Interaction of a close-in extrasolar planet with the magnetic field of its host star

Randy Olivier Laine

UNIVERSITÉ D'ORLÉANS

ÉCOLE DOCTORALE ÉNERGIE - MATÉRIAUX - SCIENCES DE LA TERRE ET DE L'UNIVERS

Groupe de Recherches sur la physique des plasmas

THÈSE présentée par :

Randy O. LAINE

soutenue le: **17 juillet 2013**

pour obtenir le grade de : **Docteur de l'Université d'Orléans**

Discipline: Physique

MODÉLISATION DE L'INTERACTION ENTRE LE CHAMP MAGNÉTIQUE D'UNE ÉTOILE ET UNE PLANÈTE EXTRASOLAIRE PROCHE

THESE dirigée par :

Douglas N.C. Lin	Professeur, UC Santa Cruz, UCO/LICK Observatory, Co-Directeur de thèse
Michel Tagger	Directeur de Recherche, CNRS, LPC2E, Co-Directeur de thèse

RAPPORTEURS :

Fabrice Mottez	Chargé de Recherche, CNRS, LUTh, Observatoire de Paris, Meudon
Philippe Zarka	Directeur de Recherche, CNRS, LESIA, Observatoire de Paris, Meudon

JURY :

Thomas Chust	Chargé de Recherche, CNRS, LPP, Ecole Polytehnique, Palaiseau
Thierry Dudok De Wit	Professeur des Universités, Université d'Orleans, LPC2E, Président du Jury
Douglas N.C. Lin	Professeur, UC Santa Cruz, UCO/LICK Observatory
Fabrice Mottez	Chargé de Recherche, CNRS, LUTh, Observatoire de Paris, Meudon
Michel Tagger	Directeur de Recherche, CNRS, LPC2E, Université d'Orléans
Philippe Zarka	Directeur de Recherche, CNRS, LESIA, Observatoire de Paris, Meudon

To my parents,
Sylvain and Jeannette Laine,
my first academic work is dedicated with love.

Acknowledgments

First of all, I would like to express my heartfelt gratitude to Doug ("Professor") Lin for his warm welcome when I first came to Santa Cruz for a research internship, and for his ongoing mentorship during the thesis. I have learned about perseverance in research, genuine hospitality, and making puns from you more than any single other person. I remember the many hours we spent discussing and scratching our heads over papers, ideas, and problems, as well as the passion, hard work, and care for your students that you have exemplified. I would also like to thank Michel Tagger for his willingness to co-direct this thesis and eagerness to help me contact other scientists. Thank you for taking the time, despite being over-booked with leadership responsibilities, to regularly check on the progress of the work. Finally, I thank Steve Balbus, who has initiated me to astrophysical gas dynamics, for introducing me to Doug Lin and later to Philippe Zarka, through whom I then met Michel Tagger.

The work for this thesis was carried out in the Astronomy and Astrophysics department at the University of California Santa Cruz, at the Laboratoire de Physique et Chimie de l'Environnement et de l'Espace in Orléans, France, and during two month-long visits at the Kavli Institite for Astronomy and Astrophysics, at Peking University, Beijing, China. I would thus like to thank for their financial support, UCO/LICK and Doug Lin in Santa Cruz, California, the University of Orléans and the LPC2E in Orléans, the Ecole Normale Supérieure in Paris, and the KIAA in Beijing. I also feel blessed to have had the privilege to meet and befriend many wonderful people in all these places. Daniel during my internship, Héloise and Matthieu in Orléans, all the families in Christian Life Center, the graduate students at UCSC and LPC2E, and the Chinese students Bin, Chelsea, Liang, Munan, Shangfei, Wendy, Xiaochen, and Xiaojia.

I have greatly benefited from the contribution of numerous members of the UCSC community. Shawfeng Dong, with whom I have had many interesting discussions, has guided me with learning linux and Fortran, and I have had the pleasure to meet his growing family. Ian Dobbs-Dixon has helped me learn IDL. I was so eager to learn fast that I came to see him again and again; he has been very kind and patient. He also jokingly taught me that if I thought I had made some progress, I may just go home and enjoy the rest of the day, instead of staying longer and finding a mistake that would spoil the rest of the evening! I must say, I have never followed that advice and indeed at times commuted back home thinking about a mistake I had just found. Pascale Garaud has helped me start the numerical computations for the time-periodic magnetic interaction. Katherine Kretke, another student of Doug, was the first astrophysics graduate student I befriended. She suggested that "a graduate student is a machine that turns coffee into

papers." I hardly drink coffee... I also enjoyed discussing about planets and magnetic dynamos with Jonathan Fortney and Gary Glatzmaier, both experts in their respective fields. The astronomy and astrophysics community in Santa Cruz is outstanding for its friendliness, exemplified for example by Raja GuhaThakurta and Enrico Ramirez-Ruiz. Several visitors also contributed to the project: Jim Pringle is the one who suggested to our attention the time-dependent diffusion model which we used for our first paper, and I have had interesting discussions with Andrew Cumming about unipolar induction and with Jean-Michel Désert about stellar spots.

Back in France, I would like to thank the entire team in Orléans who have welcomed me, with a special thank you to Jean-Mathias Griessmeier for his input on the magnetic field of extrasolar planets, the administrative staff Isabelle Langer, Catherine Hong, and Colin Royer for their help, and the graduate students Fabrice Duruisseau, Hugo Breuillard, Gisèle Krysztofiak, and Patxi Ritter for their friendliness. I have also had the pleasure to meet Philippe Zarka to talk about Alfvén waves, which then led to meeting Fabrice Mottez, Thomas Chust, and Sebastien Hess for a lively discussion again over Alfvén waves. I have also met Fabrice Gaillard to talk about the conductivity of rocks, thanks to Michel Tagger.

I would now like to express my appreciation to collaborators on various past and ongoing aspects of the project, Tristan Guillot on the project about CoRoT-2b, Fabio de Colle on a 3D simulation of the magnetic interaction, as well as Yuezhen Niu and Bin Dai on a related project about the planetary ionosphere.

Lastly but not least, Thomas Chust, Thierry Dudok de Wit, Fabrice Mottez, and Philippe Zarka have kindly accepted to be on the jury for the Ph.D. defense, and I thank them for their encouragements and comments, especially for the reviewers' reports.

Randy O. Laine

randy.laine@wustl.edu

Contents

Chapter 1

Introduction and overview

1.1 Zooming in

The past two decades have witnessed the creation of a new sub-field within astrophysics. In parallel to the study of our Solar System, the field of extrasolar planets has advanced and is advancing at a tremendous pace. Within the seven hundred or so extrasolar planets confirmed to date, we focus on the so-called "close-in" planets which orbit their host stars within roughly 0.1 AU (a class of planets that is not found in our Solar System). The concept that planets can indeed migrate from their birth locations toward their host stars has received wide theoretical and numerical support.

Close-in planets experience a set of uniquely intense interactions with their host stars (for example, gravitational tides and stellar irradiation). Within this set of intense interactions, the magnetic interaction between a close-in planet and its host star has comparably received limited attention. In order to reach quantitative conclusions, it is necessary to further specify the problem, for example, choose a magnetic field geometry and use or develop a model of interaction. We thus adopt a stellar magnetic field with dipolar geometry (as opposed to higher order geometries or a geometry determined by the stellar wind), and we use two models to respectively study the time-dependent and time-independent magnetic interactions. Finally, the magnetic interaction may trigger numerous effects, and we primarily pay attention to the effects of the ohmic dissipation (as an energy source) and Lorentz torques on the planet's internal structure and orbital angular momentum.

1.2 Outline of the thesis

In addition to the introduction and conclusion (the first and last chapters), this thesis contains 5 chapters: chapters 2 and 3 provide background information, chapter 4 is a transition chapter that outlines the main questions and reviews the relevant bibliography, and chapters 5 and 6 describe the scientific results.

In **chapter 2**, we set the physical context of the study. We review important concepts of Magnetohydrodynamics (MHD) such as magnetic diffusion and advection, electromagnetic induction, electromotive force, magnetic Reynolds number, charge separation, and Eddy

currents.

In **chapter 3**, we briefly review the observational methods used to detect extrasolar planets, describe some of the close-in planets' notable characteristics, and outline the main theoretical model for planetary system formation and evolution. We also dedicate a section to discuss the relevant characteristics of stars (primarily their magnetic dipole strengths, spin rates, and mass loss rates through winds) and their subsequent evolution in time.

In **chapter 4** (the transition chapter), we describe the three key astrophysical themes in this thesis. 1) A first endeavour consists in characterizing the Lorentz torque associated with the magnetic interaction, in particular its effect on a planet's semi-major axis and migration. 2) A related task is to calculate the ohmic dissipation associated with the currents induced in the planet and to assess its effect on the radii of hot-Jupiters. 3) Finally, we also describe a method that may be used to obtain constraints (or estimates) of the stellar magnetic field strength and the electric conductivity (and possibly state of differentiation) of a close-in super-Earth which interacts magnetically with its host star.

In **chapter 5**, we model the time-dependent interaction between a gas giant planet and the dipolar magnetic field of its host star that arises from the diffusion of the stellar field in the planet. Although the study is applicable to a system {star + close-in planet} at any stage of its evolution, we primarily use the model in the context of a young system with typically strong stellar magnetic fields. In the first part of the chapter, we describe a semi-analytical model used to solve the magnetic diffusion equation and calculate the associated ohmic dissipation. We conclude with an estimate of the effect of the Lorentz torque on the planet's migration. In the second part of the chapter, we focus on the situation in which the close-in planet fills its Roche lobe, and the ohmic dissipation drives a mass loss through Roche lobe overflow. In doing so, we expand the approach used in the first part of the chapter into a self-consistent model in which the internal structure and mass loss rate adjust to the ohmic dissipation. We conclude with an estimate of the mass loss rate and associated change in the planet's angular momentum while varying the parameters of the system.

In **chapter 6**, we turn to the time-independent magnetic induction of electric currents in a planet. Contrary to the model described in the previous chapter which was primarily relevant for close-in gas giants and young stars, the present model may be relevant for close-in gas giants and rocky planets as well as for young and more mature systems. We sequentially describe in detail the calculation of each component of the model and compare the well-known tidal dissipation and torque with the ohmic dissipation and Lorentz torque associated with the magnetic interaction. We also suggest two astrophysical applications of the model. First, the ohmic dissipation may provide a mechanism for explaining the inflated aspect (*i.e.* unexplained large radii) of some hot-Jupiters (we apply our model to CoRoT-2b). Second, instead of assuming a stellar field strength and a planetary electric conductivity in order to deduce the Lorentz torque and ohmic dissipation experienced by the planet, we propose that observational constraints on the torques or energy sources applied on the planet can inversely help to constrain the stellar magnetic field strength and the electric conductivity of a rocky planet's outer layers. Estimations of the electric conductivity may furthermore shed light on the degree of differentiation of the extrasolar planet's crust.

In **chapter 7** (conclusion and perspectives), we take a critical look on our results, zoom out to consider them in a larger context, and outline a few promising issues.

La découverte en 1995 de la première planète autour d'une étoile semblable au Soleil a marqué le début d'une croissance extraordinaire dans l'étude de la formation et évolution des systèmes planétaires et la caractérisation individuelle des planètes extrasolaires. A ce jour, plus de sept cent planètes extrasolaires ont été découvertes. Parmi ces planètes, nous nous intéressons aux planètes très proches de leur étoile (demi-grand axe inférieur a 0.1 unité astronomique). Ces planètes se distinguent par des interactions très intenses avec leur étoile. Nous modélisons l'interaction magnétique entre une planète et le champ magnétique dipolaire de son étoile et calculons l'énergie dissipée et le moment angulaire échangé lors de cette interaction. Ces paramètres physiques sont important d'un point de vue astrophysique puisque l'énergie et moment angulaire peuvent changer le rayon d'une planète gaseuse et son demi-grand axe planétaire.

En plus des chapîtres d'introduction et de conclusion (chapîtres 1 et 7), ce manuscrit de thèse est divisé en cinq chapîtres. Le chapître 2 décrit le context physique de notre étude et rappelle de nombreux concepts comme la diffusion et advection magnétique, l'induction électromagnétique, la force électromotive, le nombre de Reynolds magnétique, la séparation de charge induite, et les courants de Eddy. Dans le chapître 3, nous décrivons brièvement les principales techniques observationelles utilisées pour détecter des planètes extrasolaires. Nous décrivons aussi les idées principales du modèle de formation des systèmes planétaires ainsi que les caractéristiques stellaires importantes dans notre étude. Le chapître 4 est une transition qui décrit les thématiques astrophysiques majeures abordées dans cette thèse et présente une revue bibliographique. Nos résultats sont décrits aux chapîtres 5 et 6: nous étudions l'interaction magnétique périodique dans le temps au chapître 5 et l'interaction magnétique indépendente du temps au au chapître 6.

Chapter 2

Physical analysis of the problem

The physics involved in modelling the formation and evolution of planetary systems is so diverse that any astrophysical object or phenomenon can be analyzed or modelled using different sub-fields of physics, depending on the aspects of the problem of interest. This chapter thus presents a brief analysis of the magnetic interaction under investigation in order to set the physical framework, which is then applied to close-in extrasolar planets in the magnetosphere of their host stars.

Contents

Nous présentons dans ce chapître le contexte physique de notre étude, le reste de ce manuscrit se concentrant sur les aspects astrophysiques. Nous rappelons d'abord les équations d'induction électromagnétique et de diffusion-advection du champ magnétique. Nous décrivons ensuite le mode Transverse Electrique (périodique dans le temps, donnant lieu à un courant induit alternatif) et le mode Transverse Magnétique (indépendent du temps, donnant lieu à un courant induit continu) qui seront étudiés séparemment aux chapîtres 5 et 6. Enfin, nous notons l'importance des conditions aux limites et introduisons l'analogie des circuits électriques utilisée au chapître 6 pour l'étude du mode Transverse Magnétique.

2.1 Magnetic diffusion and induction

In this section, we review the basic concepts that lead to the diffusion equation of an external magnetic field into a body with a non-zero electric conductivity. We both discuss the time-periodic (relevant for chapter 5) and the time-independent cases (relevant for chapter 6).

General description

We assume that a body bounded by a closed surface S is placed for the first time in contact with an external magnetic field $\mathcal{B}_{ext}$ which can be time dependent or independent and is present everywhere except, initially, within the body. Because of $\mathcal{B}_{ext}$, the field in the body $\mathcal{B}$ changes from zero to a non-zero value. This change occurs first near the boundary S and, with time, increasingly deeper inside the body. The time derivative of the magnetic field is accompanied with an electric field $\mathcal{E}$ (Maxwell-Faraday equation)

$$\frac{\partial \mathcal{B}}{\partial t} = -\nabla \wedge \mathcal{E}. \tag{2.1}$$

If the electrical conductivity σ in the body is non-zero, an electric current density $\mathcal{J}$ is induced through Ohm's law (here written with σ as a scalar)

$$\mathcal{J} = \sigma \mathcal{E}, \tag{2.2}$$

as well as a corresponding magnetic field through Maxwell-Ampere equation (where the displacement current is neglected)

$$\nabla \wedge \mathcal{B} = \mu_0 \mathcal{J}, \tag{2.3}$$

where μ_0 is the vacuum magnetic permeability. Combined together, the previous equations lead to the diffusion equation for the magnetic field inside the conductor

$$\frac{\partial \mathcal{B}}{\partial t} = -\nabla \wedge (\eta \nabla \wedge \mathcal{B}), \tag{2.4}$$

where $\eta = (\mu_0 \sigma)^{-1}$ is the magnetic diffusivity. If η is constant in space, the diffusion equation becomes

$$\frac{\partial \mathcal{B}}{\partial t} = \eta \triangle \mathcal{B}. \tag{2.5}$$

The evolution of the total field in the body is analogous to that of a diffusion process. A change in magnetic field in the body is coupled with the induction of an electric and magnetic fields (the latter only in the presence of a non-zero electric conductivity). The effect of this induced magnetic field is to reduce its causes (Lenz's law), *i.e.* changes in magnetic field in the body. As in the heat diffusion, the presence of the Laplacian operator indicates that the solution will be the smoothest possible, *i.e.* local inhomogeneities of the magnetic field in the body will tend to be smoothed out through diffusion.

Diffusion of a time-independent external magnetic field

For a time-independent external magnetic field $\mathcal{B}_{ext}$, the field $\mathcal{B}(\mathbf{r})$ inside the body at location $\mathbf{r}$ increases with time from zero to the external value. Therefore, at each location, $\partial\mathcal{B}/\partial t$ tends to zero after some time, the induced current density decreases in amplitude, and the external field thus diffuses in the body with a characteristic time scale $\tau = \mu_0\sigma L^2$ (L is a characteristic size of the body and σ is the electric conductivity). Stated differently, after a characteristic time τ, the field has penetrated a characteristic distance $L(\tau) = \sqrt{\tau/\mu_0\sigma} = \sqrt{\tau\eta}$ (this formula is derived from a dimensional analysis, and we have omitted numerical coefficients).

Diffusion of a periodic external magnetic field, Eddy currents, and skin depth

On the other hand, a time-periodic external magnetic field (with an amplitude oscillating around zero) induces time-periodic (Eddy) currents. Contrary to the time-independent case, these currents do not decay but instead continually dissipate the magnetic energy. The "skin depth" δ is the distance over which the amplitude of the field decreases by a factor e^1, and it is typically written as $\delta = \sqrt{2\eta/\omega}$, where ω is the radial frequency of the time-periodic external magnetic field. The higher the electric conductivity, the stronger the Eddy currents, and the more difficult it is for the external magnetic field to diffuse in the conductor. More generally, a time variable field can be decomposed into its time-independent and time-periodic Fourrier components, each diffusing as described above.

2.2 Motional induction

In this section, we review the concept of motional induction which, in the presence of a magnetic field, determines the electric fields present in different frames of references moving relative to each others. It is a kinematic effect relevant for the study of a planet moving relative to the stellar magnetosphere.

In addition to magnetic diffusion, changing frame of reference is another way to induce an electric field in the presence of an external magnetic field. Instead of stating it in general terms, we apply it to our astrophysical (non-relativistic) system. We assume that a star has a magnetic dipole m which spins with the star with angular velocity ω_* and generates a dipolar magnetic field $\mathcal{B}_*$. A planet orbits this star with angular velocity ω_p (which is also denoted n in celestial mechanics). We call $(\mathcal{R}^p)$ the frame centered on the planet and translating around the star at the planetary orbital angular velocity ω_p, and we call $(\mathcal{R}^*)$ the frame translating around the star on the planet's orbit but with the angular velocity of the stellar spin ω_*. The velocity of the frame $(\mathcal{R}^p)$ relative to the frame $(\mathcal{R}^*)$ is $v_{p/*} = a\omega_{p/*} = a\left(\omega_p - \omega_*\right)$; it is also the velocity of the planet relative to the unperturbed stellar magnetospheric plasma that co-rotates with the star. We call $\mathcal{E}^*$ and $\mathcal{E}^p$ respectively the total electric fields in the frames centered on the planet and translating around the star with angular velocities respectively equal to that of the stellar spin and that of the planetary orbit. These electric fields are

$$\mathcal{E}^p = \mathcal{E}^* + v_{p/*} \wedge \mathcal{B}_*, \tag{2.6}$$

and the magnetic field is the same in both frames of references. The equation above is sometimes written with a negative sign $\mathcal{E}^p = \mathcal{E}^* - \upsilon_{*/p} \wedge \mathcal{B}_*$, but it would then be expressed with the velocity $\upsilon_{*/p}$ of the frame $(\mathcal{R}^*)$ in the frame $(\mathcal{R}^p)$. If we assume that $\mathcal{E}^* = 0$ (*i.e.* no electric field in the unperturbed stellar magnetosphere, for example because of the high conductivity along field lines), then the electric field in the frame of the planet is purely the motionally induced field $\mathcal{E}^p = \upsilon_{p/*} \wedge \mathcal{B}_*$.

The motional field is a kinematic effect and does not require the planet or any conductor to be present. Nevertheless, the presence of a planet with conductivity σ enables charges to move under the motionally induced electric field. Contrary to a Coulombian electric field which curl is zero, the curl of the induced motional electric field is non zero, and it is able to carry a charge around a closed loop (*i.e.* an electric current) at the expense of work.

2.3 Full equation and magnetic Reynolds number

We now combine both concepts (magnetic diffusion and motional induction) and discuss some important parameters (such as the magnetic Reynolds number and time scales) with which one can compare the relative strengths of these effects.

When both the magnetic diffusion and the motional electric field are taken into account, the equation that describes the evolution of the magnetic field inside the planet is,

$$\frac{\partial \mathcal{B}}{\partial t} = \nabla \wedge (\upsilon_{p/*} \wedge \mathcal{B}) - \nabla \wedge (\eta \nabla \wedge \mathcal{B}), \tag{2.7}$$

which becomes, if η = constant,

$$\frac{\partial \mathcal{B}}{\partial t} = \nabla \wedge (\upsilon_{p/*} \wedge \mathcal{B}) + \eta \triangle \mathcal{B}. \tag{2.8}$$

The first and second terms on the right hand side of the previous equation corresponds respectively to the magnetic advection (and its associated motional induction) and magnetic diffusion. The dimensionless parameter that compares their respective strengths is the magnetic Reynolds number

$$R_m = \frac{\upsilon_{p/*} L}{\eta} = \upsilon_{p/*} L \mu_0 \sigma, \tag{2.9}$$

where L is a characteristic length-scale. This parameter is obtained by taking the ratio of the advection term $\nabla \wedge (\upsilon_{p/*} \wedge \mathcal{B}) \sim (\upsilon_{p/*} \mathcal{B})/L$ with the diffusion term $\eta \triangle \mathcal{B} \sim \eta \mathcal{B}/L^2$. The motional induction is negligible if $R_m \ll 1$, *i.e.* $\upsilon_{p/*} \ll \eta/L = (\mu_0 \sigma L)^{-1}$. The regime in space plasmas may differ drastically from that in laboratory plasmas primarily because of the large differences in the sizes involved in each respective regime. Near and inside a hot-Jupiter, $\sigma \approx 10^{-5} - 10^5$ ohm^{-1} m^{-1}, $\upsilon \approx 10^5$ ms^{-1}, $R_p \approx 10^8$m (the scale height, another characteristic size, is $H \approx 10^5$m near the surface), and the magnetic Reynolds number is almost always larger than unity (except when the planet orbits the star near co-rotation, *i.e.* $\upsilon_{p/*} \approx 0$, and for negligibly conducting gas in the planet). Table 2.1 summarizes these numerical estimates.

μ_0	$\upsilon_{p/*}$	σ	L	R_m
$4\pi \times 10^{-7}$	10^5	10^{-5}	$L = R_p = 10^8$	$R_m \approx 10^2$
$4\pi \times 10^{-7}$	10^5	1	$L = R_p = 10^8$	$R_m \approx 10^7$
$4\pi \times 10^{-7}$	10^5	10^5	$L = R_p = 10^8$	$R_m \approx 10^{12}$
$4\pi \times 10^{-7}$	10^5	10^{-5}	$L = H = 10^5$	$R_m \approx 10^{-1}$
$4\pi \times 10^{-7}$	10^5	1	$L = H = 10^5$	$R_m \approx 10^4$
$4\pi \times 10^{-7}$	10^5	10^5	$L = H = 10^5$	$R_m \approx 10^9$

Table 2.1: Table giving the values of the magnetic Reynolds number for a few reasonable sets of parameters for the interaction of a planet with the stellar magnetosphere. Except when $\upsilon_{p/*} \approx 0$ (the planet is orbiting with a period very near that of the stellar spin) or $\sigma_0 \approx 0$, the system is typically in the regime with $R_m \gg 1$ where magnetic advection and its associated motionally induced electric field is dominant.

The characteristic time scale τ associated with the full equation is

$$\tau = \frac{L^2}{\eta} \frac{1}{1 + R_m}. \tag{2.10}$$

Again, we find that for small magnetic Reynolds number, diffusion is dominant, and $\tau \approx \tau_{diffusion} = L^2/\eta$. Inversely, for large magnetic Reynolds number, the motional induction term dominates and $\tau \approx \tau_{advection} = L/\upsilon$ which is typically smaller than an orbital period. Of course, the analysis using the magnetic Reynolds number is local (as opposed to macroscopic) and ignores boundary conditions, which are discussed later in this chapter.

2.4 Transverse Electric (TE) mode in a planet

The simplest geometry is obtained by assuming that the stellar spin and planetary orbital axes are aligned. The stellar magnetic moment $\mathbf{m}$ can be decomposed in its components $m_\parallel$ parallel to the planet's orbital axis and a component $m_\perp$ perpendicular to the planet's orbital axis. It amounts to decomposing the stellar dipolar field into respectively a time-independent and a time-periodic components (as seen by the planet in a circular orbit in the ecliptic plane).

The interaction of the planet with the time-periodic component corresponds to the Transverse Electric (TE) mode. Eddy currents are induced (within a depth corresponding to a few skin depths) and an alternative current (AC) circuit is established within the planet (Sonett et al. 1975 [109], Campbell 1983 [20], Laine et al. 2008 [73]).

2.5 Transverse Magnetic (TM) mode in a planet

The interaction of the planet orbiting in the presence of the time-independent component of the stellar magnetic field corresponds to the Transverse Magnetic (TM) mode

(Colburn 1980 [24], Goldreich & Lynden-Bell 1969 [51], Laine & Lin 2012 [72]). We neglect diffusion when discussing the TM mode and thus assume that the external magnetic field permeates the planet. For a planet in a vacuum, the motionally induced electric field $\mathcal{E}_v$ in the planet triggers a charge separation on a time scale, typically negligible, $\tau = \epsilon/\sigma$ (ϵ being the local electric permittivity) which locally decreases the electric field (Sonett & Colburn 1967 [108]). If allowed to build up, the electrostatic (Coulombian) electric field associated with the charge separation $\mathcal{E}_{sep}$ cancels the electromotive field (*i.e.* $\mathcal{E}_{sep} = -\mathcal{E}_v$).

2.5.1 A very idealized scenario

We now describe a slightly different idealized scenario as pictured in figure (2.1) to avoid the effect of boundary conditions. The idealized conditions are later removed to emphasize the importance of boundary conditions.

We assume that the external magnetic field is time-independent, uniform in space, in the z direction, occupies all space, and permeates the planet. We assume that the planet is infinite in the y direction (like an infinite cylinder), surrounded by vacuum, initially at rest, and starts to move at time t=0 in the x direction at speed $v_{p/*}$.

In the frame moving with the planet, there is an electric field $\mathcal{E} = v_{p/*}\mathcal{B}$ in the direction of -y. If the plasma in the planet has zero conductivity, then there is no further interaction between the plasma and the stellar field. If the plasma has a small electric conductivity σ, then the motional electric field generates a volumic current $\mathcal{J} = \sigma\mathcal{E}$. The plasma in the volumic current is acted upon by the magnetic field through a Lorentz force which points in the direction of -x and thus tends to oppose the motion of the planetary plasma. Concurrently, the induced electric current density also generates an induced magnetic field through the Ampere equation. The drawing of the field lines looks as if the total magnetic field (the sum of the induced magnetic field and unperturbed external field) is dragged in the direction of the planet leading to the concept that field and plasma are drawn toward co-motion, the extent of which depends on the strength of the interaction.

Equivalently, one can follow, in the field's frame (associated with the stellar magnetosphere), the motion of the plasma charges which move with the planet. These charges experience a Laplace force $F = qv_{p/*}\mathcal{B}$ which makes positive and negative charges drift in opposite directions; the current associated with this drift has the same effect as the induced current in the previous paragraph.

2.5.2 Lifting the hypothesis of vacuum around the planet

In the vacuum surrounding the planet, the magnetic field lines (defined as the tangent to the magnetic field vector) have no physical meaning. Nevertheless, the field on each side of the planetary boundary are coupled through magnetic tension. Therefore, if the planet is surrounded by and moving through a conducting plasma, then the motion of the planetary plasma perturbs the field which threads the planet, this perturbation is communicated to the field outside the planet (magnetic tension), and this perturbation of the field outside the planet is in turn communicated to the plasma through the electric conductivity as described above. The combination of magnetic tension and Lenz' law (acting as an inertia) leads to the generation and propagation of Alfvén waves. The magnetic field induced in the planet

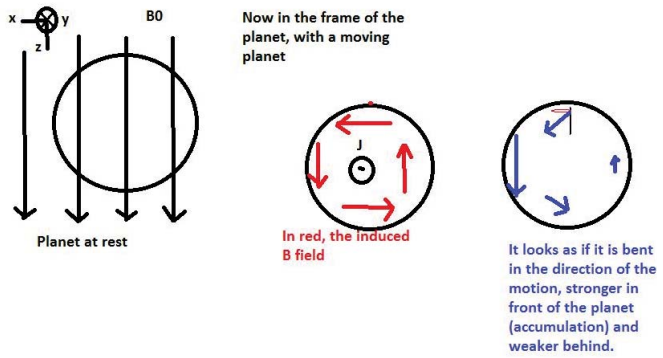

Figure 2.1: Idealized geometry used to discuss the interaction of an external magnetic field with a conductor without needing to consider boundary conditions. The impact and importance of the boundary conditions are discussed in the subsequent subsections. The planet is assumed here to be infinite in the y direction. The magnetic field is uniform, time-independent, and permeates the planet. The planet is at rest in the picture on the left, and in motion in the +x direction in the pictures in the middle and on the right. The picture in the middle shows the magnetic field induced in the planet (in red), and the picture on the right shows the total magnetic field (in blue) in the planet, which is the sum of the external magnetic field (in black) and the induced magnetic field (in red)

.

rapidly decays to zero outside the planet. Far from it, the stellar magnetosphere is thus unperturbed, except along the field lines threading the planet along which Alfvén waves can travel.

2.5.3 Considering boundary conditions

In the idealized scenario, we assumed the planet to be infinite in the direction of the induced current in order to avoid boundaries. In other words, we assumed that there were adequate sources and sinks of charges or currents to carry the induced currents. We now consider a spherical planet of radius R_p. In the TE mode, solutions can be found with currents confined in the planet. The planet can thus be studied in isolation, but boundary conditions on the current are in fact important as soon as the current crosses the surface of the planet.

The effect of boundary conditions is readily seen in the TM mode (time-independent), for example, if the planet is surrounded by a very resistive medium (such as vacuum as in the idealized description above). In this case, the currents (induced in the -y direction) will result in a charge separation and a coulombian electric field $\mathcal{E}_{sep}$. This coulombian field opposes the motionally induced field, and the total electric field in the planet is accordingly decreased. If the total field is decreased to zero in the planet through charge separation, then the induced currents are also quenched.

Inversely, if the charges are allowed to leave the planet at a sufficient rate, then $\mathcal{E}_{sep}$ does not build up. This condition is equivalent to assuming a closed (or infinite) loop through

the medium outside the planet with adequate electric conductivity. It is also equivalent to the assumption, implicit in the neglect of boundary conditions, that there are adequate sources and sinks of charges and currents. When the boundary conditions are taken into account, whether the electric field in the planet is reduced or not depends on the electric conductivity in the planet relative to that along closed loops through the outer medium (Drell et al. 1965 [36] discusses a variant where the charges leave the planet through photoelectric effect (when photons can cause electrons to become unbounded) and not because of the electric conductivity of the outside medium). Therefore, the characteristics, especially electric conductivities, of the plasma along the entire path of the current must be considered (Alfven 1981 [2]), as is the case in electric circuit models (Piddington & Drake 1968 [91], Goldreich & Lynden-Bell 1969 [51]).

2.5.4 Electric circuit analogy in TM mode

In our astrophysical application, the resistances along the entire circuit are the resistances of the planet $\mathcal{R}_p$, of the plasma at the foot of the flux tube on the stellar surface $\mathcal{R}_*$ (the resistance along the flux tube,$\mathcal{R}_f$, is neglected). In this electric circuit analogy, there are two independent and symmetric circuits, each involving one hemisphere of the planet, one hemisphere of the star (in fact, just the volume corresponding to the footprint of the flux tube), and the corresponding flux tube (as represented in figure 2.2).

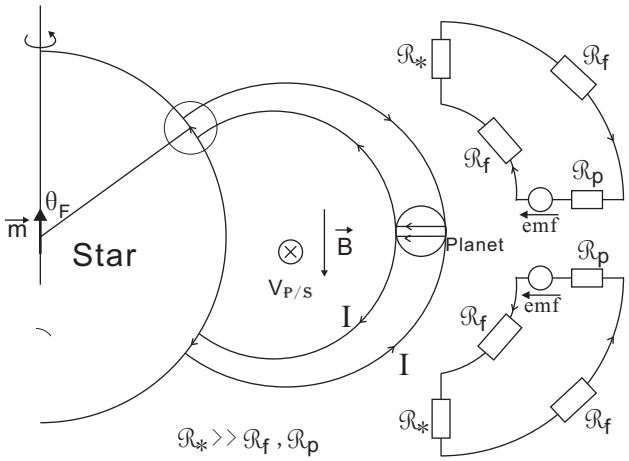

Figure 2.2: Schematic representation of the system as an electric circuit (from Laine & Lin 2012 [72]). In the figure $v_{p/*}$ is written $V_{p/s}$.

Advantages and drawbacks/limits

There is a long standing discussion about the description of phenomena with a $(\mathcal{E}, \mathcal{J})$ or $(v, \mathcal{B})$ approach (also see Saur 2004 [97]). For example, Eugene Parker criticizes electric

circuit analogies in favor of a $(v, \mathcal{B})$ approach, primarily because he has in mind cosmical plasmas with very high electric conductivities (resulting in $\mathcal{E} = 0$) and so low density that ohm's law does not apply (Parker 2007 [87]). On the other hand, Alfvén points out that electric analogies are useful and relevant, and that an $(\mathcal{E}, \mathcal{J})$ approach is essential in some cases (Alfvén 1981 [2]).

Electric circuit analogies are a macroscopic representation of an $(\mathcal{E}, \mathcal{J})$ description. These models are easier to grasp intuitively, involve macroscopic calculations (not unlike the Q-value in the calculation of tidal torques), and explicitly make use of the electric current. On the other hand, a natural consequence of using macroscopic values is the loss of the precision that comes from microscopic considerations. Electric circuit analogies sometimes can at best represent an average and, therefore, may also neglect geometric coefficients. More significantly, the electric circuit analogy makes the assumption that the macroscopic electric current is the same in every part of the circuit, *i.e.* that information about changes in electric potential at one location are rapidly transmitted to all parts of the circuit. In our astrophysical objects of interest, this information is transmitted along field lines at the Alfvén speed $v_A = \mathcal{B}/\sqrt{\mu_0 \varrho}$ (in the frame of the plasma attached to the field lines), where ϱ is the volumic mass of charged particles (Alfvén 1942 [3]). Nevertheless, if the gas is fully ionized or if the collision frequency of charged particles with neutrals is large, then ϱ is roughly the gas volumic mass.

2.6 Concluding remarks

We have briefly discussed some of the important physical aspects which are in the background of the present astrophysical study. Although seemingly straightforward, these concepts lead to an exceedingly complex, rich, and diverse array of phenomena. In trying to model the interaction of an astrophysical body with an external magnetic field, one may take a combination of numerous approaches, depending on the level of detail desired (order of magnitude or precise calculation), the tools used (analytical, semi-analytical, fully numerical), the level of approximation made (ideal MHD, resistive MHD, plasma physics if ohm's law does not apply, two-fluid approximation, assumption of local thermodynamic equilibrium or not), the model used (Alfvén wing, unipolar inductor (TM mode), TE mode), the scale (geographical extent) of the study, and perhaps more importantly the degree of homogeneity (*e.g.* the Moon as a homogeneous body interacting with the Solar wind (homogeneous, moderate scale), the impact of magnetized impurities on the surface of the Moon interacting with the Solar wind (local), a pure Alfvén wing (homogeneous), the transition between the immediate surrounding of a planet and its Alfvén wing (moderate scale, inhomogeneous), the reflection of Alfvén waves at a discontinuity (local, inhomogeneous), a unipolar inductor and its complete electric circuit as in chapter 6 (large scale), etc.).

Expounding on each of these topics is beyond the scope of the present work, but the following list of articles include additional physical discussions in an astrophysical context: Drell 1965 [36] (pure linear Alfvén wing for a man-made satellite in the Earth's magnetic field), Schwartz et al. 1969 [100] (interaction of the Moon with the Solar wind), Neubauer 1980 [83] (non-linear Alfvén wing), Crary & Bagenal 1997 [26] (transition from an Alfvén

wing to a unipolar inductor), Deift & Goertz 1973 [47] (local discussion of the generation of an Alfvén wave; part of a series of 4 papers, [47], [49], [28], [48])), Saur 2004 [96] (Alfvén wing and unipolar inductor for Io), Saur et al. 2004 [97] (a review article for the Io-Jupiter interaction), and Southwood & Kivelson 1991 [110] (a discussion of electric currents along magnetic field lines).

Chapter 3

Onward to extrasolar systems

This chapter briefly reviews the main methods used to detect extrasolar planets, summarizes the current theory of planetary system formation, and ends with important background information about stars and stellar magnetospheres.

Contents

Ce chapître présente un survol du vaste domaine qu'est l'étude de la formation et évolution des systèmes planétaires. De nombreux ouvrages de vulgarisations et de références existent dont nous avons inclu une courte liste en début de section (3.2).

Dans la première section de ce chapître (3.1), nous présentons la partie observationelle de l'étude des systèmes planétaires, en particulier les méthodes d'observations et certaines caractéristiques importantes des planètes découvertes jusqu'à maintenant. Les méthodes les plus couramment utilisées dans la recherche de planètes extrasolaires sont les vitesses radiales, le transit, l'astrométrie, l'imagerie directe, et les microlentilles gravitationelles. Les vitesses radiales et le transit sont les méthodes de détections ayant eu, jusqu'à maintenant, le plus de succès (plus de 90% des détections). Cependant, ces méthodes sont

toutes complémentaires. Par example, les vitesses radiales et transit sont plus sensibles aux planètes massives sur une orbite proche, contrairement à l'astrométrie et aux microlentilles gravitationelles qui détectent plus facilement les planètes sur des orbites longues. En outre, les microlentilles permettraient aussi la détection de lunes et planètes n'orbitant pas une étoile.

L'étude des caractéristiques d'ensemble des planètes révèle une diversité inattendue (3.1.3). Par example, les masses des planètes extrasolaires varient continuement entre la limite de détection (une masse terrestre) jusqu'aux masses correspondantes aux naines brunes. Leurs eccentricités de même varient de 0 à 1, sauf pour les planètes proches de leur étoile.

Cette observation attire notre attention sur les interactions entre une étoile et une planète proche de l'étoile. Nous présentons d'abord le cas bien connu des marées gravitationelles, puis nous décrivons le cas des planètes enflées que nous étudions plus en détail au chapître 4. Nous mentionnons enfin le déficit apparent de planètes très proches de leur étoile qui pourrait être causé par deux effets complémentaires: un mécanisme qui donne du moment angulaire à la planète vers 0.04-0.08 unité astronomique, et un mécanisme qui retire du moment angulaire lorsque la planète est très proche de son étoile ($<$0.04 UA).

Dans la deuxième section de ce chapître (3.2), nous résumons la partie théorique de l'étude des planètes extrasolaires. D'après le modèle standard, les particules solides dans le disque protoplanétaire augmentent en taille au cours de nombreuses collisions. Plusieurs étapes clés de cette croissance de 40 ordres de grandeur (depuis la masse d'une particule micrométrique jusqu'à une masse terrestre) ne sont pas encore bien comprises, en particulier comment les grains solides peuvent grandir en taille alors que les collisions entre particules au delà du mètre peuvent détruire les grains, et comment les particules ont le temps de devenir une planète lorsque des arguments théoriques mènent à penser que ces particules solides peuvent migrer jusqu'à l'étoile en un temps bien inférieur au temps associé à la formation des planètes à partir des grains. Pour comprendre la formation des planètes, il est donc nécessaire d'étudier également les turbulences et inhomogenéités de pression qui peuvent faciliter les collisions (pour permettre la croissance en taille) et créer des zones stables (où la migration planétaire est (temporairement) arrêtée).

Après cette description des étapes et problèmes principaux de la formation des planètes, nous présentons (dans la sous-section 3.2.4) les paramètres stellaires utilisés dans notre modèle (en particulier, champ magnétique, période de rotation, et perte de masse par vent stellaire).

3.1 Introduction to the field of extrasolar planets

3.1.1 From one to many Solar systems

Seven objects in our Solar System, the Sun, Moon, Mercury, Venus, Mars, Jupiter, and Saturn can be seen with naked eyes and, together with the few hundred brightest stars in the firmament, have been the subject of wonder, careful observation, and analysis for several millennia. They guided sailors and explorers, inspired poets, and provided the impetus for the compilation of astronomical tables which, with the scientific method, brought the dawn of modern astronomy and celestial mechanics. Further painstaking observation and analysis gradually improved our knowledge of the constituents of our own Solar System with, for example, the discovery of Uranus, Neptune, Pluto, planetary rings, Kepler, Kuiper and Oort belts, planetary magnetic field, Solar wind, and interplanetary magnetic field. Concurrently, development in observational techniques, fruitful interactions with theoretical physics, and progress in the study of stars and interstellar medium provided concepts such as accretion, proto-planetary disks, minimum mass nebula, winds and jets, stellar composition, resonance and instability, magnetosphere, bow shocks, etc. The discovery of each of these astronomical objects, concepts, or phenomena could be a remarkable story to be told in its own right.

Collectively, these advances have shaped a scenario of planetary system formation and evolution which, along its main lines, explains somewhat satisfactorily (ignoring a few gaps in the understanding) the key features of our Solar System, such as, to name only a very few, the low inclination, low eccentricity, prograde planetary orbits, and the sharp separation between small rocky planets in the inner part of the Solar System and giant planets in the outer part. Nevertheless, theories of planetary system formation and evolution were constructed based on observations from our own Solar System, which resulted in a built-in methodological bias toward predicting the formation of planetary systems similar to ours.

The discovery in 1995 of the first extrasolar planet, Pegasus-51b, to orbit around a Solar-type star has rekindled the theoretical interest in the formation and evolution of planetary systems and led the way for hundreds of new systems to be discovered and studied. Fascinating worlds around stars in a "far far away galaxy" have abounded in popular culture, and it is no longer science fiction.[1] To date, over 700 extrasolar planets have been discovered around nearby stars, a few thousands candidates await confirmation, and several projects have been dedicated to searching for extrasolar planets (CoRoT, Kepler, etc). Figure (3.1) shows the masses and semi-major axes of the planets that have been discovered so far.

3.1.2 How can extrasolar planets be detected?

Five main techniques are currently used to search for extrasolar planets: radial velocity, transit, astrometry, direct imaging, and gravitational microlensing. We briefly review their respective strengths, weaknesses, and biases, with an emphasis on their complementarity. We refer the interested reader to the large body of specialized works (for example, the

[1] It must be pointed out, however, that all these planets have been discovered in our local neighborhood; astronomers are still far from detecting planets in a "far far away galaxy."

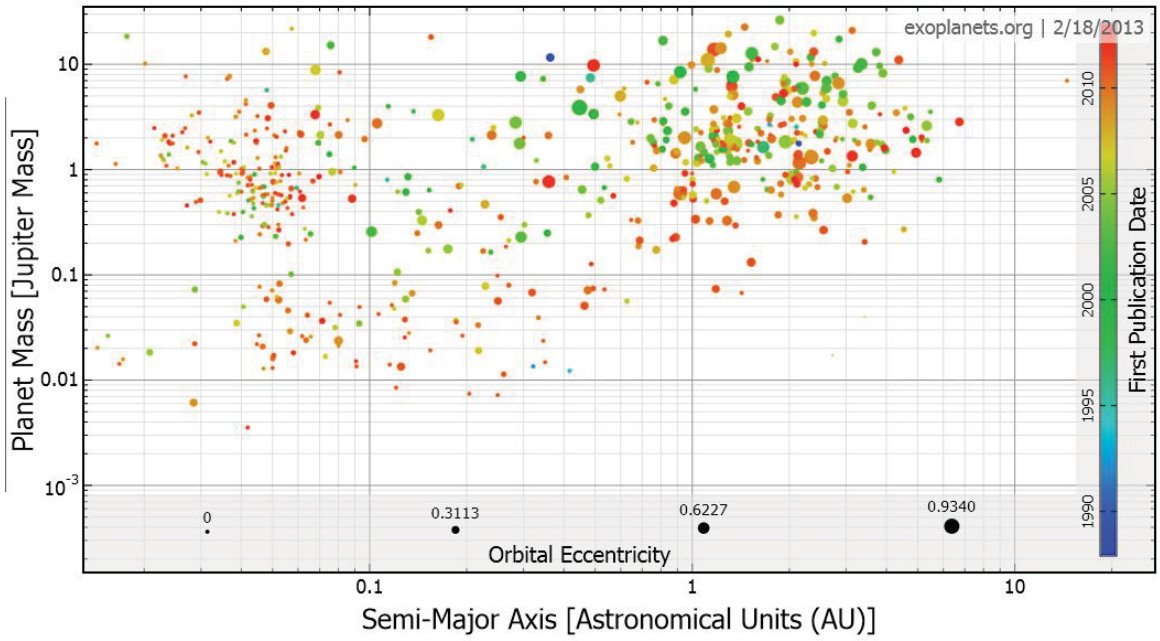

Figure 3.1: Plot of the masses as a function of semi-major axes of the extrasolar planets referenced on http://exoplanets.org/ as of mid-February 2012. The color codes the age of first publication and shows the recent massive increase in number of discoveries, especially among lower mass planets). The size of the dot gives a qualitative idea of the eccentricity of the planet, which shows that planets close to their stars tend to have smaller eccentricities.

volume "Exoplanets" edited by Sara Seager (Seager 2010 [101]).

Radial velocity

Radial velocity has been the most successful method (about 70% of the verified detections), and it is the technique used in the detection of Pegasus-51b, the first extrasolar planet discovered around a Solar type star (Mayor & Queloz 1995 [81]). The radial velocity technique detects the Doppler shifts in the stellar spectral lines due to the motion of the star around the center of mass of the {planet + star} binary system. Like astrometry, it is an indirect method which infers the presence of a planet through its perturbation on the stellar motion.

This method is efficient for detecting close-in and massive (heavy) planets. The Doppler shift is proportional to $M_p sin(i)$, with M_p the mass of the planet and i the angle between the orbital plane and the observer. The degeneracy (M_p and i are both unknown) cannot be lifted with this technique alone, and only a lower boundary estimate of the mass is obtained. This method is also affected by noise in the stellar light, for example, due to oscillations of the stellar surface, stellar activity cycles, changes in granulation, and variations in stellar magnetic fields.

In fact, Doppler shifts in stellar spectra have been used for a century to measure the radial motions of stars with proper motion larger than a few kms^{-1}, and this method was early on suggested as a way to detect extrasolar planets (Struve 1952 [112]). However, a Jupiter-mass planet orbiting a Solar-mass star at 0.05 AU (respectively an Earth-mass planet at 1 AU) is associated with a stellar radial velocity of the order of 100 ms^{-1} (respectively 10 cms^{-1}). Detecting such small Doppler shifts is one of the greatest technical challenge to this method.[2]

Transit

The transit technique detects the small dip in the stellar flux reaching the telescope when an extrasolar planet transits between the star and the observer (about a 1% dip in the stellar luminosity for a transiting hot-Jupiter and 0.01 % for an Earth-like planet). Charbonneau et al. 2000 [22] detected the first transiting extrasolar planet, and this method has so far been used to discover about 20% of the verified extrasolar planets. Thousands of candidates have also been found with the space missions Kepler and CoRoT. This method is also more sensitive to large planets and biased toward close-in planets since the probability of transit increases sharply with decreasing semi-major axis. Therefore, this technique theoretically can detect much fewer planets than radial velocity. It is also highly sensitive to variations in stellar activity.

Nevertheless, this method provides unique information about the planet such as the radius of the planet and a spectra of the planetary atmosphere (a transition spectra during "primary eclipse" when the planet transits in front of the star, and an emission spectra just before the "secondary eclipse" when the planet is about to be eclipsed by the star). Such

[2]In effect, instead of analysing a single spectral line, observers statistically analyze the temporal variations of a stellar spectrum against a known stable reference set of spectral lines.

information makes this method particularly useful in the study of the planet's habitability, albedo, and atmospheric composition. Because the optical depth is wavelength dependent, the observation of transits at different wavelengths allows to probe different depths in the planet's atmosphere (Gillon et al. 2010 [46], Snellen et al. [107]) and to infer temperature inversions (Machalek et al. 2009 [79], Parmentier & Guillot 2011 [88]). Attempts to detect retrograde orbits and the angle between the stellar spin axis and the planet's orbital axis have been made through the Rossiter-McLaughlin effect (Winn et al. [116]), and planetary winds may be inferred through the detection of a warm spot on the planet that is offset from the planet-star axis (Knutson et al. 2007 [70]). Used together, the radial velocity and transit methods can yield an estimate of the planet's mean density and, therefore, internal bulk composition.

Astrometry

Astrometry measures the semi-major axis of a star's elliptic motion around the center of mass of the binary system {planet + star}. It, therefore, detects more readily massive planets (like radial velocity) and planets with a large semi-major axis, which makes this method complementary to the transit and radial velocity methods. It also measures both the mass M_p and the angle $sin(i)$. Nevertheless, implementing this technique is challenging because of the Earth's atmosphere and the exquisite angular resolution required. Interferometry and space missions such as Hipparcos and Gaia are, therefore, favored. So far, no verified detection of an extrasolar planet has yet been made through astrometry.

Direct imaging

Direct imaging may be the first method that comes to mind, but it is in fact extremely difficult to achieve because it requires a small angular resolution (0.3 arcsec for a planet at 1AU around the nearest star), and because the planetary flux represents only a tiny fraction of the stellar flux (over 20 magnitude differences in the visible). The contrast can be enhanced with a coronograph and also by observing at longer wavelengths, for example in the IR (which corresponds to the peak of the planet's flux). This technique is, therefore, more suitable for large planets with strong internal energy (for example, young planets; but young stars have stronger fluxes as well) and around relatively faint stars. Close-in planets have a higher temperature and flux, but angular resolution requires long-baseline interferometry techniques. In spite of these technical difficulties, this method is actively pursued because it may potentially yield the most comprehensive set of information on planetary atmospheres. A handful of planets have been detected via IR imaging.

Gravitational microlensing

When a star (the lens) passes in the line of sight between the observer and a star (or stars) further away in the background, the light from the background star(s) is bent around the lens (a relativistic effect). The background star appears as a ring (or as multiple sources if the axisymmetry is broken), and these sources appear brighter as the light is focused on the observer by the lens. This amplification varies with time, and the lensing configuration

typically happens only once. If a planet orbits the lens, it also contributes to and slightly modifies the lensing event (thus called microlensing), and this perturbation to the primary lensing event is the signature of the extrasolar planet (Giannini & Lunine 2013 [45]). The magnification of the planet's flux is such that a study considered the possibility of detecting chemical compounds (such as water or methane) in the atmosphere (Spiegel et al. 2005 [111]).

Statistical calculations estimate that a few gravitational (two) microlensing events should occur per year per ten million stars (potential lenses) observed along the galactic bulge (Mao & Paczynski 1991 [80]). Since such events may happen only once and are limited in duration, this method requires in practice networks of teams around the globe that monitor for gravitational lensing events. They alert in real-time specialized centers which then carefully gather and analyze photometric data for the presence of an extrasolar planet around the lens.

In spite of this apparent low theoretical yield, the microlensing method is complementary to the other ones (about 20 detections so far). Its sensitivity is higher for planets beyond the snow line (a few AUs for mature Solar-type stars), and it does not require observations spanning a few planetary periods. It is, therefore, particularly suitable for detecting planets with very long orbital periods. In addition, microlensing is much less sensitive than the other methods to variability in the host star (the lens) and can thus be used to detect planets around a wide range of stars. In some cases, the planet itself could be the primary lens, and this method can potentially detect wandering planets (planets not orbiting a host star). Finally, the probability of detection and the duration of the perturbation in a microlensing event are proportional to $\sqrt{M_p}$, but the amplitude of the perturbation is independent of the mass of the (micro)lens. Microlensing is thus suitable to detect small planets (Queloz 2006 [93]), and potentially even moons around extrasolar planets as an additional departure to the symmetry expected in microlensed light.

Other methods

The five methods described above are the ones commonly used. Many more are being investigated, and we mention below a few others: pulsar timing variation, magnetic interaction with the host star, and the detection of planets in disks.

Pulsar timing variation. The first confirmed detection of an extrasolar planet *around a Solar-type star* was achieved in 1995. Nevertheless, the very first confirmed detection of extrasolar planets occurred in 1992 through pulsar timing variation (Wolszczan & Frail 1992 [117]). Instead of directly measuring the motion of the star (astrometry) or the doppler shift in the star's light (radial velocity), pulsar timing variation searches for anomalies in the periodicity of a pulsar's radio pulses. Because of the precise rotation period of millisecond pulsars, Earth-size planets with large orbits can be detected.

Magnetic interaction with the host star: Radio-waves and spots on the star. Radio emissions from Jupiter have been detected in 1955 (Burke & Franklin 1955 [16]) and correlated to the presence and position of Io (Bigg 1964 [11]), which is an obstacle in the

presence of the magnetized flow in Jupiter's magnetosphere. An extrasolar planet similarly constitutes an obstacle to a magnetized plasma. Zarka 2007 [121] suggests an empirical scaling relationship between the energy flux incident on a planet and the energy emitted by the planet in radio waves. These radio-waves could thus be another signature of extrasolar planets, and this method may also provide invaluable information about the magnetic environment of the extrasolar planets. The presence of a close-in planet in the magnetosphere of its host star may also lead to a spot on the star circulating on the star with a period close to that of the planet, which may be another observable evidence of the presence of the planet (Laine & Lin 2012 [72]).

Detection of planets in disks. New generation telescopes such as Alma may provide the angular resolution necessary to indirectly detect planets through their influence on the disks. Indeed, the presence of a planet can perturb the disk. For example, a massive planet may scatter debris or open a gap in the disk in a detectable pattern (Casassus et al. [21]).

3.1.3 Some important or unexpected features of extrasolar planets

The search for extrasolar planets have so far focused on nearby Solar-type stars, preferentially with stable fluxes and near the plane of the Milky Way. All the data about extrasolar planets in this section (also see figure 3.1), unless otherwise stated, are from http://exoplanets.org which, as of June 2013, references 733 confirmed planets and over 3000 Kepler candidates (which await confirmation).

Planets seem to be very diverse

Planetary mass. The sample of confirmed extrasolar planets presents a fairly smooth continuum of masses, from a few Earth-masses ($0.01 M_J$, neighboring the lower detection limit) to masses of Brown Dwarfs, with a small and relatively less populated parameter space around $0.1 M_J$ (M_J stands for "Jupiter-mass").[3]

Eccentricity. Planets may have any eccentricity, but there is a clear trend toward small eccentricities for close-in planets (with orbital periods smaller than 7 days). This trend can be accounted by the gravitational tides raised by a star on its close-in planet(s), which can circularize the orbit of a gas giant planet in a few million years (Rasio et al. 1996 [94]). Secular resonances between planets and tidal interactions with the disk or star can result in changes in the planet's semi-major axis (*i.e.* gravitational potential energy), eccentricity (*i.e.* angular momentum and gravitational potential energy), internal energy, and orbital inclination (Papaloizou & Terquem 2010 [86], Wu & Lithwick 2011 [119]).

Semi-major axis. Extrasolar planets also exhibit a wide range of semi-major axes,

[3] This relatively smooth gradient of planetary masses indicates that there is no strong constraint on the mass of a planet. The end product may therefore simply be the result of the history of the system and the surface density of material available in the disk. Since gas giants, in the standard model, are built from large solid cores, one also must investigate the mechanisms involved in the transition from large super-Earth cores to gas giants planets (through accretion) and *vice-versa* (through evaporation).

from 0.0058 (Kepler-42 c) to 14.5 AU (HR 8799e, which is an outlier since the second furthest planet detected is HD150706b at 6.7 AU).

Planets can be on very small orbits

Although planets have been detected at a wide range of semi-major axes, we focus on the so-called close-in planets (a $<$ 0.1 AU) of which the first extrasolar planet discovered, Pegasus-51b, is a prototype (with a mass comparable to that of Jupiter ($Msini = 0.46M_J$) and a semi-major axis $a = 0.052\ AU$). All 16 planets discovered between 1995 and 1999 (as referenced on http://exoplanets.org) were gas giants planets, and 5 of these have a semi-major axis $a < 0.1\ AU$. Observations over time confirmed the existence of such a class of "close-in" gas giants, which were then called "hot-Jupiters."[4]

The discovery of close-in planets have rekindled the theoretical prediction that planets can gradually migrate while staying on quasi-Keplerian orbits by exchanging angular momentum with the gas in the protoplanetary disk (Goldreich & Tremaine 1979 [52], Terquem & Papaloizou 2007 [113]).[5]

The present work focuses on these close-in planets, which interact with their host stars in unique ways. In particular, tidal and magnetic interactions between the planet and the star result in angular momentum exchanges (which influence the end stages of planetary migration) and ohmic dissipation (which may explain the large planetary radii of some close-in planets). Chapter 4 describes in more details the questions that will be addressed in this work.

3.2 Theory of planetary system formation and evolution

There are now numerous reference textbooks available on planetary system formation and evolution, such as Murray & Dermott 2000 [82], Armitage 2010 [4] with its associated online lecture notes (Armitage 2010 [5]), and the more general book edited by S. Seager (Seager 2010 [101]). R. Alexander also provides concise online lecture notes (Alexander 2011 [1]).

We briefly outline in this section the main stages and components of the standard model of planetary system formation.

[4]The discovery of hot-Jupiters was both expected and surprising. Indeed, the radial velocity method is much biased toward detecting massive close-in planets. Nevertheless, this discovery was also surprising because gas giants, according to the standard model, form through fast accretion of gas onto a massive solid core, which is expected to form far enough from the star where large amount of material can be found in the solid phase. Planets with masses comparable to large rocky planets and ice giants have also been detected on surprisingly close-in orbits.

[5]Planets may, therefore, be highly mobile and enter or move out of secular resonance with each other. Within the standard model, a vision of planets forming in neatly defined, stable, and non-interacting isolated orbits no longer holds. Furthermore, the concept of migration introduces an additional time-scale in the standard model of planetary system formation.

3.2.1 Planet formation

From gas and dust to planetesimals

The material used to form planets is contained in the protoplanetary disk, which is a disk of gas and dust orbiting a central star and extending up to a few hundred AUs.[6] Dust particles are solid particles amounting to a few percent of the disk mass. A disk of mass a few percent that of the star corresponds to the minimum mass required to build the planets in our Solar System, but more massive disks can exist as well.

Near the star, most of the material is in gas form and somewhat ionized by stellar radiation and wind. In fact, very near the star, the stellar magnetic field energy dominates; ionized gas is accreted along the magnetic field lines, which results in a truncated disk around the edge of the stellar magnetosphere. The temperature in the disk decreases with increasing distance from the star, and the "snow line" corresponds to the distance at which solid water can form out of the gas phase.[7]

If particles orbit smoothly around the star on Keplerian orbits and laminar flows, then there is little chance for collisions and growth. Local turbulence, vortexes, and regions of local pressure maxima in the disk are therefore necessary to increase the collision rate or create local high density of solid building material. The study of the causes of such local turbulence, vortexes, and high density locations is an important current research topic.

As dust particles collide with each other, they bind through Van der Walls forces, and agglomerate into larger and larger particles.[8] At small sizes, hydrodynamical effects dominate, and the collision cross section is the area of the particles. At larger sizes, gravitational effects dominate; they increase the collisional cross-section through gravitational focusing and also trigger dynamical effects such as secular resonances and tidal interactions. Particles of all sizes presumably primarily form where the temperature is low enough, but they can also spiral inward through gravitational interactions, which results in a redistribution in space of the solid material.

From planetesimals to planets

Solid agglomerates are typically called planetesimals when they become large enough (above the km size) that their interactions become dominated by gravitational effects (before that, they may be called dust or grains). As numerous planetesimals collide and grow above a few thousand kilometers in size, they may be called planetary cores (if they are on the way to becoming a gas giant), super-Earths, mini-Neptunes, etc., depending on

[6] The star and proto-planetary disk form from the collapse of a molecular cloud. The star can also be part of a multiple system.

[7] Each chemical compound has its own line (the radius at which is solidifies), but water is one of the dominant compounds (apart from hydrogen and helium) because the disk has much hydrogen and oxygen. The condensation line of silicate would be another important radius.

[8] Collisions have in fact two competing effects. At small relative velocities and small sizes, particles stick together, but at high relative velocities and large sizes, the collisions may break down particles. It is therefore a dynamic equilibrium process. Calculations of the speed distribution of particles in a disk indicate that particles with a size around the meter tend to break each other up. How to overcome this "meter barrier" (and several other barriers) is a current area of active research.

the characteristic that is being stressed (*e.g.* their mass, composition, etc.) and using our own Solar System as a reference. These large bodies may exchange angular momentum with the disk and spiral inward or outward, interact with each other through secular resonances, collide, or accrete a gaseous envelope of diverse composition and mass.

Planetary cores, when massive enough, may accrete and retain a gaseous envelope. If the gas surface density in the disk is high enough, this envelope may reach masses comparable to that of the core. As more mass is continually accreted, the accretion rate enters in a phase of drastic increase (it "runs away" instead of being in a quasi-hydrostatic balance) and leads to the formation of giant gas envelopes as described by the run-away core-accretion model (Bodenheimer & Pollack 1986 [13]). Gravitational instability where particularly massive disks (it is unclear how common massive disks are) can become unstable and collapse into gas giants (bypassing the need to first form a planetary core) is a competing scenario (Cameron 1978 [19], Boss 1997 [14]).

3.2.2 Gravitational and hydrodynamical effects

Gas and dust: Hydrodynamics

In the absence of gas, dust particles would orbit the star in Keplerian orbits (neglecting gravitational interactions between dust particles). On the other hand, the gas pressure exerts a small (usually outward) force on the gas and decreases the stellar effective gravity. Since the orbital velocity is such that the corresponding inertial acceleration compensates the gravity, a lower effective gravity results in a lower orbital velocity, and the gas therefore orbits at a slightly sub-Keplerian speed (by about half a percent). The dust thus encounters a headwind of gas, feels a corresponding drag, loses angular momentum, and drifts radially toward the star with a time scale of about 10^5 years.[9] Describing how planets can form before the particles have significantly drifted inwardly is a key problem of planet formation. Elements of answer include local pressure maxima that can trap particles or instabilities and vortexes that oppose migration.

Planetesimals and disk: Planet migration

As solid particles increase in size above a few km, their dynamics is no longer affected by the hydrodynamics of the gas. The gas in the disk still interacts with the planetesimal through gravitational forces, but an axisymmetric disk exerts no overall torque on a planet when the interactions are averaged over a period. However, the presence of a planet, if massive enough, can introduce an asymmetry in the disk (through non-axisymmetric density waves), which results in angular momentum exchange between the disk and the planet.

When the interaction is calculated precisely and averaged over an orbit, the torque between an annulus of gas and the planet is zero except at precise resonant locations

[9] The drag is often modelled as an Epstein drag (force proportional to the relative velocity) or Stokes drag (force proportional to the square of the relative velocity) depending on whether the particles are respectively smaller or larger than the gas mean free path. Regardless of the regime, the particles migrate toward the star on a tiny timescale.

where the gas' angular velocity $\Omega(r)$ is a multiple of the relative angular velocity between the planet and the gas $m\left(\Omega(r) - \Omega_p\right) = \pm\Omega(r)$ (Goldreich & Tremaine 1979 [52]). In the frame of the planet, these locations along the planet/star axis follow $r = \left(1 \pm \frac{1}{m}\right)^{2/3} a$ (where $m = \infty$ corresponds to the "co-rotation radius," and the other locations correspond to "Lindblad resonance" locations).

These interactions result in a transfer of angular momentum from smaller to larger semi-major axes. In other words, a planet gives angular momentum to the gas beyond the planetary semi-major axis, pushing the gas outward. The planet also receives angular momentum from the gas at smaller semi-major axes, and the gas thus moves inward. Overall, the net exchange of angular momentum for the planet is typically negative. A planet with masses lower than a few Earth-masses spirals inward (type I migration) toward the star with a time scale as short as a few $10^4 - 10^5$ years and inversely proportional to the planet's mass. Massive planets (*e.g.* gas giants), however, interact so strongly with the disk that the outward (inward) motion of the gas outside (inside) of the planet's radius results in a "gap" (a ring of low density in the disk around the semi-major axis of the planet). In such a case, the gas giant's inward migration is locked to that of the disk accretion (type II migration), which occurs on a time-scale less than 10^6 years and independently of the planet's mass. Within the runaway accretion scenario, to become gas giants, planetary cores must accrete their envelopes within this time scale, or other mechanisms must exist to slow the inward migration of planetary cores (*e.g.* Baruteau 2008 [7]).

3.2.3 Subsequent evolution of planets

Collisions in the early stages of planet formation result in high planetary internal energies, and the interior of planetary cores may melt and differentiate. Planets which form a little later (after most planetesimals have already collided with each other) may escape this intense phase of giant impacts, and another differentiation mechanism may be necessary.

The mechanisms leading to the presence or absence of a planetary dynamo have not yet been clearly established either, although convection, heat flux, enough electric conductivity, and differential motion (through spin) are expected to be important (see Christensen & Aubert 2006 [23] and Jones 2011 [67] for scaling laws in our Solar System). There are to date no measurement of extrasolar planetary magnetic field, although theoretical studies are being carried out (*e.g.* Gaidos et al. 2010 [43], Zuluaga et al. 2013 [123]), and a recent work attempts to infer the size of a planetary magnetosphere through lags of the onset of transit at UV and optical wavelengths (Vidotto et al. 2010 [114]).

Regardless of the specifics of these mechanisms, young planets have high intrinsic fluxes which radiate away their internal energy. The radius of a gas giant planet decreases (tje planet contracts) as the planets ages, cools down, and sees its internal energy decrease. The study of the mechanisms that slow down such contraction is an active area of research. Candidates include sources of internal energy such as gravitational tides, stellar irradiation, giant impacts and, of interest here, ohmic dissipation. Since we are focusing on close-in planets, the surface temperature and strong irradiation may also play key roles as boundary conditions and because they move the convective zone deeper inside the planet (Fortney et al. 2011 [41]).

The protoplanetary disk

This section is kept to a minimum here as disks have already been mentioned before. In addition, protoplanetary disks are not directly involved in our model since the interaction of a close-in extrasolar planet with the magnetosphere of its host star occurs within or near the magnetospheric cavity. In addition, the gas in the disks, although essential to the formation and early evolution of planetary systems, is thought to disappear within a few 10^6 to 10^7 years (the material left over after the gas has disappeared is called a debris disk). Since gas giants accrete their massive envelopes before the gas in the disk goes away, this time scale is, therefore, a strong constraint for models of planet formation.[10]

A related and relevant aspect worth mentioning here is the impact of the effective viscosity in the disk near the cavity, which controls the inward transport of mass in the disk. The interplay between the disk mass accretion and the magnetic torque between the disk and the star determines the extent of the magnetosphere and its position with regard to the co-rotation radius (Bouvier et al. 2007 [15], Lin & Ju in preparation [78]).

3.2.4 The star

The purpose of this section is to outline the evolution of the star, in particular its radius, surface magnetic field, spin rate, temperature, mass loss rate through winds, and mass accretion. These parameters all affect the electromagnetic interaction with a close-in planet: the radius and surface magnetic field strength determine the field strength at the location of the planet, the stellar spin rate affects the relative velocity (between the planet and the stellar magnetosphere) and thus the motional electric field, the stellar surface temperature determines the electric conductivity of the stellar plasma at the foot of the flux tube intersecting the planet (which we call "the footprint" for conciseness), and finally the winds (and, to a smaller extent, accretion rates) set the density and thus the Alfvén velocity between the planet and the star. We will describe the parameters corresponding to Solar-type stars at three stages: TTauri stars (a few 10^6 years), young main sequence stars (up to a few 10^8 years), and main sequence stars. For each stage, we provide fiducial values for the parameters, while keeping in mind that there can be much variability.

TTauri star

Main characteristics. After the proto-stellar stage, low-mass stars enter the pre-main sequence as TTauri stars. They have large radii (2-4 Solar radii) leading to a large total luminosity, spin periods which are moderate (6-10 days) at first but decrease as contraction occurs (1-6 days), a relatively low temperature ($T \approx 4000K$), strong winds, and a strong magnetic field.

[10] Observations of young stars indicate that most stars older than 10 million years are no longer surrounded by a gas and dust disk. These observations suggest a lifetime for protoplanetary disk of a few million years. The gas and dust disappear as it is accreted onto gas giants, onto the star, or as it escapes from the disk (pushed by the strong stellar wind or by gravitational escape). Nevertheless, larger (solid) particles may still be present in the disk as they do not scatter the stellar light and are therefore much more difficult to detect.

Winds and accretion rates. For our purpose, Classical TTauri stars (CTTS) and Weaklined TTauri stars (WTTS) are fairly similar, except for the absence of disk and accretion in WTTS. CTTS typically still have a proto-planetary disk, strong winds (a few hundreds of kms^{-1} and mass loss rates of $10^{-9} - 10^{-8} M_{\odot}/year$), strong accretion $(10^{-10} - 10^{-8} M_{\odot}/year)$[11], with associated strong emission lines, active jets, and accretion hot-spots. Weaklined TTauri stars (WTTS) no longer have a disk (or the disk has become optically thin), and they show little accretion and weaker winds. There is little information about TTauri stars winds at small semi-major axes, but they may be as low as low as 50-200km/s with mass loses between $10^{-10} - 10^{-7} M_{\odot}/year$ (Vidotto et al. 2010 [114]). We use a larger value for the winds, keeping in mind that the effects of the wind and mass loss rate both contribute in establishing the mass density profile between the planet and the star (in other words, to reduce the uncertainty on the mass density profile of the flux tube, both the uncertainties on the wind speeds and mass loss rates should be reduced).

Magnetic field. Several recent studies measuring Zeeman splitting infer the surface magnetic field strength of TTauri stars to be around a few kilo Gauss. The field is found to have dipolar, octopolar, and higher order components, which relative strengths vary from star to star (Johns-Krull 2007 [66], Yang & Johns-Krull 2011 [120]; for review papers, see Hussain 2012 [63] or Gregory et al. 2010 [53]; Bouvier & al. 2007 [15] also have empirical formulas for the surface field strength). Nevertheless, although the field just above the stellar surface is complex, the large scale geometry of the magnetosphere is well ordered and that of a modified dipole (Gregory al. 2008 [54]).[12]

Evolution toward main sequence

CTTS accrete much matter from the disk, which ought to increase their angular momentum. In addition, as a star ages, it also contracts and significantly spins up to reach periods as small as a day. However, when the disk is still present (a few to tens of million years), magnetic bracking and locking act to limit the spin up. Later, outflow through winds carries angular momentum away through its interaction with the stellar magnetic field, which gradually spins the star down (the Sun has an equatorial spin period of about 24 days). The stellar magnetic field also decreases with time, but it is difficult to be more quantitative. For order of magnitude estimates, it is possible to use a spin angular velocity dependence with time $\omega_* \sim t^{-1/2}$ (with stellar spin periods $P_* \approx 25$ days to a month for $t = 5 \times 10^9$years (Ivanov & Papaloizou 2011 [65])). For the stellar surface magnetic field, Bouvier uses $\mathcal{B}_* \infty P_*^{\alpha}$ for CTTS with α close to 1.2, but the dependence on the stellar

[11] This corresponds to $6 \times 10^{12} - 10^{14}$kg s^{-1}. For example, the accretion rate for AA Tau is estimated (from line emission) to be around $10^{-9.6}$ to $10^{-8.5}$ $M_{\odot}$yr^{-1} with an average around $10^{-9.2}$ (Donati et al. 2010, [33]), and that of V2219 Oph between 3.2×10^{-8} and 4×10^{-9} $M_{\odot}$yr^{-1} (Donati et al.2007 [32], Gregory et al. 2008 [54]).

[12] For example, Gregory et al. 2008 [54] models BP Tau and V2129 Oph (both have a stronger octopole than dipole field at the surface), and finds the large scale structure of the field to be "simpler and well ordered," with about 20-40 % larger surface flux through open field lines than obtained with an ideal dipolar geometry. These studies primarily attempt to understand stellar accretion and interactions with the disk, and model the geometry near the surface of the star in order to explain low latitude accretion hot spots. Indeed, in systems where the inner boundary of the disk is close to the star, the accretion of the gas at the inner boundary and along magnetic field lines may occur in the region with complex geometry and map onto the star at low latitude regions (Gregory & al 2008).

radius is comparatively much stronger $\mathcal{B}_* \propto R_*^{-3}$ (Bouvier et al. 2007 [15] and references therein). discussing planetary dynamos, Jones 2011 [67] derives three different scaling laws with $\mathcal{B} \propto \omega^{\alpha}$ where $\alpha = 1/10, 1/2$ and 1 respectively.

In parallel to the stellar evolution, planetary cores form within a few million years, migrate, and may accrete massive gas envelopes. In other words, young planets which have migrated to the inner parts of the planetary system through type I or type II migration first encounter the magnetic fields of TTauri stars. Planets which later migrate through interaction with other planets would encounter the fields of young (or more mature) main sequence stars.

Summary

We provide here some stellar fiducial parameters which may be used in numerical estimates and in the writing of scaling laws. Calculations for a real system would of course require the precise numerical values for the parameters. The list below is also summarized in table (3.1).

For TTauri stars (up to about 10^7 years). We use $M_\star = M_\odot$, $R_* = 3R_\odot$ (2-4 $R_\odot$), $T_* = 4000$K (surface), spin periods (spin angular velocity ω_*) with a wide possible range from 1 day (after the spin up phase) to 10 days (before the spin up phase), $\mathcal{B}_* = 2000$G as the dipolar surface field (1-3kG), outflow due to winds at velocity $v_{wind} = 400$km/s with (isotropic) mass loss rate $\dot{M} = 10^{-8} M_\odot/yr$. These parameters may all have a wide range, and the wind speed may be smaller in the magnetosphere.

For young stars (up to a few 10^8 years). We use values estimated for a star such as CoRoT-2, $M_\star = M_\odot$, $R_* = 0.9R_\odot$, $T_* = 5600$K (surface), Spin period of 3.5 days days (which is lower than expected from the star's age, but the star can also have been spun up by a planet migrating inward; we used the stellar spin rate of CoRoT-2), $\mathcal{B}_* = 300G$ as the dipolar surface field (very poorly known), outflow due to winds at velocity $v_{wind} = 200$km/s with (isotropic) mass loss rate $\dot{M} = 10^{-11} M_\odot/$yr.

For mature stars (above 10^9 years). We use $M_\star = M_\odot$, $R_* = 0.9R_\odot$,[13] $T_* = 5600$K (surface), Spin period of 24 days, $\mathcal{B}_* = 30$G as the dipolar surface field, outflow due to winds at velocity $v_{wind} = 100$km/s with mass loss rate $\dot{M} = 3 \times 10^{-14} M_\odot/$yr.

3.2.5 Stellar magnetosphere

Three radii are defined in this section: the boundary of the magnetosphere, the co-rotation radius, and the radius of the magnetospheric cavity (the first two being the most important ones).

Magnetospheric radius. The stellar magnetosphere is the volume around the star where the magnetic energy is dominant, primarily over the gas pressure and wind volumic kinetic energy.[14] Assuming a constant wind speed and mass loss rate, the wind ram

[13] We chose $R_* = 0.9R_\odot$ for a young star because we had in mind CoRoT2 as a model; we then also keep $R_* = 0.9R_\odot$ for mature stars.

[14] Gold coined the term "magnetosphere" to describe the region in the Earth's outer atmosphere where

	TTauri stars	Young Stars	Mature stars
Mass	$M_\odot$	$M_\odot$	$M_\odot$
Radius	$2-4R_\odot$	$0.9R_\odot$	$0.9R_\odot$
Temperature	4000 K	5600 K	5600 K
Spin period	1-10 days	3.5 days	24 days
Surface field	2000 G (1-3 kG)	a few hundred G	30G
Wind	400 km/s	200 km/s	100 km/s
Mass loss	$10^{-8}M_\odot$/yr	$10^{-11}M_\odot$/yr	$3\times10^{-14}M_\odot$/yr

Table 3.1: Table giving the fiducial values for key parameters of stars at three stages of evolution (TTauri, young main sequence, and mature stars). The values for the young star is modelled after CoRoT-2, but the magnetic field strength is very approximative. We kept the stellar radius and temperature for a mature star similar to that of a young star
.

pressure $\varrho v^2/2$ is proportional to $\varrho = \dot{M}/(4\pi v a^2)$, and it thus decreases proportionally to a^{-2} (where a is the distance to the star). Since the magnetic energy decreases as a^{-6} (for a dipolar geometry, the field decreases as a^{-3}, and the magnetic pressure is proportional to $\mathcal{B}^2$), it dominates near the star (except for an exceedingly weak surface field), and the location of the magnetospheric boundary is determined by the balance of magnetic pressure, gas pressure, and stellar wind ram pressure.[15]

A young planet which migrates toward its star (through its gravitational interactions with the disk) first encounters a magnetized wind and then, as it enters the magnetosphere, a strong magnetic field. Discussing the extent of the magnetosphere is, therefore, relevant for the present study for several reasons. It first determines the location where the interaction becomes important, and it shows that the number of planets which may potentially interact magnetically with their host stars is non-negligible. It also allows an estimation of the magnetic field strength felt by the planet and of the orbital angular velocity of the planet when it starts to interact with the stellar magnetosphere, which are all important values in the study of the end stages of planetary migration.

The previous paragraphs dealt with a static scenario. However, proto-planetary disks and stellar spin rates, outflows, and magnetic dynamos are dynamic, and disks also experience viscosity and accretion toward the star. The precise location of the stellar magnetosphere (or of any magnetized astrophysical body) thus depends on numerous factors such as the stellar magnetic dipole's strength, the surrounding plasma pressure, the outgoing magnetized wind ram pressure, and the incident disk accretion pressure (when a proto-planetary disk is still present).

When disk accretion is present, the radius of the boundary may be a little smaller than the co-rotation radius as defined above (Papaloizou 2007 [85], Ghosh & Lamb 1978 [44]). Assuming a dipolar geometry, Bouvier & al. 2007 [15] determines the boundary R_T

the dynamics of the ionized gas is dominated by the Earth's magnetic field (Gold 1959 [50]).

[15] For large magnetosphere (*e.g.* Jupiter's), the inertial forces becomes large and affect the co-rotation of the plasma (Hill 1979 [60], Hill 1980 [61]).

(notation from Bouvier's paper) of the magnetosphere of a TTauri star (with accretion) to be about $7R_*$ (*i.e.* $\approx 14R_\odot$)

$$\frac{R_T}{R_*} = \frac{\mathcal{B}_*^{4/7} R_*^{5/7}}{\dot{M}^{\,2/7} (2GM_*)^{1/7}} \tag{3.1}$$

$$= 7.1 \left(\frac{\mathcal{B}_*}{1kG}\right)^{4/7} \left(\frac{\dot{M}}{10^{-8} M_\odot \mathrm{yr}^{-1}}\right)^{-2/7} \left(\frac{M_*}{0.5 M_\odot}\right)^{-1/7} \left(\frac{R_*}{2R_\odot}\right)^{5/7}. \tag{3.2}$$

This formula does not explicitly include the stellar spin rate, but it nevertheless yields a boundary for the magnetosphere near the expected location of the co-rotation radius (see below). However, dynamic changes in disk accretion rates and stellar field strengths also result in a dynamic magnetospheric boundary (Lin & Ju, in preparation [78]).

Co-rotation radius. When a proto-planetary disk is present, the ionized gas in the disk interacts with the magnetic field in a way that is qualitatively similar to the planet-stellar magnetosphere interaction that is developed later in this work. The effect of this interaction depends on the location of the gas with regard to the co-rotation radius, a_{co}, which is given by

$$a_{co} = \left(\frac{GM_*}{\omega_*^2}\right)^{1/3}, \tag{3.3}$$

where G is the gravitational constant, M_* is the stellar mass, and ω_* is the stellar spin angular velocity. In other words, a particle (gas or planet) on a Keplerian orbit with a semi-major axis equal to the co-rotation radius has an orbital period equal to that of the stellar spin period. When a particle has a semi-major axis larger (smaller) than the co-rotation radius, it is said to orbit outside (inside) co-rotation. This important vocabulary will be used again when discussing the effect of an induced Lorentz torque on the angular momentum of extra-solar planets. The co-rotation radius corresponds to $a_{co} \approx 14R_\odot = 0.064AU$ (for $M_* = M_\odot$ and a stellar spin period of 6 days) and to $a_{co} \approx 0.08AU$ for a stellar spin period of 8 days.

Qualitatively, because of the magnetic interaction, the gas orbiting outside co-rotation gains angular momentum and moves outward while the gas which orbits inside co-rotation loses angular momentum and migrates towards the star. Applied to a planet, the semi-major axis as compared with the co-rotation radius determines whether the Lorentz torque pushes the planet away or pulls it toward the star (which is discussed in more details in section 6.5.1).

This qualitative result (a planet outside co-rotation is pushed further away from the star; a planet inside co-rotation is pulled further inward toward the star) may at first seem counter-intuitive if only velocities are considered. Indeed, the Lenz law would seem to indicate that a planet would like to orbit at co-rotation and thus to move inward (outward) toward the radius of co-rotation if the planet is outside (inside) co-rotation. It is however not the case because the planet is within a gravitational potential. In addition, the important physical quantity is the angular momentum. When the planet is outside (inside) co-rotation, the Lorentz torque is positive (negative), which increases (decreases) the planet's angular momentum which, within the gravitational potential, pushes (pulls)

the planet outward (inward). The same argument is applied below to gas instead of a planet.

Radius of the magnetospheric cavity. The interaction between the disk and the magnetosphere opens a "magnetic cavity" in the disk. Because the gas within co-rotation loses angular momentum and is accreted onto the star along field lines, and the gas outside co-rotation gains angular momentum and is pushed away, the disk thus becomes truncated (Bouvier et al. 2007 [15], Lin et al. 1996 [77]). Weak magnetic fields of course result in a small magnetospheric cavity which does not extend to the co-rotation radius. However, if the magnetic field is strong enough (so that the magnetic energy is still the dominant energy even outside the co-rotation radius), then the magnetospheric cavity may also be expected to extend in the neighborhood or further than the co-rotation radius.

This radius (also called "truncation radius") is not as important as the other two in this thesis (older stars have no disk, and close-in planets are likely to be within the truncation radius). Nevertheless, if the planet is still embedded in the disk, then the geometry of the magnetic interaction can be rather more complicated. Overall, unless the magnetic field is weak (which also results in a weak magnetic interaction), the magnetosphere can be expected to clear a magnetospheric cavity, and the geometry adopted in this work is that of a planet inside the cavity (or in a disk that is very thin near the star).

As a summary, we have discussed in this sub-section the primary factors which influence the size and extent of the stellar magnetosphere. We emphasized its dynamic character and its relevance to the rest of the present work. As a first approximation, the co-rotation radius can be used as a rough estimate of the boundary of a young star's magnetosphere. When the star is more mature and without a disk, the boundary is determined by the energy balance between magnetic energy and stellar wind ram pressure.

3.3 Concluding remarks

We have briefly reviewed some of the characteristics of the known extrasolar planets and outlined the scenario of planetary system formation and evolution. Numerous questions pertaining to the formation and evolution of planetary systems are outstanding, and we have pointed out some of them in this chapter. In the next chapter, we describe the main questions addressed in this thesis and review the state of the theory relevant to the interaction between an astrophysical body and a magnetic field.

Chapter 4

Description of the main questions and bibliographical review

The previous chapters have set the physical and astrophysical context of the present work. In this chapter we describe the main questions addressed in this thesis and summarize key recent relevant papers.

Contents

Dans la première partie de ce chapître, nous présentons les thématiques majeures de la thèse: la charactérisation du couple de Lorentz et de la dissipation ohmique associés à l'interaction magnétique entre une planète proche de son étoile et le champ magnétique dipolaire stellaire. En particulier, 1) nous calculons l'effet du couple de Lorentz sur la migration planétaire, et 2) nous montrons que la dissipation ohmique dans la planète permet d'expliquer l'aspect "enflé" de certaines Jupiter chaudes. Finalement, 3) nous décrivons une approche théorique qui permet d'estimer l'intensité du champ magnétique stellaire et la conductivité électrique de la croûte des planètes telluriques en interaction

magnétique avec le champ magnétique dipolaire de leur étoile. Cette méthode permettrait donc également d'estimer indirectement la température et degré de différentiation de ces planètes. La deuxième partie de ce chapître est une revue bibliographique des thématiques décrites ci-dessus.

4.1 Description of the main questions

4.1.1 Overview

Within the sample of all known extrasolar planets, we focus specifically on those near or inside the stellar magnetosphere (*i.e.* roughly within 0.1 AU of the star). In the subsequent chapters, we will show that the magnetic interaction is associated with both an ohmic dissipation and a Lorentz torque on the planet, their intensities depending on the parameters of the system.

1) We seek to understand better the contribution of the magnetic interaction to the end stages of planetary migration; in order to do so, the most important parameter to calculate is the rate of angular momentum exchange between the planet and the star.

2) We also seek to explain why some close-in extrasolar planets seem to have a surprisingly large radius (compared to their masses). An energy source in a planet could explain such radius, and we therefore seek to calculate the ohmic dissipation associated with the magnetic interaction.

3) Furthermore, assuming that a close-in super-Earth interacts magnetically with its host star, we suggest a general method that uses observational constraints on the rate of semi-major axis variation or on the planet's surface temperature in order to obtain constraints on the stellar magnetic field strength and the electric conductivity of the planet's outer layers. Since observational data on planets and stellar magnetic fields are sparse, a method that can theoretically infer any additional information is valuable.

4) Finally, the magnetic interaction between the planet and the star may result in observable spots on the star which drift on the stellar surface with an angular velocity comparable to that of the planet, instead of that of the stellar spin. We only mention this topic here and describe it more in the last chapter which discusses potentially fruitful further investigations. We now describe each of first three topics in more detail.

4.1.2 Planetary migration: Angular momentum exchange

Overview

Young planets migrate toward their stars through type I or type II migration with respective time scales of $10^5 - 10^6$ years and a few 10^6 years (Armitage 2010 [4]). Variations in semi-major axes are induced by changes in angular momentum. At least five mechanisms may change the planet's orbital angular momentum: 1) gravitational tidal torques with the disk, 2) planetary mass loss through Roche lobe overflow (the mass lost is accreted onto the star and gives angular momentum to the planet), 3) gravitational tidal torques with the star, 4) Lorentz torque resulting from the magnetic interaction between the planet and the star, and 5) secular interactions between planets (we will not consider further this scenario in this thesis). We briefly consider the effects of these mechanisms and the changes in semi-major axis they may induce (the Lorentz torque and the mass loss are the two mechanisms studied in this thesis).

Tidal interactions with the disk. Overall, the tidal torques with the disk usually remove angular momentum from the planet and result in inward planetary migration.

These torques are short-lived and disappear within the first 10^7 years of the system (which corresponds to the life time of the gas disk). In addition, when the planet is well within the magnetospheric cavity, the overall interaction with the disk is zero (Armitage 2010 [4]). It is nevertheless a mechanism that is able to efficiently decrease large semi-major axes, and most close-in planets have probably migrated through tidal interactions with the disk.

Tidal torque between the planet and the star. Tidal interactions between the planet and the star occur throughout the life of the system. However, tidal torques decrease with semi-major axis as a^{-6} (Dermott 1970 [30]) and they are thus negligible except for close-in planets. Section 6.5.1 analyses these torques in more detail. The tidal (and Lorentz) torques both remove angular momentum from the planet if it is inside co-rotation and add angular momentum to the planet if it is outside co-rotation (Dermott1970 [30], Laine & Lin 2012 [72]).

Mass loss rate through Roche lobe overflow The Roche lobe is the equipotential surface on which the gravitational forces of the star and planet cancel each other. The distance from the center of the planet to the Lagrangian L1 (the point on the Roche lobe nearest to the planet; it is located between the planet and the star) is the Hill's radius and is given by

$$R_H = a \left(\frac{M_p}{3M_*} \right)^{1/3}. \tag{4.1}$$

If the ohmic dissipation in the planet is able to trigger a mass outflow, this mass will first overflow the Roche lobe through the L1 point. As it passes beyond the L1 point, it becomes gravitationally bound to the star; it can then be accreted onto the star, thus giving angular momentum to the planet. In the context of a magnetic interaction, younger systems (associated with stronger stellar magnetic field and a planet that may not yet have fully contracted) and close-in planets (with smaller Roche lobes) favor the mechanism of mass loss through Roche lobe overflow. In addition, this effect gives angular momentum to the planet when it is both inside and outside co-rotation. We investigate this scenario in section 5.4.

Lorentz torque Similarly to the tidal torque with the star, the Lorentz torque adds angular momentum to the planet if it is outside co-rotation and removes angular momentum from the planet if it is inside co-rotation (Laine & Lin 2012 [72], also see section 6.5.1). In addition, since it is associated to the magnetic interaction, it is stronger for young systems and close-in planets.

Discussion

One of the goals of this work is to better characterize the angular momentum exchange associated with the magnetic interaction of a planet and its host star.

The sample of hot-Jupiters is now complete, with a little less than one hot-Jupiter per hundred stars (Wu & Lithwick 2011 [119]).[1]. The sparsity of very close-in planets may point to the existence of mechanisms which may limit the migration of planets into the star or inversely destroy planets which migrate too close to the star. Destruction of a

[1] To say that the sample is complete means that astronomers have, with high degree of confidence, detected all hot-Jupiters orbiting near the stars which have been observed.

planet could occur through evaporation, disruption of the internal structure, or by pulling the planet into the star (which may be a way to increase the metallicity of the stellar envelope).

More generally, understanding the angular momentum exchange is necessary in order to model the end stages of planetary migration. The location of the boundary of the stellar magnetosphere, co-rotation radius, and disk truncation radius relative to each other is important. We show in figure 4.1 all six possible set of positions (numbered from scenario 1 to scenario 6) of these three radii relative to each others, and we indicate the qualitative effects and characteristic time scales of the four mechanisms listed above.

Depending on the direction and strengths of the torques, a planet may migrate all the way into the star or instead reach a stable orbit (which may not be permanently stable) either when the sum of the torques is equal to zero or when there is no torque. For example, in scenario 4 of Figure 4.1, when the planet is sufficiently inside the magnetospheric cavity, it no longer interacts with the disk (also see for example Lin et al. 1996 [77]). If the tidal torque at that location (between the magnetospheric cavity and the disk truncation radius) is negligible, then the planet is not experiencing any torques. When the disk is still present (in young systems), the precise position of the three radii relative to each other depends on the specifics of each system and is not well understood yet.

We denote the co-rotation radius, boundary of magnetosphere, and disk truncation radius respectively by a_{co}, r_M, and r_{disk}. We also denote the semi-major axis of the planet with "a". In scenario 1, the inward migration of a planet is likely to be halted in the range of semi-major axis $a_{co} < a < r_{disk}$. It may potentially also be halted for $a_{disk} < a < a_M$, but the magnetic interaction (leading to the Lorentz torque and mass loss) of a planet still embedded in the disk has not been explicitly studied. If the presence of the disk weakens the magnetic interaction, then the planet may not be halted in this region. In scenario 2, the migration may be halted for $a_{co} < a < a_M$ but the previous remark still applies. The potential locations where the migration may be halted (or the absence of such locations) can be seen for all six scenarios. In order to be quantitative, it is however necessary to estimate the order of magnitude of the Lorentz torque and angular momentum transfer associated with the mass loss, which is one of the goal of this thesis.

When the disk has evaporated, there are only 2 qualitatively distinct configurations, which can be represented for example by the scenarios 3 and 4 (and after removing the disk). After the disk has vanished and the star has spun up (to spin periods of a few days), the system is most likely in the scenario 3 (after about 10^7 years). As the star then spins down and the magnetic field decreases, the system can later be represented by the scenario 4.

4.1.3 Inflated hot-Jupiters

A fraction of the hot-Jupiters have transiting radii significantly (up to 20 %) larger than that predicted from numerical simulations (Figures (4.2) and (4.3) show planets for which measurements of the radius during transit are available). [2]

[2]These simulations include the basic physics (thermodynamics and radiative transfer of a spherical body in hydrostatic equilibrium, but the planetary radius may in fact depend on numerous parameters

Even after accounting for the stellar irradiation, the radii of over 40 planets are still unexplained. It has been suggested that an *ad hoc* dissipation inside the planet of an additional energy (in addition to the planet's naturally expected internal energy) of 1% of that of the stellar irradiation on the planet may explain most of the super-inflated planets (Guillot & Havel 2011 [58], also see figure (4.3)). Theories attempting to account for this inflation thus involve an input of heat in the convective zone (below a few tens of bars), for example ohmic heating through the interaction of planetary winds with planetary magnetic fields (Batygin & Stevenson 2010 [8], Batygin et al. 2011 [9])[3], ohmic heating through interaction with stellar magnetic fields (Laine et al. 2008 [73], Laine & Lin 2012 [72], Laine & al., in preparation [74]), tidal heating (Bodenheimer et al. 2001 [12], Gu et al. 2003 [56], Gu et al. 2004 [55]), mechanisms (for example planetary winds) that can transport a fraction of the stellar irradiation below the convection zone (Showman & Guillot 2002 [106], Guillot & Havel [58]), or some mechanisms that can trap energy in the planet, for example through a gray atmosphere, *i.e.* atmospheric opacities low in the visible wavelengths but high in the infrared (Guillot 2010 [57]). We examine the effect of ohmic dissipation due to currents induced inside a close-in planet as it interacts with the magnetosphere of its host star. In section 6.7, we find that the time-independent interaction can adequately account for the observed radius of CoRoT-2b, one of the most inflated planet (which radius is otherwise unexplained).

4.1.4 Gathering information about planets: Remote sounding

Although the amount of information available about extrasolar planets has increased tremendously in the past two decades, it remains limited (little more than semi-major axis, mass, orbital inclination, and sometimes surface temperature can be routinely known). We suggest that the observational information currently available about close-in super-Earths, complemented with either an orbital constraint (*e.g.* an estimate or observational constraint on the semi-major axis rate of change) or an energetic constraint (*e.g.* an estimate of the temperature of the planet's night side) may be sufficient to infer an estimate of the stellar magnetic field and the electric conductivity of the planet's outer layers.

Indeed, an orbital or energetic constraint would provide an estimate of the strength of the interaction (Lorentz torque or ohmic dissipation) and thus of the magnetic field strength and planet's conductivity. To our knowledge, such approach has never been carried out for extrasolar planets.

---

and effects, including the planetary mass, stellar irradiation, planetary temperature profile, presence of a core, internal energy, and entropy, as well as the convective and radiative mechanisms in the planet which determine the transport of energy. The black body equilibrium temperature for a gas giant at 0.05 AU with zero albedo around a Solar-type star is about 1500K, but very few actual measurements of the "surface" temperatures of transiting gas giants have been made since they require extensive measurements that must be fitted against numerical models which are themselves not yet well constrained. A few surface temperatures have been inferred, for example, for CoRoT-2b, which is also one of the more extremely inflated planet (Guillot & Havel 2011 [58]).

[3] In the model by Batygin & Stevenson, the winds at the surface of a close-in planet (for example driven by the strong temperature gradient between the day-side and the night-side of a planet which spin is synchronized with its orbit), if ionized, can interact with the planetary magnetic field.

4.2 Bibliographical review

We summarize the literature on the topics relevant to the present thesis. Relatively few works have been published on the magnetic interaction between a star and an extrasolar planet, but much work has been done on binary stars interacting magnetically (of which Campbell 1983 [20] is an example that is used in chapter 5) and on our Solar System, primarily the interaction of Io with Jupiter's magnetosphere and of the Moon interacting with the magnetized Solar wind.

4.2.1 Planet-induced stellar spots: A potentially observable evidence for star-planet interactions

Observational studies

As early as 2000, Cuntz et al. 2000 [27], taking inspiration from magnetic interactions between stars and from star-planet tidal interactions, raised the possibility that close-in exoplanets may interact magnetically with their stars in a way that would induce detectable stellar activity (in fact, tidal interactions can raise diverse types of excitations which are dissipated at the stellar surface and induce a local enhanced activity). He considers the interaction between the stellar surface magnetic field $\mathcal{B}_*$ and the planetary surface magnetic field $\mathcal{B}_p$ and suggests that the energy E released by the interaction scales as $E = \mathcal{B}_*\mathcal{B}_p/(d-d_m)^2 d_{mag}^2$ where d_{mag} is the size of the planet's magnetosphere as determined by $\mathcal{B}_p$ and the strength of the stellar wind, and $d - d_{mag}$ is the distance from the star to the planet's magnetosphere (this calculation assumes that the fields decrease as the square of the distance and that the interaction occurs at a distance d_{mag} from the planet).

Writing shortly afterwards, Shkolnik (Shkolnik et al. 2003 [105], Shkolnik 2004 [102] (PhD thesis)) reports the observation of chromospheric enhancements (CaII and K lines) on HD 179949 (with a companion at 0.045AU) which drift on the star with a 3-day orbit (stellar period is unknown but estimated to be smaller than 9 days). These spots have been found on observations separated by over a year, near the sub-planetary point, and with about a 2.5% enhancement for potassium; however, only 3 observations had been carried out. Further observations (Shkolnik et al. 2005 [104]) find similar enhanced activity again in HD 179949 (this time the K spots lead the sub-planetary point by 60 degrees), in υAnd (the CaII spot is offset from the sub-planetary point by 169 degrees), and possibly in τ Bootis (Walker et al. 2008 [115]).

Shkolnik et al. 2008 [103] reaches a slightly different conclusion as it reports an on/off nature of the enhanced activity: 4 out of 7 observations showing enhancements with a period of 3 days (presumably induced by the planet) whereas the other 3 observations show modulations with a 7-day period, presumably that of the star (also see Scandariato et al. 2013 [98] for X-ray and visible wavelengths). Finally, a few more recent studies have reported inconclusive results (so far), for example Fares et al. 2010 [39] or Poppenhaeger et al. [92], which searches X-ray and visible modulations in *υAnd* (cf. Shkolnik2005 [104] for the CaII modulations).

Overall, these observations are promising, but they are difficult and sparse, and a clear pattern has not yet emerged. We point out, in agreement with Shkolnik et al., that an

on/off nature of the spots is not contradictory with a magnetic interaction, although some periodicity may be expected. For example, in the context of a unipolar interaction, the magnetic interaction has feedback mechanisms which may result in the interaction being at times not valid (for example, see section 6.3.5). In addition, reconnection (which we have not yet included in the model) may also result in an intermittent interaction (magnetic interaction as considered in this thesis punctuated by episodes of reconnection).

Combining expertises (in measuring stellar magnetic field strength and geometry and in monitoring for stellar enhancements), Donati et al. (including Shkolnik) report several pioneering measurements of a stellar magnetic field (of τBoo). The period of the star is estimated around 3 days, which indicates that the stellar spin is synchronized with that of the planet. More relevantly, they detect minute CaII H & K enhancements but although yet able to discriminate between a planet induced enhancement or a variability intrinsic to the star. In addition, they point out that the estimate of the time scale needed to bring the entire star to spin in synchronicity with the planet's orbit is 3×10^{10} years, and they thus conclude that only the outer layers of the star have achieved synchronicity. We point out (see section 6.5.1) that the Lorentz torque in the unipolar inductor may be stronger than the tidal torques, and lead to quicker full synchronization of the stellar spin/planetary orbit (Donati et al. 2008 [103]). Although more work about this specific system would be needed, the synchronization time scale for the star could thus be shorter than expected.

Theoretical models

On the theoretical side, Li et al. suggest that the presence of a close-in super-Earth around a White Dwarf may induce enough heat near the star's magnetic pole to be detectable as Hα emissions (Li et al. 1998 [76]). They assume that the planet has a very high electric conductivity (similarly to the ideal unipolar inductor described in section 6.2). The heating occurs primarily in the atmosphere of the star in a sheet of thickness Δd (thickness of the current sheets) and depth H. The heating rate is proportional to $H/\Delta d$, but Li et al. point out that these two parameters are difficult to estimate. One of the contribution of our model is to introduce a way to calculate the depth of the footprint (the footprint is the volume in the stellar atmosphere where the current crosses the magnetic field lines on the star). The thickness of the current sheets do not intervene in our model, but Goldreich & Lynden-Bell 1969 [51] includes a quick analytical calculation of the expected thickness of such sheets in the flux tube.

Lanza 2009 [75] studies the star-planet interaction in the context of a force free model (an example of force free field is a field that verifies an equation such as $\nabla^2\mathcal{B} + \alpha^2\mathcal{B} = 0$). The energy is taken from the rearrangement of the field lines (from a configuration where different field lines have different parameter α (as defined above), which is associated with a higher energy, to a configuration where α is uniform (and thus associated with a lower energy)). The intermittent character of the observations corresponds to the lapses where the field regains its original, higher energy configuration. Lanza notes that the energy needed to account for the observation is about 10^{21}W, that this value is larger than what is available through reconnection, and that it nevertheless matches an order of magnitude estimate of the energy released through the mechanism under consideration. We point out that the ohmic dissipation associated with the unipolar inductor model could also energy

of this order of magnitude.

Ip et al. run numerical simulations for the reconnection of a magnetized planet with different geometries of the stellar coronal magnetic field (Ip et al. 2004 [64]). The calculation of the energy available is however carried out as an analytic order of magnitude estimate and is found to be a few times 10^{19}W (indeed lower than the 10^{21}W suggested as necessary in Lanza 2009 [75] quoted above).

4.2.2 Energy input in a hot-Jupiter

Two models (in addition to the one presented in this work) investigate the possibility of explaining the inflation of hot-Jupiter through a magnetic mechanism.

Buzasi proposes that the interaction between a magnetized hot-Jupiter and the stellar magnetic field may account for the inflated character of the planet. The energy input comes from the interaction between both magnetospheres, and the order of magnitude of the energy available is obtained from a scaling law used to describe the heating through magnetic storms in the Earth's magnetosphere. The order of magnitude of the energy is comparable to that from the unipolar inductor model, and it is large enough to explain the planetary inflation. The model nevertheless also requires a mechanism through which the energy dissipated in the planet's magnetosphere can be injected deep into the planet's convective region, and Buzasi proposes that field aligned currents and an induced potential difference can do so (Buzasi 2013 [17]).

Batygin & Stevenson (Batygin & Stevenson 2010 [8], Batygin et al. 2011 [9]) propose a model in which the ionized planetary winds interact with the planet's magnetic field (it is a variant of the unipolar inductor model). The winds may be fuelled, for example, by strong temperature gradients between the day and night side of a close-in planet which spin and orbit are synchronized. The winds are assumed parallel to the planet's latitudes (flowing in the $\mathbf{e}_\phi$ direction in spherical coordinates). The cross-product between the winds and the component of the planet's magnetic field in the $\mathbf{e}_\theta$ direction thus results in currents in the radial direction, which may then travel and be dissipated inside the planet.

Most mechanisms that account for an extra energy source must indeed also include a mechanism to transport the heat into the planet, but a few models naturally dissipate the heat inside the planet (*e.g.* radioactive heating, giant impact, and the unipolar inductor model in which the stellar magnetic field is present inside the planet (see chapter 6)).

4.2.3 Magnetic interaction and angular momentum exchange

The impact of a magnetic interaction on the angular momentum exchange between two bodies has been extensively studied for binary stars and stars with disks, but fewer work has been done so far for extrasolar planets. Fleck considers the angular momentum exchange induced by the distortion in the stellar field due to the presence of the planet (Fleck 2008 Fleck [40]). In this model, the torque is proportional to $\mathcal{B}_\phi \mathcal{B}_p$ where $\mathcal{B}_\phi$ and $\mathcal{B}_p$ are respectively the poloidal and toroidal components of the perturbed stellar magnetic field. The time scales found are short (which means that the power of the interaction can be significant).

We also point out the study by Papaloizou 2007 [85], which briefly estimates the effect of the time-periodic magnetic interaction (star-planet) when the planet is well within the magnetospheric cavity. The stellar field is taken to be non-axisymmetric, and the interaction under study is thus presumably the time-periodic interaction, as in the TE mode studied in chapter 5. Papaloizou concludes that the effect of this interaction is unlikely to be significant. Nevertheless, the estimate of the electric conductivity of a gas giant used in the paper (taken from Zhang et al. 1996 [122]) is that of the core of Jupiter and Saturn, which is likely a large overestimate of the effective electric conductivity involved in the interaction for most systems. In the model by Papaloizou, the strength of the interaction is proportional to the skin depth (it is found to be about $10^{-5}R_p$ (R_p being the planetary radius)), which would be larger for a more reasonable electric conductivity. In fact, in the model we consider for the time-periodic interaction (in chapter 5), we also find that in the regime where the skin depth is very small, the strength of the interaction indeed decreases roughly proportionally with the skin depth (instead of being insensitive to the electric conductivity).

4.3 Concluding remarks

The astrophysical questions of interest presented in this chapter and underlying the present work may be tackled with a variety of approaches and with a wide range of approximations (from a scaling law and order of magnitude estimate to a full problem (which we do not tackle).[4] Nevertheless, they are current problems which still need to be better characterized. Although many comments (which significance we did not appreciate until the completion of the work) have already been included in the previous chapters, the next two chapters present the bulk of the present work.

[4] About such solution for the full problem, Papaloizou comments, "Finding the response of a general steady state magnetospheric accretion flow to an orbiting protoplanet is a very difficult problem. Accordingly we consider possible simplifications" (Papaloizou 2007 [85]).

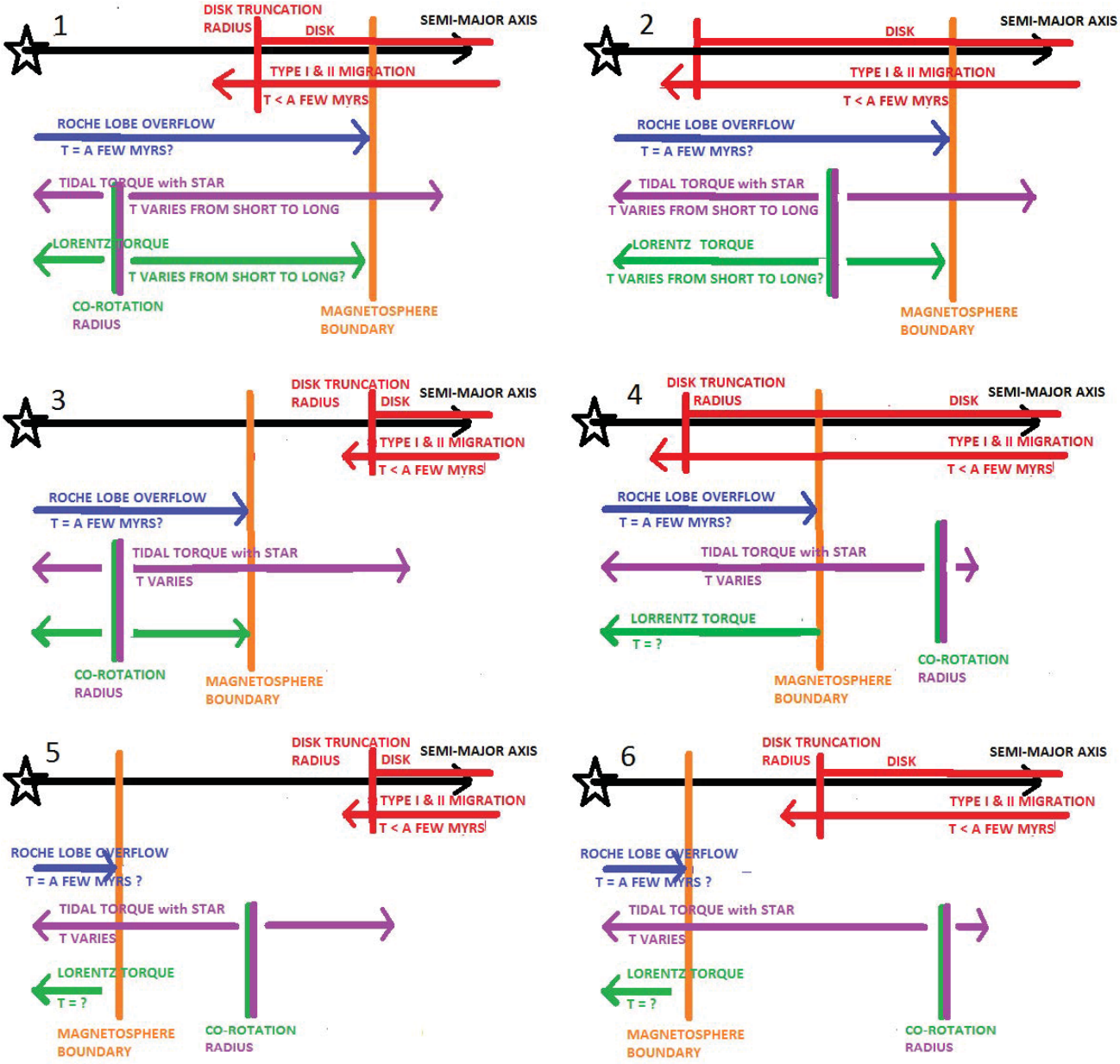

Figure 4.1: The figure shows qualitatively the characteristic time scales (denoted with "T") and the effects on the angular momentum of the planet caused by the tidal interaction with the disk (red arrow), mass loss through Roche lobe overflow (blue arrow), tidal torque with the star (purple arrow), and Lorentz torque (Green arrow). The direction of the arrow indicates the direction of change of semi-major axis due to the corresponding torque. The three radii discussed in section 3.2.5 (the boundary of the magnetosphere, the disk truncation radius, and the co-rotation radius) are respectively indicated by the orange, red, and green-purple vertical line. The position of these three radii relative to each others is important. Of course, some scenarios are more likely than others, but all six possible relative positions are shown, labelled with the number near the star. The figure is not to scale, and the relative positions change with time (age of the system). One of the results from the present work is a better characterization of the transfer of angular momentum associated with the Lorentz torque and the mass loss.

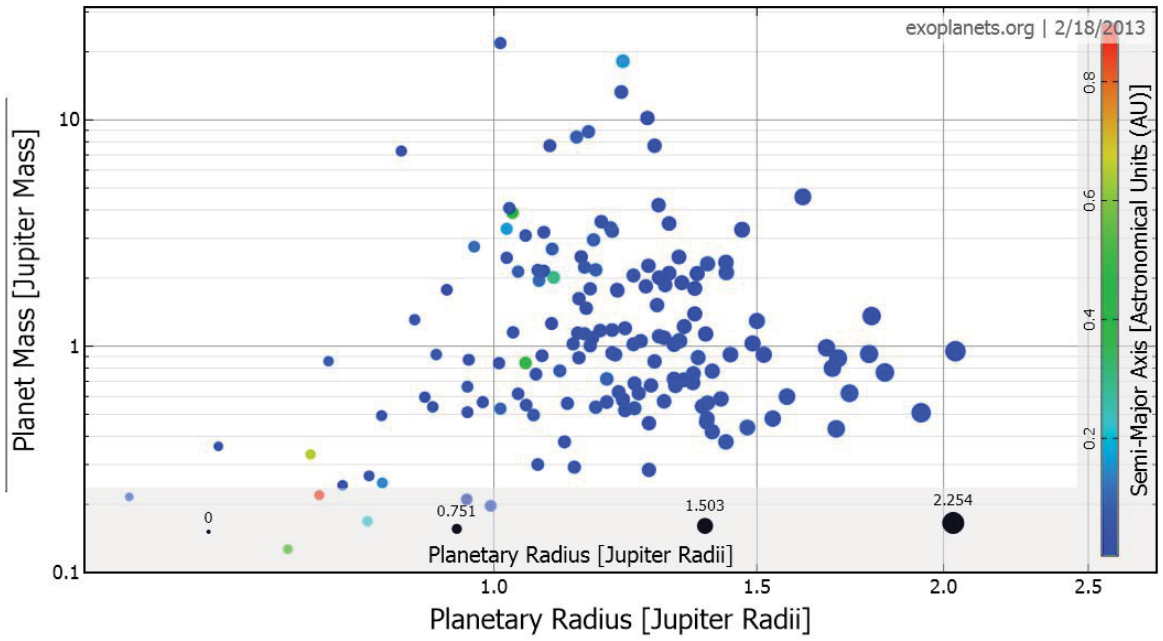

Figure 4.2: Plot of the planetary masses as a function of the planetary transiting radii (obtained from http://exoplanets.org in February 2013). The color indicates the semi-major axis and shows that most of these planets are close to their stars. The size of the dot provides an idea of the transiting radii (which is redundant with the x-axis but may provide an additional visual cue). One can for example see that most planets with a mass comparable to that of Jupiter have a radius significantly larger than that of Jupiter.

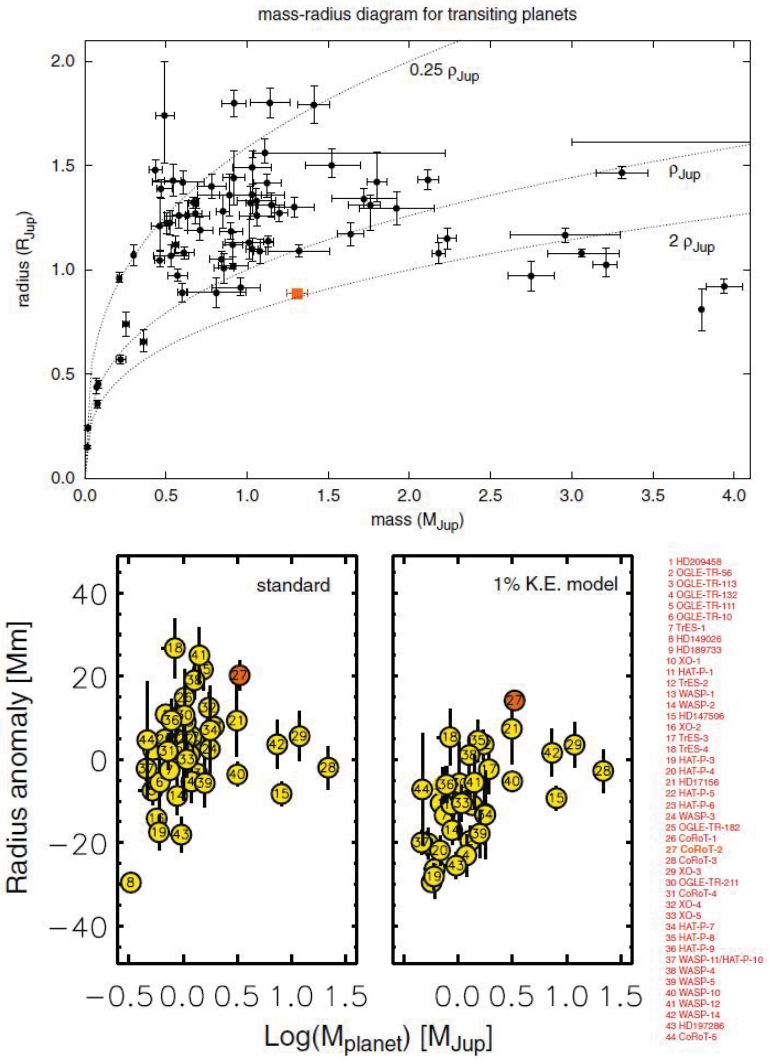

Figure 4.3: The **figure on top** is a mass-radius relationship for transiting planets from Cabrera et al. 2010 [18]. CoRoT-13b, the focus of the paper by Cabrera, is highlighted in orange. This diagram shows that the radii of these transiting planets are inflated such that their mean densities are smaller than that of Jupiter. The **bottom figure** is from Guillot & Havel 2011 [58] and presents the difference between the measured transiting radii of a sample of transiting planets and their radii expected from numerical models (units in Megameters). In the left panel, the radii are calculated using standard numerical models which include stellar irradiation. It shows that the irradiation may explain some of the inflated radii, but by no means all. In the right panel, the radii are calculated using the standard models, including irradiation and an additional *ad hoc* energy (deposited at the center of the planet) amounting to 1% of the irradiation incoming on the planet. CoRoT2b is the planet in red, one of the most inflated planet relatively to the expected radius.

Chapter 5

TE mode in a hot-Jupiter: Ohmic dissipation, torque, and mass loss

Planets migrate toward their stars on time scales of a few million years. To better understand the final fate of such planets, it is necessary to investigate the mechanisms of angular momentum exchange and their characteristic time scales. The main goal of this chapter is to estimate the angular momentum that can be transferred to a planet through its interaction with the time-dependent component of the stellar dipolar field. We use a semi-analytic approach to model the diffusion of the stellar field in the planet (section 5.2). For a chosen magnetic diffusivity profile, we then calculate the ohmic dissipation associated with the Eddy currents and the time scale on which the Lorentz torque transfers angular momentum to the planet (section 5.3). We finally calculate the mass loss rate through Roche lobe overflow that may be induced by the ohmic dissipation and the angular momentum gained by the planet if this mass is accreted onto the star (section 5.4). A table of symbols is provided in table 5.4 in the appendix (section 5.6.5).

Contents

Les planètes gaseuses géantes migrent vers leur étoile de part leur interaction gravitationelle avec le disque proto-planétaire. Ces planètes approchent donc à proximité de la magnétosphère d'une étoile TTauri. Lorsque l'orbite de la planète est à l'extérieur (à l'intérieur) du rayon de co-rotation avec la rotation de l'étoile, le couple gravitationel de marée et le couple de Lorentz donne (retire) du moment angulaire à la planète. Lorsque la vitesse de rotation de l'étoile diminue après la phase de contraction, le rayon de co-rotation augmente au delà de l'orbite de la planète proche, et le temps charactéristique de migration dans ce cas dépend alors de l'intensité de l'interaction gravitationelle et magnétique. Il est donc important de connaître les phénomènes qui contribuent à freiner la migration planétaire alors que la planète est encore en dehors de la co-rotation ainsi que les temps charactéristiques associés aux variations du demi-grand axe.

Dans ce contexte, nous calculons l'intensité maximale de l'interaction magnétique entre une étoile jeune (TTauri ou au début de la séquence principale) et une planète gaseuse proche. Nous modélisons dans ce chapître l'interaction Transverse Electrique qui correspond à la diffusion de la composante périodique du champ magnétique stellaire dans la planète. Un courant électrique alternatif est alors induit dans la planète ainsi qu'une dissipation ohmique et un couple de Lorentz. Nous exprimons le champ stellaire à l'aide d'un champ scalaire poloidal que nous décomposons en composantes harmoniques sphériques. Nous choisissons ensuite un profil de diffusivité magnétique dans la planète et résolvons l'équation de diffusion magnétique pour ce profil. Nous calculons que la dissipation ohmique est de l'ordre de 2×10^{21}W (en moyenne sur une orbite), et le couple de Lorentz sur la planète peut arrêter la migration en un temps characteristique d'environ 30 millions d'années (ce qui n'est typiquement pas assez rapide). Nous multiplions alors la diffusivité magnétique par un facteur 10^{α} avec α de -6 à 9 et montrons que la dissipation ohmique ne dépend que faiblement de la diffusivité magnétique.

En plus du couple de Lorentz, la planète peut recevoir du moment angulaire si elle perd de la masse par le point de Lagrange L1 du lobe de Roche et lorsque cette masse est accrétée par l'étoile. Plusieurs facteurs facilitent une telle perte de masse: les planètes jeunes ont un grand rayon de part leur énergie interne, le lobe de Roche est petit pour les planètes proches de leur étoile, et les dissipations de marées et ohmiques sont des sources supplémentaires d'énergie. Nous étudions le cas le plus favorable: une planète jeune soumise à une interaction de marée assez forte pour que la planète remplisse son lobe de Roche. Nous calculons alors la perte de masse associée à l'ajout de la dissipation ohmique et montrons que cet effet permet un transfert de moment angulaire vers la planète à un taux suffisant pour arrêter la migration, mais seulement dans ce cas optimal et transitoire.

5.1 Structure of the chapter

Overview of the problem

Planets in young systems encounter strong TTauri star magnetic fields as they migrate toward their stars through Type I or Type II migration. This early interaction is a key stage in the retention or destruction of the planet. If the planet's inward migration may be slowed down until the disk evaporates and the stellar magnetic field starts to decay, then the planet may remain on a stable Keplerian orbit. One mechanism to slow down the inward migration is to provide angular momentum to the planet. We investigate the plausibility of this scenario for a young close-in hot-Jupiter around a TTauri star.

This chapter focuses on the interaction of a hot-Jupiter with a time periodic stellar field with a specific emphasis on estimating its effect on the end stages of planetary migration (Laine & al 2008 [73]). It is divided in two main parts. In the first part, we use a semi-analytical model to calculate the diffusion of the stellar field into the planet, the ohmic dissipation associated with the Eddy currents, and the order of magnitude of the time scale on which the Lorentz torque transfers angular momentum to the planet. We show that this mechanism is likely to be inadequate in halting migration in most systems but that it may be barely adequate in the most favorable conditions.

In the second part, we use the tools developed in the first part and study the planetary mass loss by Roche lobe overflow that may be induced by the ohmic dissipation in the planet. Such mass loss, if accreted onto the star, is another way to provide angular momentum to the planet and slow inward migration. Although favorable conditions for such mass loss are likely to be transitory, we show that the associated Lorentz torque may be sufficient to halt inward migration and result in significant mass loss.

Detailed summary of the chapter

In section 5.2, we describe the semi-analytical approach used to model the diffusion of the time-dependent component of the stellar dipolar magnetic field in the planet. This approach has been used, for example, by Campbell 1983 [20] in the case of binary stars. This section is the most mathematical one and can be at first skipped by a reader primarily interested in the astrophysical results. A detailed overview of the argument is also provided here.

We adopt a spherical geometry for the planet and thus assume that the magnetic diffusivity profile $\eta(r)$ only has a radial dependence. We also assume the planet to be on a circular Keplerian orbit and the stellar spin axis to be aligned with the axis of planetary orbit. We neglect the effect of the planetary spin on the magnetic diffusion (for example, the planet may be tidally locked and always present the same face to the star). This interaction of a planet with the stellar magnetic field gives rise to both diffusion and motional induction. We focus here on the effect of the diffusion of the time-periodic

component of the field, *i.e.* that generated by $m_\perp$, the component of the stellar magnetic moment which is in the plane of the planet's orbit (perpendicular to the orbital axis).

We, therefore, start with the equation of magnetic diffusion (subsection 5.2.1). Since the magnetic diffusivity is non-uniform in the planet (and assumed to be infinite outside the planet), this equation does not reduce to the well known heat diffusion equation. In order to solve it, we first express the magnetic field with a potential scalar $\mathcal{B} = \nabla \wedge (\nabla \wedge (\phi \mathbf{e}_r))$, which we then write as a sum of spherical harmonics ($\phi = \mu_0 \sum_{l,m} C_l^m G_l(r) Y_l^m(\theta, \varphi) e^{i\omega t}$). The main components are the synodic angular velocity ω ($exp(i\omega t)$ thus models the time periodicity of the stellar field seen by the planet) and the orthogonal base of spherical harmonics functions $\{Y_l^m\}$ which model the angular dependence of the poloidal scalar ϕ (l and m being indices that label the different functions in the base). The only unknowns to be determined are the $\{G_l\}$ functions which model the radial dependence of the poloidal scalar, and the $\{C_l^m\}$ coefficients which determine the respective "weight" of each $G_l(r)Y_l^m(\theta, \phi)$.

Such decomposition is helpful for several reasons: the time-dependence of the magnetic field is explicitly shown, the time derivative is thus simple to calculate, and we can also first focus on solving a scalar (ϕ) instead of a vector. After some algebra, the partial differential diffusion equation on the magnetic field can be transformed into a second order ordinary differential equation for the radial part of the poloidal scalar (the unknown functions $G_l(r)$). The equation is slightly different inside and outside the planet since the magnetic diffusivity profile is assumed infinite outside the planet, and is to be defined inside the planet. It is thus more convenient to separate it into two equations, respectively for $G_l(r)$ inside the planet (first equation) and outside the planet (second equation), both equations only differing by the value of the magnetic diffusivity.

$$\frac{d^2 G_l(r)}{dr^2}(r) - \left[\frac{l(l+1)}{r^2} + \frac{i\omega}{\eta}\right] G_l(r) = 0 \tag{5.1}$$

$$\frac{d^2 G_l(r)}{dr^2}(r) - \left[\frac{l(l+1)}{r^2}\right] G_l(r) = 0. \tag{5.2}$$

Subsection 5.2.1 ends after the derivation of these two equations, and subsections 5.2.2 and 5.2.3 respectively solve each of them.

In subsection 5.2.2, we focus on the **poloidal scalar outside the planet** ϕ. Since the corresponding equation for the $G_l(r)$ has an analytical solution, the poloidal scalar outside the planet is entirely determined except for the coefficients C_l^m. In addition, the poloidal scalar outside the planet ϕ can be decomposed as the sum of the contribution of the stellar field and the contribution of the field induced in the planet (but seen at a location outside the planet), $\phi = \phi_* + \phi_p$ where ϕ_* is the stellar contribution and ϕ_p is the contribution of the induced field.

ϕ_* is also determined since the stellar field is assumed to be a simple dipolar magnetic field. We thus start with the standard vectorial formula for a dipolar magnetic field $\mathcal{B}_*$ and then find the analytical expression of the potential vector ψ_* (using $\mathcal{B}_* = -\nabla\psi_*$). An independent calculation (in appendix) shows that the poloidal scalar ϕ_* is related to the potential scalar ψ_* with the relation $\psi_* = -\partial\phi_*/\partial t$, which we use to find the expression

of ϕ_*. Some algebra is then needed to rearrange the formula and express ϕ_* using the Legendre polynomials. It is useful to do so in order to remain with an orthogonal base of functions related to the spherical harmonics base.

ϕ_p, the contribution of the induced field to the total poloidal scalar outside the planet is not known. However, as an induced field, its angular dependence mirrors that of its cause (*i.e.* ϕ_p depends on the same Legendre polynomials as ϕ_*). In addition, its radial part is the analytic solution to the corresponding equation in (5.2). We can therefore write an expression for ϕ_p where the only unknown are numerical coefficients. It may also be useful to point out that these unknown coefficients are written with the notations $(\alpha_1,\alpha_2,\alpha_3,\alpha_4,\beta_1,\beta_2,\gamma_1,\gamma_2,\gamma_3,\gamma_4)$.

By the end of section 5.2.2, we thus have an analytic expression for the total poloidal scalar outside the planet which radial and angular dependence is determined. We then turn in section 5.2.3 to the **poloidal scalar inside the planet**. The unknown are the $G_l(r)$ functions and the C_l^m coefficients. Assuming that the magnetic diffusivity profile $\eta(r)$ in the planet is known, the $G_l(r)$ can be found numerically by solving equation (5.1), and the only unknowns left are the coefficients C_l^m.

The unknown coefficients C_l^m in the expression of the poloidal scalar inside the planet and the coefficients $(\alpha_1,\alpha_2,\alpha_3,\alpha_4,\beta_1,\beta_2,\gamma_1,\gamma_2,\gamma_3,\gamma_4)$ in the expression of the poloidal scalar outside the planet can then be found through the condition of continuity of the poloidal scalar at the boundary of the planet. We equate the poloidal scalars outside and inside the planet for $r = R_p$ and obtain a set of linear equations, which we solve for the C_l^m. The determination of the $G_l(r)$ and the C_l^m concludes section 5.2.

Section 5.3 derives the expression of the ohmic dissipation associated with the currents induced in the planet. Since the cause of these currents is the diffusion of the magnetic field in the planet's magnetic diffusivity profile, we express the ohmic dissipation using the coefficients and functions calculated previously. In order to obtain numerical results, we need to specify the magnetic diffusivity profile. For a simple magnetic diffusivity profile in the planet, we find an ohmic dissipation $\mathcal{P} \approx 2 \times 10^{21} Js^{-1}$. Because the magnetic diffusivity profile is uncertain (and different for each system considered), we also study the dependence of the total ohmic dissipation on the value of the magnetic diffusivity. We, therefore, artificially multiply the magnetic diffusivity by a factor 10^α (while keeping the shape of the profile, *i.e.* the functional dependence on the radius, unchanged). We find that the total ohmic dissipation is insensitive to this change over a large range of orders of magnitude.

Relating the ohmic dissipation to the work of the Lorentz force, we finally obtain an order of magnitude of the Lorentz torque and find that it transfers angular momentum to the planet on a time scale about an order of magnitude too slow to reasonably oppose type I or type II migration (assuming the planet is still interacting tidally with the protoplanetary disk). We conclude the section by pointing out that this time scale is adequate if extreme (tough still reasonable) values are chosen, *i.e.* strong TTauri star magnetic fields and fast stellar spin. In addition, we describe how the values calculated would scale if applied to main sequence stars.

The previous two sections form the first part of this chapter. In the second part, we investigate the possibility that the ohmic dissipation, under some favorable conditions, may

induce mass loss through Roche lobe overflow. Estimating the mass loss rate is in itself a relevant pursuit. Indeed, the conditions under which hot-Jupiters may lose a significant fraction of their envelopes and become either super-Earths or rocky planets with a small gaseous envelope (a type of planet which is not found in our Solar System but seems to exist around other stars) are not well characterized. Nevertheless, in line with the general direction of this chapter, our main interest in estimating the mass loss rate is to estimate the angular momentum that can be transferred to the planet as the mass lost is accreted onto the star.

In **Section 5.4**, we build a simple self-consistent analytic model in order to relate the mass loss rate to the ohmic dissipation. Subsection 5.4.1 presents the model and the conditions that we adopt. Very young close-in planets have large radii due to the intense stellar irradiation and a large internal energy. We assume that the planet fills its Roche lobe and calculate the mass loss resulting from the addition of the ohmic dissipation. It, therefore, does not entail re-inflating a mature planet but rather slowing down the contraction and/or inducing mass loss through ohmic dissipation during a transitory stage of the planet's lifetime (when it has not yet fully contracted). This idealized scenario, therefore, provides the maximum mass loss possible. If the planet does not fill its Roche lobe when it is in equilibrium with stellar radiation and tidal dissipation, then part of the ohmic dissipation is used to first inflate the planet's equilibrium radius. The expansion of a gas caused by an energy source may be modelled in different ways, and we choose to consider a quasi-hydrostatic situation. We model the planet with a polytropic interior and an isothermal outer layer, calculate the magnetic diffusivity profile, and write the equations of mass, momentum, and energy conservation.

In subsection 5.4.2, we apply the method developed in section 5.2 to a young planet which fills its Roche lobe. We calculate the ohmic dissipation and mass loss rate while varying in turn one of the following parameters of interest: the planet's mass, semi-major axis, stellar mass, stellar luminosity, stellar dipolar strength, angle between the stellar magnetic dipole and spin axis, and the synodic angular velocity. Under the favorable (ideal) conditions considered above and for our fiducial values of a hot-Jupiter, we find an initial rate of mass loss of about $3 \times 10^{-7} M_* \mathrm{yr}^{-1}$ (if an evolutionary simulation was run, this value would be the initial slope of the curve). If this outflow is accreted onto the star, it would provide angular momentum to the planet, with corresponding orbital changes occurring in a few million years. Although the mass loss rate calculated should be seen as an upper limit, it may nevertheless provide a sufficient barrier to inward migration. We conclude the section with an attempt at formulating a generalized scaling law which would give a quick estimate of the ohmic dissipation and mass loss rate for any values of the parameters listed above.

More details about the calculations and a table of symbols (table 5.4, section 5.6.5) are provided in the appendix.

5.2 Diffusion of the magnetic field

5.2.1 The equations

We center the set of coordinates (x, y, z) on the planet and (x_0, y_0, z_0) on the star as indicated in the figure (5.1).

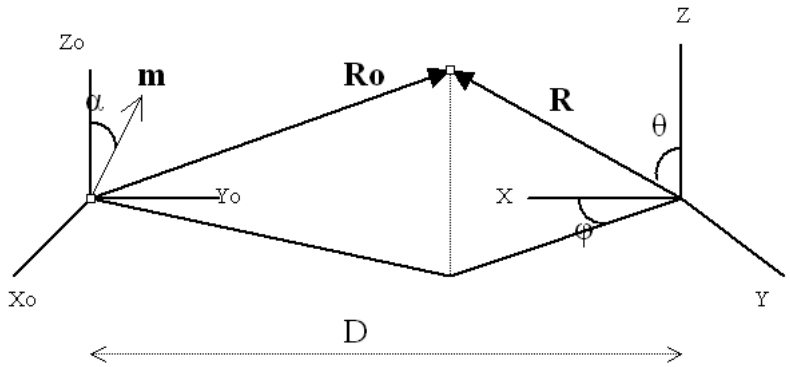

Figure 5.1: The geometry of the system. The star is on the left, at the center of the set of axes (x_0,y_0,z_0), and the planet is on the right, at the center of the set of axes (x,y,z).

The equation of diffusion of the stellar magnetic field into the planet is

$$\frac{\partial \mathcal{B}}{\partial t} = -\nabla \wedge (\eta \nabla \wedge \mathcal{B}), \tag{5.3}$$

as obtained from Ohm's law $\mathcal{J} = \sigma\mathcal{E}$, Maxwell-Faraday's equation $\partial\mathcal{B}/\partial t = -\nabla \wedge \mathcal{E}$, and Maxwell-Ampere's equation $\nabla \wedge \mathcal{B} = \mu_0\mathcal{J}$ (also see section 2.1). The stellar field is poloidal and will be expressed as a potential scalar ψ (see below). Before doing so, we now express the total magnetic field with a potential scalar ϕ such that,

$$\mathcal{B} = \nabla \wedge (\nabla \wedge (\phi \mathbf{e}_r)), \tag{5.4}$$

and then decompose ϕ on the spherical harmonics base and account for the time periodicity with a factor $exp(i\omega t)$

$$\phi = \mu_0 \left[\sum_{l,m} C_l^m G_l(r) Y_l^m(\theta, \varphi) \right] e^{i\omega t}, \tag{5.5}$$

where the Y_l^m are the spherical harmonic functions, the G_l are the corresponding radial components to be determined (cf. equation (**??**) below), the C_l^m are coefficients to be determined, and $\omega = \omega_p - \omega_*$ is the synodic period. We can therefore write the time derivative of the magnetic field (*i.e.* the left hand side of equation (5.3))

$$\frac{\partial \mathcal{B}}{\partial t} = i\omega \nabla \wedge (\nabla \wedge (\phi \mathbf{e}_r)). \tag{5.6}$$

Equation (5.3) thus becomes

$$i\omega\nabla\wedge(\nabla\wedge(\phi\mathbf{e}_r)) = -\nabla\wedge(\eta\nabla\wedge\mathcal{B}). \tag{5.7}$$

After integrating once, we get

$$i\omega\nabla\wedge(\phi\mathbf{e}_r) = -\eta\nabla\wedge\mathcal{B}, \tag{5.8}$$

where we choose the particular solution for which the integration gradient is zero.[1] We replace $\mathcal{B}$ in the right hand side of (5.8) by its decomposition in spherical harmonics (equations (5.4)) and (5.5)), develop the curls, and identify terms by terms using the spherical harmonics base (see section (5.6.1) in the appendix). We then obtain the equations for $G_l(r)$ both in the planet (with a magnetic diffusivity profile $\eta(r)$) and outside the planet (with $\eta=\infty$)

$$\frac{d^2G_l(r)}{dr^2}(r) - \left[\frac{l(l+1)}{r^2} + \frac{i\omega}{\eta}\right] G_l(r) = 0 \tag{5.9}$$

$$\frac{d^2G_l(r)}{dr^2}(r) - \left[\frac{l(l+1)}{r^2}\right] G_l(r) = 0. \tag{5.10}$$

5.2.2 The poloidal scalar outside the planet

Outside the planet, $\eta=0$ and the equation for the radial part of ϕ is

$$\frac{d^2G_l(r)}{dr^2}(r) - \left[\frac{l(l+1)}{r^2}\right] G_l(r) = 0. \tag{5.11}$$

This equation has analytical solutions which are the linear combinations of $\{r^{l+1}\}$ (corresponding to the contribution of the stellar field) and $\{r^{-l}\}$ (corresponding to the contribution of to the field induced in the planet). In the remaining of this subsection, we will therefore express the poloidal scalars outside the planet due respectively to the star ϕ_* and to the planet ϕ_p (ϕ_p corresponds to the field induced in the planet by the stellar magnetic field, but seen at a position $\mathbf{r}$ located outside the planet)

Contribution of the Stellar field

We express here the poloidal scalar corresponding to the stellar magnetic field. We decompose the stellar magnetic moment m into its components respectively parallel $m_\parallel = mcos\alpha$ and perpendicular $m_\perp = msin\alpha$ to the stellar spin axis (where α is the angle between the dipole and the orbit axis). Quadrupolar and higher order fields are neglected. In the formula, vectors are in bold when there is an ambiguity. The magnetic vector potential $\mathcal{A}_*$ (such that $\mathcal{B}_* = \nabla\wedge\mathcal{A}_*$), magnetic scalar potential ψ_* (such that $\mathcal{B}_* = -\nabla\psi_*$),

[1] As pointed out by P. Mottez, a more general calculation may be carried out without neglecting the gradient.

and magnetic field are

$$\mathcal{A}_* = \frac{\mu_0}{4\pi}\frac{\mathbf{m}\wedge\mathbf{r}_0}{r_0^3} \tag{5.12}$$

$$\psi_* = \frac{\mu_0}{4\pi}\frac{\mathbf{m}\cdot\mathbf{r}_0}{r_0^3} \tag{5.13}$$

$$\mathcal{B}_* = \frac{\mu_0}{4\pi}\left(\frac{3\mathbf{r}(\mathbf{m}\cdot\mathbf{r}_0)}{r_0^5} - \frac{\mathbf{m}}{r_0^3}\right) \tag{5.14}$$

$$= B_*(R_*)\left(\frac{R_*}{r_0}\right)^3 (2cos\theta, sin\theta, 0)\,. \tag{5.15}$$

We also write $\mathbf{m} = (sin\alpha cos\omega t, sin\alpha sin\omega t, sin\alpha)$ and $\mathbf{r}_0 = \mathbf{d} + \mathbf{r} = (rsin\theta sin\varphi, a - rsin\theta cos\varphi, rcos\theta)$ where $\mathbf{d}$ is the vector semi-major axis from the star to the planet. We thus write the potential scalar of the stellar field (see section 5.6.2 in the appendix, especially equation 5.79)

$$\psi_* = -\frac{\mu_0 m sin\alpha}{4\pi d^3} r P_1^1 (2cos\varphi sin\omega t + sin\varphi cos\omega t) - \frac{3}{2}\frac{\mu_0 m sin\alpha}{4\pi d^4} r^2 \left[P_2^0 sin\omega t - P_2^2\left(\frac{1}{2}cos2\varphi sin\omega t + \frac{1}{3}sin2\varphi cos\omega t\right)\right], \tag{5.16}$$

where $P_1^1 = -sin\theta$, $P_2^2 = 3sin^2\theta$, and $P_2^0 = (3cos^2\theta - 1)/2$ are Legendre associated polynomials. This expression was obtained as a Taylor expansion of $\psi_* = (\mu_0/4\pi)(\mathbf{m}\cdot\mathbf{r}_0/r_0^3)$ using $\mathbf{r}_0 = \mathbf{d} + \mathbf{r}$, and after some algebra in order to express it explicitly with Legendre polynomials.

We also show in the appendix (equation (5.60)) that $\psi_* = -\partial\varphi_*/\partial r$. After integration of ψ_* in the previous equation (equation (5.16)), we obtain an expression for ϕ_*,

$$\phi_* = \frac{\mu_0 m sin\alpha}{8\pi d^3} r^2 (2cos\varphi sin\omega t + sin\varphi cos\omega t) P_1^1 + \frac{\mu_0 m sin\alpha}{8\pi d^4} r^3 \left[P_2^0 sin\omega t - \left(\frac{1}{2}cos2\varphi sin\omega t + \frac{1}{3}sin2\varphi cos\omega t\right) P_2^2\right]. \tag{5.17}$$

We have thus obtained the expression of the poloidal scalar corresponding to the stellar magnetic field. Legendre polynomials have been explicitly used because they are an orthogonal base and will allow identifying terms. We remind that r denotes the distance to the center of the planet and d is the distance between the planet and the star. The radial dependence of the stellar poloidal scalar ϕ_* is in $\{r^{l+1}\}$ (a set of solutions of equation (5.11)).

Contribution of the induced field

We now express ϕ_p, the poloidal scalar outside the planet due to the field induced in the planet. The radial dependence of ϕ_p follows $\{r^{-l}\}$ (the other set of solutions of equation 5.11), and the dependence of ϕ_p on the spherical harmonics is similar to that of its cause, *i.e.* ϕ_*. We therefore express ϕ_p using the same Legendre polynomials as for ϕ_*, although

the radial dependence is different (ϕ_p corresponding to the r^{-l} whereas ϕ_* corresponding to r^{l+1} (cf. the discussion of equation (5.11))

$$\phi_p = \mu_0 P_1^1 \left[\frac{\cos\varphi}{r}(\alpha_1 \sin\omega t + \alpha_2 \cos\omega t) + \frac{\sin\varphi}{r}(\alpha_3 \sin\omega t + \alpha_4 \cos\omega t)\right] + \frac{\mu_0 P_2^0}{r^2}(\beta_1 \sin\omega t + \beta_2 \cos\omega t) + \mu_0 P_2^2 \left[\frac{\cos 2\varphi}{r^2}(\gamma_1 \sin\omega t + \gamma_2 \cos\omega t) + \frac{\sin 2\varphi}{r^2}(\gamma_3 \sin\omega t + \gamma_4 \cos\omega t)\right]. \quad (5.18)$$

The total poloidal field outside the planet as defined in equation (5.4) is $\phi_{out} = \phi_* + \phi_p$, and its radial part is the solution of (5.11). At the boundary of the planet, we will match this expression with that of the poloidal scalar inside the planet in order to solve for the unknown coefficients (α_1, α_2,α_3,α_4, β_1,β_2, γ_1, γ_2, γ_3, and γ_4).

5.2.3 The poloidal scalar inside the planet

As found previously, the radial part of the poloidal scalar inside the planet follows the equation

$$\frac{d^2 G_l(r)}{dr^2}(r) - \left[\frac{l(l+1)}{r^2} + \frac{i\omega}{\eta}\right] G_l(r) = 0, \quad (5.19)$$

which we solve numerically.

The numerical solver

For a known conductivity profile σ (to be specified in the following sections), we first use a Newton-Raphson-Kantorovich approach to numerically solve equation (5.19) for $G_l(r)$ (*i.e.* the radial part of the total poloidal scalar ϕ inside the planet).

For each l and m, we decompose C_l^m and $G_l(r)$ into their respective real and imaginary parts, $G(r) = Y_1(r) + iY_2$ and $C_l^m = \mu_l^m + i\nu_l^m$. We also write the derivatives $Y_3(r) = Y_1'(r)$ and $Y_4(r) = Y_2'(r)$. Equation (5.19) then become

$$Y_3'(r) = -\frac{\omega}{\eta(r)} Y_2(r) + \frac{l(l+1)}{r^2} Y_1(r) \quad (5.20)$$

$$Y_4'(r) = \frac{\omega}{\eta(r)} Y_1(r) + \frac{l(l+1)}{r^2} Y_2(r). \quad (5.21)$$

Using $G_l(r) \sim r^{l+1}$ for $r \sim 0$ (the symbol $\sim$ indicate the behavior near a limit) and $G_l(r) \sim r^{l+1} + r^{-1}$ for $r \sim R_p$, we obtain the boundary conditions

$$G_l'(R_p) + \frac{l}{R_p} G_l(R_p) - (2l+1) R_p^l = 0 \quad (5.22)$$

$$G_l'(r \simeq 0) - \frac{l+1}{r} G_l(r \simeq 0) = 0, \quad (5.23)$$

We then match at $r = R_p$ the expressions for the total poloidal scalars inside and outside the planet. The total poloidal scalar inside the planet depends on the coefficients C_l^m, and the total poloidal scalar outside the planet depends on the coefficients (α_1, α_2,α_3,α_4, β_1,β_2, γ_1, γ_2, γ_3, and γ_4). These coefficients are thus obtained together through continuity of the total poloidal scalar at the boundary of the planet. We give in appendix (section (5.6.3) the linear equations used to calculate the coefficients (μ_1^1, μ_1^{-1}, ν_1^1, ν_1^{-1}, α_1, α_2,α_3,α_4), (μ_2^0, ν_2^0, β_1,β_2), and (μ_2^2, μ_2^{-2}, ν_2^2, ν_2^{-2}, γ_1, γ_2, γ_3, γ_4).

5.3 Conductivity profile and ohmic dissipation rate

General expression for the ohmic dissipation

Once the coefficients above have been determined and a magnetic diffusivity profile has been obtained, we can calculate the ohmic dissipation. The stellar magnetic field diffuses inside the planet and generates an electric field $\mathcal{E}$ and its associated volumic current $\mathcal{J}$ inside the planet. The corresponding ohmic dissipation inside the planet is $\mathcal{P}_{vol} = Re(\mathcal{J})\ Re(\mathcal{E})$. Using $\mathcal{E} = \frac{1}{\sigma}\mathcal{J}$, $\mathcal{J} = \frac{1}{\mu_0}\nabla \wedge \mathcal{B}$, and $\nabla \wedge \mathcal{B} = \frac{-i\omega}{\eta}\nabla \wedge (\phi \mathbf{e}_r)$ (obtained from equation (5.8)), we can write:

$$\mathcal{P}_{vol} = \frac{\omega^2}{\mu_0 \eta} \| \nabla \wedge (\phi \mathbf{e}_r) \|^2. \tag{5.24}$$

We then integrate the volumic ohmic dissipation to calculate the total ohmic dissipation

$$\mathcal{P} = \int_r < \mathcal{P}_{\theta,\varphi} > r^2 dr, \tag{5.25}$$

where $< \mathcal{P}_{\theta,\varphi} >$ is the volumic ohmic dissipation integrated over θ and φ and is given in the appendix section (5.6.4) as a function of the G_l and C_l^m.

Fiducial set of parameters and corresponding ohmic dissipation

We apply the previous scheme to a specific fiducial system (summarized in table 5.1: a planet with $M_p = 0.63 M_J$, $R_p = 1.4 R_J$, $a = 0.04 AU$, and a TTauri star with $m = 4 \times 10^{34} Am^2$, which corresponds to a surface field $\mathcal{B}_*(R_*) = \mu_0 m/(4\pi R_*^3) \approx 3000G$ for $R_* = 4R_\odot$ and to a field at the location of the planet $\mathcal{B}_*(a) \approx 180$G (it corresponds to the maximum reasonable value for the field of a TTauri star based on observations). At 0.04 AU, the Keplerian angular velocity is $\omega_p \approx 2.5 \times 10^{-5} \mathrm{s}^{-1}$. We adopt a relative angular velocity between the stellar spin and the planetary orbit $\omega = |\omega_p - \omega_*| = 10^{-5} s^{-1}$ which corresponds to a stellar spin of 5 days. Finally, we use $sin\alpha = 1$, which maximizes the value of the time periodic component of the magnetic dipole.

We at first adopt an *ad hoc* magnetic diffusivity profile (the magnetic diffusivity η is related with the electric conductivity σ through $\eta = (\mu_0 \sigma)^{-1}$) in the planet: $\eta(r) = 10^3 exp\left[25 \left(\frac{r}{R_p}\right)^2\right]$ based on preliminary estimates (later calculations show that it is in

Mass of planet	$M_p = 0.63 M_J$
Radius of planet	$R_p = 1.4 R_J$
Semi-major axis	$a = 0.04 AU$
Stellar magnetic dipole strength	$m = 4 \times 10^{34} Am^2$
Stellar radius	$R_* = 4 R_\odot$
Stellar surface field	$\mathcal{B}_*(R_*) = \mu_0 m/(4\pi R_*^3) \approx 3000G$
Field at 0.04 AU	$\mathcal{B}_*(a) \approx 180$G
Synodic angular velocity	$\omega = \lvert\omega_p - \omega_*\rvert = 10^{-5} s^{-1}$
Tilt angle	$sin\alpha = 1$

Table 5.1: Table giving the fiducial values for key parameters used to calculate the ohmic dissipation.

fact a lower estimate of the conductivity in the deep interior by one or two order of magnitude). Using these values and the magnetic field strength of a TTauri star, we numerically calculate a corresponding total ohmic dissipation, averaged over a synodic period, $\mathcal{P} \approx 2 \times 10^{21} Js^{-1}$. This value is in fact comparable to ωE_B, where E_B is the time average of the magnetic energy of the stellar field at the location of the planet.

The solution we obtain for the radial part of the poloidal scalar for this electric conductivity profile is plotted in figure 5.2.

Skin depth

The characteristic length scale associated with the diffusion of a time periodic magnetic field of period τ is $L = \sqrt{\eta\tau}$. However, $\eta(r)$ here varies with radius and becomes smaller with depth into the planet, and the characteristic length scale L(r) is a function of radius. We define the scale height H(r) associated with the magnetic diffusivity such that $\eta(r + H(r))/\eta(r) = \exp(1)$. We, therefore, define an effective penetration depth r_{eff}, which corresponds to the radius at which the scale height H(r) is comparable to the classical skin depth $\delta_0 = \sqrt{2\eta/\omega}$. In other words, $H(r_{eff}) = \sqrt{2\eta(r_{eff})/\omega}$.

The scale height H(r) for a magnetic diffusivity profile $\eta = 10^\alpha exp(25r^2/R_p^2)$ (where $\alpha = 3$ in our example) is

$$H = \frac{R_p^2}{[2]25r} \tag{5.26}$$

where the factor [2] should be included if one derives H such that $\eta(r+H) = \exp(1)\eta(r)$, but is absent if one defines H such that $\eta = 10^\alpha exp(r/H)$.

The classical skin depth δ is

$$\delta_0 = \sqrt{\frac{2\eta}{\omega}} = \sqrt{2} \times 10^{5/2} \times 10^{\alpha/2} exp\left[12.5\left(\frac{r^2}{R_p}\right)^2\right], \tag{5.27}$$

where the numerical values are given for $\omega = 10^{-5}\mathrm{s}^{-1}$. For $\alpha = 3$, we get an effective penetration depth $r_{eff} \approx 0.7 R_p$ which is coherent with the graphs of $G_l(r)$. For $\alpha > 9$

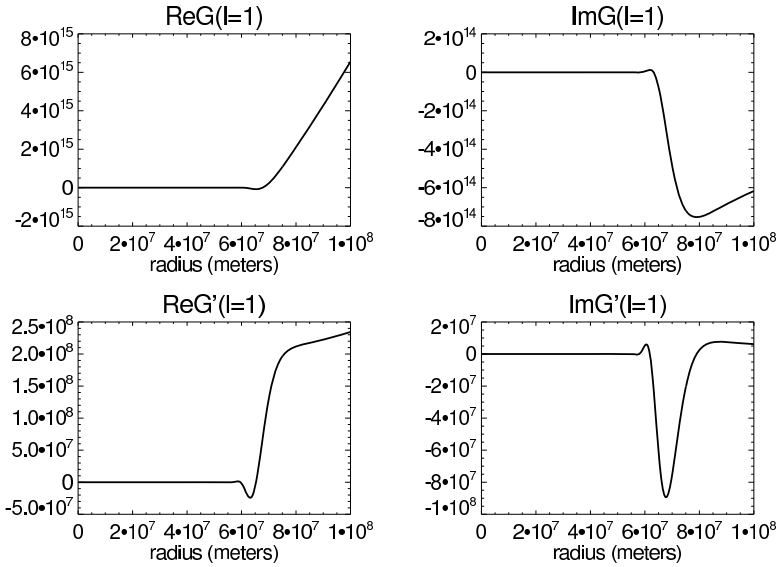

Figure 5.2: Real and imaginary parts of $G_{l=1}(r)$ and its first derivative, for $R_p = 10^8 m = 1.4\ R_J$, $a = 0.04\ AU$, and $\eta(r) \simeq 10^3 \exp(25r^2/R_p^2)$. The shape of $G_2(r)$ is very similar to that of $G_1(r)$, but the amplitude of $C_2^m G_2(r)$ is much smaller than the amplitude of $C_1^m G_1(r)$ (i.e, $|C_2^m G_2(r)| \ll |C_1^m G_1(r)|$).

(*i.e.* a body with very little conductivity), the effective skin depth is comparable to 90 % of the radius. For such large magnetic diffusivity, the magnetic field diffuses fully into the planet.

Ohmic dissipation for a wide range of magnetic diffusivity

The magnetic diffusivity profile is dependent on numerous parameters, such as the planetary composition, the model for the planet's internal structure, or the boundary conditions (*e.g.* surface temperature and pressure). The ohmic heating may also exert a feedback on the internal structure and thus on the magnetic diffusivity. Since the model does not so far account for such feedback, we run several independent calculations for a wide range of magnetic diffusivity. We keep the magnetic diffusivity profile proportional to $exp\left[25\left(\frac{r}{R_p}\right)^2\right]$ but vary the coefficient in front from 10^{-3} to 10^{12}. The results are summarized in the table 5.2.

This series of calculations indicate that the total ohmic dissipation does not vary much over a range of magnetic diffusivity of many orders of magnitude ($\alpha \approx 0$ to 9, with $\eta = 10^{\alpha} exp(25r^2/R_p^2)$). Qualitatively, a large electric conductivity leads to a small skin depth because the magnetic energy is efficiently dissipated. Therefore, larger electric conductivity (smaller magnetic diffusivity) results in a smaller volume of dissipation, but a strong volumic ohmic dissipation. Inversely, a smaller electric conductivity (larger magnetic diffusivity) results in a smaller ohmic dissipation per unit volume, but also a deeper

$\eta(r) = 10^{-3} \times \exp(25(r/R_p)^2)$	$\mathcal{P} = 1.26 \times 10^{21}\ Js^{-1}$
$\eta(r) = 10^{0} \times \exp(25(r/R_p)^2)$	$\mathcal{P} = 2.7 \times 10^{21}\ Js^{-1}$
$\eta(r) = 10^{3} \times \exp(25(r/R_p)^2)$	$\mathcal{P} = 2.18 \times 10^{21}\ Js^{-1}$
$\eta(r) = 10^{5} \times \exp(25(r/R_p)^2)$	$\mathcal{P} = 1.71 \times 10^{21}\ Js^{-1}$
$\eta(r) = 10^{7} \times \exp(25(r/R_p)^2)$	$\mathcal{P} = 1.12 \times 10^{21}\ Js^{-1}$
$\eta(r) = 10^{9} \times \exp((25(r/R_p)^2)$	$\mathcal{P} = 2.33 \times 10^{20}\ Js^{-1}$
$\eta(r) = 10^{10} \times \exp((25(r/R_p)^2)$	$\mathcal{P} = 2.5 \times 10^{19}\ Js^{-1}$
$\eta(r) = 10^{12} \times \exp(25(r/R_p)^2)$	$\mathcal{P} = 2.5 \times 10^{17}\ Js^{-1}$

Table 5.2: Table giving $\mathcal{P}$ as a function of η, with a wide range of value for η.

effective penetration of the field into the planet, and thus a larger volume where ohmic dissipation occurs.

For $\alpha < -3$, the effective skin depth is less than a few percent and corresponds to a completely different regime. For $\alpha > 9$ the effective penetration depth is comparable to the radius of the planet. In other words, further increasing α lead to lower electric conductivity and lower ohmic dissipation per unit volume (proportionally to $\sigma = (\mu_0\eta)^{-1}$), but it does not increase the volume where dissipation occurs, which thus explains the finding that the ohmic dissipation decreases for very large magnetic diffusivities.

Ohmic dissipation and migration

We assume that the planet orbit is prograde and defines the positive convention for angular momentum. We have defined in section (3.2.5) (about stellar magnetospheres) the co-rotation radius as the semi-major axis at which a planet in Keplerian orbit would have an orbital period equal to the stellar spin period. If the planet orbits the star outside co-rotation (*i.e.* with a semi-major axis larger than the co-rotation radius), then the interaction due to Lenz's law would result in a positive torque on the planet; the planet thus gains angular momentum and moves out, and the star loses angular momentum and spins down. If the planet orbits inside co-rotation (*i.e.* with a semi-major axis smaller than the co-rotation radius), then the interaction results in a negative torque on the planet. It loses angular momentum and move inward where as the star gains angular momentum and spins up (Campbell 1983 [20], Laine et al. 2012 [72]).

We here simply compare the ohmic dissipation in the planet with the energy associated with a change in the planetary orbit (inward or outward). The change in the planet's total energy $|E = GM_pM_*/2a|$ when the planet migrates from 0.05AU to 0.04AU is $\Delta E \approx 2 \times 10^{36} J$. A force dissipating energy at rate $\mathcal{P}$ would produce a work comparable to ΔE in about $t \approx 3 \times 10^7$ years. This time-scale is typically longer than those associated with planetary migration by a factor 10. As the planet approaches the star outside co-rotation, if it steadily loses angular momentum to an external sink, then the inward migration cannot be stopped by the Lorentz torque; the planet continues to spiral inward, passes the co-rotation radius, and may fall into the star (once the planet is inside the co-rotation radius, the Lorentz torque becomes negative and the planet steadily loses angular momentum).

However, $\mathcal{P}$ could be increased by increasing $|\omega| = |\omega_p - \omega_*|$. The value of $|\omega|$ used in the previous calculation is $10^{-5}s^{-1}$. For a planetary orbit of 3 days, this value of ω corresponds to a stellar spin period of 5 days (the planet being inside co-rotation) or 2 days (the planet being outside co-rotation). If the star were to spin with a 1.3-day period, then $|\omega| \approx 3 \times 10^{-5}s^{-1}$ which would bring the time scale down to $t \approx 3 \times 10^6$ years. In this case, the torque exerted by the star on the planet orbiting outside co-rotation may marginally counter-balance the planetary inward migration.

Alternatively, for the fiducial values we have chosen for a young main sequence star ($R_* = 0.9R_\odot$ and a surface field $\mathcal{B}_*(R_*) = 0.03$ Tesla), we obtain a magnetic dipole strength $m = 7.5 \times 10^{31}\mathrm{Am}^2$ and a field at the location of the planet at 0.04AU of 0.35G. Extrapolating with a dependence of the ohmic dissipation on the inverse square of the magnetic field, the interaction with a young main sequence star at 0.04AU would be decreased by a factor 2.8×10^5. The corresponding ohmic dissipation is energetically non-negligible (it may raise the temperatures of the night side of a planet by 200K), but it does not significantly affect the dynamics of the planet. At 0.01AU, the stellar field at the location of the planet is about 22G (around a young star with surface field equal to 300G). The ohmic dissipation at that location is about 60 times weaker than that around the TTauri-star.

Summary

We thus conclude the first part of this chapter with the following progress and results. 1) We adapted an analytic approach first developed for binary stars to the interaction of a planet with the time-periodic component of the stellar dipolar magnetic field. 2) We show that the total ohmic dissipation does not depend much on the strength of the magnetic diffusivity profile, for a wide range of reasonable values of the magnetic diffusivity. 3) In the context of young systems in which planets are approaching their host stars through type I and type II migration, we show that the interaction investigated here may halt inward migration on a time-scale comparable to that of planetary migrations through gravitational torques with the disk, but only in the most favorable regime (maximum stellar magnetic field strength and large relative angular velocity ω, *i.e.* a star spinning rapidly). The interaction with a main sequence star is found to be significantly weaker, and the favorable regime is presumably only achieved around TTauri stars (which also corresponds to the regime where type I and type II migration occur).

5.4 Planetary mass loss

5.4.1 Model

Line of thought

Another mechanism that can give angular momentum to the planet is planetary mass loss through Roche lobe overflow. The Roche lobe is the equipotential surface on which the gravitational influence of the star and planet are equal. The Lagrangian L1 is the point on the Roche lobe nearest to the planet, and it is located between the planet and the star. The distance from the center of the planet to the Lagrangian L1 is the Hill's radius and is

given by

$$R_H = a\left(\frac{M_p}{3M_*}\right)^{1/3} \tag{5.28}$$

If the ohmic dissipation in the planet is able to trigger a mass outflow, this mass will first overflow the Roche lobe through the L1 point. It will then be accreted onto the star; this mass loses angular momentum and gives angular momentum to the planet. We now explore the impact of the ohmic dissipation on the planetary mass loss rate and the associated indirect gain of planetary angular momentum. We use a basic analytical model of the internal structure of a planet and self-consistently calculate the mass loss rate. This model allows us to calculate the ohmic dissipation and mass loss rate as we vary the planet's mass, semi-major axis, the star's mass, luminosity, and dipolar strength, the tilt angle α, and the relative angular velocity ω.

We consider a very young planet which is still in the quasi-hydrostatic contraction phase. We assume that the planet has migrated to a close-in radius and experiences strong stellar irradiation (and strong tidal dissipation). At 0.04AU, the Hill's radius of a Jupiter-mass planet is about $6R_J \approx 0.47R_\odot$. The stellar flux received by the planet increases as the planet approaches the star as a^{-2}. The ohmic dissipation increases as $\mathcal{B}^2 \propto a^{-6}$ for a dipolar geometry and in the absence of any adjustment in the internal structure (in our self-consistent model, we will see that $\mathcal{P} \propto a^{-4}$). Typically, the input of energy through irradiation is larger than that due to ohmic dissipation and thus sets the planet's surface temperature.

Bodenheimer & al. investigate the radius of close-in planets in equilibrium with stellar irradiation, and with an energy source such as tidal dissipation (Bodenheimer & al. 2001 [12]). They find a relation

$$log\frac{R_p}{R_\odot} = A(M_p) + B(M_p) log\frac{W}{L_\odot} + C(M_p)\left(log\frac{W}{L_\odot}\right)^2 \tag{5.29}$$

with $(A, B, C) = (3.11, 1.01, 0.0642)$ for planetary parameters similar to HD 209458. The formula is a fit to the results from numerical simulations and is valid for an energy W between $10^{-8}L_\odot$ and $10^{-5}L_\odot$. A tidal dissipation $W_{tide} = 10^{-8}L_\odot$ corresponds to a radius $R_p \approx 0.13R_\odot$, and $W_{tide} = 10^{-5}L_\odot$ corresponds to $R_p \approx R_H$. Instead of tidal dissipation, the ohmic dissipation calculated above (which is about $10^{-5}L_\odot$) could be used to maintain the planetary radius near the Roche lobe. However, there would not be much energy left to drive a significant mass loss. Nevertheless, if the planet is still in the quasi-hydrostatic equilibrium contraction phase, a tidal energy lower than $10^{-5}L_\odot$ may be sufficient to maintain the planet near the Roche lobe. As the planet ages, its equilibrium radius (without additional heating) decreases, and more and more additional heating is required.

In the following sections, we thus adopt the most favorable conditions in order to derive the maximum mass loss rate achievable. We assume that the young planet fills its Roche lobe due to its high internal energy, a large stellar irradiation, and a large tidal dissipation. We then add the ohmic dissipation and calculate the associated mass loss rate. If the planet does not fill its Roche lobe when it starts to interact magnetically with its host star,

then part of the ohmic dissipation would first be used to inflate the planet before a mass loss can be driven.

Planetary internal structure

To calculate the planet's electric conductivity profile, We model the planet's internal structure with a polytropic interior topped by an isothermal layer in equilibrium with the stellar radiation. The strong stellar irradiation leads to an extended isothermal layer.

In the isothermal region, the equations for the state variables are

$$T(r) = constant = T_0 \tag{5.30}$$

$$P(r) = P_0\ exp\left[\frac{GM_p}{\alpha T}\left(\frac{1}{r}-\frac{1}{R_p}\right)\right] \tag{5.31}$$

$$\varrho(r) = \frac{P(r)}{\alpha T} \tag{5.32}$$

where $T_0 \approx 1500$K is determined as the black body equilibrium with the stellar radiation at 0.04AU and $\alpha = \mathcal{N}_a k_B/(\mu \mathcal{M}_H)$ (where $\mathcal{N}_a$ is the Avogadro constant, k_B the Boltzmann constant, $\mathcal{M}_H$ the hydrogen molar mass, and μ a coefficient which depends on the ionisation rate ($\mu = 1$ for hydrogen atoms, and $\mu = 0.5$ for fully ionized hydrogen gas, and we usually choose μ close to unity)). The angle between the stellar magnetic field and the stellar spin axis is also denoted α, but it is usually expressed as sin α.

In the polytropic interior we use the following equations,

$$P(r) = K\varrho^{\gamma}(r), \tag{5.33}$$

$$\frac{dP}{dr}(r) = -\frac{d\phi_g}{dr}(r)\varrho(r) \tag{5.34}$$

$$\triangle\phi_g(r) = 4\pi\ G\ \varrho(r) \tag{5.35}$$

where the value of γ is chosen below, $\phi_g = -\frac{GM_p(r)}{r}$ is the gravitational potential with $M_p(r)$ the mass contained within radius r, and $\triangle$ is the laplacian (in the Poisson equation).

Using equations (5.33), equation (5.34) becomes $K\gamma\varrho^{\gamma-1}(r)\frac{d\rho}{dr}(r) = -\varrho(r)\frac{d\phi_g}{dr}$. We then integrate and obtain $\phi_g(r) = Constant\ -\ \frac{K\gamma}{\gamma-1}\rho^{\gamma-1}(r)$. Replacing ϕ_g in the poisson equation (5.35), finally obtain,

$$\triangle\rho^{\gamma-1}(r) = -\frac{\gamma-1}{K\ \gamma}\ 4\pi G\varrho(r) \tag{5.36}$$

We use $\gamma = 2$ which reasonably approximates the internal structure and has the advantage of leading to an analytic solution (de Pater & Lissauer 2001 [29], Ogilvie & Lin 2004 [84]). In spherical coordinates, the previous equation becomes:

$$\frac{1}{r^2}\frac{d}{dr}\left(r^2\frac{d}{dr}\varrho(r)\right) = -\frac{2\pi G}{K}\varrho(r). \tag{5.37}$$

and we obtain the equations for the state variable in the polytropic region,

$$\varrho(r) = \varrho_c \frac{sinkr}{kr} \tag{5.38}$$

$$P(r) = K\varrho_c^2 \left(\frac{sinkr}{kr}\right)^2 \tag{5.39}$$

$$T(r) = \frac{P}{\alpha\varrho} = \frac{K}{\alpha}\varrho_c \frac{sinkr}{kr} \tag{5.40}$$

$$K = \frac{2\pi G}{k^2} \tag{5.41}$$

where the ϱ_c is the value of the density at the center of the planet. We call $r_=$ the boundary between the isothermal and polytropic region and solve for the three unknown ϱ_c, k, and $r_=$ using the three equations $P_{iso}(r_=) = P_{conv}(r_=)$, $T_{iso}(r_=) = T_{conv}(r_=)$, and that the total mass is equal to M_p.

Magnetic diffusivity profile

We use the following equation for the magnetic diffusivity (adapted from the Saha's equation for hydrogen, multiplied by a factor 10 to better account for the ionization of metals at low temperature and pressure ionization in the deep interior), also see section 6.3 for a more precise derivation.

$$\eta(r) = 10^{-2} \frac{\sqrt{P(r)}}{T^{3/4}(r)} exp\left(\frac{78909}{T}\right). \tag{5.42}$$

Derivation of the mass loss

We use the sound speed c_s (with $c_s^2 = dP/d\varrho \approx 10^4 T$) to relate dP/dr with $d\varrho/dr$,

$$\frac{dP}{dr} = \frac{dP}{d\varrho}\frac{d\varrho}{dr} = \frac{d\varrho}{dr}c_s^2 \tag{5.43}$$

The mass conservation in steady state $4\pi r^2 \varrho(r) \upsilon(r) = \dot{M}$ relates $d\varrho/dr$ with the gas velocity assuming that $\dot{M}$ is constant),

$$\frac{1}{\varrho}\frac{d\varrho}{dr} = -\frac{1}{r^2\upsilon}\frac{dr^2\upsilon}{dr} \tag{5.44}$$

The steady state momentum equation $\upsilon(d\upsilon/dr) + (1/\varrho)(dP/dr) = -dU/dr$ can then be re-written in a classic form (Frank et al. 2002 [42]),

$$\left(1 - \frac{c_s^2}{\upsilon^2}\right)\frac{d}{dr}\left(\frac{\upsilon^2}{2}\right) = -\frac{dU}{dr}\left(1 - \frac{2c_s^2}{r}\frac{1}{dU/dr}\right) \tag{5.45}$$

where $U(r) \approx \frac{-GM_\star}{a}\left[\left(1 - \frac{M_p}{M_\star}\right)\left(\frac{a}{a-r} + \frac{(a-r)^2}{2a^2}\right) + \frac{M_p}{M_\star}\left(\frac{a}{r} + \frac{r^2}{2a^2}\right)\right]$ is the gravitational potential for the (planet + star) system (Gu & al. 2003 [56], Murray & Dermott 2000 [82]).

The left-hand side of (5.45) is zero at the sonic point r_s (the location where the speed of the flow equals the sound speed, *i.e.* $\upsilon = c_s$), and the right hand side can thus be used to solve for r_s (assuming the sound speed is known in the isothermal region (for example using $c_s^2 \approx 10^4 T$).

Under the assumption that the mass loss is driven by the ohmic dissipation and that the stellar irradiation determines the temperature, the energy equation in steady state reduces to

$$\frac{1}{r^2}\frac{d}{dr}\left[r^2 \varrho(r)\upsilon(r)\left(\frac{\upsilon^2}{2} + h(r) + \phi_g(r)\right)\right] = \mathcal{P}_{vol} \tag{5.46}$$

where h is the enthalpy and ϕ_g is the gravitational potential (of the planet alone as felt by a gas particle). We use the mass conservation $\dot{M} = 4\pi r^2 \varrho \upsilon$ and integrate the energy equation between the Roche lobe and r_{pn}, the radius corresponding to the maximum penetration of the field into the planet,

$$\dot{M}\left[\frac{\upsilon^2}{2}(R_H) - \frac{\upsilon^2}{2}(r_{pn}) + h(R_H) - h(r_{pn}) + \phi_g(R_H) - \phi_g(r_{pn})\right] = \mathcal{P}. \tag{5.47}$$

This equation effectively links the mass loss rate with the ohmic dissipation, with the dominant term in brackets being typically $\phi_g(r_{pn})$. The conservation of mass finally links the mass loss rate with the density and velocity at the sonic point,

$$\begin{cases} \rho(r_s) = \frac{\dot{M}}{4\pi r_s^2 c_s(r_s)} \\ P(r_s) = \alpha\ \rho(r_s) T(r_s) \\ \alpha = \frac{\mathcal{N}_a k_B}{\mu \mathcal{M}_H} \end{cases} \tag{5.48}$$

where $\mathcal{N}_a$ is the Avogadro constant, k_B the Boltzmann constant, $\mathcal{M}_H$ is the hydrogen molar mass, μ a coefficient which depends on the ionisation rate ($\mu = 1$ for hydrogen atoms, and $\mu = 0.5$ for fully ionized hydrogen gas, and we usually choose μ close to unity).

5.4.2 Ohmic dissipation and mass loss for different sets of parameters

Iterative method

Using this approximative internal structure model ($T(r)$, $P(r)$, $\varrho(r)$, $\eta(r)$ profiles), we calculate the ohmic dissipation and mass loss rate while varying in turn each of the following parameters: planet's mass M_p , semi-major axis a , the star's mass M_* , luminosity L_* , and dipolar strength m , the tilt angle α, and the relative angular velocity ω. Instead of solving directly for the self-consistent solution, we instead use an iterative approach.

For a chosen initial set of parameters for the {star + planet} system (such as masses, semi-major axis, etc.), we use the polytropic and isothermal approximation to determine the corresponding internal structure of the planet $T_0(r)$, $P_0(r)$, $\varrho_0(r)$, and $\eta_0(r)$ (here, the subscripts refer to the iteration step). We then calculate successively the ohmic dissipation $\mathcal{P}_0$ (corresponding to the variables with subscript 0 using the method outlined in sections 2 and 3), the corresponding mass loss rate $\dot{M}_0$ using the energy equation (5.47), the values of

$\varrho_1(r_s)$ and $P_1(r_s)$ at the sonic point (which is determined from the momentum equation). These values of density and pressure finally serve to determine the variables $(T_1, P_1, \varrho_1, \sigma_1$ in the isothermal region. The variables in the polytropic region are then obtained by continuity at the isothermal-polytropic boundary. Having thus obtained the new profiles $T_1(r)$, $P_1(r)$, $\varrho_1(r)$, and $\eta_1(r)$, we pursue the iteration until the ohmic dissipation and mass loss rate reach an equilibrium.

We then vary some of the parameter(s) (*e.g.* M_p), and iterate again until we obtain the ohmic dissipation and mass loss rate corresponding to this new set of parameters for the {planet + star} system. We also verified that the convergence is robust in the sense that artificially changing, for example, the ohmic dissipation during one of the iterations does not affect the final value. Similarly, we also verified that the values after convergence of the mass loss rate and ohmic dissipation depend only on the chosen set of parameters (but do not depend on the starting point of the iterations).

$\mathcal{P}$ and $\dot{M}$ as a function of planetary and stellar parameters

We plot the equilibrium values of $\mathcal{P}$ and $\dot{M}$ in the graphs presented in figures (5.3) and (5.4). From each group of plots, we also obtain $\mathcal{P}$ and $\dot{M}$ as a power law depending on the parameter that is being varied, all the others being kept constant at the value of the fiducial model given above. These functions are given in the table below (table 5.3).

Mass loss, angular momentum exchange, and planetary migration

The mass loss rate associated with the fiducial parameters $M_p = 1.63 M_J$, $a = 0.04 AU$, $M_* = M_\odot$, $L_* = 1.5 L_\odot$, $sin\alpha = 1$, $\omega = 10^{-5}\text{s}^{-1}$, and $m = 4 \times 10^{34}$ Am^2 (*i.e.* a field strength at the location of the planet or $\mathcal{B}_*(a) \approx 180$G) is $\dot{M} \approx 10^{13}$ kgs^{-1}. If we assume that a large fraction of this mass loss is accreted onto the star through the L1 point, we can link the mass loss with the variation of semi-major axis (Gu et al. 2003 [56]),

$$\frac{\dot{a}}{a} = -2\frac{\dot{M}}{Mp} \tag{5.49}$$

This exchange of angular momentum therefore acts on a time scale τ a few times $M_p/\dot{M}$, *i.e.* a few 10^6 years. Such angular momentum exchange is thus comparable to that needed to stall the early migration within 0.04AU during the TTauri phase (assuming a strong magnetic dipole $m = 4 \times 10^{34}$Am^2).

Attempts toward generalized power laws

The exponents calculated in table (5.3) correspond to variations of only one parameter at a time. In order to extrapolate to any specific real hot-Jupiter, it would be interesting to see if the exponents could be brought together into a single power law. If the variables are separable and each contribute independently to the ohmic dissipation and mass loss, we would get the following relations,

Ohmic dissipation rate $\mathcal{P}$ and mass loss rate $\dot{M}$	Varying Parameter
$\mathcal{P}_1 = 3.3 \times 10^{21} \left(\frac{M_p}{0.63\ M_J}\right)^{2.16}$ W $\dot{M}_1 = 1.2 \times 10^{13} \left(\frac{M_p}{0.63\ M_J}\right)^{2.4}$ kg s^{-1}	$0.25\ M_J \leq M_p \leq 1.7\ M_J$
$\mathcal{P}_2 = 3.3 \times 10^{21} \left(\frac{a}{0.04\ AU}\right)^{-4}$ W $\dot{M}_2 = 1.2 \times 10^{13} \left(\frac{a}{0.4\ AU}\right)^{-3.8}$ kg s^{-1}	$0.015\ AU \leq a \leq\ 0.08\ AU$
$\mathcal{P}_3 = 3.5 \times 10^{21} \left(\frac{\lvert\omega\rvert}{10^{-5}}\right) - 1.5 \times 10^{20}$ W $\dot{M}_3 = 1.4 \times 10^{13} \left(\frac{\lvert\omega\rvert}{10^{-5}}\right) - 1.3 \times 10^{12}$kg s^{-1}	$7 \times 10^{-6} \leq \lvert\omega\rvert \leq\ 7.3 \times 10^{-5}$
$\mathcal{P}_4 = 3.3 \times 10^{21} \left(\frac{m}{4\times10^{34}}\right)^{2.18}$ W $\dot{M}_4 = 1.2 \times 10^{13} \left(\frac{m}{4\times10^{34}}\right)^{2.3}$ kg s^{-1}	$6 \times 10^{33} \leq m \leq\ 4 \times 10^{34}$
$\mathcal{P}_5 = 3.3 \times 10^{21} \sin^{2.17}(\alpha)$ W $\dot{M}_5 = 1.2 \times 10^{13} \sin^{2.28}(\alpha)$kg s^{-1}	$0.3 \leq \sin(\alpha) \leq 1$
$\mathcal{P}_6 = 3.3 \times 10^{21} \left(\frac{M_\star}{M_\odot}\right)^{-0.53}$ W $\dot{M}_6 = 1.2 \times 10^{13} \left(\frac{M_\star}{M_\odot}\right)^{-0.5}$ kg s^{-1}	$0.5\ M_\odot \leq M_\star \leq\ 1.5\ M_\odot$
$\mathcal{P}_7 = 3.3 \times 10^{21} \left(\frac{L_\star}{1.5\ L_\odot}\right)^{-0.5}$W $\dot{M}_7 = 1.2 \times 10^{13} \left(\frac{L_\star}{1.5\ L_\odot}\right)^{-0.8}$ kg s^{-1} $\mathcal{P}_7 = 7.5 \times 10^{19} \left(\frac{L_\star}{1.5\ L_\odot}\right)^{5.9}$W $\dot{M}_7 = 1.25 \times 10^{11} \left(\frac{L_\star}{1.5\ L_\odot}\right)^{5.8}$ kg s^{-1}	$0.5\ L_\odot \leq L_\star \leq\ 2.6\ L_\odot$ $2.6\ L_\odot \leq L_\star \leq\ 5\ L_\odot$

Table 5.3: Table giving $\mathcal{P}$ and $\dot{M}$ as a function of the parameter that is being varied.

$$\mathcal{P} = 3.3 \times 10^{21} W \left(\frac{M_p}{0.63\ M_J}\right)^{2.2} \left(\frac{a}{0.04\ AU}\right)^{-4} \left[\left(\frac{|\omega|}{10^{-5}\mathrm{s}^{-1}} - 0.045\right)\right] \left(\frac{m}{4 \times 10^{34}\mathrm{A\ m}^2}\right)^{2.2} (\sin\ \alpha)^{2.2} \left(\frac{M_\star}{M_\odot}\right)^{-0.5} \left(\frac{L_\star}{1.5\ L\odot}\right)^{-0.5} \tag{5.50}$$

$$\dot{\mathcal{M}} = 1.2 \times 10^{13}\mathrm{kg\ s}^{-1} \left(\frac{M_p}{0.63\ M_J}\right)^{2.4} \left(\frac{a}{0.04\ AU}\right)^{-3.8} \left[\left(\frac{|\omega|}{10^{-5}\mathrm{s}^{-1}} - 0.1\right)\right] \left(\frac{m}{4 \times 10^{34}\mathrm{A\ m}^2}\right)^{2.3} (\sin\ \alpha)^{2.3} \left(\frac{M_\star}{M_\odot}\right)^{-0.5} \left(\frac{L_\star}{1.5\ L\odot}\right)^{-0.8}. \tag{5.51}$$

We test these laws against our numerical model. The first set of parameters that we consider is $M_p = 1.5 M_J$ and $a = 0.03 AU$, all the other parameters being kept equal to the fiducial parameters with the TTauri star. The numerical calculation yields $\mathcal{P} = 4.2 \times 10^{22}$W and $\dot{\mathcal{M}} = 1.5 \times 10^{14}$kg s^{-1}. Using the formula under the assumption of separation of variables, we get $\mathcal{P} = 7 \times 10^{22}$W and $\dot{\mathcal{M}} = 2.9 \times 10^{14}$kg s^{-1}.

We now consider a set of parameters in which all parameters are taken different from their fiducial values: $M_p = 1.5 M_J$, $a = 0.03 AU$, $\omega = 2.9 \times 10^{-5} s^{-1}$, $m = 2 \times 10^{34}\ Am^2$, $M_\star = 1.5 M_\odot, _\star = 0.8_\odot$ (the value of ω corresponds, for example, to a system in which the planet is at Keplerian augular velocity and the star has a period of 1 or 4 days). The numerical calculation yields $\mathcal{P} = 1.7 \times 10^{22}$W and $\dot{\mathcal{M}} = 7 \times 10^{13}$kg s^{-1}. Under the assumption of separation of variables, we get from the generalized formula $\mathcal{P} = 3.5 \times 10^{22}$W and $\dot{\mathcal{M}} = 1.6 \times 10^{14}$kg s^{-1}, which again is not exact but a reasonable order of magnitude estimate (within a factor of a few).

The assumption of separation of variables is, therefore, only approximative, but nevertheless may provide a quick estimate (only at the level of order of magnitude) of the ohmic dissipation and mass loss under the assumptions outlined above. Nevertheless, even if a more exact generalized formula is still unknown, the iterative procedure described above could be used to calculate the ohmic dissipation, mass loss rate, and gain of angular momentum for any given set of parameters.

5.5 Concluding remarks

We briefly summarize this chapter's original contributions. The semi analytical model of the time-periodic magnetic diffusion has been developed for binary stars (Campbell 1983 [20]) and applied to estimate their circularization and spin-orbit synchronization time scales. We instead use the model to study the impact of the magnetic diffusion on planetary migration. We find that the energy associated with the work of the Lorentz force is typically too weak by an order of magnitude to directly oppose type I and II planetary migration. It may nevertheless be sufficient if the system is in particularly favorable conditions (high magnetic field strength, high stellar spin rate). Of course, it may also be sufficient in

cases where the planet loses its interaction with the disk (for example when the planet is well within the magnetospheric cavity or after the disk has evaporated, cf. Papaloizou 2007 [85]). Another contribution is the introduction of the "effective skin depth" and more significantly the qualitative conclusion that the total ohmic dissipation remains fairly constant in spite of large changes in the order of magnitude of the magnetic diffusivity (it may nevertheless be interesting to test this conclusion for a variety of magnetic diffusivity profiles).

The idea that mass loss through Roche lobe overflow may increase the planet's angular momentum is not new (*e.g.* Gu et al. 2003 [56] from which we borrow equation (5.49) relating the mass loss rate and the angular momentum transfer). Our contribution lies in self-consistently relating the mass loss rate to the ohmic dissipation and in the approximative scaling relations.

5.6 Appendix

5.6.1 Equations for the $G_l(r)$

Summary

The equation of diffusion the stellar magnetic field into the planet is

$$\frac{\partial \mathcal{B}}{\partial t} = -\nabla \wedge (\eta \nabla \wedge \mathcal{B}). \tag{5.52}$$

We write the solenoidal field with axisymmetry as

$$\mathcal{B} = \nabla \wedge (\nabla \wedge (\phi \mathbf{e}_r)) \tag{5.53}$$

$$\phi = \mu_0 \left[\sum_{l,m} C_l^m G_l(r) Y_l^m(\theta, \varphi) \right] e^{i\omega t}, \tag{5.54}$$

where ϕ is decomposed on the spherical harmonics. The Y_l^m are the spherical harmonic functions, the G_l are the corresponding radial components to be determined, the C_l^m are coefficients to be determined, and $\omega = \omega_p - \omega_*$ is the synodic period.

We replace $\partial\mathcal{B}/\partial t$ by $i\omega\nabla \wedge (\nabla \wedge (\phi \mathbf{e}_r))$ in the left hand side of (5.54), and obtain after integrating equation (5.54) once,

$$i\omega \nabla \wedge (\phi \mathbf{e}_r) = -\eta \nabla \wedge \mathcal{B}. \tag{5.55}$$

Calculation of the LHS and RHS of equation (5.55)

LHS. The curl of a vector $\mathbf{A}$ in spherical coordinates is

$$\nabla \wedge \mathbf{A} = \frac{1}{r sin\theta} \left(\frac{\partial}{\partial \theta}(A_\phi sin\theta) - \frac{\partial A_\theta}{\partial \varphi} \right) \mathbf{e}_r + \frac{1}{r} \left(\frac{1}{sin\theta} \frac{\partial A_r}{\partial \varphi} - \frac{\partial}{\partial r}(r A_\varphi) \right) \mathbf{e}_\theta + \frac{1}{r} \left(\frac{\partial}{\partial r}(r A_\theta) - \frac{\partial A_r}{\partial \theta} \right) \mathbf{e}_\varphi. \tag{5.56}$$

Therefore, using $\phi \mathbf{e}_r$ in place of $\mathbf{A}$, we write

$$\nabla \wedge (\phi \mathbf{e}_r) = 0 \cdot \mathbf{e}_r + \frac{1}{r}\left[\frac{1}{sin\theta}\frac{\partial \phi}{\partial \varphi}\right]\mathbf{e}_\theta + \frac{1}{r}\left(-\frac{\partial \phi}{\partial \theta}\right)\mathbf{e}_\varphi, \tag{5.57}$$

which yields the left hand side of (5.55).

RHS. Taking the curl of the previous equation, we obtain the magnetic field $\mathcal{B} = \nabla \wedge \nabla \wedge (\phi \mathbf{e}_r)$,

$$\begin{aligned}
\mathcal{B}_r &= \frac{1}{rsin\theta}\left\{\frac{\partial}{\partial \theta}\left[\frac{1}{r}\left(-\frac{\partial \phi}{\partial \varphi}\right)sin\theta\right] - \frac{\partial}{\partial \varphi}\left[\frac{1}{rsin\theta}\frac{\partial \phi}{\partial \varphi}\right]\right\} \stackrel{def}{=} -\nabla^2\phi = \frac{l(l+1)}{r^2}\phi \\
\mathcal{B}_\theta &= \frac{1}{r}\left[-\frac{\partial}{\partial r}\left(-\frac{\partial \phi}{\partial \theta}\right)\right] = \frac{1}{r}\frac{\partial^2 \phi}{\partial r \partial \theta} \\
\mathcal{B}_\varphi &= \frac{1}{r}\left[\frac{\partial}{\partial r}\left(\frac{1}{sin\theta}\frac{\partial \phi}{\partial \varphi}\right)\right] = \frac{1}{rsin\theta}\frac{\partial^2 \phi}{\partial r \partial \varphi}.
\end{aligned} \tag{5.58}$$

The second equal sign in the expression for $\mathcal{B}_r$ is by definition of the laplacian of a scalar, and the third is from $r^2\nabla^2 Y_l^m = -l(l+1)Y_l^m$.

From the previous set of equation, we can thus write as an intermediate summary,

$$\begin{aligned}
\mathcal{B}_r &= -\nabla^2\phi = \frac{l(l+1)}{r^2}\phi \\
\mathcal{B}_\theta &= \frac{1}{r}\frac{\partial^2 \phi}{\partial r \partial \theta} \\
\mathcal{B}_\varphi &= \frac{1}{rsin\theta}\frac{\partial^2 \phi}{\partial r \partial \varphi}.
\end{aligned} \tag{5.59}$$

We interrupt here the flow of the calculation in order to derive a relationship useful for the calculation. We can express the magnetic field with a potential scalar ψ such that $\mathcal{B} = -\nabla\psi$. Using the previous set of equation, we can thus also write the following relationship between the potential scalar ψ and the poloidal scalar ϕ,

$$\psi = -\frac{\partial \phi}{\partial r}. \tag{5.60}$$

We now turn back to the calculation of the right hand side of equation (5.55). We take the curl of the set of equations (5.59) (by using the components of $\mathcal{B}$ obtained in equation (5.59) instead of $\mathbf{A}$ in equation (5.56)), simplify it, and obtain the right hand side of (5.55).

$$-\eta\left(\nabla \wedge \mathcal{B}\right)_r = 0 \tag{5.61}$$

$$-\eta\left(\nabla \wedge \mathcal{B}\right)_\theta = \frac{-\eta}{rsin\theta}\frac{\partial}{\partial \varphi}\left(\frac{l(l+1)}{r^2}\phi\right) + \frac{\eta}{r}\frac{\partial}{\partial r}\left(\frac{1}{sin\theta}\frac{\partial^2 \phi}{\partial r \partial \varphi}\right) \tag{5.62}$$

$$-\eta\left(\nabla \wedge \mathcal{B}\right)_\varphi = \frac{-\eta}{r}\frac{\partial}{\partial r}\left(\frac{\partial^2 \phi}{\partial r \partial \theta}\right) + \frac{\eta}{r}\frac{\partial}{\partial \theta}\left(\frac{l(l+1)}{r^2}\phi\right). \tag{5.63}$$

As a reminder, we showed (see equation (5.57)) that the LHS of equation (5.55) is

$$i\omega\nabla \wedge (\phi \mathbf{e}_r) = 0 \cdot \mathbf{e}_r + \frac{i\omega}{rsin\theta}\frac{\partial \phi}{\partial \varphi}\mathbf{e}_\theta - \frac{i\omega}{r}\frac{\partial \phi}{\partial \theta}\mathbf{e}_\varphi. \tag{5.64}$$

We can now equate the left hand side (equation (5.64)) and right hand side (equation (5.63)) of equation (5.55) (which is simply an integrated version of the magnetic diffusion equation). Identifying the terms in the RHS (equation 5.63) and LHS (equation 5.64) along the $\mathbf{e}_\theta$ direction, we obtain

$$\frac{i\omega}{rsin\theta}\frac{\partial\phi}{\partial\varphi} = \frac{-\eta}{rsin\theta}\frac{\partial}{\partial\varphi}\left(\frac{l(l+1)}{r^2}\phi\right) + \frac{\eta}{r}\frac{\partial}{\partial r}\left(\frac{1}{sin\theta}\frac{\partial^2\phi}{\partial r\partial\varphi}\right). \tag{5.65}$$

Finally, we now use again the decomposition of the poloidal scalar in spherical harmonics $\phi = \mu_0 \sum_{l,m} C_l^m G_l(r) Y_l^m(\theta,\varphi) e^{i\omega t}$, which we insert into the previous equation and find

$$\mu_0 \sum_{l,m} C_l^m \left[\frac{d^2G}{dr^2} - \left(\frac{l(l+1)}{r^2} + \frac{i\omega}{\eta}\right) G\right] \frac{\partial Y_l^m}{\partial\theta}(\theta,\varphi) e^{i\omega t} = 0 \tag{5.66}$$

(identifying the terms along the $\mathbf{e}_\varphi$ direction would yield the same equation).

We therefore obtain the equations for $G_l(r)$ inside the planet (with $0 < \eta < \infty$) and outside the planet (with $\eta = \infty$),

$$\frac{d^2G}{dr^2} - \left(\frac{l(l+1)}{r^2} + \frac{i\omega}{\eta}\right) G = 0 \tag{5.67}$$

$$\frac{d^2G}{dr^2} - \left(\frac{l(l+1)}{r^2}\right) G = 0. \tag{5.68}$$

5.6.2 Equations for the stellar poloidal scalar outside the planet

We write $\mathbf{m} = (sin\alpha cos\omega t, sin\alpha sin\omega t, sin\alpha)$ and $\mathbf{r}_0 = \mathbf{a} + \mathbf{r} = (rsin\theta sin\varphi, a - rsin\theta cos\varphi, rcos\theta)$, which leads to

$$\mathbf{m}\cdot\mathbf{r}_0 = m\left[rcos\alpha cos\theta + dsin\alpha sin\omega t + rsin\alpha sin\theta(sin\varphi cos\omega t - cos\varphi sin\omega t)\right]. \tag{5.69}$$

We also write $\mathbf{r}_0 = \mathbf{d} + \mathbf{r}$ (where $\mathbf{d}$ is the vector semi-major axis from the star to the planet), which gives $r_0^2 = d^2\left(1 - 2rsin\theta cos\varphi/d + r^2/d^2\right)$ and,

$$\frac{1}{r_0^3} = \frac{1}{d^3}\left[1 + \frac{3r}{d}sin\theta cos\varphi + \left(\frac{r}{d}\right)^2\left(\frac{15}{2}sin^2\theta cos^2\varphi - \frac{3}{2}\right) + o\left(\frac{r^2}{d^2}\right)\right]. \tag{5.70}$$

The scalar potential due to the star is $\psi_* = \frac{\mu_0\mathbf{m}\cdot\mathbf{r}_0}{4\pi r_0^3}$. In the product of $1/r_0^3$ and $\mathbf{m}\cdot\mathbf{r}_0$, we keep the terms of order r/d^3 and r^2/d^4 and drop the terms which are independent of time (which do not result in TE modes) and constant in space (as it is a scalar potential). The term of order r/d^3 is

$$\psi_1 = \frac{\mu_0 m}{4\pi d^3}\left[3rsin\alpha sin\theta cos\varphi sin\omega t + rsin\alpha sin\theta(sin\varphi cos\omega t - cos\varphi sin\omega t)\right] \tag{5.71}$$

$$= \frac{\mu_0 m}{4\pi}\frac{r}{d^3}sin\alpha sin\theta(2cos\varphi sin\omega t + sin\varphi cos\omega t) \tag{5.72}$$

$$= -\frac{\mu_0 m}{4\pi}\frac{r}{d^3}sin\alpha P_1^2(2cos\varphi sin\omega t + sin\varphi cos\omega t) \tag{5.73}$$

where $P_1^2 = -sin\theta$ is a Legendre associated polynomial.

The term of order r^2/d^4 is

$$\begin{aligned}
\psi_2 &= \frac{\mu_0 m}{4\pi d^4} r^2 sin\alpha \left[sin\omega t \left(\frac{15}{2} sin^2\theta cos^2\varphi - \frac{3}{2} \right) + 3sin^2\theta \left(cos\varphi sin\varphi cos\omega t - cos^2\varphi sin\omega t \right) \right] && (5.74)\\
&= \frac{\mu_0 m}{4\pi d^4} r^2 sin\alpha \left[sin\omega t \left(\frac{9}{2} sin^2\theta cos^2\varphi - \frac{3}{2} \right) + cos\omega t \left(\frac{3}{2} sin^2\theta sin2\varphi \right) \right] && (5.75)\\
&= \frac{3}{2} \frac{\mu_0 m}{4\pi d^4} r^2 sin\alpha \left[sin\omega t \left(3sin^2\theta \left(\frac{1+cos2\varphi}{2} \right) - 1 \right) + cos\omega t \left(sin^2\theta sin2\varphi \right) \right] && (5.76)\\
&= \frac{3}{2} \frac{\mu_0 m}{4\pi d^4} r^2 sin\alpha \left[sin\omega t \left(\frac{3}{2} sin^2\theta cos2\varphi - \frac{(3cos^2\theta - 1)}{2} \right) + \frac{1}{3} cos\omega t \left(3sin^2\theta sin2\varphi \right) \right] && (5.77)\\
&= \frac{3}{2} \frac{\mu_0 m}{4\pi d^4} r^2 sin\alpha \left[sin\omega t \left(\frac{1}{2} P_2^2 cos2\varphi - P_2^0 \right) + \frac{1}{3} cos\omega t \left(P_2^2 sin2\varphi \right) \right] && (5.78)
\end{aligned}$$

where $P_2^2 = 3sin^2\theta$ and $P_2^0 = (3cos^2\theta - 1)/2$ are Legendre associated polynomials. The stellar potential scalar $\psi_* = \psi_1 + \psi_2$ is thus

$$\begin{aligned}
\psi_* &= -\frac{\mu_0 m}{4\pi} \frac{r}{d^3} sin\alpha P_1^2 (2cos\varphi sin\omega t + sin\varphi cos\omega t)\\
&+ \frac{3}{2} \frac{\mu_0 m}{4\pi d^4} r^2 sin\alpha \left[sin\omega t \left(\frac{1}{2} P_2^2 cos2\varphi - P_2^0 \right) + \frac{1}{3} cos\omega t \left(P_2^2 sin2\varphi \right) \right] && (5.79)
\end{aligned}$$

5.6.3 Set of linear equations for $\{C_l^m$, α, β, and $\gamma\}$

μ_l^m and ν_l^m are respectively the real and imaginary parts of C_l^m; α_1, α_2,α_3,α_4, γ_1, γ_2, γ_3, and γ_4 are coefficients in the expression of the induced poloidal scalar ϕ_p inside the planet. The linear set of equation that we solved for the coefficients (μ_1^1, μ_1^{-1}, ν_1^1, ν_1^{-1}, α_1, α_2,α_3,α_4), (μ_2^0, ν_2^0, β_1,β_2), and (μ_2^2, μ_2^{-2}, ν_2^2, ν_2^{-2}, γ_1, γ_2, γ_3, γ_4). The values of $G_l(r)$ considered are for $r = R_p$ the radius of the planet.

$$\begin{cases}
(\mu_1^1 - \mu_1^{-1}) Re(G_1) + (-\nu_1^1 + \nu_1^{-1}) Im(G_1) - \alpha_2 \frac{1}{R_p} \sqrt{\frac{8\pi}{3}} = 0\\
(-\nu_1^1 - \nu_1^{-1}) Re(G_1) + (-\mu_1^1 - \mu_1^{-1}) Im(G_1) - \alpha_4 \frac{1}{R_p} \sqrt{\frac{8\pi}{3}} = \frac{m \ sin\alpha}{8\pi \ d^3} R_p^2 \sqrt{\frac{8\pi}{3}}\\
(-\nu_1^1 + \nu_1^{-1}) Re(G_1) + (-\mu_1^1 + \mu_1^{-1}) Im(G_1) - \alpha_1 \frac{1}{R_p} \sqrt{\frac{8\pi}{3}} = 2\frac{m \ sin\alpha}{8\pi \ d^3} R_p^2 \sqrt{\frac{8\pi}{3}}\\
(-\mu_1^1 - \mu_1^{-1}) Re(G_1) + (\nu_1^1 + \nu_1^{-1}) Im(G_1) - \alpha_3 \frac{1}{R_p} \sqrt{\frac{8\pi}{3}} = 0\\
(\mu_1^1 - \mu_1^{-1}) Re(\dot{G_1}) + (-\nu_1^1 + \nu_1^{-1}) Im(\dot{G_1}) + \alpha_2 \frac{1}{R_p^2} \sqrt{\frac{8\pi}{3}} = \frac{m \ sin\alpha}{8\pi \ d^3} 2R_p \sqrt{\frac{8\pi}{3}}\\
(-\nu_1^1 - \nu_1^{-1}) Re(\dot{G_1}) + (-\mu_1^1 - \mu_1^{-1}) Im(\dot{G_1}) + \alpha_4 \frac{1}{R_p^2} \sqrt{\frac{8\pi}{3}} = 2\frac{m \ sin\alpha}{8\pi \ d^3} 2R_p \sqrt{\frac{8\pi}{3}}\\
(-\nu_1^1 + \nu_1^{-1}) Re(\dot{G_1}) + (-\mu_1^1 + \mu_1^{-1}) Im(\dot{G_1}) + \alpha_1 \frac{1}{R_p^2} \sqrt{\frac{8\pi}{3}} = 0\\
(-\mu_1^1 - \mu_1^{-1}) Re(\dot{G_1}) + (\nu_1^1 + \nu_1^{-1}) Im(\dot{G_1}) + \alpha_3 \frac{1}{R_p^2} \sqrt{\frac{8\pi}{3}} = 0
\end{cases} \qquad (5.80)$$

$$\begin{cases} (\mu_2^2+\mu_2^{-2})Re(G_2(R_p))+(-\nu_2^2-\nu_2^{-2})Im(G_2(R_p))-\gamma_2\frac{1}{R_p^2}12\sqrt{\frac{2\pi}{15}}=0 \\ (-\nu_2^2+\nu_2^{-2})Re(G_2(R_p))+(-\mu_2^2+\mu_2^{-2})Im(G_2(R_p))-\gamma_4\frac{1}{R_p^2}12\sqrt{\frac{2\pi}{15}}=-\frac{1}{3}\frac{m\ \sin\alpha}{8\pi\ d^4}R_p^3 12\sqrt{\frac{2\pi}{15}} \\ (-\nu_2^2-\nu_2^{-2})Re(G_2(R_p))+(-\mu_2^2-\mu_2^{-2})Im(G_2(R_p))-\gamma_1\frac{1}{R_p^2}12\sqrt{\frac{2\pi}{15}}=-\frac{1}{2}\frac{m\ \sin\alpha}{8\pi\ d^4}R_p^3 12\sqrt{\frac{2\pi}{15}} \\ (-\mu_2^2+\mu_2^{-2})Re(G_2(R_p))+(\nu_2^2-\nu_2^{-2})Im(G_2(R_p))-\gamma_3\frac{1}{R_p^2}12\sqrt{\frac{2\pi}{15}}=0 \\ (\mu_2^2+\mu_2^{-2})Re(\dot{G}_2\ (R_p))+(-\nu_2^2-\nu_2^{-2})Im(\dot{G}_2\ (R_p))+2\gamma_2\frac{1}{R_p^3}12\sqrt{\frac{2\pi}{15}}=0 \\ (-\nu_2^2+\nu_2^{-2})Re(\dot{G}_2\ (R_p))+(-\mu_2^2+\mu_2^{-2})Im(\dot{G}_2\ (R_p))+2\gamma_4\frac{1}{R_p^3}12\sqrt{\frac{2\pi}{15}}=-\frac{m\ \sin\alpha}{8\pi\ d^4}R_p^2 12\sqrt{\frac{2\pi}{15}} \\ (-\nu_2^2-\nu_2^{-2})Re(\dot{G}_2\ (R_p))+(-\mu_2^2-\mu_2^{-2})Im(\dot{G}_2\ (R_p))+2\gamma_1\frac{1}{R_p^3}12\sqrt{\frac{2\pi}{15}}=-\frac{3}{2}\frac{m\ \sin\alpha}{8\pi\ d^4}R_p^2 12\sqrt{\frac{2\pi}{15}} \\ (-\mu_2^2+\mu_2^{-2})Re(\dot{G}_2\ (R_p))+(\nu_2^2-\nu_2^{-2})Im(\dot{G}_2\ (R_p))+2\gamma_3\frac{1}{R_p^3}12\sqrt{\frac{2\pi}{15}}=0 \end{cases} \tag{5.81}$$

$$\begin{cases} \mu_2^0 Re(G_2(R_p))-\nu_2^0 Im(G_2(R_p))-\beta_2\frac{1}{R_P^2}\sqrt{\frac{4\pi}{5}}=0 \\ -\nu_2^0 Re(G_2(R_p))-\mu_2^0 Im(G_2(R_p))-\beta_1\frac{1}{R_P^2}\sqrt{\frac{4\pi}{5}}=\sqrt{\frac{4\pi}{5}}\frac{m\ \sin\alpha}{8\pi\ d^4}R_p^3 \\ \mu_2^0 Re(\dot{G}_2\ (R_p))-\nu_2^0 Im(\dot{G}_2\ (R_p))+\beta_2\frac{2}{R_P^3}\sqrt{\frac{4\pi}{5}}=0 \\ -\nu_2^0 Re(\dot{G}_2\ (R_p))-\mu_2^0 Im(\dot{G}_2\ (R_p))+\beta_1\frac{2}{R_P^3}\sqrt{\frac{4\pi}{5}}=\sqrt{\frac{4\pi}{5}}\frac{m\ \sin\alpha}{8\pi\ d^4}3R_p^2 \end{cases} \tag{5.82}$$

5.6.4 Ohmic dissipation

The ohmic dissipation is,

$$\mathcal{P}=\int_r <\mathcal{P}_{\theta,\varphi}> r^2 dr \tag{5.83}$$

where $<\mathcal{P}_{\theta,\varphi}>$ is given by

$$\begin{aligned} <\mathcal{P}_{\theta,\varphi}>=\frac{\mu_0\omega^2}{\eta r^2}\Big\{&\cos^2\omega t\left[\left(A_{11}^2+A_{12}^2\right)+3\left(A_{17}^2+A_{18}^2\right)+\frac{3}{\pi}A_{15}^2\right] \\ &+\sin^2\omega t\left[\left(A_{13}^2+A_{14}^2\right)+3\left(A_{19}^2+A_{20}^2\right)+\frac{3}{\pi}A_{16}^2\right] \\ &+\sin\omega t\cos\omega t\left[\left(A_{12}A_{14}+A_{11}A_{13}\right)+3\left(A_{17}A_{19}+A_{18}A_{20}\right)+\frac{3}{\pi}A_{15}A_{16}\right]\Big\}. \end{aligned}$$

and the A_{ij} are give by,

$$\begin{cases} A_{11}(r) \overset{def}{=} (\nu_1^1 - \nu_1^{-1})Re(G_1(r)) + (\mu_1^1 - \mu_1^{-1})Im(G_1(r)) \\ A_{12}(r) \overset{def}{=} (\mu_1^1 + \mu_1^{-1})Re(G_1(r)) - (\nu_1^1 + \nu_1^{-1})Im(G_1(r)) \\ A_{13}(r) \overset{def}{=} (\mu_1^1 - \mu_1^{-1})Re(G_1(r)) - (\nu_1^1 - \nu_1^{-1})Im(G_1(r)) \\ A_{14}(r) \overset{def}{=} -(\nu_1^1 + \nu_1^{-1})Re(G_1(r)) - (\mu_1^1 + \mu_1^{-1})Im(G_1(r)) \\ A_{15}(r) \overset{def}{=} \nu_2^0 Re(G_2(r)) + \mu_2^0 Im(G_2(r)) \\ A_{16}(r) \overset{def}{=} \mu_2^0 Re(G_2(r)) - \nu_2^0 Im(G_2(r)) \\ A_{17}(r) \overset{def}{=} (\nu_2^2 + \nu_2^{-2})Re(G_2(r)) + (\mu_2^2 + \mu_2^{-2})Im(G_2(r)) \\ A_{18}(r) \overset{def}{=} (\mu_2^2 - \mu_2^{-2})Re(G_2(r)) + (-\nu_2^2 + \nu_2^{-2})Im(G_2(r)) \\ A_{19}(r) \overset{def}{=} (\mu_2^2 + \mu_2^{-2})Re(G_2(r)) - (\nu_2^2 + \nu_2^{-2})Im(G_2(r)) \\ A_{20}(r) \overset{def}{=} (-\nu_2^2 + \nu_2^{-2})Re(G_2(r)) - (\mu_2^2 - \mu_2^{-2})Im(G_2(r)) \end{cases} \tag{5.84}$$

5.6.5 Table of symbols

$\mathcal{B}_*$, m	Stellar dipolar magnetic field, Stellar magnetic dipole
α	Tilt angle (angle between the stellar magnetic dipole m and the stellar spin axis)
$m_\perp$	Component of the dipole perpendicular to the stellar spin axis ($m_\perp = msin\alpha$)
$m_\parallel$	Component of the dipole in the direction parallel to the stellar spin axis ($m_\parallel = mcos\alpha$)
ψ_*	Stellar magnetic scalar potential ($\mathcal{B}_* = -\nabla\psi_*$)
A_*	Stellar magnetic vector potential ($\mathcal{B}_* = \nabla \wedge A_*$)
ϕ	Potential scalar ($\mathcal{B} = \nabla \wedge (\nabla \wedge (\phi e_r))$
ϕ_*	Potential scalar outside of the planet due to the stellar field
ϕ_p	Potential scalar outside of the planet due to the field induced in the planet
$\phi_* + \phi_p$	Total potential scalar outside the planet
$(\alpha_i\ \beta_i\ \gamma_i)$	Unknown coefficients in ϕ_p (α_1,α_2,α_3,α_4,β_1,β_2,γ_1,γ_2,γ_3,γ_4)
P_1^1,P_2^0,P_2^2	Legendre Associated Polynomials (involved in ϕ_*)
$Y_l^m(\theta, \varphi)$	Spherical harmonics function (in the decomposition of ϕ inside the planet)
$G_l(r)$	Radial dependence of the decomposition of ϕ inside the planet
C_l^m	Coefficients in the decomposition of ϕ inside the planet
Y_1, Y_2	$G(r) = Y_1(r) + iY_2(r)$ (real and imaginary parts; indices l are implied)
Y_3, Y_4	$G'(r) = Y_3 + iY_4$ (time derivaties; indices l implied)
μ_l^m, ν_l^m	$C_l^m = \mu_l^m + i\nu_l^m$ (real and imaginary parts)

ω, ω_p, ω_*	Synodic angular velocity, planet's orbital angular velocity, stellar spin angular velocity
$\mathbf{d}$	Vector from the center of the star to the center of the planet
$\mathbf{r}$	Vector position centered on the planet
$\mathbf{r}_0$	Vector position centered on the star ($\mathbf{r}_0 = \mathbf{d} + \mathbf{r}$)
μ_0	Vacuum magnetic permeability
$\sigma(r)$	Electric conductivity profile in the planet
$\eta(r)$	Magnetic diffusivity profile in the planet ($\eta = (\mu_0\sigma(r))^{-1}$)
M_p,R_p,a	Mass of the planet, Radius of the planet, semi-major axis
M_*,R_*,L_*	Mass, Radius, and Luminosity of the star
$R_\odot$,$L_\odot$	Solar radius and luminosity
δ_0	Standard formula for the skin depth ($\delta_0 = \sqrt{2\eta/\omega}$)
$H(r)$	Scale height of the magnetic diffusivity
r_{eff}	Estimate of the radius where the stellar field diffusion stops, $H(r_{eff}) = \sqrt{2\eta(r_{eff})/\omega}$
$\mathcal{P}_{vol}$	Ohmic dissipation per unit volume
$< \mathcal{B}_{\theta,\varphi} >$	$\mathcal{P}_{vol}$ integrated over θ and φ
$\mathcal{P}$	Total ohmic dissipation (units: Watts)
T,P,ϱ,ϱ_c	Temperature, Pressure, density profiles in the planet, and density at the center of planet
K, γ, k	Coefficients in the polytropic equation ($P(r) = K\varrho^\gamma(r)$) and ($\varrho(r) = \varrho_c sin(kr)/kr$)
$r_=$	Transition radius between the isothermal and polytropic layers of the planet
P_{iso},T_{iso}	T and P profiles in the isothermal layers of the planet
P_{conv},T_{conv}	T and P profiles in the convective (polytropic) layers of the planet
h	Volumic enthalpy of the gas in the planet
ϕ_g	Gravitational potential of the gas in the gravitational field of the planet
$U(r)$	Gravitational potential of the system {planet + star}
c_s, r_s	Sonic velocity of the gas and Sonic radius
r_{pn}	Radius in the planet where the stellar field diffusion stops (not calculated numerically)
ϕ_g	Gravitational potential of the gas in the gravitational field of the planet
$U(r)$	Gravitational potential of the system {planet + star}
k_B, $\mathcal{N}_a$	Boltzman constant, Avogadro number
α	Coefficient such that $P = \alpha\varrho T$ (perfect gas law) (not the tilt angle)
ϕ_g	Gravitational potential of the gas in the gravitational field of the planet
$U(r)$	Gravitational potential of the system {planet + star}
$\dot{M}$	Mass loss rate through Roche lobe overflow

Table 5.4: Main symbols used in the chapter.

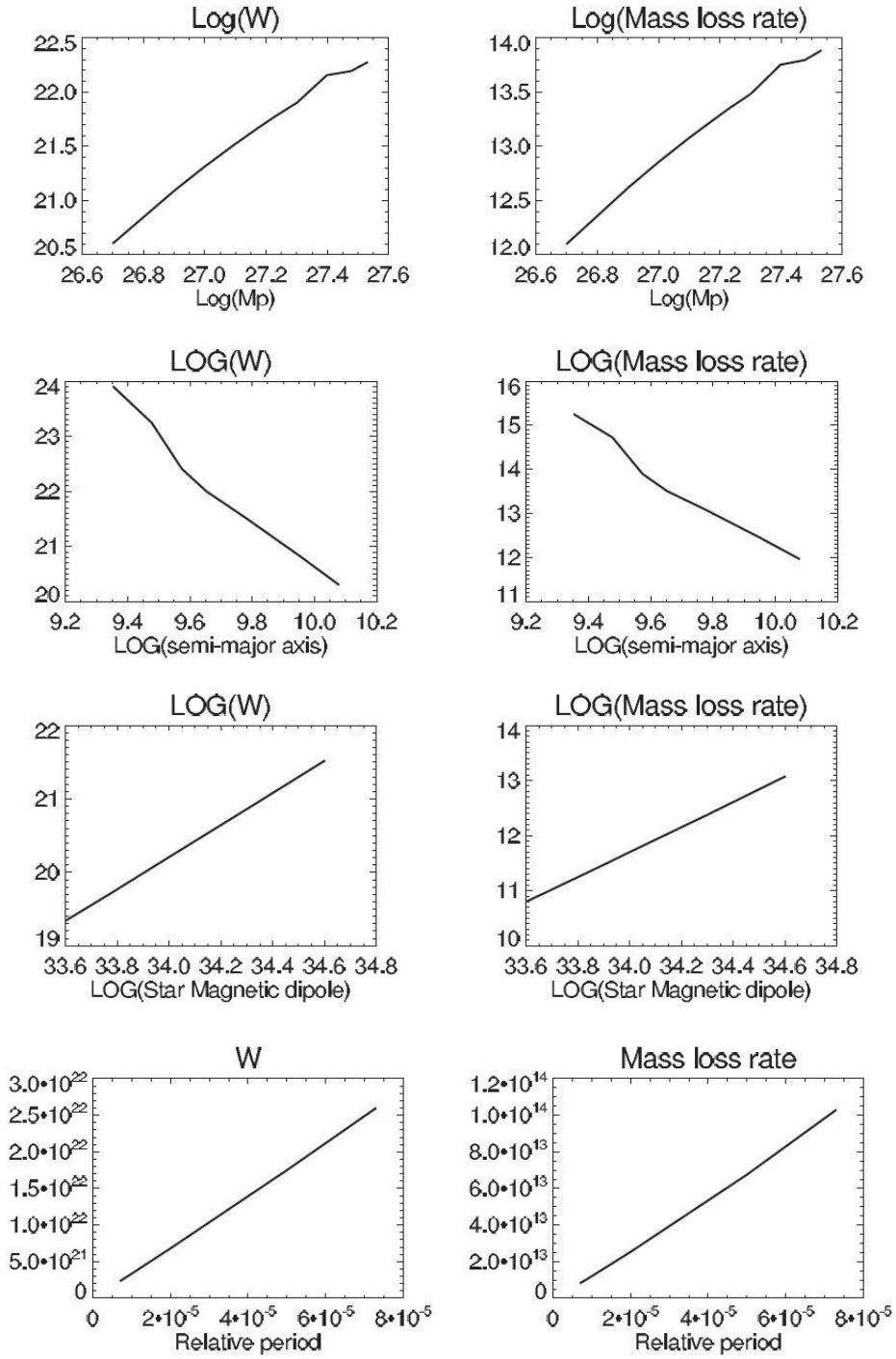

Figure 5.3: Ohmic dissipation rate (left) and mass loss rate (right) for different 1) planetary masses, 2) semi-major axes, 3) Stellar magnetic dipole strengths, 4) Relative (synodic) periods

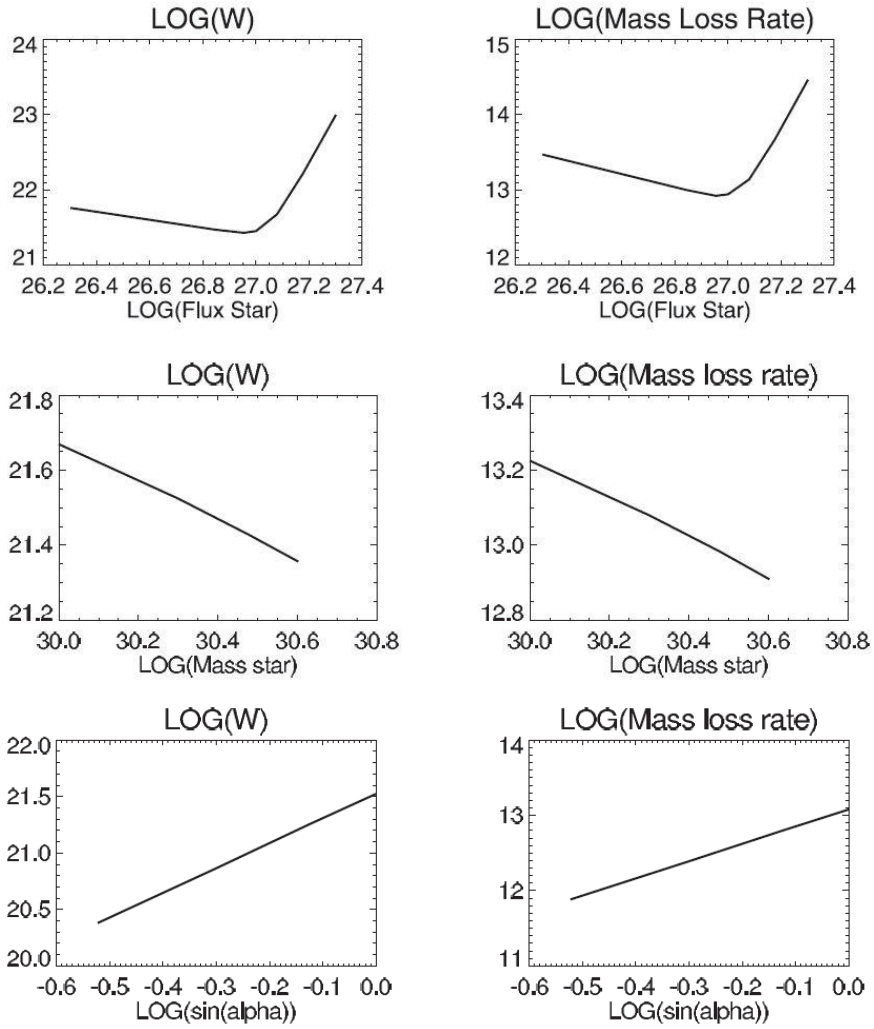

Figure 5.4: Ohmic dissipation rate (left) and mass loss rate (right) for different 5) Stellar fluxes (W) 6) Stellar masses 7) tilt angles

Chapter 6

TM mode in a close-in super-Earth and a hot-Jupiter

We now turn to the Transverse Magnetic mode, which we model as a unipolar inductor. We focus on the motional induction in the planet due to the time-independent component of the stellar magnetic dipole (generated by the component $m_{\parallel}$ of the magnetic dipole parallel to the orbital axis). As in the previous chapter, we adopt a dipolar stellar magnetic field and a planet in a close-in circular Keplerian orbit, and we assume that it is permeated by the stellar field. The motional electric field is present in any frame moving relative to the frame of the magnetosphere, but the presence of the planet introduces an electric conductivity that allows a current to flow across field lines. The charge separation induced across the planet can flow along field lines, and the electric current crosses the foot of the flux tube on the stellar surface. We describe in detail the different components of a self-consistent unipolar inductor model and derive the ohmic dissipations and Lorentz torques on the planet and star. We then apply it to two systems, an extremely inflated hot-Jupiter, and a rocky planet on an extremely close orbit. These two examples illustrate the model's potential contributions to the inflation of hot-Jupiters and to the remote sounding of the electric conductivity and thus composition of the outer layers of rocky planets. A table of the symbols (table 6.1 is provided in appendix (section 6.9.5).

Contents

Dans ce chapître, nous étudions le mode d'interaction Transverse Magnétique. Il correspond à l'induction d'une force électromotrice dans la planète dû au mouvement de la planète dans la magnétosphère de son étoile. Nous utilisons une analogie de circuit électrique correspondant à un inducteur unipolaire. Dans ce modèle, un courant induit dans la planète (par une force électromotrice) circule dans une boucle fermée constituée par la planète, le flux de tube magnétique associé à la planète, et le pied du flux de tube au niveau de l'atmosphère de l'étoile. Une analogie en circuit électrique dans laquelle le courant total est le même en tout point du circuit est valide tant que les ondes d'Alfvén se propagent rapidement pour communiquer tout changement de potentiel électrique en un point au reste du circuit.

Le modèle d'induction unipolaire est décrit dans la **section (6.2)**. Nous présentons d'abord le modèle d'inducteur unipolaire idéal (6.2.1) dans lequel la planète est représentée par un générateur idéal sans résistance interne. Nous modifions alors ce modèle pour tenir compte de la contribution de la résistance de la planète (6.2.2). La section suivante (**section (6.3)**) décrit les différents paramètres du modèle. Nous écrivons les équations permettant de calculer la conductivité électrique dans la planète et atmosphère de l'étoile ainsi qu'un systéme d'équations analytiques qui décrit simplement leur profil de temperature et pression (6.3.1). Nous présentons ensuite notre calculation de la resistance intégrée de la planète et du pied du flux de tube dans l'atmosphere stellaire (6.3.2). Nous introduisons un paramètre libre, la profondeur du pied de flux de tube, dont la valeur permet

de déterminer l'ensemble des paramètres (intensité du courant, dissipation ohmique, résistances, etc.) de facon cohérente (6.3.3). Nous présentons aussi deux conditions de validité du modèle: la condition classique de temps de trajet des ondes d'Alfvén (6.3.4), et une nouvelle condition dans laquelle la dissipation ohmique dans le pied du tube de flux, lorsqu'elle provoque une augmentation de la température et de la conductivité électrique, favorise le co-mouvement du flux de tube avec l'étoile plutôt qu'avec la planète. Cet effet rend alors la condition associée au trajet des ondes d'Alfvén plus difficile à remplir (6.3.5).

Nous analysons alors les différents sous-régimes d'interactions et illustrons chaque sous-régime par un example (6.4). Nous étudions ensuite l'effet de la dissipation ohmique et du couple de Lorentz et les comparons avec la dissipation et couple associés aux interactions gravitationelles de marées (6.5). Finalement, nous appliquons notre modèle à deux problèmes astrophysiques. Nous suggérons d'abord que le modèle d'interaction unipolaire, lorsqu'il s'applique, permet d'estimer la conductivité électrique des couches externes d'une planète solide ainsi que l' intensisté du champ magnétique stellaire. Nous illustrons cela en étudiant Kepler-78b (KIC 8435766b), une planète tellurique très proche de son étoile (6.6). Enfin, nous montrons que la dissipation ohmique associée au modèle d'induction unipolaire est suffisante pour expliquer l'aspect enflé de CoRoT-2b, une des planètes géantes proches de son étoile dont le large rayon est encore inexpliqué (6.7). Une table des symboles est fournie en appendix (table 6.1 en section 6.9.5).

6.1 Structure of the chapter

Description of the unipolar inductor model (section 6.2). We first describe the ideal unipolar inductor (**subsection 6.2.1**) which models the planet as a generator with negligible internal resistance and the footprint as an electric "load." This model is for example used in the classic paper Goldreich & Lynden-Bell 1969 [51]. The field lines threading the planet act as electric wires and the entire flux tube (field lines + plasma) is assumed to be co-moving with the planet (because of its assumed large electric conductivity relative to that in the footprint) and drifting on the stellar atmosphere. A difference of potential is induced across the planet and is communicated without change across the foot of the flux tube on the stellar atmosphere (also more concisely called "the footprint") where it drives an induced current and its associated ohmic dissipation. The planet is thus a unipolar inductor with zero resistance. In **subsection 6.2.2**, we modify this model in order to more realistically include the resistance of the planet. The field lines (and the plasma attached to them) are no longer assumed to be co-moving with the planet and drifting across the footprint. Instead, they may drift relative to both the planet and footprint, the respective relative drift depending on the electric resistances involved (the smaller the resistance of the planet compared to that of the footprint, the closer the field lines and attached plasma are to co-move with the planet and drift on the footprint, as in the case of the ideal unipolar inductor). The planet and the footprint are equivalent to two generators in series with non-negligible internal resistances. Once the integrated resistances of the planet and the footprint are calculated, the electric current, ohmic dissipation, and torque on the planet and footprint can be analytically determined.

Calculation of the resistances and validity condition (section 6.3). We describe the derivation of the resistances involved in the circuit. We start with a description of a basic analytical structure of the planet and stellar atmosphere (for the cases where a more precise determination is not available) and the corresponding electric conductivity profile (**subsection 6.3.1**). This analytical structure is appropriate for the planetary and stellar atmospheres, but it neglects pressure ionization and degeneracy in the deep planetary interior. Nevertheless, such approximation in the interior is sufficient to grasp the key physics of the interaction, does not affect the order of magnitude of the integrated resistance of the planet, and the analytical structure enables us to provide a fully self-consistent model even for systems for which the internal structure have not yet been simulated numerically.

We then introduce the integral formulas used for the calculation of the resistance of the planet and of the footprint (**subsection 6.3.2**). These integral equations are written in a formal form, and the boundaries of the integrals must be first determined. The boundaries of the integral for the planet and the upper boundary of the integral for the footprint are easily determined (**subsection 6.3.3**), but the lower boundary in the integral of the footprint is determined self-consistently with the condition of validity of the electric circuit model (cf. **subsections 6.3.4 and 6.3.5** where we calculate the Alfvén travel times).

Analysis of finer aspects of the model (sections 4 and 5). We analyze the different regimes of interaction in the unipolar inductor model in **section 4**. We also analyze the Lorentz torque and its effect on the planet's angular momentum and we compare the Lorentz torque and ohmic dissipation with the well known tidal torque and dissipation (**section 5**).

Application to astrophysical problems (sections 7 and 8). We first describe how the model may be used as a way to remotely infer the electric conductivity of the outer layers of a close-in rocky planet. We illustrate the method by estimating constraints on the electric conductivity and differentiation of Kepler-78b, a newly discovered rocky planet (**section 7**). We also apply our model to the strongly inflated hot-Jupiters. Instead of the simple analytical structure derived here, we use an internal structure of CoRoT-2b as obtained from numerical evolutionary codes and show that an interaction of the type unipolar inductor between CoRoT-2b (one of the most inflated planet relative to its mass and stellar irradiation) and its host star can provide the extra energy source needed to account for the planet's inflated radius (**section 8**).

More details about the calculation and a table of symbols (table 6.1 is provided in appendix (section 6.9.5).

6.2 Ideal and general unipolar inductor models

6.2.1 Ideal Unipolar inductor

Electric field, difference of potential, and current

This section derives the electric field, electric current, ohmic dissipation, and torque in the ideal unipolar inductor model (*e.g.* Goldreich & Lynden Bell 1969 [51]) for a close-in extrasolar planet (Laine & Lin 2012 [72]).

In the ideal unipolar inductor model, the inductor (here, the planet) is assumed to have a large electric conductivity compared to that in the rest of the electric circuit. The electric circuit equivalent is that of a generator with an internal resistance negligible compared to that of the load (we will later study the condition required for the validity of an electric circuit approximation).

We call ω_p the planet Keplerian angular velocity, ω_* the stellar spin angular velocity, $v_{p/*}$ the velocity of the planet in the frame translating around the star on the orbit of the planet but at the stellar spin angular velocity, a the semi-major axis, and $\mathcal{B}_*(a)$ the stellar magnetic field seen by the planet. In this chapter, we are interested in the magnetic interaction between the time-independent component of the stellar dipolar field and the planet in a circular Keplerian orbit. We, therefore, use the component of the magnetic dipole $m_{\|}$ which is parallel to the stellar (and orbital) axis. In this simple geometry, the magnetic field seen by the planet in the orbital plane is thus perpendicular to the orbital motion. In the frame of the planet, a motionally induced electric field $\mathcal{E}_0$ (see chapter 2) is given by

$$\mathcal{E}_0 = v_{p/*}\mathcal{B}_*(a) = (\omega_p - \omega_*)a\frac{\mu_0 m}{4\pi a^3}, \tag{6.1}$$

which corresponds to a generator that maintains a difference of potential U_0 across the diameter of the planet

$$U_0 = 2R_p\mathcal{E}_0 = 2R_p(\omega_p - \omega_*)a\frac{\mu_0 m}{4\pi a^3}. \tag{6.2}$$

In fact, because of the spherical shape of the planet, the difference of potential U depends on the geometry of the motional electric field and on the latitude and longitude

(for example, $U(\theta,\varphi) = U_0 sin\theta cos\varphi$)). The electric conductivity along the magnetic field lines is assumed to be high so that the difference of potential U_* at the foot of the flux tube in the stellar atmosphere is the same as that across the planet, *i.e.* $U_* = U_0$. We will equivalently call "the foot of the flux tube in the stellar atmosphere" as "the footprint."

The footprint is an ellipse of lengths y_* (the direction along which the current flows and across which U_* is applied) and x_* the length in the other direction (here y_* and x_* are twice the length of the axes of the ellipse)

$$y_* = \frac{1}{s} R_p \left(\frac{R_*}{a}\right)^{3/2} \tag{6.3}$$

$$x_* = 2R_p \left(\frac{R_*}{a}\right)^{3/2}, \tag{6.4}$$

where $s \stackrel{def}{=} cos\theta_F \approx \sqrt{1-\frac{R_*}{a}}$ (which is about 1 except for extremely close in systems), with θ_F the angle between the stellar spin axis and the location of the foot of the flux tube. We can also write $sin\theta_F \approx \sqrt{\frac{R_*}{a}}$. The electric field in the footprint is thus

$$\mathcal{E}_* = \frac{U_*}{y_*} = 2\frac{\mu_0 m}{4\pi a^3}(\omega_p - \omega_*) a \left(\frac{a}{R_*}\right)^{3/2} s. \tag{6.5}$$

which is independent of the radius of the planet. The cross section of the current across the footprint is $x_* d_{pn}$ where the depth of penetration d_{pn} represents the height of the footprint across which the current flows perpendicularly to the field lines. The footprint has a planar geometry since its size is small compared to the radius of the star, and the total resistance of the foot of the flux tube in the stellar atmosphere $\mathcal{R}_*$ is thus readily calculated (also see section (6.9.1))

$$\mathcal{R}_* = \frac{y_*}{x_*}\frac{1}{\Sigma_*} = \frac{1}{2s\Sigma_*}, \tag{6.6}$$

with s defined as above. We called $\Sigma_* = \int_z \sigma_p dz$ the height integrated Pedersen conductivity in the footprint, where the boundaries of integration need to be specified. In the approximation of a quasi-isothermal atmosphere, the Pedersen conductivity decreases with depth (P increases while T remains roughly constant). In that case, the integral reaches a maximum value after a few scale heights. Since the ideal unipolar inductor model assumes that the resistance of the footprint is the largest, the electric current is

$$I = \frac{U_*}{\mathcal{R}_*} = 4R_p\,(\omega_p - \omega_*)\,a\frac{\mu_0 m}{4\pi a^3}\Sigma_* s. \tag{6.7}$$

This macroscopic expression could also be derived by integrating the current density $\mathcal{J} = \sigma_p \mathcal{E}_*$.

It is also important to note that each hemisphere of the planet is considered independently with its corresponding footprint on each hemisphere of the star (for example, see figure (6.1) in which the resistances of the flux tube and planet are negligible). Therefore, the above values of the current and resistances, and the values below for the ohmic dissipation and torques are for one of the two equivalent hemispheres corresponding to two similar but independent electric circuits.

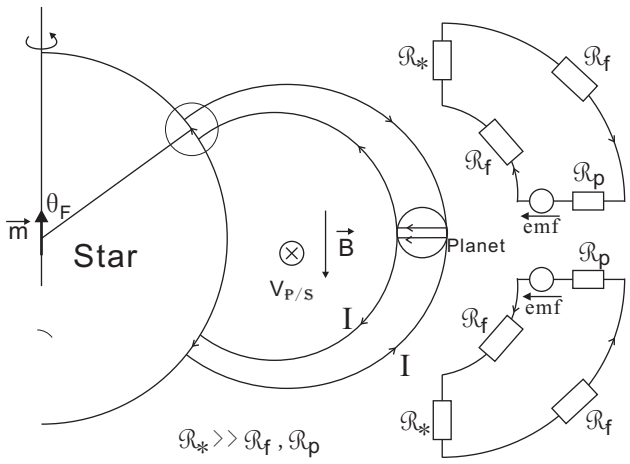

Figure 6.1: Schematic representation of the system as an electric circuit (from Laine & Lin 2012 [72], also shown earlier in this manuscript as figure 2.2). In the figure $v_{p/*}$ is written $V_{p/s}$. The figure shows the angle θ_F between the stellar spin axis and the location of the footprint on the stellar surface. In the ideal unipolar inductor model, the resistances of the planet and flux tube are neglected.

Ohmic dissipation and torque

We consider the torques on the planet and star due to the Lorentz force, with the axis of the torques being the axis of stellar spin and planetary orbital motion, and the convention for the positive direction of torques is the one corresponding to the stellar spin. The ohmic dissipation in the footprint $\mathcal{P}_*$ (*e.g.* the one on the Northern hemisphere of the star), torque on the planet (on its northern hemisphere) $\mathcal{T}_p$, and torque $\mathcal{T}_*$ exerted on one corresponding footprint are

$$\mathcal{P}_* = U_* I = \mathcal{R}_* I^2 = 8 R_p^2 (\omega_p - \omega_*)^2 a^2 \left(\frac{\mu_0 m}{4\pi a^3} \right)^2 \Sigma_* s \tag{6.8}$$

$$|\mathcal{T}_p| = \int\int\int a \wedge \mathcal{J} \wedge \mathcal{B}_*(a) dV = 8 R_p^2 a^2 \left(\omega_p - \omega_*\right) \left(\frac{\mu_0 m}{4\pi a^3} \right)^2 \Sigma_* s \tag{6.9}$$

$$|\mathcal{T}_*| = \int_x \int_y \int_z r \wedge \mathcal{J} \wedge \mathcal{B}_*(R_*) dV = |\mathcal{T}_p| \tag{6.10}$$

In the calculation of $\mathcal{T}_p$, we used $\int_{xz} \mathcal{J} dx dz = I$ and $\int_y = 2R_p$. To calculate $\mathcal{T}_*$, we used $\int_y dy = y_*$, $\int_{xz} \mathcal{J} dx dz = \mathcal{I}$, $r = R_* sin\theta_F$, $\mathcal{B}_*(R_*) = 2\mu_0 m cos\theta_F / (4\pi R_*^3)$ (i.e. the projection of the stellar surface field in the radial direction, perpendicular to the current).

6.2.2 General unipolar inductor

In the ideal unipolar inductor model, the flux tube (*i.e.* the field lines and the plasma attached to it) is described as being anchored on (co-moving with) the secondary (Io or an extrasolar planet) because of the high electric conductivity assumed in the secondary, and as drifting against the surface of the primary (Jupiter or the host star). This drag on the stellar surface results in the ohmic dissipation and torque calculated above.

In our general model, we include both the resistance of the planet $\mathcal{R}_p$ and that of the footprint $\mathcal{R}_*$, and we do not impose that the field lines and plasma are co-moving with the planet. Rather, the extent to which the flux tube and its plasma is brought to co-motion with either the planet or the footprint is dependent upon their relative resistances. In fact, the presence of the planet disturbs the field and plasma velocity at the location of the planet and of the footprint. The plasma at both locations experience a motionally induced electric field $\mathcal{E}_*$ and $\mathcal{E}_p$, with their respective differences of potential U_p and U_*. The electric field vectors are in opposite directions, but since they are on opposite sides of a common closed loop (composed of the planet, the footprint, and the flux tube), they provide work to electric charges in the same direction along the closed loop, and the differences of potential U_* and U_p thus add up in an electric circuit analogy to U_0 as calculated above ($U_{Tot} = U_0 = U_* + U_p$). The planet and footprint thus act like two generators in additive series.

A solution of the full problem would require solving the MHD and momentum equations for the magnetic field and plasma velocity both in the planet and footprint, derive the motional electric fields and the associated current density (these are local equations), and link both locations together with the condition that the total current in the loop is determined by the total resistance (a macroscopic condition). We assume that such a solution exists and use the macroscopic expressions,

$$U_p = U_{Tot}\frac{\mathcal{R}_p}{\mathcal{R}_{Tot}} \tag{6.11}$$

$$U_* = U_{Tot}\frac{\mathcal{R}_*}{\mathcal{R}_{Tot}}. \tag{6.12}$$

The set of macroscopic equations for the planet and its footprint on the stellar atmosphere is

$$U_0 = 2R_p a(\omega_p - \omega_*)\frac{\mu_0 m}{4\pi a^3} \tag{6.13}$$

$$U_p = U_0\frac{\mathcal{R}_p}{\mathcal{R}_p + \mathcal{R}_*} \tag{6.14}$$

$$U_* = U_0\frac{\mathcal{R}_*}{\mathcal{R}_p + \mathcal{R}_*} \tag{6.15}$$

$$I = \frac{U_0}{\mathcal{R}_p + \mathcal{R}_*} \tag{6.16}$$

$$\mathcal{P}_{Tot} = U_0 I = \frac{U_0^2}{\mathcal{R}_p + \mathcal{R}_*} \tag{6.17}$$

$$\mathcal{P}_p = U_p I = \mathcal{P}_{Tot}\frac{\mathcal{R}_p}{\mathcal{R}_p + \mathcal{R}_*} \tag{6.18}$$

$$\mathcal{P}_* = U_* I = \mathcal{P}_{Tot} \frac{\mathcal{R}_*}{\mathcal{R}_p + \mathcal{R}_*} \tag{6.19}$$

$$|\mathcal{T}_p| = |\mathcal{T}_*| = \frac{\mathcal{P}_{Tot}}{|\omega_p - \omega_*|} = \mathcal{T}, \tag{6.20}$$

where $\mathcal{T}_*$ has the sign of $\omega_p - \omega_s$ and $\mathcal{T}_p = -\mathcal{T}_*$.

In the rest of this chapter, we first calculate the resistances involved and discuss the condition under which an electric circuit analogy is adequate (section 6.3). We then analyze the different regimes of interaction within the unipolar inductor model (section 6.4), and we analyze the ohmic dissipation and Lorentz torque and compare them with the tidal dissipation and torque (section 6.5). We finally apply the model to the remote sounding of a super-Earth (section 6.6) and to explain the inflation of the radius of a hot-Jupiter (section 6.7).

6.3 Determination of the parameters in the model

In this section, we determine the resistance of the planet $\mathcal{R}_p$ and the resistance of the footprint $\mathcal{R}_*$, which are used to calculate (using the formulas in the previous section) the total electric current I, the ohmic dissipation in the planet $\mathcal{P}_p$ and in the footprint $\mathcal{P}_*$, and the torque on the planet $\mathcal{T}_p$ and on the footprint $\mathcal{T}_*$. We only write the key formulas in this section and include more details in the appendix.

The internal structure (T,P) and electric conductivity profiles of the planet and stellar atmosphere must first be calculated. For most planetary systems, this information is not readily available, and we thus developed a basic analytic model which allows a rapid estimate of the (T,P) profile and the calculation of the ionization fraction and electric conductivity profiles of the planet and footprint.

The outline of this section is as follows. We first summarize (subsection 6.3.1) the equations for the internal structure of the planet and stellar atmosphere and for the electric conductivity profiles. We then provide the integral formula used to calculate the resistance of the planet and star (subsection 6.3.2). They are formal formulas for which the lower and upper boundaries must be defined before a specific numerical calculation can be carried out. We thus specify the lower and upper bounds for the integral of the planet, and the upper bound for that of the footprint (subsection 6.3.3). The lower bound of the integral of the footprint is a free parameter which is determined self-consistently with the condition that ensures the validity of an electric circuit analogy (subsection 6.3.4). Finally, we also introduce another condition for the validity of the model which we discuss in subsection 6.3.5.

6.3.1 Planet's and footprint's analytical internal structure and electric conductivity profiles

Key formulas for the electric conductivity

In the presence of a magnetic field, one can define three electric conductivities, σ_0, the parallel electric conductivity (in the direction parallel to the field lines), σ_p, the Pedersen

electric conductivity (in the direction perpendicular to the field lines and parallel to the electric field), and σ_H, the Hall electric conductivity (parallel to $\mathcal{E} \wedge \mathcal{B}$). In the present summary, we only consider the parallel and Pedersen conductivities,

$$\sigma_0 = A_4 \frac{T^{3/4}}{\sqrt{P}} \left[\exp\left(\frac{-E_H}{2kT}\right) + \sqrt{f_K} \exp\left(\frac{E_H - E_K}{2kT}\right) \right] \quad (6.21)$$

$$\sigma_p = \frac{\sigma_0}{1 + A_3^2 \frac{T}{P^2} \mathcal{B}_*^2(r)}, \quad (6.22)$$

where $A_4 \approx 6.1 \times 10^6$, and $A_3 = 2.9 \times 10^3$ only depend on physical constants, T and P are the gas temperature and pressure, $E_H = 13.6$eV and $E_K = 4.34$eV are the ionization energies of hydrogen and potassium, k is the Boltzmann constant, and f_K is the fraction of potassium (typically $f_K = 10^{-6}$).

We have only considered the thermal ionization of hydrogen and potassium. At lower temperature, potassium is the main contributor of free electrons (since its thermal ionization energy is much lower than that of hydrogen). However, its contribution is limited because of its lower fraction number. The thermal ionization fraction (and thus the electric conductivity) increases with temperature and decreases with pressure. The contribution of the pressure ionization deeper in a gas giant's interior is neglected in our analytical model (which therefore underestimates the electric conductivity of the deep interior by one or two orders of magnitude (*e.g.* Huang & Cumming 2012 [62], Batygin et al. 2011 [9])).

The factor $A_3^2 T(r) \mathcal{B}_*^2(r)/P(r)$ in the denominator of the Pedersen conductivity is equal to $(\omega_e/\nu_e)^2$ where ω_e is the electron gyrofrequency and ν_e is the electron-neutral collision frequency. When $(\omega_e(r)/\nu_e(r))^2 \gg 1$, the electrons experience few collisions, and they spiral along field lines but do not drift across field lines ($\sigma_p(r) \ll \sigma_0(r)$ in this situation). Inversely, when $(\omega_e(r)/\nu_e(r))^2 \ll 1$, the large collision rate allow electrons to drift across field lines, and $\sigma_p(r) \approx \sigma_0(r)$. The situation in the planet and footprint corresponds to the limit $\sigma_p(r) \approx \sigma_0(r)$ (as will be made clear in the discussion about "electromagnetic effective radius").

Planet's internal structure

When no precise internal structure model of the planet is available, we assume that the hot-Jupiter has an isothermal outer layer (which temperature is determined by the black body equilibrium with the intense stellar irradiation)

$$T = T_0 \quad (6.23)$$

$$P(r) = P_0 \exp\left[\beta_p (1 - x)\right] \quad (6.24)$$

$$\varrho(r) = \varrho_0 \exp\left[\beta_p (1 - x)\right], \quad (6.25)$$

where $x = r/R_p$, T_0, P_0, and ϱ_0 are respectively the temperature, pressure, and density at the planet's transiting radius, and $\beta_p = GM_p/(\alpha T_p R_p) = R_p/H_p$ where R_p is the planet's radius and $H_p = \alpha T_p R_p^2/(GM_P)$ is the scale height in the isothermal region. As in the previous chapter, $\alpha = \mathcal{N}_a k_B/\mu\mathcal{M}_H$ where $\mathcal{N}_a$ is the Avogadro constant, k_B is the Boltzman constant, $\mathcal{M}_H$ is the mass density of hydrogen, and $\mu\mathcal{M}$ is the gas mass density.

If we assume a fully hydrogen atom composition, $\alpha \approx 8300$ and $\beta_p \approx 339$. The most straightforward definition of α is such that the perfect gas law is written $P = \alpha \varrho T$.

We also assume a polytropic planetary interior ($P = K\varrho^2$) for which an analytical solution exists),

$$\varrho_c(r) = \varrho_{c,0}\frac{\sin kr}{kr} \tag{6.26}$$

$$P_c(r) = K\varrho_p^2(r) = P_{c,0}\left(\frac{\sin kr}{kr}\right)^2 \tag{6.27}$$

$$T_c(r) = \frac{P}{\alpha\varrho_p} = T_{c,0}\frac{\sin kr}{kr} \tag{6.28}$$

where $K = 2G\pi/k^2$, $k = \pi/(fR_p)$ with f a free parameter close to one which is used to ensure that the polytropic-isothermal boundary occurs at an appropriate location, $\varrho_{c,0}$, $P_{c,0}$, and $T_{c,0}$ are respectively the density, pressure, and temperature at the center of the planet.

Structure of the footprint

When no precise (T,P) profile of the stellar atmosphere is available, we assume that the stellar photosphere and chromosphere (until the transition region with the corona) is isothermal, such that

$$\begin{aligned} P(r) &= P_0 exp\left[\beta_*(1-x)\right] \\ \varrho(r) &= \varrho_0 \exp\left[\beta_*(1-x)\right] \\ T(r) &= T_0 \end{aligned} \tag{6.29}$$

where the subscript 0 denotes the top of the photosphere and $\beta_* = GM_*/(\alpha T_* R_*) = R_*/H_*$ where R_* is the stellar radius and $H_* = \alpha T_* R_*^2/(GM_*)$ is the scale height.

Electric conductivity profile of a hot-Jupiter and footprint

The electric conductivity of a hot-Jupiter and the stellar footprint have the same expression, and we re-write equation (6.84),

$$\sigma_p(r) \approx \sigma_0(r) = A_4\frac{T^{3/4}}{\sqrt{P}}\exp\left(\frac{-E_H}{2kT}\right)\left[1+\sqrt{f_K}\,\exp\left(\frac{E_H-E_K}{2kT}\right)\right] \tag{6.30}$$

where $A_4 \approx 6.1 \times 10^6$ and where T and P are the temperature and pressure of respectively the planet or the footprint. In the stellar footprint, the contribution of the potassium to the electric conductivity is negligible compared that that of hydrogen, and it reduces to $\sigma_p(r) \approx \sigma_0(r) = A_4\frac{T^{3/4}}{\sqrt{P}}\exp\left(\frac{-E_H}{2kT}\right)$.

These comments and formulas conclude the summary of the planet's and footprint's structure and electric conductivity (see appendix for more details).

6.3.2 General formula for the resistances of the planet and footprint

Resistance of the planet

Assuming that the electric conductivity profile $\sigma_p(r)$ (with spherical symmetry) of a gas giant planet is known, we calculate the total integrated resistance $\mathcal{R}_p$ of one hemisphere of the planet (for example that corresponding to $z > 0$) with the following formula,

$$\mathcal{R}_p^{-1} = \int_{z=0}^{R_{max}} \int_{y=0}^{\sqrt{R_{max}^2 - z^2}} dydz \left(\int_{x=0}^{\sqrt{R_{max}^2 - z^2 - y^2}} \frac{dx}{\sigma_p(r)} \right)^{-1} \tag{6.31}$$

The electric conductivity profile $\sigma_p(r)$ has a radial symmetry. However, the geometry of the current is not precisely known, and the primary local constraint is the charge conservation. Nevertheless, the motionally induced electric field $\mathcal{E} = \upsilon_{p/*} \wedge \mathcal{B}$ can be thought of as axial (*i.e.* parallel to an axis of a cartesian set of coordinates) with ($\upsilon_{p/*}$, $\mathcal{B}$, $\mathcal{E}$) forming a direct orthogonal base. Unless the magnetic field is drastically distorted in the planet and is no longer primarily vertical (perpendicular to the orbital plane), the electric field and electric current can be thought, for example, as in the x direction (with the magnetic field in the z direction and $\upsilon_{p/*}$ in the y direction), with (x,y,z) forming a Cartesian coordinate system (as in figure 6.11 in the appendix).

Within this framework, an infinitesimal parallelepiped with sides of length dx, dy, dz, has an infinitesimal resistance $\delta\mathcal{R}_{xyz}$

$$\delta\mathcal{R}_{xyz} = \frac{1}{\sigma_p(r)} \frac{dx}{dydz}, \tag{6.32}$$

with the electric current encountering a cross-section dydz and moving along a length dx across the parallelepiped. The triple integral in equation (6.31) is thus simply the integral of all the infinitesimal parallelepipeds which are contained in the planet (as a sphere), first in series along the x direction, and then in parallel in the y and z direction (the intermediate steps are as follows),

$$\begin{aligned}
\delta\mathcal{R}_{yz} &= \int_x \delta\mathcal{R}_{xyz} = 2 \int_{x=0}^{\sqrt{R_{max}^2 - z^2 - y^2}} \frac{1}{\sigma_p(r)} \frac{dx}{dydz} \\
\delta\mathcal{R}_z^{-1} &= \int_y \delta\mathcal{R}_{yz}^{-1} = 2 \int_{y=0}^{\sqrt{R_{max}^2 - z^2}} dydz \left(2 \int_{x=0}^{\sqrt{R_{max}^2 - z^2 - y^2}} \frac{dx}{\sigma_p(r)} \right)^{-1} \\
\mathcal{R}^{-1} &= \int_z \delta\mathcal{R}_z^{-1} = \int_{z=0}^{R_{max}} \int_{y=0}^{\sqrt{R_{max}^2 - z^2}} dydz \left(\int_{x=0}^{\sqrt{R_{max}^2 - z^2 - y^2}} \frac{dx}{\sigma_p(r)} \right)^{-1}
\end{aligned} \tag{6.33}$$

The boundaries of the integral reflect the fact that the planet is a sphere. We present in the appendix our rationale for adopting this formula instead of the more commonly used $\mathcal{R}_\perp = (\int_z \sigma(z) dz)^{-1}$ or $\mathcal{R}_\parallel = R_p^{-2} \int_z dz/\sigma(z)$.

In fact, the above formula (equation 6.31) corresponds to the resistance of one hemisphere of the planet (both hemisphere being in parallel). Indeed, the integral in the z direction is from 0 to R_{max} (which will be defined below, but for the time being is roughly

equal to the radius of the planet). The integral in the x and y directions are both from $-R_{max}$ to R_{max}, but because of the symmetry, we can write $\int_{-Rmax}^{Rmax}(...)dx = 2\int_{0}^{Rmax}(...)dx$ and $\int_{-Rmax}^{Rmax}(...)dy = 2\int_{0}^{Rmax}(...)dy$ (where the symbol (...) represent the integrand). Both factors 2 cancel each other and we obtain the above formula. The argument in this paragraph can also be seen in the detail of the derivation as presented in equation (6.33).

Resistance of the footprint

The geometry of the footprint (in the stellar atmosphere) is simpler than that of the planet. Since its depth is typically much less than its length and width, it can be approximated with a planar geometry. In other words, the electric conductivity $\sigma_p(z)$ is a function of the local height z, and the current flows perpendicularly to the gradient of electric conductivity, as the red arrow (horizontal) in figure 6.10 in appendix. In this geometry, the following formula is adequate

$$\mathcal{R}_* = \mathcal{R}_\perp = \left(2s\int_z \sigma(z)dz\right)^{-1} = \frac{1}{2s\Sigma_*} \tag{6.34}$$

$$\Sigma_* = \int_{zmin}^{zmax} \sigma_p(z)dz, \tag{6.35}$$

where Σ_* is the height integrated electric conductivity in the footprint, and $s \stackrel{def}{=} cos\theta_F$ where θ_F is the angle between the stellar spin axis and the location of the footprint (as can be seen in figure 6.1).

For an isothermal stellar photosphere, we can write $\sigma_p(z) = E_* P^{-1/2}$ where $E_* = A_4 T^{3/4} \exp\left(\frac{-E_H}{2kT}\right)\left[1+\sqrt{f_K}\exp\left(\frac{E_H-E_K}{2kT}\right)\right]$. The height integrated Pedersen conductivity can then be integrated analytically, and we obtain

$$\Sigma_* = \int_z E_* P^{-1/2} dz = \int_{Pmax}^{Pmin} E_* \frac{R_*}{\beta_*}\frac{dP}{P^{3/2}} = \frac{2E_*H_*}{\sqrt{P_{min}}}\left(1-\sqrt{\frac{P_{min}}{P_{max}}}\right) \tag{6.36}$$

$$\mathcal{R}_* = \frac{\sqrt{P_{min}}}{4sE_*H_*}\left(1-\sqrt{\frac{P_{min}}{P_{max}}}\right)^{-1}, \tag{6.37}$$

where H_* is the scale height in the photosphere (and we will see below that $P_{min} = P_{1*} = 2.9\times10^3\sqrt{T}\mathcal{B}_*(R_*)$ is the pressure at which the Pedersen and parallel conductivity become comparable). We can also note that Σ_* has a maximum value $\Sigma_{*,max} = 2E_*H_*/\sqrt{P_{min}}$, but the footprint typically does not extend so deep that Σ_* reaches its maximum value.

6.3.3 Lower and upper boundaries of the integrals

The previous equations are written in a formally, and the upper and lower boundaries must be specified in order to carry out actual numerical calculations.

Planet's and footprint's upper boundaries: Defining an "effective electromagnetic radius"

Defining the upper boundaries is equivalent to specifying an "effective electromagnetic (EM) radius" to the planet and the star. For example, the "transiting radius" of an extrasolar planet is the radius as defined by transit, and the "electromagnetic radius" is that defined for the purpose of calculating the integrated resistance. We call r_{1p} and r_{1*} respectively the EM effective radii of the planet and star. For a set of coordinates centered on the planet (respectively, on the star), the volume where $r > r_{1p}$ (respectively $r > r_{1*}$) is thus considered as part of the interplanetary medium.

Far from the planet, the pressure is low, and the parallel conductivity is much larger than the Pedersen conductivity perpendicular to the field lines ($\sigma_0 \gg \sigma_p$). As one approaches the planet, the pressure increases (which increases the collision frequency and thus increases the electron's ability to move across field lines). We define r_{1p} as the location where the parallel and Pedersen conductivities become comparable. Quantitatively, we adopt r_{1p} such that $\omega_e(r_{1p}) = \nu_e(r_{1p})$, *i.e.* the radius for which the electron-neutral collision frequency is equal to the electron gyrofrequency. when this condition is satisfied, the $\sigma_p = \sigma_0/2$, and the Pedersen conductivity approaches the parallel conductivity asymptotically for $r < r_{1p}$ (r=0 at the center of the planet). In turn, r_{1*} is defined similarly, *i.e.* such that $\omega_e(r_{1*}) = \nu_e(r_{1*})$. In other words, since the electric field is perpendicular to the magnetic field lines, as soon as the Pedersen conductivity is non-negligible compared to the parallel conductivity, electrons will cross the field line in large quantity, and the corresponding plasma ought to be included in the planet and star respectively.

Planet's lower boundary

As can be seen in equation (6.31), we adopt $r = 0$ as the lower boundary of the integral in the resistance (of one hemisphere of the planet).

Footprint's lower boundary.

In the model we developed, the lower boundary of the footprint is intimately associated with the condition of circuit closure associated with the Alfvén wave travel time (in short, "the closure condition"). It is a free parameter which is used to coherently calculate the footprint resistance so that the closure condition is verified. It is in fact the only parameter that needs to be solved for, all the other ones being determined once the values of the parameters for the system (such as mass of the planet, radius, surface temperature, semi-major axis, stellar radius, mass, surface temperature, magnetic field strength, spin period, mass loss rate through winds) are chosen. We thus discuss in the next section the determination of the footprint's lower boundary together with the closure condition.

We refer to the footprint's lower boundary with several notations, all containing the subscript "pn" (for penetration, since we will see that the definition of the lower boundary of the footprint is determined by the depth of penetration of the Alfvén wave). We call d_{pn} "the depth of penetration" *i.e.* the depth of the footprint, r_{pn} is the radius of the footprint's lower boundary ($r = 0$ is the center of the star), $x_{pn} = r_{pn}/R_*$ is the dimensionless radius,

and $P_{pn} = P(x_{pn})$ is the radius of the bottom of the footprint.

6.3.4 Lower boundary of the footprint and formal closure condition

Overview of the closure condition

In an electric circuit with a single loop, the electric current I is the same everywhere, and the differences of potential across multiple generators are added before calculating the current. In addition, changes in electric potential at any location is communicated to the rest of the circuit within a time-scale short compared to the oscillation period (for an alternative current), or the time-scale between two interruptions of the circuit (for a circuit with switches as the one considered here).

In the astrophysical system under consideration, information about changes in potential propagates along field lines at the Alfvén speed $\upsilon_A = \mathcal{B}/(\sqrt{\mu_0 \varrho})$. Waves emitted near the surface of the planet first travel to the stellar electromagnetic effective surface r_{1*} and then deeper into the footprint down to a depth d_{pn} to be determined (if we were to call the radius of the lower boundary of the footprint $r_{*,min}$, then $r_{*,min} + d_{pn} = r_{1*}$).

We call $t_{A,FT}$ the time it takes for an Alfvén wave to travel along the flux tube between the planet and the top of the footprint (from r_{1p} to r_{1*}), $t_{A,*}$ the time it takes for an Alfvén wave to travel from the top of the footprint to a depth d_{pn}, and t_{max} the time it takes the flux tube to slip through a planetary diameter (t_{max} is the characteristic lifespan of the circuit). We also write $t_0 = 2R_p/\upsilon_{p/*}$ which is the minimum value for t_{max} (it is the advection time of the unperturbed plasma across a length equal to the planetary diameter). With these notations, the condition for the electric circuit analogy can be expressed (Goldreich & Lynden-Bell 1969 [51]),

$$t_A < t_{max} \tag{6.38}$$

$$t_{max} = \frac{2R_p}{\upsilon_{p/*}} \frac{\mathcal{R}_{Tot}}{\mathcal{R}_p} = t_0 \left(1 + \frac{\mathcal{R}_*}{\mathcal{R}_p}\right) \tag{6.39}$$

$$t_A = 2(t_{A,FT} + t_{A,*}), \tag{6.40}$$

where t_A is the time it takes for an Alfvén wave to go from the planet to the bottom of the footprint and back to the planet (*i.e.* the total travel time). In the previous equation, both $t_{A,*}$ and t_{max} (the latter through its dependence on $\mathcal{R}_*$) are functions of d_{pn}. The depth of penetration is thus determined by solving the condition $t_A = t_{max}$ which means that Alfvén waves cannot go deeper into the footprint than d_{pn} and still be reflected back (conveying the contribution of the footprint) to the planet within a time-scale t_{max}. Once d_{pn} is thus determined, $\mathcal{R}_*$ can be self-consistently calculated as well as the remaining macroscopic values (current, ohmic dissipations, and torques). Figure 6.2 illustrates a case where this condition for the closure of the circuit is not met and a case where it is met.

We now derive the expressions for t_A (the total Alfvén travel time), t_{max} (the total time available for the Alfvén waves to propagate from the planet to the footprint, into the footprint, and back to the planet), and $\mathcal{R}_*$ (the total integrated resistance of the footprint).

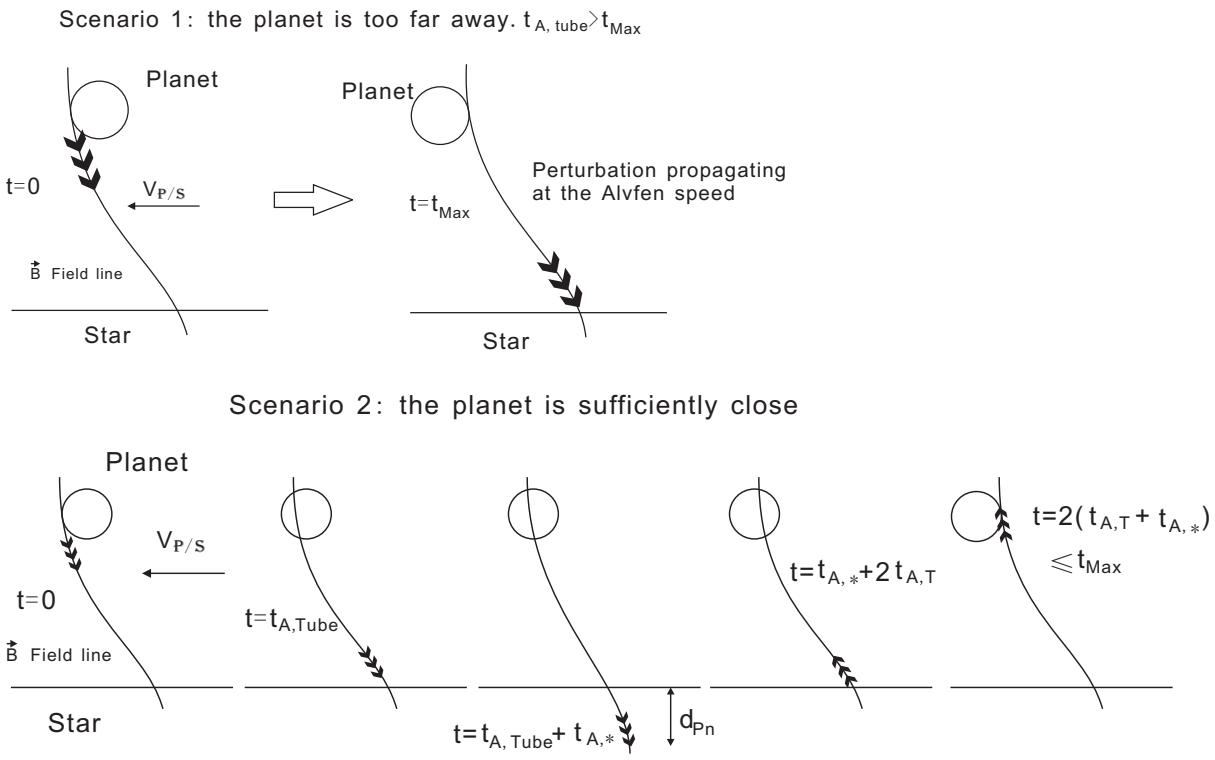

Figure 6.2: Propagation of an Alfvén wave between a planet and its host star. The planet's motion relative to the stellar field induces an potential drop across the flux tube in the proximity of the planet. This information propagates along the flux tube toward the host star with an Alfvén speed. Due to finite diffusion and the relative motion between the planet and the stellar magnetosphere, the net field lines also slip through the planet. **Top figure: no closure**. In this illustration the time-scale required for the Alfvén wave to reach the host star is long compared with that required for the slippage of the field. The circuit is not established in this case. **Bottom figure: closure condition satisfied**. In this illustration, the time available t_{max} is large enough, and an electric circuit analogy can be used.

We also emphasize their dependence on d_{pn}, the thickness of the flux tube which determines the lower boundary of the integral used to calculate the resistance of the footprint).

Alfvén travel time t_A

The Alfvén travel time t_A can be decomposed into two parts: t_{A*} the Alfvén travel time in the footprint, $t_{A,FT}$ the Alfvén travel time along the flux tube between the planet and the star. In fact, the Alfvén waves in the flux tube go through three distinctive regions: the planet's atmosphere above the effective electromagnetic radius of the planet (which density is determined in our model by the atmosphere of the planet), the flux tube proper (which density is determined by the stellar wind), and the chromosphere of the star. We can thus write $t_A = t_{A*} + t_{A,p} + t_{A,FT,0} + t_{A,chro}$ where $t_{A,p}$ is the Alfvén travel time through the gas which density is dominated by the planet's atmosphere above r_{1p}, $t_{A,FT,0}$ is the Alfvén travel time through the gas which density is dominated by the stellar wind, and $t_{A,chro}$ is the Alfvén travel time which density is dominated by the stellar chromosphere above r_{1*}.

Travel time in the footprint t_{A*} The Alfvén speed in the footprint is

$$\upsilon_{A,*}(x) = \frac{\mathcal{B}_*(x)}{\sqrt{\mu_0 \varrho(x)}} = \frac{\mathcal{B}_*(R_*)}{\sqrt{\mu_0 \varrho_0}} \exp\left(\frac{-\beta_*}{2}(1-x)\right), \tag{6.41}$$

where we assumed the magnetic field to be constant.

The Alfvén travel time in the footprint from $x_1 = r_1/R_p$ to a location x_{pn} (in the isothermal photosphere) to be determined is therefore

$$t_{A,*} = \int_{r=r_{pn}}^{r_1} \frac{dr}{\upsilon_{A,*}} = \frac{2H_*}{\upsilon_{A,*}(x_1)}\left(\frac{\upsilon_{A,*}(x_1)}{\upsilon_{A,*}(x_{pn})} - 1\right) = \frac{2H_*}{\upsilon_{A,*}(x_1)}\left(\sqrt{\frac{P(x_{pn})}{P_{1*}}} - 1\right), \tag{6.42}$$

For a TTauri star, $H_* = 1.1 \times 10^6$m, $\beta_* = 1922$, $P_1 = 3.7 \times 10^4$Pa, $\varrho_1 = 1.1 \times 10^{-3}$, $\mathcal{B}_*(R_*) = 0.2$T, and $\upsilon_{A,*}(x_1) = 5.3$km/s.

For a main sequence star, $H_* = 1.4 \times 10^5$m, $\beta_* = 4576$, $P_1 = 6.5 \times 10^3$Pa, $\varrho_1 = 1.4 \times 10^{-4}$, $\mathcal{B}_*(R_*) = 0.03$T, and $\upsilon_{A,*}(x_1) = 2.26$km/s.

Travel time along the flux tube dominated by the stellar wind $t_{A,FT,0}$**.** Assuming that the stellar wind mass loss rate $\dot{M}$ is isotropic and assuming a constant stellar wind υ_{wind} in the magnetosphere, the mass density profile of the stellar wind is $\varrho_{FT} = \dot{M}/(4\pi r^2 \upsilon_{wind})$ (where r denotes the distance to the center of the star). Assuming a dipolar magnetic field, the Alfvén speed is $\upsilon_{A,FT}(r) = \mathcal{B}_*(r)/\sqrt{\mu_0 \varrho(r)}$ along the flux tube. The Alfvén travel time along the flux tube between the planet and footprint $t_A = \int dr/\upsilon_A$ can thus be written (for TTauri, young, and mature main sequence stars)

$$t_{A,FT,0}(r) \approx 489s \left(\frac{a}{0.04AU}\right)^3 \left(\frac{\mathcal{B}_*(R_*)}{0.2T}\right)^{-1} \left(\frac{R_*}{3R_\odot}\right)^{-3} \left(\frac{\dot{M}}{10^{-8}M_\odot/yr}\right)^{1/2} \left(\frac{\upsilon_{wind}}{400km/s}\right)^{-1/2} \tag{6.43}$$

$$t_{A,FT,0}(r) \approx 5.4 \times 10^3 s \left(\frac{a}{0.04AU}\right)^3 \left(\frac{\mathcal{B}_*(R_*)}{0.03T}\right)^{-1} \left(\frac{R_*}{0.9R_\odot}\right)^{-3} \left(\frac{\dot{M}}{10^{-11}M_\odot/yr}\right)^{1/2} \left(\frac{\upsilon_{wind}}{200km/s}\right)^{-1/2}$$

$$t_{A,FT,0}(r) \approx 2.4\times10^3 s \left(\frac{a}{0.04AU}\right)^3 \left(\frac{\mathcal{B}_*(R_*)}{0.003T}\right)^{-1} \left(\frac{R_*}{0.9R_\odot}\right)^{-3} \left(\frac{\dot{M}}{10^{-14}M_\odot/yr}\right)^{1/2} \left(\frac{\upsilon_{wind}}{100km/s}\right)^{-1/2}$$

Travel time in the stellar chromosphere $t_{A,chro}$. We also calculate the Alfvén travel time between r_{1*} and the top of the chromosphere below the transition region with the corona (where we assume that the density becomes comparable to that imposed by the stellar wind). The chromosphere has a roughly isothermal profile until the transition region with the corona, where the density drops rapidly. We thus approximate the region above r_{1*} by extending the density $\varrho = \varrho_0 exp[\beta_*(1-x)]$ (see equation 6.30). The Alfvén speed is $\upsilon_{A,*} = \mathcal{B}_*/\sqrt{\mu_0\varrho}$ where $\mathcal{B}_*$ is the magnetic field at the surface of the star. The Alfvén travel time from r_1 to the top of the chromosphere is thus (the calculation is similar to that for $t_{A,*}$)

$$t_{A,chro} = \frac{2H_*}{\upsilon_{A,*}(r_1)}. \tag{6.44}$$

Travel time in the planetary atmosphere $t_{A,p}$. We call $t_{A,p}$ the Alfvén travel time between r_{1p} and the top of the atmosphere where it merges with the interplanetary space. The (T,P) profile in the planetary atmosphere may be highly variable (depending on the stellar irradiation, opacities and clouds, composition, and mass loss if applicable, etc.). Since P_{1p} is small (around 11Pa for a temperature of 1500K and a stellar field strength at the planet of 1G), the transition is at most within 10-15 scale heights. With an approximation of an isothermal atmosphere, the Alfvén travel time is calculated as above,

$$t_{A,p} = \frac{2H_p}{\upsilon_{A,p}(r_1)}. \tag{6.45}$$

$t_{A,p}$ may be negligible if the planetary's atmosphere is evaporated (for a close-in super-Earth) or if the stellar wind ram pressure is so strong that the transition from the planet's atmosphere to the flux tube dominated by the stellar wind occurs near r_{1p}. We include both $t_{A,p}$ and $t_{A,chro}$ as part of $t_{A,FT}$, the travel time along the flux tube.

Summary: Calculation of the total Alfvén travel time t_A. The Alfvén travel time from the planet effective EM radius through the planet's atmosphere, stellar wind along the flux tube, stellar chromosphere, footprint, and back to the planet is thus

$$t_A = 2(t_{A,FT} + t_{A,*}), \tag{6.46}$$

where $t_{A,FT} = t_{A,p} + t_{A,FT,0} + t_{A,chro}$. It is important to note that only $t_{A,*}$ depend on d_{pn}.

Maximum time available to close the circuit t_{max}

We now express t_{max} the maximum time available for the Alfvén waves to travel before a field line have diffused or is advected across the planet's diameter. It is equal to

$$t_{max} = \frac{2R_p}{\upsilon_{p/*}}\left(\frac{\mathcal{R}_p + \mathcal{R}_*}{\mathcal{R}_p}\right) = t_0\left(1 + \frac{\mathcal{R}_*}{\mathcal{R}_p}\right), \tag{6.47}$$

where $t_0 = 2R_p/v_{p/*}$ is the advection time of the unperturbed plasma across a distance equal to the planet's diameter.

The time available to close the circuit t_{max} is sensitive to the ratio of the resistances $\mathcal{R}_*/\mathcal{R}_p$. This ratio is large when the planet is more conductive than the footprint (of which the ideal unipolar inductor is a limiting case). In this regime, the plasma in the flux tube co-moves more tightly with the planetary plasma than with the plasma at the footprint, and the flux tube drifts slowly across the planet's diameter. This drift relative to the planet is self consistent with a motional electric fields $\mathcal{E}_p = \mathcal{E}_0\mathcal{R}_p/(\mathcal{R}_p + \mathcal{R}_*)$ (the subscript 0 indicates the background, unperturbed, value) and a drift velocity relative to the planet of $(\omega_p - \omega_*)a\mathcal{R}_p/(\mathcal{R}_p + \mathcal{R}_*)$. This reduced angular velocity leads to $t_{max} > t_0$.

Detailed equation of closure condition

We write in detail the closure condition $t_{max} = 2(t_{A,*} + t_{A,FT})$.

$$\frac{2R_p}{v_{p/*}}\left(1 + \frac{\sqrt{P_{1*}}}{4sE_*H_*}\left(1 - \sqrt{\frac{P_{1*}}{P_{pn}}}\right)^{-1}\frac{1}{\mathcal{R}_p}\right) = 2\left[t_{A,FT} + \frac{2H_*}{v_{A,*}(x_1)}\left(\sqrt{\frac{P_{pn}}{P_{1*}}} - 1\right)\right]. \quad (6.48)$$

The footprint is defined between the pressure P_{1*} (top of the footprint, corresponding to the radius r_{1*}) and P_{pn} which is the maximum pressure in the footprint. The different terms in the previous equation have the following physical meanings: $\frac{2R_p}{v_{p/*}} = t_0$ is the unperturbed advection time-scale across a distance equal to the diameter of the planet, $1 + \frac{\sqrt{P_{1*}}}{4sE_*H_*}\left(1 - \sqrt{\frac{P_{1*}}{P_{pn}}}\right)^{-1} = \mathcal{R}_*$ is the resistance of the footprint, $\mathcal{R}_p$ is the resistance of the planet, $t_{A,FT}$ is the Alfvén travel time along the flux tube (it includes $t_{A,p}$, $t_{A,FT,0}$ and $t_{A,*}$), and $\frac{2H_*}{v_{A,*}(x_1)}\left(\sqrt{\frac{P_{pn}}{P_{1*}}} - 1\right) = t_{A,*}$ is the Alfvén travel time in the footprint.

The maximum pressure P_{pn} may vary from P_{1*} to a few times larger than P_{1*}. For $P_{pn} \approx P_{1*}$, the left hand side of equation (6.48) is very large and the right hand side small. As P_{pn} increases, the left hand side decreases while the right hand side increases. This coupled variation of t_{max} and $t_{A,*}$ ensures that a solution exists. Solving for $\xi = \sqrt{P_{pn}/P_{1*}}$ (and thus determining P_{pn} and d_{pn}) simultaneously determines $\mathcal{R}_*$, the total current, the ohmic dissipations, and the Lorentz torque.

6.3.5 A lower bound for d_{pn}

The previous calculation determines the depth of penetration d_{pn}, and we now briefly discuss some constraints on the upper and lower limits for d_{pn}. The depth of penetration is limited to at most a few scale heights because the Alfvén speed is small in the footprint (and decreases quickly as the density increases).

In the other limit (lower limit on d_{pn}), although decreasing d_{pn} increases $\mathcal{R}_*$ and t_{max} (which enhances the circuit closure condition), the ohmic dissipation in the footprint $\mathcal{P}_*$ provides a negative feedback mechanism and a lower bound to d_{pn}. Indeed, the ohmic dissipation in the footprint is efficiently radiated away and conducted to neighborhood regions. However, if the volume of the footprint is too small to absorb the ohmic heating

and radiate or conduct it away, then the temperature and electric conductivity locally increase, which decreases $\mathcal{R}_*$ and establishes an upper boundary to the ratio $\mathcal{R}_*/\mathcal{R}_p$ and to t_{max}. Thus d_{pn} cannot be arbitrarily small.

The footprint has a depth d_{pn} and an area $\pi(y_*/2)(x_*/2) = \pi R_p^2(R_*/a)^3/(2s)$. Once deposited in the corresponding volume, the heat is radiated away and diffuses into the neighboring regions. In the optically thin region, the temperature depends on a balance between the heating rate (here, the ohmic dissipation $\mathcal{P}_*$) and the cooling rate Λ_{Tot}. Cooling rates vary sharply for temperatures between 6000 and 10000K, and we use a range for the cooling rate per unit volume $\Lambda_{vol} = (10^{-39} - 10^{-37}) n_e n_H = \lambda_0 \chi n^2$ where the numerical factor $\lambda_0 = 10^{-39} - 10^{-37}$ have the units of Wm^3, χ is the ionization fraction (around 10% - 50%), n is the plasma number density (adapted from Draine 2010 [34]). The cooling rate for the entire volume of the foot print, Λ, is

$$\Lambda_{Tot} = \int \Lambda_{vol} dV = \frac{\pi}{2s} R_p^2 \left(\frac{R_*}{a}\right)^3 \lambda_0 \chi \int_z n^2 dz = \frac{\pi}{2s} R_p^2 \left(\frac{R_*}{a}\right)^3 \lambda_0 \chi \frac{H_*}{2} \left(\frac{P_{1*}}{kT}\right)^2 \left(\xi^4 - 1\right), \tag{6.49}$$

where the last equal sign comes from a change of variable $dz = -H_* dP/P$ (with P=nkT). For a planet like CoRoT2b and its host star and $\lambda_0 = 10^{-39} - 10^{-37}$ we typically find $\Lambda \approx 10^{24} - 10^{26}(\xi^4 - 1)$ (Λ is expressed in watts), where we used $P_{1*} = 6500$Pa (which depends on the magnetic field strength according to equation (6.82)). Since the energy is dissipated in the footprint but may be radiated away from a larger area, we allow the effective area for the purpose of the cooling to be at most the size of the planet's cross-section. If the dissipation occurs in the optically thick region, the cooling function may be replaced by the black body radiation.

6.4 Analysis of the different regimes and illustrative example

In this section, we describe how the strength of the interaction ($\mathcal{P}_{Tot}$, $\mathcal{P}_p$, $\mathcal{P}_*$, and $\mathcal{T}$) vary with the parameters of the system ($\mathcal{B}_*(R_*)$, a, R_p, etc.). Since the model is later applied to the inflation of a hot-Jupiter, we particularly focus on how the total ohmic dissipation, which depends on the strength of the interaction, is shared between the planet and the footprint and vary with the planetary resistance.

To illustrate the different regimes, we also carry out the numerical applications for a recently discovered extremely short-period rocky planet around Kepler-78b (KIC 8435766) (Sanchis-Ojeda et al. 2013 [95]) which has the following relevant parameters: a late G-type star with $T_* = 5143$K, $R_* = 0.73 R_\odot \approx 5 \times 10^8$m, $M_* = 0.84 M_\odot$, $P_* = 12.5$ days (spin orbit, with an age estimated above 7.5×10^8 years), orbital period $P_p = 8.5$h ($a = 9.1 \times 10^{-3} AU = 2R_\odot \approx 3.1 R_*$), $M_p < 8 M_\oplus$, and $R_p \approx 1.1 R_\oplus$. The largest uncertainties are for the stellar radius (and thus ratio R_*/a), planetary radius, and planetary mass. In the numerical applications, we use the largest planetary mass and radius within the confidence interval, which are $R_p = 1.37 R_\odot$ and $M_p = 8 M_\odot$, which correspond to a particularly dense planet.

Planetary and footprint structures

Planetary structure and resistance. We assume that the planet has a constant electric conductivity ($\mathcal{R}_p = 2/(\pi R_p \sigma)$) and vary this parameter in order to illustrate the different regimes of interaction in our model.

Footprint structure and resistance At the photosphere, we use $T_0 = 5143$K, $P = 2g/3\kappa$, and $\kappa = 10^{-38}\varrho^{1/3}T^{10}$ (Bell & Lin 1994 [10]), and we obtain $\varrho_0 = 6.2 \times 10^{-4}$kgm^{-3} and $P_0 = 2.6 \times 10^4$Pa. The scale height is $H_* = 10^5$m, (with $\beta_* = 5022$), and the other relevant pressures are $P_{1*} = 2.9 \times 10^3\sqrt{T_0}\mathcal{B}_*(R_*)$ and P_{pn}. As before, we write $\xi = \sqrt{P_{pn}/P_{1*}}$.

The important electric values for the star Kepler-78 are $\sigma_p = E_*/\sqrt{P}$ (with $E_* = 2.9 \times 10^4$), the height integrated conductivity $\Sigma_* = 2E_*H_*(1-1/\xi)/\sqrt{P_{1*}}$, and the resistance of the footprint $\mathcal{R}_* = (2s\Sigma_*)^{-1}$ where $s = \sqrt{1 - R_*/a} \approx 0.82$, and $\mathcal{R}_* = \mathcal{R}_{*,min}/(1-1/\xi)$.

Closure condition

We identify two main different regimes of interaction, respectively, the "favorable closure" and "unfavorable closure" regimes. Two minor regimes could also be identified, the "quasi-favorable closure" which is the transition between the favorable and unfavorable closure regimes and the "no closure" regime. We rewrite the equation of circuit closure with different levels of detail,

$$t_{max} = 2(t_{A,FT} + t_{A*}) \tag{6.50}$$

$$t_0\left(1 + \frac{\mathcal{R}_*}{\mathcal{R}_P}\right) = 2(t_{A,FT} + t_{A,*}) \tag{6.51}$$

$$\frac{2R_p}{(\omega_p - \omega_*)a}\left(1 + \frac{\mathcal{R}_{*,min}}{\mathcal{R}_p}\frac{\xi}{\xi - 1}\right) = 2(t_{A,FT} + t_{A,*,1}(\xi - 1)) \tag{6.52}$$

where t_0 is the advection time-scale of unperturbed plasma across a distance equal to the planetary diameter, $\xi = \sqrt{P_{pn}/P_1}$ describes the depth of the footprint (from the effective radius $r_{1,*}$ to the depth of penetration r_{pn}), $\mathcal{R}_{*,min} = (2s\Sigma_*)^{-1}$ is the lower bound of the total resistance of the footprint, $\mathcal{R}_* = \mathcal{R}_{*,min}(\xi - 1/\xi)^{-1}$ so that deeper penetration increases the cross-section encountered by the current and decreases the integrated footprint resistance, $t_{A,FT}$ is the travel time along the flux tube (which may also include the travel time in the stellar chromosphere above r_{1*} ($t_{A,chro}$) and the travel time in the planetary atmosphere above r_{1p} ($t_{A,p}$)), $t_{A,*} = t_{A,*,1}(\xi - 1)$ is the travel time in the footprint (longer time for a deeper penetration, with $t_{A,*,1} = 2H_*/\upsilon_{A,*,1}$ physically being the time for the Alfvén wave to travel 2 scale heights at the location r_{1*}), and the ratio $\mathcal{R}_*/\mathcal{R}_p$ describes the relative effect the conductivity in the planet and footprint have in bringing the plasma to co-motion (a smaller resistance in the planet leading to a longer time t_{max}).

The equation above is solved for ξ as a last step (everything else being already determined), which allows a self-consistent calculation of the resistance of the footprint, the total current, ohmic dissipations, and Lorentz torque. The different regimes correspond to different ways the ohmic dissipation and Lorentz torque vary as a function of the parameters included in the model.

In discussing the different regimes, the most important factors to consider are the relative values of $\mathcal{R}_p$ and $\mathcal{R}_*$ and the fact that increasing ξ (which is by definition larger than 1) increases the right hand side and decreases the left hand side.

Favorable closure regime

The favorable closure regime corresponds to the situation where the Alfvén waves have much time to travel from the planet's to the star's effective radii, resulting in a deeper footprint, larger values of ξ (typically larger than 1.5), and smaller stellar integrated resistance.

Primary condition. The condition that most naturally allows this regime is $2t_{A,FT} \leq t_0$ (*i.e.* short Alfvén travel time). When this condition is met, closure is possible regardless of the resistances of the planet and footprint, and the values of $\mathcal{R}_p$ and $\mathcal{R}_*$ are decoupled. This is more easily met for strong stellar field, weak mass loss rates, and small orbit but near co-rotation.

For example, if we (unrealistically) assume a stellar surface field of 2500G (a TTauri field, corresponding to $\mathcal{R}_{*,min} = 2.6 \times 10^{-8}$ohm) but with moderate stellar winds of $10^{-12} M_\odot/yr$ (young main sequence star), then the condition is met ($t_{A,FT} = 34s$, including the travel time in the chromosphere), the value of $\mathcal{R}_*$ is near that of its minimum, and the circuit can be closed regardless of the planetary resistance. The total resistance is dominated by $\max(\mathcal{R}_p, \mathcal{R}_{*,min})$, and the power in the planet scales as $\mathcal{P}_p \sim U_0^2 \mathcal{R}_P / \mathcal{R}_{*,min}^2$ (if $\mathcal{R}_{*,min}$ is dominant), and $\mathcal{P}_p \sim U_0^2/\mathcal{R}_P$ (if $\mathcal{R}_p$ is dominant). Therefore, as the planetary resistance decreases from very resistive planet to very conductive planet, the ohmic dissipation in the planet increases, reaches a maximum for $\mathcal{R}_p = \mathcal{R}_{*,min}$ (corresponding to $\mathcal{P}_p = U_0^2/\mathcal{R}_{*,min}$), and then decreases when $\mathcal{R}_{*,min}$ becomes dominant.

Alternate, weaker condition. Nevertheless, the condition above is not common in planetary systems (and more unlikely with super-Earths than hot-Jupiters because of the smaller radii). When $2t_{A,FT} > t_0$, another condition that allows the favorable closure regime is $\mathcal{R}_p \ll \mathcal{R}_{*,min}$ (*i.e.* the plasma drifts slowly relative to the planet). This condition is weaker than $2t_{A,FT} < t_0$ because it leads to the favorable closure regime only when $\mathcal{R}_p/\mathcal{R}_{*,min} < t_0/2t_{A,FT}$.

For example, if we take a stellar surface field of 300G and mass loss rate of $10^{-11} M_\odot/yr$ which are reasonable for a young main sequence star, then $2t_{A,FT} > t_0$, and $\mathcal{R}_* = 9.1 \times 10^{-9}$ohm. If we take a conductive planet $\sigma = 10^2$ ($\mathcal{R}_p = 7 \times 10^{-10}$), then we obtain $\xi = 4.7$ and $\mathcal{R}_* = 1.1 \times 10^{-8}$, which is close to its minimum value. The total power $\mathcal{P}_0 = 3.7 \times 10^{27} W$ is mostly dissipated in the footprint $\mathcal{P}_* = 3.4 \times 10^{27} W$ and only a fraction is lost the planet $\mathcal{P}_p = 2.1 \times 10^{26}$W. As long as the alternate condition is met ($\mathcal{R}_p/\mathcal{R}_{*,min} < t_0/2t_{A,FT}$) then the amount of dissipation in the planet depends on its conductivity as described above, but the overall strength of the interaction is unchanged.

As a summary, the favorable closure regime is associated with relatively large values of ξ and a footprint integrated resistance near its minimum value (so a typically small value). The favorable closure regime with the condition $2t_{A,FT} > t_0$ puts no constraints on $\mathcal{R}_p$, whereas the alternate condition implies that $\mathcal{R}_p$ is also small, thus leading to a strong interaction (*i.e.* strong ohmic dissipation and Lorentz torque). In any event,

$\mathcal{R}_* > \mathcal{R}_{*,min}$, which leads to a minimum for the total resistance $\mathcal{R}_{Tot} > \mathcal{R}_{*,min}$. For each set of parameters considered, this value of $\mathcal{R}_{Tot}$ corresponds to the largest possible interaction strength.[1]

Unfavorable closure regime

The unfavorable closure regime corresponds to the case where $2t_{A,FT} \gg t_0$. It is more likely in systems with weak stellar field, large semi-major axis (but within the stellar magnetosphere), far from co-rotation, or with large mass losses. In this case, the closure of the system is possible but requires $\mathcal{R}_* > \mathcal{R}_p$, which is associated with $\xi \approx 1$ (typically $\xi < 1.01$). The fact that there is little time for Alfvén waves to travel into the footprint is consistent with the fact that a shallower footprint results in a larger $\mathcal{R}_*$ and a larger t_{max}.

In addition, since $\mathcal{R}_* > \mathcal{R}_p$, then $\mathcal{R}_{Tot} \approx \mathcal{R}_*$ and the strength of the interaction seems primarily controlled by the footprint resistance. Nevertheless, contrary to the favorable closure regime, $\mathcal{R}_*$ and $\mathcal{R}_p$ are inter-dependent in the unfavorable closure regime. Indeed, since ξ is close to 1, equation (6.52) reduces to,

$$t_0 \frac{\mathcal{R}_{*,min}}{\mathcal{R}_p} \frac{\xi}{\xi - 1} \approx 2t_{A,FT} \tag{6.53}$$

with $\mathcal{R}_* = \mathcal{R}_{*,min}(\xi - 1/\xi)^{-1} \approx \mathcal{R}_{*,min}/(\xi - 1)$. In this regime, the resistance of the footprint adapts so that the ratio $\mathcal{R}_*/\mathcal{R}_p \approx 2t_{A,FT}/t_0$ is adequate for meeting the closure condition. The extent to which $\mathcal{R}_*$ must be larger than $\mathcal{R}_{*,min}$ depends on the relative values of $\mathcal{R}_p$ and $\mathcal{R}_*$ needed to ensure closure of the circuit (for example, a value $\xi = 1.01$ corresponds to $\mathcal{R}_* = 100\mathcal{R}_{*,min}$).

To illustrate the interdependence of $\mathcal{R}_p$ and $\mathcal{R}_*$, we choose a stellar surface magnetic field equal to 30G and a stellar mass loss rate of $10^{-11} M_\odot/yr$. For $\sigma = 1$ (*i.e.* $\mathcal{R}_p = 7.2 \times 10^{-8}$ohm), we obtain $\mathcal{R}_* = 3.7 \times 10^{-6}$, $\mathcal{P}_{Tot} = 1.19 \times 10^{23}$W, mostly dissipated in the footprint $\mathcal{P}_* = 1.17 \times 10^{23}$W, with a fraction in the planet $\mathcal{P}_p = 2.3 \times 10^{21}$W.

Increasing the planet's resistance by 10 ($\sigma = 0.1$, $\mathcal{R}_p = 7.2 \times 10^{-7}$) leads to an integrated resistance at the footprint increased also by 10 ($\mathcal{R}_* = 3.7 \times 10^{-5}$), $\mathcal{P}_{Tot} = 1.19 \times 10^{22}$W, mostly dissipated in the footprint $\mathcal{P}_* = 1.17 \times 10^{22}$W, with a fraction in the planet $\mathcal{P}_p = 2.3 \times 10^{20}$W.

Therefore, within this regime, increasing the planet's resistance by a factor k results in an increase of the footprint resistance and of the total resistance by the same factor. The value of ξ, the strength of the interaction, the torque, and the ohmic dissipation are decreased by the factor k. Decreasing the planet's resistance has the opposite effect.

We plot in figure 6.3 the ohmic dissipation in the planet and the total ohmic dissipation for a wide range of planetary resistance.

[1] Because M-dwarfs have lower surface surface temperatures, they would also have higher $\mathcal{R}_{*,min}$, leading to the weak condition for favorable closure regime being more easily met. Since M-dwarfs are very common, it may be fruitful to apply the present model to these types of stars.

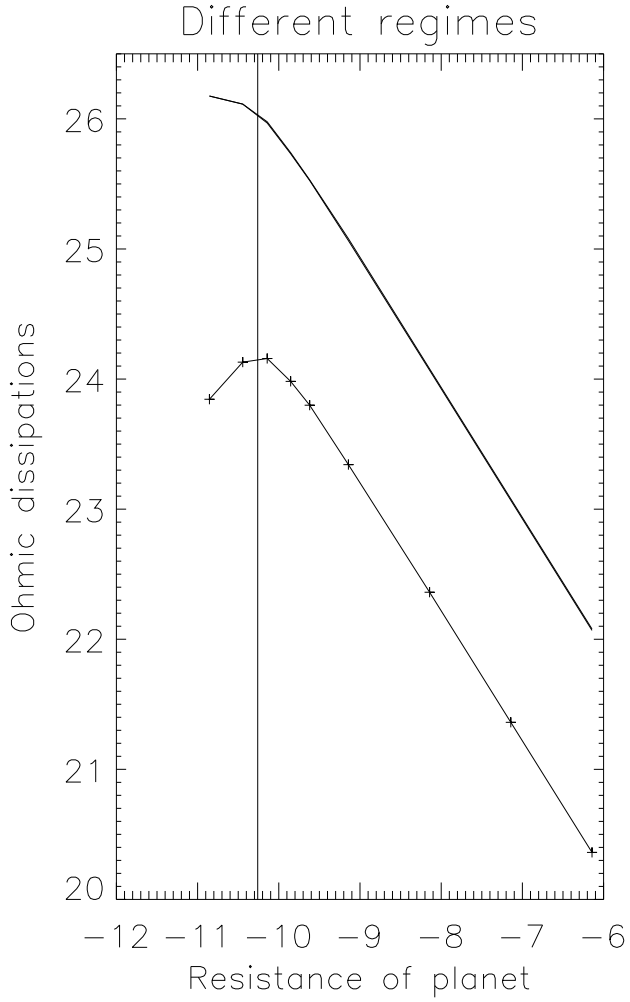

Figure 6.3: Ohmic dissipation in the planet $\mathcal{P}_p$ and total ohmic dissipation $\mathcal{P}_{Tot}$ for a range of planetary resistances. The line represents the transition between the "unfavorable closure" regime to the "favorable closure" regime. Going from right to left, *i.e.* for decreasing planetary resistance, the transition occurs when the weak condition for the favorable regime $\mathcal{R}_p < \mathcal{R}_{*,min} t_0/2t_{A,FT}$.

Quasi-favorable closure regime and no closure regimes

The **quasi-favorable closure** regime is the transition between the unfavorable and favorable closure regimes, *i.e.* the parameter space where the value of ξ, although still close to 1 (typically around 1.01-1.5), is large enough that the term $t_{A,*} = t_{A,*,1}(\xi - 1)$ becomes non negligible.

The **no closure** regime corresponds to the case where the feedback mechanism (*e.g.* ohmic heating) becomes strong enough that it prevents the condition of circuit closure as described in section 6.3.5. This regime is thus technically not a regime of interaction, but we define and name it here since it is associated with effects internal to the model which limit its applicability. Although stronger interaction is associated with larger ohmic dissipation, the no closure regime is most likely in (very) unfavorable closure regime (where the footprint is shallow) and for small planets (as their footprint is smaller, which results in a smaller volume where cooling can occur).

Planets can also move in and out of these regimes as the conditions vary in time. Conditions that may affect the regime of interaction are the strength of the stellar magnetic field (typically decreases with age), stellar spin (may increase in young systems, then typically decreases as the system ages), stellar wind (typically decreases), stellar and planetary radius (decreases with age), and the position of the planet relative to the co-rotation radius. Variations in the semi-major axis is the condition associated with sharpest and most ubiquitous changes as T_p, $\mathcal{B}_*(a)$, $\omega_p - \omega_*$, all depend on the semi-major axis.

6.5 Analysis of the Lorentz torque and ohmic dissipation

6.5.1 Lorentz torque

Qualitative analysis of the effect of the torques

The Lorentz torques have a qualitative effect similar to that of tidal torques (see Murray & Dermott 2000 [82] for a description of tidal torques). The effect of the torque is the same if the stellar magnetic dipole is parallel or anti-parallel to the stellar spin axis. **If the planet orbits outside co-rotation with the stellar spin** ($\omega_p < \omega_*$), then the Lorentz torque on the planet is positive ($\mathcal{T}_p = \mathcal{T}$), the planet gains orbital angular energy at a rate $\mathcal{P}_{orbit,p} = \mathcal{T}\omega_p$, and it moves outwards. Therefore, the Lorentz torque tends to push further out a planet orbiting outside co-rotation, or to slow the inward migration of a planet which is approaching the star from outside co-rotation.

The Lorentz torque on the star is negative ($\mathcal{T}_* = -\mathcal{T}$), the star loses spin angular energy at a rate $\mathcal{P}_{spin,*} = -\mathcal{T}\omega_*$, and it spins down.

The total energy of the system {star + planet} thus decreases at rate $\mathcal{P}_{orbit,p\&spin,*} = \mathcal{T}(\omega_p - \omega_*)$. This energy is dissipated as ohmic dissipation ($|\mathcal{P}_{Tot,ohm}| = \mathcal{T}|\omega_p - \omega_*|$) in the planet and footprint. The total energy decay rate of the binary system thus depends on the total resistance whereas the way this ohmically dissipated energy is shared between the planet and star depends on the ratio of their resistances.

If the planet is inside co-rotation, then $\mathcal{T}_p < 0$ and $\mathcal{T}_* > 0$, *i.e.* the star spins up

and the planet is pulled toward the star. The total energy decay rate of the system {planet + star} is as above.

The discussion above was for a prograde orbit. **If the planet has a retrograde orbit**, then the motion of the planet relative to the stellar magnetosphere is always as if the planet is outside co-rotation ($\mathcal{T}_p > 0$ and $\mathcal{T}_* < 0$, with a sign convention for torques positive in the direction of the stellar spin). This observationally rare (but see Winn et al. 2009 [116]) configuration results in a strong barrier to inward migration as the Lorentz torque transfers angular momentum to the planet for all semi-major axis.

Co-evolution of the co-rotation and orbital radii. If the system {planet + star} is taken in isolation (for example, excluding tidal torques on the planet, secular resonances with other planets, changes in stellar spin due to winds or contraction, etc.), then the co-rotation radius is an unstable equilibrium point (and the only equilibrium point). If the planet is outside co-rotation, the combined effects of the Lorentz torques increase both the co-rotation radius (the star spins down) and the planetary orbit. Equivalently, if the planet is inside co-rotation, the combined effects of the Lorentz torques is to decrease both the co-rotation radius (the star spins up) and the orbital radius. This co-evolution in the same direction is the attempt to reduce the interaction (Lenz law), but in the context of a gravitational potential (Laine et al. 2012 [72]). Subsection 6.5.1 builds on this qualitative description.

Torque formula

This discussion continues the qualitative discussion from subsection (6.5.1). The Lorentz torque on the planet and star have the same modulus, but are of opposite direction,

$$-8R_p^2(\omega_p-\omega_*)\frac{R_*^6}{a^4}\frac{\mathcal{B}_*^2(R_*)}{\mathcal{R}_{Tot}} = \frac{1}{2}M_p\sqrt{GM_*a}\frac{\dot{a}}{a} \tag{6.54}$$

$$8R_p^2(\omega_p-\omega_*)\frac{R_*^6}{a^4}\frac{\mathcal{B}_*^2(R_*)}{\mathcal{R}_{Tot}} = \frac{2}{5}M_*R_*^2\,\dot{\omega}_*, \tag{6.55}$$

where the left-hand side corresponds to the torque, and the right hand sides correspond respectively to the time-derivative of the orbit and spin angular momentum. Outside co-rotation, $\omega_p - \omega_* < 0$, and the star spins down and the planet moves outward due to the interaction. Inside co-rotation, $\omega_p - \omega_* > 0$, and the star spins up and the planet spirals inward.

We use $\dot{a}\ /a = (-2/3)\ \dot{\omega_p}\ /\omega_p$ and $a = (GM_*/\omega_p^2)^{1/3}$ and rewrite these equations (identical to Laine & Lin 2012 [72] but with $\mathcal{R}_{Tot}$ instead of $2s\Sigma_*$),

$$\frac{\dot{\omega}_p}{\omega_p^4(\omega_p-\omega_*)} = 24\frac{R_p^2}{M_p}\left(\frac{GM_*}{R_*^3}\right)^{-2}\frac{\mathcal{B}_*^2(R_*)}{\mathcal{R}_{Tot}} = \gamma_p \tag{6.56}$$

$$\frac{\dot{\omega}_*}{\omega_*^{8/3}(\omega_p-\omega_*)} = 20\frac{R_p^2}{M_*}\left(\frac{GM_*}{R_*^3}\right)^{-4/3}\frac{\mathcal{B}_*^2(R_*)}{\mathcal{R}_{Tot}} = \gamma_* \tag{6.57}$$

$$\dot{\omega}_* = \frac{5}{6}\left(\frac{M_p}{M_*}\right)\left(\frac{GM_*}{R_*^3}\right)^{2/3}\frac{\dot{\omega}_p}{\omega_p^{4/3}}, \tag{6.58}$$

where the last equation can be deduced from the first two. We have introduced the stellar break up angular velocity (the angular velocity at which the inertial force is equal to the gravitational force) $\omega_{break} = \sqrt{GM_*/R_*^3}$ (corresponding to a spin period of about 0.12 day or 2.8h for the Sun). Integrating the last equation, we obtain

$$\Delta\omega_* = -\frac{5}{2}\left(\frac{M_p}{M_*}\right)\left(\frac{GM_*}{R_*^3}\right)^{2/3}\Delta\left(\omega_p^{-1/3}\right) \quad (6.59)$$

$$\Delta\left(\frac{1}{\widetilde{P}_*}\right) = -\frac{5}{2}\left(\frac{M_p}{M_*}\right)\Delta(\widetilde{P}_p^{1/3}), \quad (6.60)$$

where the second equation is written with dimensionless periods ($\widetilde{P}_p = P_p/P_{Break}$ and similarly for the star). The constant coefficient in the first equation is $(5M_p/2M_*)\omega_{break}^{4/3} \approx 3.2\times10^{-9}$ for a close-in super-Earth (8 $M_\oplus$) and $\approx 4.2\times10^{-7}$ for a large hot-Jupiter (3.3 M_J) around a Sun-like star. Therefore if a hot-Jupiter is inside co-rotation and spirals inward into its star due to the Lorentz torque, the gain in stellar spin angular momentum is $1.5\times10^{-5}\mathrm{s}^{-1}$, which is enough to double the angular velocity of a star initially spinning with a 5 day period.[2]

time-scales associated with the Lorentz torque

The characteristic timescales in which this exchange of angular momentum occurs are not constant as they depend on the initial value of $\omega_{p,0}$ and also on whether the planet is far inside, far outside, or near co-rotation.

Well inside co-rotation, $\omega_p \gg \omega_*$, and the orbital decay time-scale is $\tau_{p,in} = (4\gamma_p\omega_{p,0}^4)^{-1}$. To derive this time-scale, we first consider $\dot{\omega}_p\ /(\omega_p^4(\omega_p-\omega_*)) = \gamma_p$ (from equation (6.60)). Using the approximation $\omega_p \gg \omega_*$, this equation becomes $\dot{\omega}_p\ /\omega_p^5 = \gamma_p$. After integration, it becomes $(\omega_{p,0}^{-4} - \omega_p^{-4}) = 4\gamma_p t$. The characteristic time-scale is here the time it takes for ω_p to decrease, for example, by a factor 2 (*i.e.* $\omega_p = \omega_{p,0}/2$), which corresponds to $\omega_p^{-4} - \omega_{p,0}^{-4} \approx \omega_{p,0}^{-4}$ and $\tau_{p,in} \approx 1/(4\gamma_p\omega_{p,0}^4)$. The following time-scales are derived similarly.

Well outside co-rotation, $\omega_p \ll \omega_*$ the time-scale for outward migration is $\tau_{p,out} = (3\gamma_p\omega_*\omega_{p,0}^3)^{-1}$.

Finally, **near co-rotation**, $\omega_p \approx \omega_*$, and the time-scale to move away from this unstable equilibrium position is $\tau_{p,co} = (\gamma_p\omega_*^4)^{-1}$.

For a fixed stellar spin period, $\tau_{p,in} < \tau_{p,co} < \tau_{p,out}$, but they differ only by a factor of a few if the orbital and stellar spin periods are comparable (a few days). For Earth and Jupiter around the Sun, $\gamma_{Earth} \approx 1073\mathcal{B}_*^2(R_*)/\mathcal{R}_{Tot}$ and $\gamma_{Jup} \approx 385\mathcal{B}_*^2(R_*)/\mathcal{R}_{Tot}$. Using

[2] In Laine & Lin 2012 [72], we pointed out that the change of stellar spin angular momentum due to the Lorentz torque on the star is small. Although it is typically the case when the planet is outside co-rotation (in Laine & Lin 2012 [72], we were considering the mechanisms that can stop the planetary inward migration when the planet approaches the star), the Lorentz torque on the star can nevertheless be significant when the planet is inside co-rotation and is spiralling into the star.

initial periods of 4 days, we obtain $\tau_p \approx 10^8 yrs \times \mathcal{R}_{Tot}/\mathcal{B}_*^2(R_*)$. The time-scales involved can thus be short for moderately large magnetic fields and small total resistance in the circuit.

Comparison with the gravitational tidal torque

The discovery of close-in extrasolar planets have led to an intense study on the angular momentum exchange and tidal dissipation associated with tidal interactions between a close-in extrasolar planet and its host star (Murray & Dermott 2000 [82], Bodenheimer et al. 2001 [12], Gu et al. 2003 [56], Ivanov & Papaloizou 2011 [65], Ogilvie & Lin 2004 [84], Dobbs-Dixon et al. 2004 [31]). The static torque (along the star-planet axis) only leads to deformation, but the dynamic torque (not aligned, thus introducing non-axisymmetry) depends on both the planet and the star and is parametrized by the macroscopic Q-value of the planet and star respectively. The tides raised by the planet in the star result in angular momentum exchange (between the orbital and stellar spin) and dissipation in the star. Inversely, the tides raised by the star on the planet result in eccentricity damping and spin-orbit syncrhonization, and energy dissipation in the planet.

The tides raised on the star by the planet and the Lorentz torque have the same qualitative effects on the planetary orbit and stellar spin. Nevertheless, the way energy is dissipated between the planet and star are different. The tides raised on the star by the planet dissipate the planetary and/or stellar spin energy entirely in the star, and the tides raised on the planet by the star dissipate the energy associated with the planet's eccentricity and spin asynchronicity entirely in the planet. In the electromagnetic interaction, the unipolar inductor Lorentz torque dissipates the orbital and stellar spin energy into both the planet and the star (each receiving a fraction depending on the ratio of their total resistances).[3] Therefore, the energy dissipated in the planet through the unipolar Lorentz torque may be large, even in the case of a planet in a circular orbit and spinning synchronously with its orbit (but not in co-rotation with the stellar spin).

We give the expressions of the tidal torque due to the tides in the star (Murray & Dermott 2000 [82]) and the ratio of the Lorentz and these tidal torques

$$\mathcal{T}_{tide} = \frac{3}{2}\frac{k_{2*}}{Q_*}\frac{GM_p^2}{a^6}R_*^5 \tag{6.61}$$

$$\frac{\mathcal{T}_L}{\mathcal{T}_{tide}} = \frac{8}{3}\left(\frac{Q_*}{k_{2*}}\frac{\mathcal{B}_*^2(R_*)}{\mathcal{R}_{Tot}}\right)\frac{R_p^2 R_*}{GM_p^2}\sqrt{GM_* a}. \tag{6.62}$$

These equations can also be rewritten in a form that includes some relevant energies

$$\mathcal{T}_{tide} = \left[\frac{2}{3}\frac{Q_*}{k_{2*}}\frac{1}{E_{grav}}\left(\frac{M_*}{M_p}\right)\left(\frac{a}{R_*}\right)^5\right]^{-1} \tag{6.63}$$

$$\frac{\mathcal{T}_L}{\mathcal{T}_{tide}} = \frac{2}{3}\frac{Q_*}{k_{2*}}\frac{E_{EM}}{E_{grav}}\left(\frac{M_*}{M_p}\right)\left(\frac{a}{R_*}\right)^5. \tag{6.64}$$

[3] The energy associated with an eccentricity would be dissipated through the Lorentz torque associated with the time-dependent interaction described in chapter 5, and the dissipation of the energy associated with the planet's spin asynchronicity has not been explicitly described in this work.

where $E_{grav} = GM_pM_*/a$ is the gravitational potential energy of the planet and $E_{EM} = \mathcal{T}_L = \mathcal{P}_{Tot}/|\omega_p - \omega_*|$ is the ohmic energy dissipated over a synodic period divided by 2π. The ratio is $\approx 3.1 \times 10^{-5}(Q_*/k_{2*})(\mathcal{B}_*^2(R_*)/\mathcal{R}_{Tot}) \approx 3.1$ for Jupiter orbiting the Sun at 0.04AU, and $\approx 2.8 \times 10^{-2}(Q_*/k_{2*})(\mathcal{B}_*^2(R_*)/\mathcal{R}_{Tot}) \approx 2840$ for the Earth orbiting the Sun at 0.04AU (where we used $Q_*/k_{2*} = 10^6$, $\mathcal{B}_*(R_*) = 10^{-3}$Tesla (10G, a weak field), and $\mathcal{R}_{Tot} = 10^{-5}$ohm). The stellar field could be much larger, which increases the strength of the Lorentz torque. The total resistance may be smaller in the quasi-favorable or favorable closure regime, but could be one or two orders of magnitude larger in the unfavorable closure regime. The Lorentz torque, when applicable, seems therefore generally stronger than the tidal torque except for very small semi-major axes (as their ratio is proportional to $\sqrt{a}$.

6.5.2 Ohmic dissipation

Formulas

The dissipation in one hemisphere of the planet $\mathcal{P}_p$, its corresponding footprint $\mathcal{P}_*$ (on the same hemisphere of the star), and the total ohmic dissipation associated with the interaction $\mathcal{P}_0$ are

$$\mathcal{P}_0 = 4R_p^2(\omega_p - \omega_*)^2 \frac{R_*^6}{a^4} \frac{\mathcal{B}_*^2(R_*)}{\mathcal{R}_p + \mathcal{R}_*} = \left| \frac{\mathcal{T}}{\omega_p - \omega_*} \right| \tag{6.65}$$

$$\mathcal{P}_p = \mathcal{P}_0 \frac{\mathcal{R}_p}{\mathcal{R}_p + \mathcal{R}_*} \tag{6.66}$$

$$\mathcal{P}_* = \mathcal{P}_0 \frac{\mathcal{R}_*}{\mathcal{R}_p + \mathcal{R}_*} \tag{6.67}$$

The ohmic dissipation in the planet is thus proportional to $\mathcal{B}_*^2(R_*)\mathcal{R}_p/(\mathcal{R}_p + \mathcal{R}_*)^2$. When $\mathcal{R}_p \gg \mathcal{R}_*$, the total current is $I \approx U_0/\mathcal{R}_p$, and most of the total ohmic dissipation is in the planet and is inversely proportional to the resistance ($\mathcal{P}_p \approx \mathcal{P}_0 \approx U_0^2/\mathcal{R}_p$). Inversely, when $\mathcal{R}_p \ll \mathcal{R}_*$, the footprint receives most of the energy, its resistance determines the total current, and the ohmic dissipation in the planet is proportional to its resistance $\mathcal{P}_p = U_0^2\mathcal{R}_p/\mathcal{R}_*^2$ (also see section 6.4).

Ohmic dissipation and planetary differentiation and inflation

We posit that the magnetic interaction with an undifferentiated rocky planet is stronger than with a fully differentiated one. Indeed, an undifferentiated planet has iron in its outer layers, which would decrease the total resistance by 2 or 3 orders of magnitude (iron may increase the conductivity in rocks through iron impurities interconnected networks in partial melts, which can create isolated high conductivity pathways for electrons across large distances (Quentin Williams, private communication, also see Partzsch et al. 2000 [89])). Therefore, as an undifferentiated planet migrates inward into the stellar magnetosphere, the strong interaction would either rapidly decay its orbit (if it is inside co-rotation), or the ohmic dissipation would be sufficient to ensure full differentiation, increase the total

resistance, and thus reduce the strength of the interaction. We explore further this scenario in section 6.6.

6.6 Remote sounding of a rocky planet: The example of Kepler-78b

6.6.1 Description and analysis of the system

We have until now assumed reasonable stellar magnetic field strengths and internal structures for the astrophysical bodies involved and calculated the ohmic dissipation and torque involved, with the goal of estimating their effects on the planet's internal structure and orbital evolution. We here use the inverse approach: assuming that a close-in extrasolar planet is interacting with its host star as a unipolar inductor, we use observational constraints on the dynamics and energetics of the system to infer constraints on the stellar magnetic field, the electric conductivity of the planet's outer layers, and whether or not the planet is differentiated (Laine & Lin 2013 [71], *in preparation*).

Numerous specialized variations around this theme are used for example, to place constraints on the composition of the Earth's crust (Fainberg & Singer 1987 [38]) or infer the presence of impurities in the rocks or of electrolytes in water/oceans (Kivelson et al. 2000 [69]). Although these methods usually require an *in situ* presence (or a probe), the potentially intense electromagnetic interaction between a close-in extrasolar planet and the stellar magnetosphere may provide a natural remote sounder. However, the study described here differs from the methods above since it is not based on the electromagnetic response to the electromagnetic perturbation (as for example in Zarka 2007 [121] and Driscoll & Olson 2011 [37]), but rather on the dynamical (torques) and energetic response (ohmic dissipation).

As above, we consider the newly discovered system around Kepler-78b/KIC 8435766b (Sanchis-Ojeda al. 2013 [95]). This planet was discovered in an effort to find ultra-short period planets which may be unnoticed by the Kepler standard pipeline. The orbital period is determined precisely, but there is an uncertainty on the planet's mass (only an upper bound is determined), the stellar radius, and consequently the ratio $a/R_* \approx 3.1$ has a 10% to 20% uncertainty as well.

This system is interesting because numerous parameters, usually unknown, have been estimated, or otherwise can be reasonably ignored. The stellar spin rate has been determined and is large enough compared to the planet's orbital angular velocity that $\omega_{p/*} \approx \omega_p$ is reasonably well constrained. The planet is also so small and close to the star that it is presumably bare (no atmosphere, no gaseous envelope, limited planetary mass loss). The absence of a gaseous envelope is consistent with its estimated large mean density. More significantly, a lower limit of the orbital decay time-scale has been inferred observationally,

$$\frac{a}{\dot{a}} = \frac{L_p}{2\mathcal{T}} > 4 \times 10^6 yrs \tag{6.68}$$

where $L_p = M_p\sqrt{GM_*a}$ is the angular momentum of the planetary orbit. Such observational constraints are rare, and it here constitutes an upper bound to the torque (at

the present location and time) such that $\mathcal{T} < 7.5 \times 10^{25}$Nm. Since the planet is inside co-rotation, both the Lorentz torque $\mathcal{T}_L$ and the gravitational tidal torque $\mathcal{T}_{tide}$ decrease the planet's angular momentum. The gravitational tidal torque $\mathcal{T}_{tide}$ is,

$$\mathcal{T}_{tide} = \frac{3}{2}\frac{k_*}{Q_*}\frac{GM_p^2}{a^6}R_*^5 \tag{6.69}$$

where the ratio Q_*/k_* models the strength of the interaction (smaller Q_*/k_* means stronger interaction). With a reasonable lower bound of $Q_*/k_* = 10^6$, we find that the tidal torque $\mathcal{T}_{tide} \leq 10^{24}$Nm, which is consistent with the observation. Alternatively, the observational constraint could be used to place a lower bound to $Q_*/k_* > 1.3 \times 10^4$, which is uninformative.

6.6.2 Calculation of the Lorentz torque

When applied to the Lorentz torque, the condition above gives (the entire planet) $\mathcal{T} < 7.5 \times 10^{25}$Nm. The upper limit for the torque on one hemisphere (as derived earlier) is thus halved, $\mathcal{T}_L < 3.8 \times 10^{25}$Nm. The Lorentz torque on one hemisphere is written

$$\mathcal{T}_L = 4R_p^2(\omega_p - \omega_*)a^2\left(\frac{R_*}{a}\right)^6\frac{\mathcal{B}_*^2(R_*)}{\mathcal{R}_{Tot}}. \tag{6.70}$$

Therefore, the upper limit is a strong constraint on the strength of the interaction. The requirement of weak interaction and the fact that the radius is small (leading to small t_0) would favor the "unfavorable closure" regime of interaction, where $\mathcal{R}_* > \mathcal{R}_p$, $t_{\max} > t_0$, and the footprint is shallow. In addition, although the total resistance involves both the resistances at the footprint $\mathcal{R}_*$ and in the planet $\mathcal{R}_p$, these resistances are coupled in the unfavorable closure regime in order to meet the condition circuit closure. Finally, since the order of magnitude of the planetary resistance is determined by the outer layers (as described in section 6.3.2, also see discussion in section 6.3.2 in the appendix), this method presently does not directly provide information about the interior.

Figure 6.4 shows the Lorentz torque (on one hemisphere) for a range of electric conductivities of the outer layers (assumed constant), dipolar field strength at the surface of the star, and stellar mass loss rates.

6.6.3 Constraints deduced

Conductivity and ohmic dissipation in the outer layers

Constraints on the conductivity of the outer layers of a rocky planet would provide information about the state of its crust (solid, partially melted, fully molten) and the level of differentiation it has achieved. Cold rocks in the crusts of differentiated planets (like the Earth) have a low electric conductivity, which steadily increases with temperature $\sigma = \sigma_0 exp(-E_i/kT)$. Although the conductivity depends on the type of rock, it could be as low as 10^{-6}Sm^{-1} at a few hundred Kelvin, and reach a few times 10^{-1}Sm^{-1} around 1000K (Yang et al. 2011 [120]). The conductivity of rocks also typically seems to be enhanced in

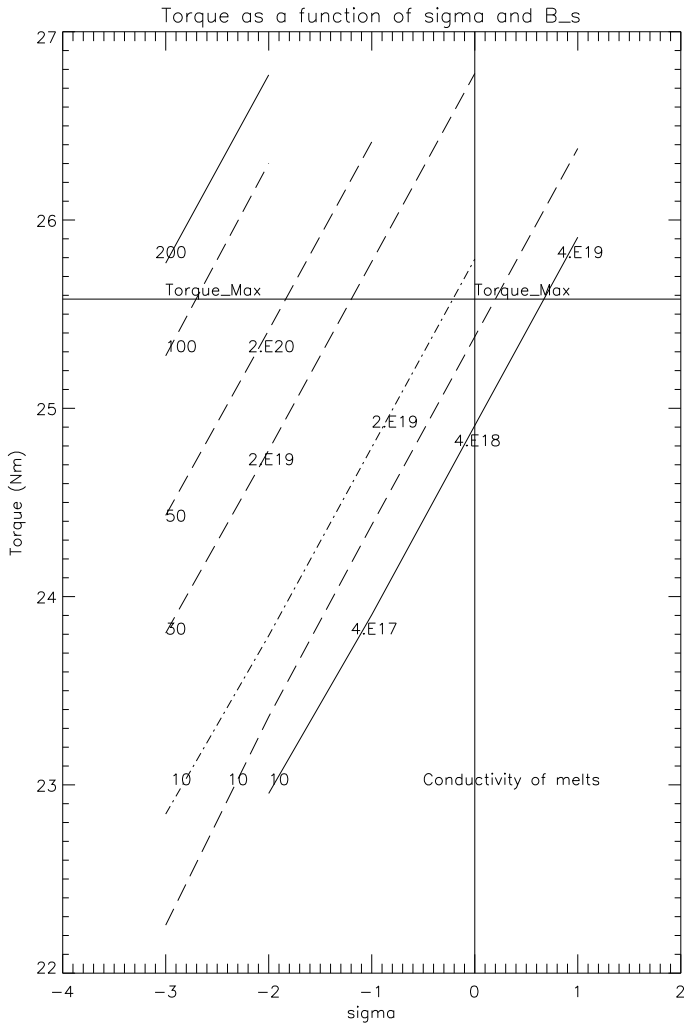

Figure 6.4: Lorentz torques (y-axis in log10 scale) on one hemisphere of the planet for a range of electric conductivities (x-axis, in log10 scale), stellar surface field dipolar strength (10G, 30G, 50G, 100G, 200G as indicated by the number on the curves), and stellar mass loss rate $10^{-10} M_{\odot}/yr$ (continuous curve), $10^{-11} M_{\odot}/yr$ (dashes), and $10^{-12} M_{\odot}/yr$ (dashes and dots). The stellar wind is taken to be 200km/s. The horizontal line corresponds to the observational constraint on the decay time-scale, and the vertical line indicates approximately the electric conductivity of rock melts. For clarity sake, we did not plot the curves corresponding to all combinations of stellar field and mass loss. The numbers in scientific notation (*e.g.* 2.E20) are the corresponding values of the ohmic dissipation in the planet.

the presence of water, impurities, and hydrogen (Karato & Wang 2013 [68]). Fully melted rocks have conductivities around $10\mathrm{Sm}^{-1}$ with the conductivity of partially melted rocks in between. Nevertheless, the presence of iron in partially melted undifferentiated rocks increase their electric conductivities by several orders of magnitude (Quentin Williams, private communication).

Assuming that the planet interacts as a unipolar inductor with its host star, the upper limit on the torque provides a strong constraint both on the stellar magnetic field and the conductivity of the planet's outer layer. For example, it appears that a stellar surface dipolar field strength above 200G would result in too strong an interaction regardless of the planet's electric conductivity or stellar mass loss rate (except for electric conductivity surprisingly low ($< 10^{-4}$)). Inversely, moderate ohmic dissipation (around 10^{19}W) can be generated even with weak surface fields ($<$30G) and reasonable electric conductivities for hot rocks ($> 10^{-3}\mathrm{Sm}^{-1}$). Overall, the results in the figure are consistent with a star with a surface dipolar field of a few tens of gausses, and an electric resistance dominated by material with conductivities between 10^{-2} and 1 Sm^{-1} (hot and partially melted differentiated rocks). Fully molten rocks with a conductivity around 10 Sm^{-1} are nevertheless not excluded, if the star has a weak surface field around 10G. In addition, the situation with a completely molten day-side with conductivities 10-$100\mathrm{Sm}^{-1}$ and a partially molten night side (due to ohmic dissipation) with conductivities around $10^{-1}\mathrm{Sm}^{-1}$ is also compatible with the calculation. Considering the range of conductivities consistent with the observation, the case of a partially melted undifferentiated planet is, however, unlikely (because the presence of iron in an undifferentiated, partially molten, outer layer would result in a much larger electric conductivity).

Upper limit on the ohmic dissipation

A strong electromagnetic interaction is accompanied with strong Lorentz torques, which decay the orbit, and strong ohmic dissipation in the planet, which raise the planet's temperature and intrinsic luminosity. The extent of the Lorentz torques was constrained above. Assuming the planet's spin is synchronized with its orbit, then the day side receives most of the stellar irradiation (about $\mathcal{P}_{irra} = 10^{21}$W). In this case, the maximum ohmic dissipation is that which is compatible with an undetectable flux from the night-side. A threshold $T_{night} < 1500K$ (Sanchis-Ojeda, personal communication) for the system under consideration corresponds to a maximum energy input on the night side $\mathcal{P}_{max} = 2\pi R_p^2 \sigma 1500^4 \approx 1.4 \times 10^{20} W$, which is larger than the ohmic dissipation expected from the calculation above. A model of the day side with albedo between 0.2 and 0.6 is found to fit the transit curves (Sanchis-Ojeda et al. 2013 [95]). Although a low albedo is more likely for a bare planet, the effect on the day side of an ohmic dissipation of 10^{20}W would correspond to a shift in albedo by 0.1 (an ohmic dissipation input of 10^{20}W together with an albedo increase by 0.1 would corresponds to an unchanged energy balance).

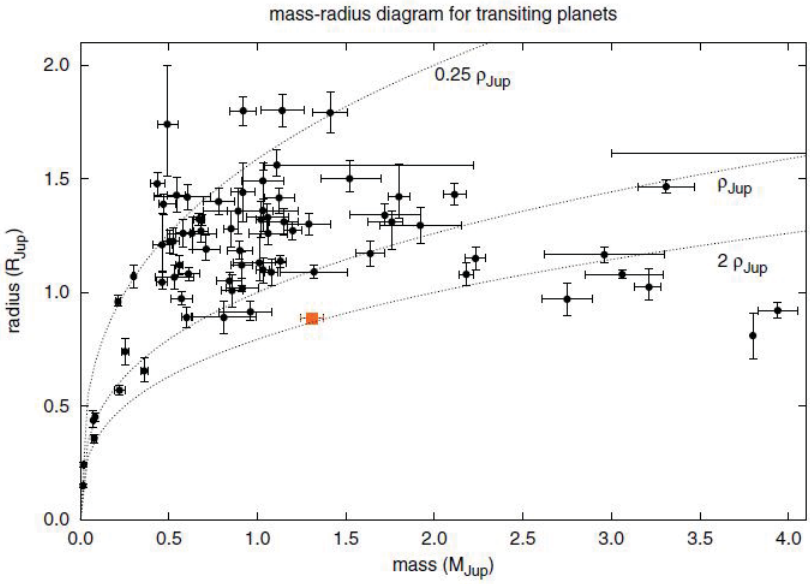

Figure 6.5: This plot from Cabrera et al. 2010 [18] shows the transiting radius as a function of mass for a sample of known extra-solar planets. The red dot is a high density planet which was the focus of the paper. This plot shows that there are many close-in gas giants with a density lower than that of Jupiter. Many of these planets in fact have a mass lower but a radius larger than that of Jupiter

6.7 Ohmic dissipation in a hot-Jupiter: The example of CoRoT-2b

6.7.1 Description of the system and astrophysical motivation

Inflated hot-Jupiters

The masses of transiting planets may be estimated using a complementary method (*e.g.* radial velocity or transit timing variations when the planet is part of a multiple system). The mean density (or a lower bound) of the planet may consequently be calculated and the radius fitted or compared to that predicted in numerical models. Figure 6.5 shows a plot of the masses and radii of a sample of close-in hot-Jupiters.

The numerical models of planetary interiors solve for the structure (T,P) as a two-point boundary problem, and the radius is such that the total mass is constant. The planet is assumed to be in quasi-hydrostatic equilibrium with its gravity, pressure, and centrifugal force, and self-consistently with its surface luminosity, which depends on the planet's entropy and any internal source of energy (Guillot & Morel 1995 [59]). The time-evolution is introduced by the change in entropy as the planet radiates heat away, and a core of variable mass may be introduced as well.

For a hot-Jupiter, such models are modified to include the impact of the stellar irradi-

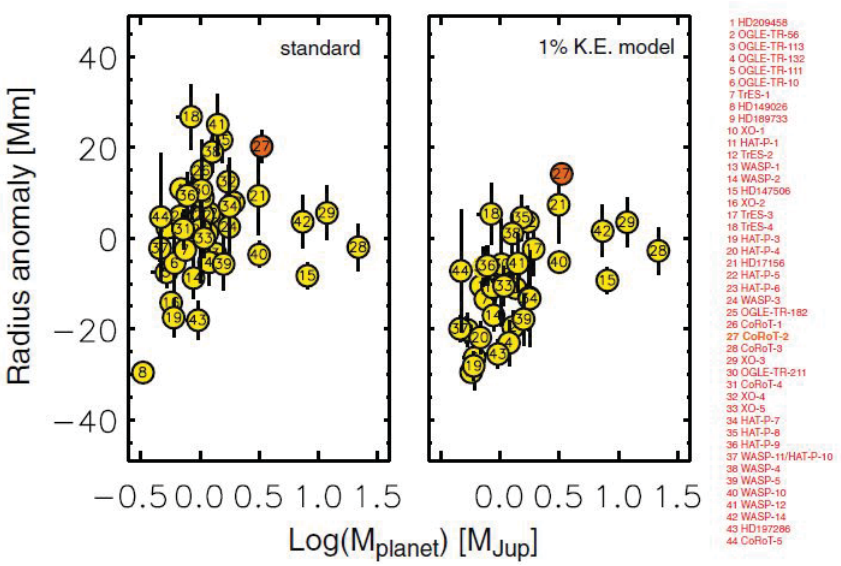

Figure 6.6: This plot from Guillot & Havel 2011 [58] shows the "radius anomaly" (observed radius minus modelled radius, in megameters) of 44 hot-Jupiters to illustrate the impact of stellar radiation and an additional energy source. In the **left panel**, the numerical models include the stellar radiation incident on the planet. It shows that many planets are too small or too large (which may require two independent sets of explanations). As the modelled radius is age dependent (especially in young systems), uncertainties on the age of the system impact the modelled radius. The **right panel** shows the radius anomaly with numerical models that include both the stellar irradiation and an additional energy source parametrized to be equal to 1% of the stellar irradiation and deposited at the center of the planet. It shows that most of the modelled radii now exceed the observed radii, except for a few outliers. CoRoT-2b, the most extreme outlier and the focus of the paper, is indicated in red.

ation as a boundary condition on the temperature near the surface of the planet, assuming variable opacities and finer refinements such as variable incident fluxes as a function of the angle of incidence (Guillot 2010 [57]). Nevertheless, the radii of some inflated hot-Jupiters, of which we take CoRoT2b as a prototype, are still larger than expected by up to 20%, even after the stellar irradiation has been taken int oaccount (see figure 6.6). Guillot & Havel 2011 [58] show that many of the radii of inflated planets could be accounted for if an additional energy heat source of 1% of the stellar irradiation is deposited at the center of the planet. The impact of this extra energy source is more extreme on lower mass hot-Jupiter (low mass hot-Jupiter need less heat to be inflated). For example, a few planets had a radius anomaly (difference between the observed and modelled radii, as plotted in figure (6.6)) larger than that of CoRoT-2b when the numerical model included no extra energy source. However, CoRoT-2b had the largest radius anomaly once the extra energy is added in the numerical models. CoRoT-2b is in fact among the planets which inflated radius may require the largest additional energy input.

The measured radii of transiting planets include an error which depends on the quality of the transit light curve and the error on the stellar radius. In addition, the age of the system is usually taken to be the age of the star as inferred from its light curve and parameters as fitted with a model.

Possible sources for the additional heating mechanism

Several mechanisms have been proposed to explain the inflated character of some hot-Jupiter: giant impacts, radio-active decay (which is not discussed here), tidal dissipation, non-gray atmosphere, wind, and a different unipolar inductor model. Giant impacts can deposit much energy into the interior of a planet, but they are rare after the infancy of the planetary system and are transient (the radius is not an equilibrium radius since the planet was inflated by a one-for-all event).

Tidal dissipation in the planet damp the planet's eccentricity and asynchronous spin-orbit, and these two parameters are damped very rapidly (Dobbs-Dixon et al. 2004 [31]). Indeed, the close-in systems have for the most part a small eccentricity. Therefore, a mechanism that continuously excites an eccentricity (or spin/orbit asynchronicity) must be posited.

In the non-gray atmosphere model, the opacity in the visible and thermal are considered to be different. If the opacity in the thermal is large and that in the visible is low, then the stellar irradiation may be deposited deep in the planet and be trapped by the large thermal opacity. For example, this model has been proposed to explain the radius of HD 209458b (Guillot 2010 [57]). This model thus brings about the question of explaining the values of the different opacities needed.

Close-in planets with a synchronous spin/orbit have strong day side-night side temperature gradients which result in strong atmospheric winds. If the winds occur deep enough, their kinetic energy could be transformed into thermal energy. A different way of tapping into the wind energy is the unipolar inductor resulting from the motion of the planetary wind (with an e_φ component) and a planetary dipolar field (with components in the e_r and e_θ directions in spherical geometry). The motion of ionized winds in a planetary magnetic field (typically thought of as the planet's intrinsic fields; but in all generalities, it could also be a field induced in the planet by the stellar magnetic field). The motionally induced electric field and its associated current could thus have a radial component which can deposit ohmic energy deeper (Batygin & Stevenson 2010 and 2011 [8] [9]). These models which aim to convert wind energy (which is driven by the irradiation) into heat below the convective zone typically parametrize (instead of directly calculating) the interaction strength with a coefficient (typically one to a few percent) that describes the conversion efficacy (also see Huang & Cumming 2012 [62] which takes a general physical approach to constrain this factor).

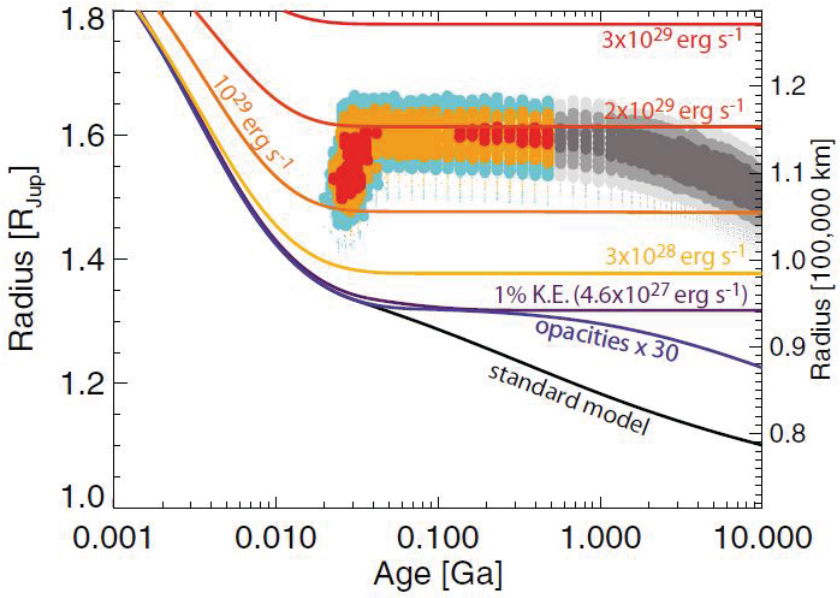

Figure 6.7: Numerical simulations of the radius of CoRoT-2b as a function of the age of the system for different models (standard model, increased thermal opacities, and various amount of *ad hoc* extra energy source (from Guillot & Havel 2011 [58])). The colored region show the observed radius within 1, 2, and 3 σ confidence (respectively red, orange, and blue color). The plot shows that increasing the opacities (non-gray atmosphere) or carrying 1% of the stellar irradiation into the convective region cannot account for the observed radius. An *ad hoc* energy source of about $2 \times 10^{22} W$ is necessary instead.

6.7.2 Ohmic dissipation and inflated radius

Fiducial parameters

We provide here the values of the relevant parameters for the CoRoT2b sytem: $M_p = 3.3 M_J$, $R_p = 1.47 R_J$, $a = 0.028 AU$ (orbital period of 1.74 days and angular velocity $\omega_p = 4.3 \times 10^{-5} \mathrm{s}^{-1}$), $M_* = M_\odot$, $R_* = 0.9 R_\odot$, $T_* = 5600 K$, and $\omega_* = 2.2 \times 10^{-5} \mathrm{s}^{-1}$ (spin period of 3.5 days). The stellar magnetic field and mass loss rate are unknown and we will use a range of reasonable values ($\mathcal{B}_*(R_*) = 10 - 300$G at the surface, and $\dot{M} = 10^{-10} - 10^{-13} M_\odot / yr$).

Numerical calculations show that the extreme inflated radius of CoRoT2b requires an extra energy dissipation of about $2 \times 10^{22} W$, which is not accounted by models that can use only a few percent of the stellar irradiation (Guillot & Havel 2011 [58], also see figure 6.7).

T,P, and Pedersen conductivity profiles

We plot the internal structure of CoRoT-2b in figure 6.8, as described with our analytical model (dotted curve in the graphs) and with tables from a numerical model (dashed

curve) with stellar irradiation but without extra *ad hoc* heating (see Guillot & Havel 2011 [58]). The last plot (bottom right) zooms in the atmosphere, and includes a temperature inversion (continuous curve).

The main difference between the analytical model and the numerical model is the simplifying assumption in our analytical model of an isothermal layer from the atmosphere to the top of the convective zone. Therefore, in the analytical model, the pressure increases with depth, but the temperature does not until the convective zone is reached. The electric conductivity profile between both models, therefore, differs most in the radiative and top of the convective layers. Nevertheless, since strongly irradiated hot-Jupiters have a thicker isothermal layer than cold gas giants, the analytical and numerical models are similar in the atmosphere (without temperature inversion) and interior, but differ significantly for pressures between a bar and 10^5 bars (which corresponds to a layer of thickness about 5×10^6meters (*i.e.* about 5% of the planetary radius)). The total resistances of the planet for the analytical model is $\mathcal{R}_p = 2 \times 10^{-6}$ ohm, and $\mathcal{R}_* = 10^{-7}$ohm for the internal structure corresponding to the numerical model without temperature inversion.

Calculation of the Ohmic dissipation

We use the (T,P) profiles from the numerical evolutionary model without dissipation and calculate the planet's resistance as well as the ohmic dissipation with our model outlined in the preceding sections. We adopt a range of magnetic field at the surface from 10G to 500G, and mass loss rates $\dot{M} = 10^{-10} - 10^{-13} M_\odot/yr$ (we assume a wind velocity of 200km/s; for the purpose of estimating the density between the planet and the footprint, variations of the wind velocity are equivalent to variations in the stellar mass loss rate). We plot in figure (6.9) the energy dissipated in CoRoT2b for both hemispheres (Laine et al. *in preparation* [74]). The Alfvén travel time $t_{A,p}$ in the atmosphere (from the wind dominated region to r_{1p} the planetary magnetic effective radius) most likely cannot be neglected in a hot-Jupiter (as it may be for a rocky planet receiving strong irradiation). Since the density profile depends on numerous parameters not included in the model, we carry out the calculation while neglecting $t_{A,p}$ (continuous curves) and with $t_{A,p}$ (dashed curves). The chromospheric Alfvén travel time was included in both calculations.

Including the Alfvén travel time in the planetary atmosphere effectively lengthens the travel time in the flux tube ($t_{A,FT}$), which is qualitatively similar to a higher stellar mass loss. The dashed curve corresponding to the calculation with $t_{A,p}$ is thus shifted to the right (higher stellar fields are needed to obtain the same ohmic dissipation in the planet). The shift occurs because longer $t_{A,FT}$ corresponds to a more unfavorable closure, thus larger footprint resistance and a weaker interaction (assuming the planetary resistance is unchanged).

We find that a stellar surface dipolar field strength between 15G (for $\dot{M} = 10^{-13} M_\odot/yr$) to 80G (for $\dot{M} = 10^{-10} M_\odot/yr$) is adequate in the case where $t_{A,p}$ is neglected. When $t_{A,p}$ is included, surface fields around 100G are adequate (see figure (6.9)), which is appropriate considering the age of the star (100-300 million years, see Wolter et al. 2011 [118], Schröter et al. 2011 [99]).

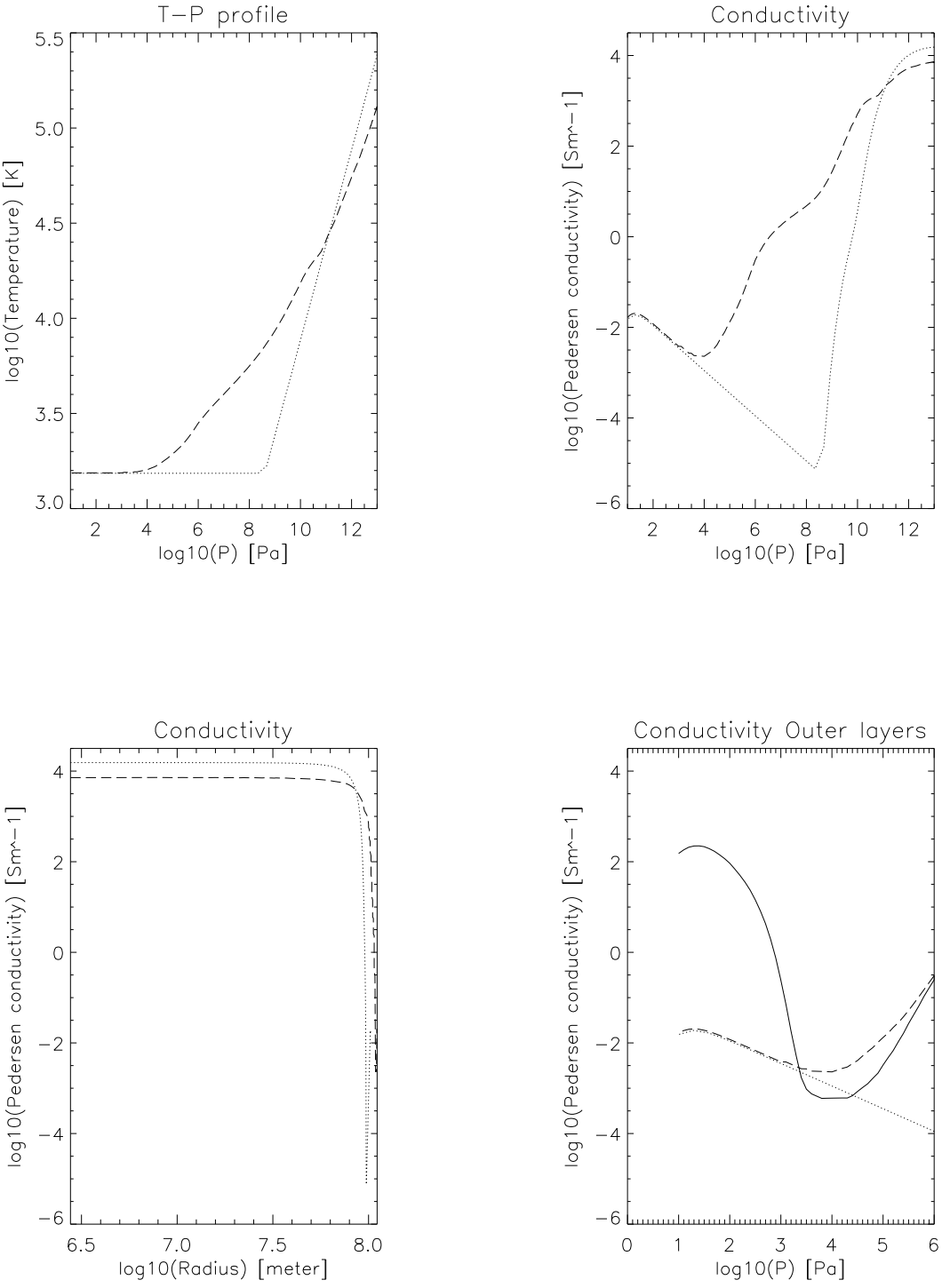

Figure 6.8: Profile for CoRoT2b, with our analytical model (**Dotted curve**), a numerical model (**Dashed curve**), and an atmosphere with a temperature inversion (**continuous curve**).

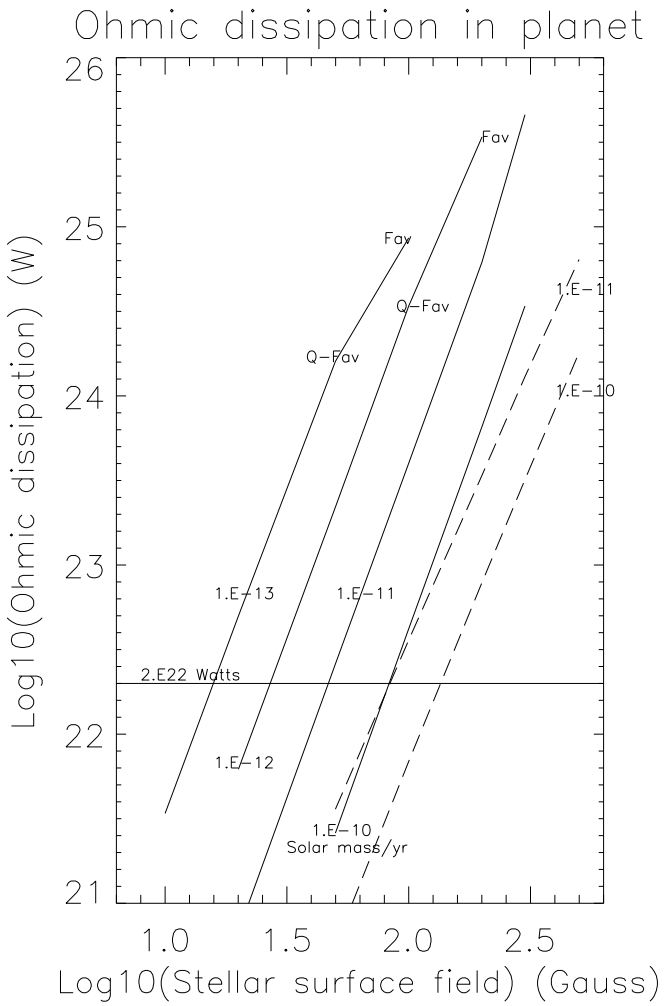

Figure 6.9: Ohmic dissipation (y-axis) for CoRoT2b (both hemisphere) for a range of magnetic fields (x-axis) and stellar mass loss rates (number on the curve, *e.g.* "1.E-10 Solar mass/yr"). The horizontal line indicates the threshold $\mathcal{P} = 2 \times 10^{22} W$ for the entire planet which is needed to account for the present radius. "Q-Fav" and "Fav" denote the locations where the regime of interaction respectively becomes Quasi-favorable or Favorable. The **continuous curves** correspond to the case where the Alfvén travel time in the planet atmosphere $t_{A,p}$ (above r_{1p}) is neglected. It corresponds to the case where the plasma density quickly becomes determined by the stellar wind density. The **dashed curve** correspond to the calculation including the travel time $t_{A,p}$. The effect of including $t_{A,p}$ is qualitatively equivalent to increasing the stellar mass loss rate (but the slope of the curves is different). The size of the footprint is such that in the parameter space considered in this plot the cooling rate is sufficient to ensure that feedback due to the ohmic dissipation does not lead to negative feedback mechanism described in section (6.3.5).

6.8 Concluding remarks

We briefly summarize this chapter's original contributions. The unipolar model has been studied in physics for two centuries (since Faraday), and it has been applied to the interaction of Jupiter and Io in 1968 by Piddington & Drake [91] and in 1969 by Goldreich & Lynden-Bell [51]. Recent works point out that extrasolar planets may also interact magnetically with their host stars (*e.g.* Ip et al. 2004 [64], Zarka 2007 [121], Lanza 2009 [75]).

We apply the ideal unipolar inductor model developed by Goldreich & Lynden-Bell [51] to the interaction of a close-in extrasolar planet and the stellar dipolar magnetosphere. We adopt the model's simple calculation of the electromotive force and condition of validity of the electric circuit analogy associated with the Alfvén waves travel time.

We generalize the model to include the resistance of the planet, develop a formula for the integrated resistance of the planet, and introduce a method to calculate the thickness d_{pn} of the footprint on the stellar atmosphere. We suggest that the ohmic dissipation in the footprint may lead to observable stellar spots (the idea of stellar chromospheric activity with a period similar to that of a close-in companion was already introduced in Shkolnik et al. 2003 [105] and its series of follow up papers). Since d_{pn} is solved self-consistently with the parameters of the system, our generalized model could quantify the location of the ohmic dissipation in the stellar atmosphere (we find that this ohmic dissipation is typically in the photosphere or bottom of the chromosphere, which is coherent with the chromospheric activity suggested by Shkolnik et al.). Our discussion about d_{pn} also includes a new condition of validity of the electric circuit analogy which relies on the temperature increase in the footprint due to the ohmic dissipation.

We also analyze the effect of the Lorentz torque on the planet's angular momentum, attempt to classify the different regimes of interaction ("favorable closure," "unfavorable closure," "quasi-favorable,"and "no closure" regimes), and precisely compare the ohmic dissipation and Lorentz torque with the well known tidal dissipation and torques. Such analysis is necessary for the study of the variations of the planet's semi-major axis.

Finally, we apply the model to two currently relevant astrophysical topics. First, we suggest that the ohmic dissipation in a hot-Jupiter is a way to explain the inflated aspect of some hot-Jupiters. The idea that an extra energy source has such effect is not new (*e.g.* Guillot & Havel 2011 [58], and several models seek to find the potential causes of such additional energy source), and the energy source proposed in our study is one candidate among many (also see Buzasi 2013 [17] with a closely related approach). It is able nevertheless to account for systems like CoRoT-2b which requires an unusual amount of heat that cannot be accounted for explained by many of the other models. Second, although most of the sections in this chapter describe how the dynamics (Lorentz torque) and energetics (ohmic dissipation) may be calculated once the physical parameters of the system (such as the masses, semi-major axis, temperatures, stellar magnetic field strength, etc.) are known (or assumed to be at certain values), we also suggest that constraints on the energetics and/or the dynamics of the system can be used to infer the values of some physical parameters (of which the stellar magnetic field and conductivity of the outer layers of a close-in super-Earth are of much astrophysical relevance). Of course, such approach

is based on the assumption that the planet and its host star are interacting according to the unipolar inductor model. Therefore, further work on the conditions of validity of the model would be useful.

6.9 Appendix

6.9.1 Electric conductivities and total resistances

We present here the equations used to derive the thermal ionization fraction and electric conductivities of a gas, assuming that its (T,P) profile is known.

Ionization fraction

Although the composition of a planet and stellar atmosphere may be complex, for the sake of calculating the ionization fraction, we consider the main contributors to be hydrogen (as the main gas constituent) and potassium (as representative of alkali metals). We assume that these elements each have only two states (ground and ionized, with number densities n_0 and n_1). Potassium (ionization energy $E_K \approx 4.34$ eV) and Hydrogen (ionization energy $E_K \approx 13.6$ eV) dominantly contribute to the total ionization fraction at different temperatures (Potassium in the planet's outer layers, and Hydrogen deeper inside) and we thus add their contributions to the free electron density linearly. We use the Saha's equation to calculate the ionization fraction,

$$\frac{n_1}{n_0} n_e = 2 \left(\frac{2\pi m_e k T}{h^2} \right)^{3/2} exp\left(\frac{-E}{kT} \right). \tag{6.71}$$

This equation can be applied to either hydrogen or potassium element, where n_1 is the number density of the element in the ionized state, n_0 is the number density of the element in the ground state, n_e is the number density of free electrons (which is equal to n_1), m_e is the electron mass, $k = 1.38 \times 10^{-23} JK^{-1}$ is the Boltzman constant $h = 6.64 \times 10^{-34} Js$ is the Plank constant, and E is the ionization energy of the element ($E = 13.6eV = E_H$ for the hydrogen element and $E = 4.34eV = E_K$ for the potassium element).

Applying the formula to hydrogen, we write $n_1 = n_e$ and $n_0 = n - n_e$, and we thus get $n_1 n_e / n_0 = \chi_H^2 n/(1-\chi_H) \approx \chi_H^2 n$ (for low ionization). We then obtain the contribution of hydrogen to the ionization fraction,

$$\chi_H = A_1 \frac{T^{5/4}}{\sqrt{P}} \exp\left(\frac{-E_H}{2kT} \right) \tag{6.72}$$

$$A_1 = \frac{(2\pi m_e)^{3/4} k^{5/4}}{h^{3/2}} \approx 0.18, \tag{6.73}$$

where we replaced number density by pressure using the perfect gas law.

The abundance of Potassium for a solar type star and protoplanetary disk is $f_K \approx 10^{-6}$, which we take to be the planetary composition ($n_0 \approx f_K n$). The contribution of potassium

to the ionization fraction is thus,

$$\chi_K = A_1 \sqrt{f_K} \frac{T^{5/4}}{\sqrt{P}} \exp\left(\frac{-E_K}{2kT}\right), \tag{6.74}$$

and the total ionization fraction is χ,

$$\chi = A_1 \frac{T^{5/4}}{\sqrt{P}} \left[\exp\left(\frac{-E_H}{2kT}\right) + \sqrt{f_K} \exp\left(\frac{-E_K}{2kT}\right)\right]. \tag{6.75}$$

Electric conductivities

Several electric conductivities are defined if electric and magnetic fields are involved. They are, σ_0, the "parallel conductivity" (parallel to the magnetic field lines or in the absence of magnetic field), σ_p, the "Pedersen conductivity" in the direction of an electric field applied perpendicular to the magnetic field, and σ_H, the "Hall conductivity" in the direction of $\mathcal{E} \wedge \mathcal{B}$. They are respectively given by (*e.g.* Baker & Martyn 1953 [6], Piddington 1954, [90]).

$$\sigma_0(r) = n_e e^2 \left(\frac{1}{m_e \nu_e} + \frac{1}{m_i \nu_i}\right) \approx \frac{n_e e^2}{m_e \nu_e} \tag{6.76}$$

$$\sigma_p(r) = n_e e^2 \left(\frac{\nu_e}{m_e\left(\omega_e^2 + \nu_e^2\right)} + \frac{\nu_i}{m_i\left(\omega_i^2 + \nu_i^2\right)}\right) \approx \sigma_0 \frac{1}{1 + \left(\omega_e/\nu_e\right)^2} \tag{6.77}$$

$$\sigma_H(r) = n_e e^2 \left(\frac{\omega_e}{m_e\left(\omega_e^2 + \nu_e^2\right)} + \frac{\omega_i}{m_i\left(\omega_i^2 + \nu_i^2\right)}\right) \approx \sigma_0 \frac{\omega_e/\nu_e}{1 + \left(\omega_e/\nu_e\right)^2}, \tag{6.78}$$

where the subscripts i and e stand for ions and electrons, n_e is the electron number density, ω_e and ω_i are the gyrofrequencies of electrons or ions; ν_e and ν_i are the collision frequencies of the electrons or ions with the neutral particles. In thermal equilibrium, $\nu_e/\nu_i \propto \sqrt{m_e/2m_i}$ (Draine 2010 [34]), which leads to $m_e\nu_e/m_i\nu_i \propto \sqrt{m_e/2m_i}$, and we neglect the contribution in the previous equations of the term corresponding to the ions.

The electron-neutral collision frequency (Draine et al. 1983 [35]) and the electron gyrofrequencies are given by

$$\omega_e(r) = \frac{e\mathcal{B}_*(r)}{m_e} \tag{6.79}$$

$$\nu_e(r) \approx 10^{-19}\, n_n \left(\frac{128kT(r)}{9\pi m_e}\right)^{1/2} \approx 10^{-19}\, P(r)\, \left(\frac{128}{9\pi m_e kT(r)}\right)^{1/2}.$$

Using (6.80) and the expression of a dipole magnetic field strength in the orbital plane $\mathcal{B}_*(r) = \mu_0 m/(4\pi r^3)$, we obtain

$$\frac{\omega_e}{\nu_e}(r) = A_3 \frac{\sqrt{T}}{P}(r)\mathcal{B}_*(r)$$

$$= \left(\frac{T}{1500K}\right)^{1/2}\left(\frac{P}{11Pa}\right)^{-1}\frac{\mathcal{B}_*(a)}{1G}$$
$$= \left(\frac{T}{5600K}\right)^{1/2}\left(\frac{P}{6500Pa}\right)^{-1}\frac{\mathcal{B}_*(R_*)}{300G} \quad (6.80)$$

$$A_3 = e\sqrt{\frac{9\pi k}{128 m_e}}10^{19} \approx 2.9\times 10^3. \quad (6.81)$$

We call r_1 the radius at which $\omega_e/\nu_e(r_1) = 1$. The pressure at this location ($P_1 = P(r_1)$) is

$$P_1 = A_3\sqrt{T(r_1)}\mathcal{B}_*(a). \quad (6.82)$$

We define r_1 and P_1 for the star and planet. When confusion is possible, we specify respectively for the star and planet r_{1p}, r_{1*}, P_{1p}, and P_{1*}. As an order of magnitude estimate, $P_1 \approx 11$Pa (*i.e.* at altitude 70km for the Earth's atmosphere) for a close-in planet with an isothermal outer layer at about 1500K and threaded by a field of 1G. Similarly, $P_1 \approx 6500$ Pa for a stellar surface temperature of 5600K and surface field of 300G. For $P(r) \ll P_1$, we get $\omega_e \gg \nu_e$ and thus $\sigma_p \ll \sigma_H \ll \sigma_0$. Inversely, for $P(r) \gg P_1$, $\omega_e \ll \nu_e$ and $\sigma_H \ll \sigma_p \approx \sigma_0$.

The expressions for σ_0 and σ_p thus reduce to

$$\sigma_0 = A_4\frac{T^{3/4}}{\sqrt{P}}\exp\left(\frac{-E_H}{2kT}\right)\left[1+\sqrt{f_K}\,\exp\left(\frac{E_H-E_K}{2kT}\right)\right] \quad (6.83)$$
$$\sigma_p = \frac{\sigma_0}{1+A_3^2\frac{T}{P^2}\mathcal{B}_*^2(r)}, \quad (6.84)$$

where $A_4 = A_1A_2 \approx 6.1\times 10^6$, and $A_3 = 2.9\times 10^3$ only depend on physical constants.

Location of the boundary for "the planet" and "footprint"

We use r_{1p} and r_{1*} as the planet or star "(electromagnetic) effective radius" for the purpose of calculating resistances. These radii could be seen as the equivalent of the "transiting radius" when talking about planetary detections. Near the planet, the Pedersen conductivity in plasma with $P(r) \ll P_{1p}$ is negligible compared to the parallel conductivity, and the electrons will travel essentially along the field lines. However, in plasma with $P(r) \gg P_{1p}$, $\sigma_p \approx \sigma_0$ and the electrons will move across the planet in the presence of the motional electric field. We, therefore, include the layers deeper than r_{1p} in the calculation of $\mathcal{R}_p$, and we similarly include the layers deeper than r_{1*} in the calculation of $\mathcal{R}_*$.

Height integrated conductivity and total resistance

There are two usual ways to calculate the planet's integrated resistance that appears in the electric circuit; we re-derive them and stress their differences. For clarity sake, we first use the approximation of a thin layer, which is for example valid when the current is confined to a thin surface layer such as the footprint in the stellar atmosphere. In this

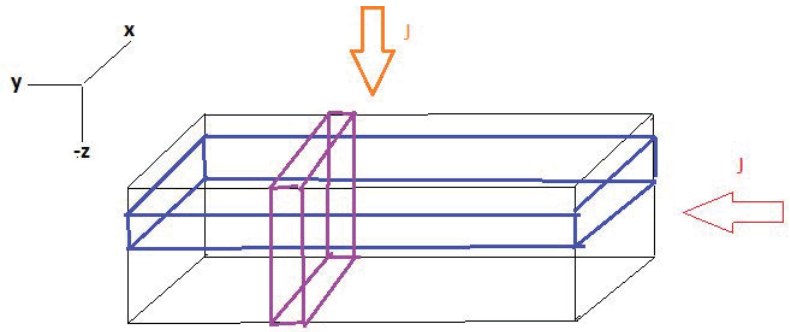

Figure 6.10: Schematic drawing of the geometry of the current in a volume with planar geometry. The electric conductivity is a function of z in the planar geometry ($\nabla\sigma$ is in the z direction). The red arrow (pointing left) corresponds to the "perpendicular" case, and the orange arrow (pointing down) corresponds to the "parallel" case.

case, we can neglect the curvature and write the electric conductivity as a function of depth $\sigma(z)$.

Current perpendicular to the electric conductivity gradient. We first consider the case where the current is along the y direction (*i.e.* perpendicular to $\nabla \cdot \sigma$) as drawn in red in figure 6.10. We define an infinitesimal resistance $\mathcal{R}_{\perp,xyz}$, where the subscripts indicate the directions in which the resistance should be integrated,

$$\mathcal{R}_{\perp,xyz} = \frac{1}{\sigma(z)} \frac{\delta y}{\delta x \delta z}. \tag{6.85}$$

In figure 6.10, $\mathcal{R}_{\perp,xyz}$ is the resistance of the volume at the intersection of the purple and blue parallelepipeds. The total resistance can be obtained through any combination of three integrals (the order does not matter in the idealized geometry). For example, by integrating in parallel in the x then z directions, and then in series in the y direction, we obtain

$$\mathcal{R}^{-1}_{\perp,yz} = \int_x \mathcal{R}^{-1}_{xyz} = \int_x \sigma(z) \frac{\delta x \delta z}{\delta y} \tag{6.86}$$

$$\mathcal{R}^{-1}_{\perp,y} = \int_z \mathcal{R}^{-1}_{xz} = \int_z \int_x \sigma(z) \frac{\delta x \delta z}{\delta y} \tag{6.87}$$

$$\mathcal{R}_{\perp} = \int_y \mathcal{R}_z = \int_y \left(\int_x \int_z \frac{\sigma(z) \delta x \delta z}{\delta y} \right)^{-1} = \frac{L_y}{L_x} \frac{1}{\Sigma}, \tag{6.88}$$

where $\Sigma = \int_z \sigma(z) dz$ is the height integrated conductivity. This formula is typically used in the calculation of the resistance of the footprint in the stellar atmosphere $\mathcal{R}_* = (2s\Sigma)^{-1}$ (where the factor $L_y/L_x = (2s)^{-1}$ accounts for the elliptical geometry of the footprint). Typically for a planetary ionosphere, $L_x = L_y$ and the total resistance is the inverse of the height integrated conductivity $\mathcal{R}_p = \Sigma^{-1}$.

If the planet is modelled as a cube, the formula may be extended to include the interior of a planet with $L_x = L_y = 2R_p$ and $\Sigma = \int_{z=0}^{R_p} \sigma(z) dz$. The resistance of one hemisphere is

then $\mathcal{R}_p = \Sigma^{-1}$ and the resistance of the entire planet is half that of each hemisphere (as the hemispheres are in parallel to each other in the global circuit).

Current parallel to electric conductivity gradient. We now consider the case where the current is along the z direction as drawn in orange (*i.e.* perpendicular to $\nabla \cdot \sigma$), and we define an infinitesimal resistance $\mathcal{R}_{\parallel,xyz}$ (different from $\mathcal{R}_{\perp,xyz}$ because of the different geometry of the current),

$$\mathcal{R}_{\parallel,xyz} = \frac{1}{\sigma(z)} \frac{\delta z}{\delta x \delta y}. \tag{6.89}$$

The total resistance can be obtained, again, through any combination of integrals along all three directions, for example by integrating in parallel in the y then x directions, and then in series in the z direction,

$$\mathcal{R}^{-1}_{\parallel,xz} = \int_y \mathcal{R}^{-1}_{xyz} = \int_y \sigma(z) \frac{\delta x \delta y}{\delta z} \tag{6.90}$$

$$\mathcal{R}^{-1}_{\parallel,z} = \int_x \mathcal{R}^{-1}_{xz} = \int_x \int_y \sigma(z) \frac{\delta x \delta y}{\delta z} \tag{6.91}$$

$$\mathcal{R}_{\parallel} = \int_z \mathcal{R}_z = \int_z \left(\int_x \int_y \frac{\sigma(z) \delta x \delta y}{\delta z} \right)^{-1} = \frac{1}{L_x L_y} \int_z \frac{\delta z}{\sigma(z)}. \tag{6.92}$$

This is, for example, the formula Dermott 1970 [30] uses to calculate the resistance of the Galilean satellite Io ($\mathcal{R}_S = 1/r_S^2 \int_0^{r_s} dr/\sigma(r)$).

Analysis. We call the previous resistances $\mathcal{R}_\perp$ and $\mathcal{R}_\parallel$ which are derived for a planar geometry when the current is respectively perpendicular and parallel to the gradient of electric conductivity,

$$\mathcal{R}_\perp = \left([2s] \int_z \sigma(z) dz \right)^{-1} \tag{6.93}$$

$$\mathcal{R}_\parallel = \frac{1}{R_p^2} \int_z \frac{dz}{\sigma(z)}, \tag{6.94}$$

where [2s] is the factor that would be included for the calculation of the resistance of the footprint using the formula for $\mathcal{R}_\perp$.

Impact of a curvature. These formulas represent two limiting cases, both present in a more realistic planet. For example, we can imagine a two-layer planet with an interior with high and uniform conductivity, encased in an outer layer with low and uniform conductivity, and threaded by an induced unipolar current along the x direction as in figure 6.11. In this case, the current and gradient of electric conductivity are parallel on the faces labelled AA and perpendicular on the faces labelled BB.

Neglect of low and high conductivities. In addition, the value of $\mathcal{R}_\perp$ primarily depends on regions of high electric conductivity, whereas the value of $\mathcal{R}_\parallel$ primarily depends on region of low electric conductivity. In other words, $\mathcal{R}_\perp$ neglects very resistive regions and $\mathcal{R}_\parallel$ neglects very conductive regions. These formulas are reasonable for a planar symmetry as in figure (6.10) when the gradient of conductivity is parallel or perpendicular to the current. However, in a spherical symmetry with an electric conductivity varying with

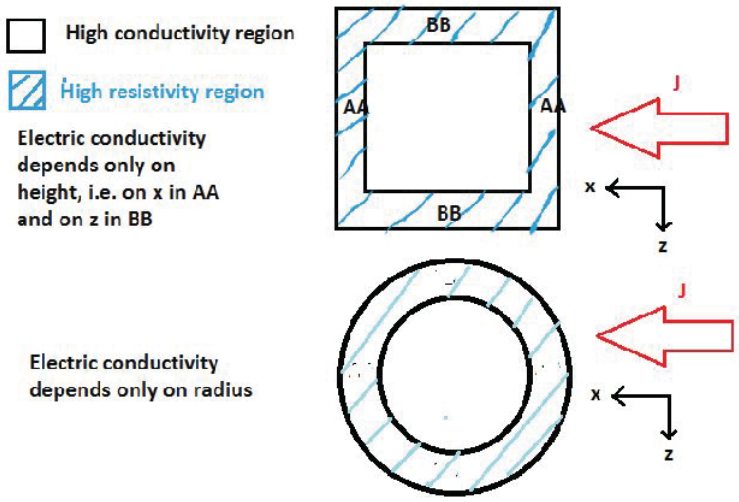

Figure 6.11: Schematic drawing of a two layer cubical and spherical planet, with a homogeneous high conductivity inner region encased in a homogeneous low conductivity outer layer. The spherical case is quite similar, for example, to a cold terrestrial planet.

radius but with a non-radial current, either formulas will neglect respectively the regions of high and low electric conductivity along the path of the current through the planet. For example, a very resistive outer layer will much reduce the unipolar inductor currents induced inside the planet (a current generated in the planet cannot avoid the outer layers on its way toward the surface of the planet). Yet, using $\mathcal{R}_\perp$ would neglect this effect.

A generalized formula. We assume that the planet is spherically symmetric and that the current is in the x direction (because of the spherically symmetric, the x direction is not special, but we do assume that the current vector density has a general identifiable direction). We therefore write,

$$\delta\mathcal{R}_{xyz} = \frac{1}{\sigma_p(r)}\frac{dx}{dydz} \tag{6.95}$$

The total resistance for one hemisphere of the planet is the integral first in series in the x direction and then in parallel in the y and z directions,

$$\delta\mathcal{R}_{yz} = \int_x \delta\mathcal{R}_{xyz} = 2\int_{x=0}^{\sqrt{R_{max}^2-z^2-y^2}} \frac{1}{\sigma_p(r)}\frac{dx}{dydz} \tag{6.96}$$

$$\delta\mathcal{R}_z^{-1} = \int_y \delta\mathcal{R}_{yz}^{-1} = 2\int_{y=0}^{\sqrt{R_{max}^2-z^2}} dydz\left(2\int_{x=0}^{\sqrt{R_{max}^2-z^2-y^2}} \frac{dx}{\sigma_p(r)}\right)^{-1} \tag{6.97}$$

$$\mathcal{R}^{-1} = \int_z \delta\mathcal{R}_z^{-1} = \int_{z=0}^{R_{max}}\int_{y=0}^{\sqrt{R_{max}^2-z^2}} dydz\left(\int_{x=0}^{\sqrt{R_{max}^2-z^2-y^2}} \frac{dx}{\sigma_p(r)}\right)^{-1}. \tag{6.98}$$

Approximation made. The generalized formula is not exact since the path of the current and geometry of the electric field are not precisely known. Nevertheless, for a geometry in

which the current vector density are overall unidirectional, the generalized formula provides a better approximation for the total resistance of a planet. More importantly, the order of the integration matters in a realistic geometry, and the order chosen in the formula above assumes that the general direction of the current is to move across the planet.

General trends. In all three formulas described above, the general trend is that the total resistance decreases with the size of the planet.

In addition, the more inhomogeneous the electric conductivity in the planet, the larger the differences between the formulas. For example, for a constant electric conductivity σ, the formulas differ only by a geometrical coefficient: $\mathcal{R}_\perp = \mathcal{R}_\parallel = (R_p\sigma)^{-1}$ and the generalized formula gives $\mathcal{R} = 2/(\pi R_p\sigma)$. Nevertheless, for a planet with two layers of equal depth $R_p/2$ each and conductivities $\sigma(inner)$ and $\sigma(outer)$, we obtain $\mathcal{R}_\perp = (2/R_p)\ 1/[\sigma(inner) + \sigma(outer)]$ and $\mathcal{R}_\parallel = (2/R)[1/\sigma(inner) + 1/\sigma(outer)]$. For a radius $R_p = 10^8$, a conductive interior $\sigma(inner) = 10^5$, and a resistive outer layer $\sigma(outer) = 1$, we would get $\mathcal{R}_\perp = 2\times10^{-13}$, $\mathcal{R}_\parallel = 5\times10^{-9}$, and $\mathcal{R} \approx 6\times10^{-9}$. For planets with electric conductivity increasing toward the center, $\mathcal{R}_\parallel$ is the better approximation of $\mathcal{R}$. If instead $\sigma(inner) = 1$ and $\sigma(outer) = 10^5$, the values of $\mathcal{R}_\perp$ and $\mathcal{R}_|$ are unchanged (since they are 1D integrals), $\mathcal{R} \approx 7.5\times10^{-14}$, and $\mathcal{R}_\perp$ is the better approximation.

Finally, since the current induced inside the planet goes, on its way out, through the planetary layers in series, the presence of a resistive outer layer encasing the planet would dominate in the calculation of the total resistance (since even currents going through the conductive interior also encounter the resistive outer layer). This case is illustrated by the first two-layer example above. Alternatively, the total resistance of a planet with a conductive outer layer encasing a much less conductive interior is dominated by the conductive outer layer since currents may flow across the planet without going through the interior. This case is illustrated by the second two-layer example above. As a summary, the order of magnitude of the planetary is set by the radius and the electric conductivity of its outer layers. The strength and profile of the electric conductivity in the interior determines the finer value.

6.9.2 Structure, conductivity, and resistance of a hot-Jupiter

We now write the equations for the state variables (T,P,ϱ) in order to calculate the resistances and the Alfvén travel time. We favor analytical models in order to focus on understanding the different regimes of interaction. An analytical structure of the footprint is adequate since it is at most a few scale heights in depth. Our analytical model for a gas giant omits the degeneracy and pressure ionization in the interior, but its impact on the total resistance of the planet is negligible compared to the other (observational or modelling) uncertainties on the outer layers.

T-P internal structure: Analytical model

We model a hot-Jupiter with an analytical polytropic interior topped with an isothermal layer. The black body equilibirum temperature with the stellar irradiation,

$$T_{bb} = \left(\frac{L_*}{16\pi a^2 \sigma}\right)^{1/4} = T_* \sqrt{\frac{R_*}{2a}}. \tag{6.99}$$

At 0.04AU, it corresponds to 1700K (for a TTauri star with $T = 4000$K and $R_* = 3R_\odot$) and 1300K (for a main sequence star with $T = 5600$K and $R_* = 0.9R_\odot$). At 0.028 AU (as for CoRoT2b), it corresponds to 2000K around a TTauri star and 1500K around a main sequence star. Strong stellar irradiation of a hot-Jupiter tends to push the boundary of the convective interior deeper. The previous formula assumes that the heat received by the planet is re-radiated by its entire surface.

Our model for a hot-Jupiter here is the CoRoT-2b system, with parameters $M_p = 3.3M_J \approx 6.3 \times 10^{27}$kg, $R_p = 1.43R_J \approx 10^8$m, $a = 0.028AU \approx 4.2 \times 10^9$m (orbital period of 1.74 days), $T_* = 5600$K, $P_{ast} = 3.5$days (*i.e.* $\omega_p - \omega_* = 2.1 \times 10^{-5}\text{s}^{-1}$), $R_* = 0.9R_\odot$ which corresponds to a planetary equilibrium temperature $T_0 = 1500$K (assuming the heat received is redistributed to the entire surface of the planet).

Temperature, pressure, and density at the transiting radius R_p. Using the opacity for molecules (converted in SI units from Bell & Lin 1994 [10]), $\kappa = 10^{-11}\varrho^{2/3}T^3$, we obtain the temperature, pressure, density, and opacity (in agreement with the values used for example in Guillot 2010 [57]) at the transiting radius,

$$\begin{aligned} T_0 &= 1500K & (6.100)\\ P_0 &= 3.8 \times 10^4 Pa & (6.101)\\ \varrho_0 &= 3 \times 10^{-3} kgm^{-1} & (6.102)\\ \kappa_0 &= 7 \times 10^{-4} m^2 kg^{-1}. & (6.103) \end{aligned}$$

Isothermal region. The temperature, Pressure, and density profiles in the isothermal region are,

$$\begin{aligned} T &= T_0 & (6.104)\\ P(r) &= P_0 \exp\left[\beta_p(1-x)\right] & (6.105)\\ \varrho(r) &= \varrho_0 \exp\left[\beta_p(1-x)\right], & (6.106) \end{aligned}$$

with $x = r/R_p$. In the previous equations, $\beta_p = GM_p/(\alpha T R_p) = R_p/H_p$ where $H_p = \alpha T R_p^2/(GM_P)$ is the scale height in the isothermal region. If we assume a fully hydrogen atom composition, $\alpha \approx 8300$ and $\beta_p \approx 339$. The most straightforward definition of α is such that the perfect gas law is written $P = \alpha\varrho T$.

Planet's convective region. We adopt a polytrope equation $P = K\varrho^2$, which has an analytical solution (such model is inaccurate for a fine modelling of the planet's internal structure, but adequate enough to build a usable model of its interaction with the star),

$$\varrho_c(r) = \varrho_{c,0}\frac{\sin kr}{kr} \tag{6.107}$$

$$P_c(r) = K\varrho_p^2(r) = P_{c,0}\left(\frac{\sin kr}{kr}\right)^2 \quad (6.108)$$

$$T_c(r) = \frac{P}{\alpha\varrho_p} = T_{c,0}\frac{\sin kr}{kr}, \quad (6.109)$$

where $K = 2G\pi/k^2$. We write $k = \pi/(fR_p)$ with f a free parameter close to one and approximate the mass of the planet as $M_p = \int_{r=0}^{R_p} 4\pi r^2 \varrho_c(r) = \varrho_{c,0}(4R_p^3 f^3/\pi)$ (Ogilvie & Lin [84]). We therefore obtain the following values at the center of the planet,

$$\varrho_{c,0} = \frac{\pi M_p}{4R_p^3 f^3} \quad (6.110)$$

$$P_{c,0} = K\varrho_{c,0}^2 = \frac{\pi G M_p^2}{8R_p^4 f^4} \quad (6.111)$$

$$T_{c,0} = \frac{GM_p}{2\alpha R_p f}. \quad (6.112)$$

Boundary between the isothermal and polytropic region. We define $r_=$ to be the transition radius between the isothermal and polytropic region, $x_= = r_=/R_p$, and S(r) the sinus cardinal function, $S(r) = sin(kr)/kr$ or similarly $S(x) = sin(\pi x/f)/(\pi x/f)$. From the continuity of T and ϱ, we calculate the values at the boundary

$$S(x_=) \stackrel{def}{=} \frac{\sin(\pi x_=/f)}{\pi x_=/f} = \frac{2\alpha R_p T_0}{GM_p} f \quad (6.113)$$

$$\varrho(r_=) = \frac{\alpha\pi T_0}{2GR_p^2}\frac{1}{f^2} \quad (6.114)$$

$$P(R_=) = \frac{\pi\alpha^2 T_0^2}{2GR_p^2 f^2}. \quad (6.115)$$

The isothermal region stretches above $r_=$. We choose f so that the pressure at the surface matches the pressure P_0 found with the opacity. For $f = 0.978$ (and $R_p = 10^8$m, $M_p = 3.3M_J$, $T_0 = 1533$K), we find the following values at the transition with the convective region, $S(x_=) \approx 5.71 \times 10^{-3}$, $x_= \approx 0.973$, $\varrho(r_=) \approx 31$kg m^{-3}, and $P(r_=) \approx 4 \times 10^8$Pa.

Numerical simulations for strongly irradiated gas giants indicate that the transition occurs deeper than 3×10^7 Pa for young planets (less than 10^9 years), 10^8 Pa (for a few billion years), and 10^9Pa (for old planets). Our analytical model underestimates the temperature a few scale heights below the transiting radius (we assume an isothermal outer layer instead of radiative) and overestimate the central temperature and pressure, but it nevertheless places the transition with the convective zone at a reasonable pressure. We can also reproduce the increase of the pressure at the transition with increasing stellar irradiation.

Boundary with the interplanetary medium and effective radius. The planetary atmosphere extends above the transiting radius. We define the effective radius r_1 as the radius at which the Pedersen conductivity becomes comparable to the parallel conductivity. Above that location, the current is mainly carried through the parallel conductivity; below,

the current starts to cross significantly the planet though the Pedersen conductivity. We use this radius as the transition between the planet and the flux tube and as the outer bound in the integrals in the calculation of the planetary total resistance. Hence the lowest pressure included in the planet corresponds to $P_{min} = P_1 = 2.9 \times 10^3 \sqrt{T_p}\mathcal{B}_*(a) \approx 11$ Pa (for CoRoT2b, threaded by a field of 1G).

Electric conductivity in a hot-Jupiter

Within the effective radius, the Pedersen conductivity is comparable to the parallel electric conductivity $\sigma_p(r) = \frac{\sigma_0}{1+\omega_e^2/\nu_e^2} \approx \sigma_0$ (cf. equation (6.84)), and we write,

$$\sigma_p(r) = A_4 \frac{T^{3/4}}{\sqrt{P}} \exp\left(\frac{-E_H}{2kT}\right)\left[1 + \sqrt{f_K}\,\exp\left(\frac{E_H - E_K}{2kT}\right)\right] \tag{6.116}$$

where $A_4 \approx 6.1 \times 10^6$.

Calculation of $\mathcal{R}_\perp = \left(\int_r \sigma_p(r)dr\right)^{-1}$ for a hot-Jupiter

. We calculate here the three resistances described in section 6.9.1 in order to illustrate their differences. We first calculate $\mathcal{R}_\perp$, which is accurate if the current is perpendicular to the gradient of electric conductivity, such as in the case of a current going through a thin ionized layer at constant height (for example in the $\mathbf{e}_\theta$ direction in a ionosphere). We then calculate $\mathcal{R}_\parallel$, which is accurate if the current is parallel to the gradient of electric conductivity, such as the case of a current incident (for example radially) on a thin ionized layer. Using our more general formula, we finally calculate $\mathcal{R}_p$ (our generalized formula, which is the value we use in later numerical applications).

We decompose the height integrated conductivity of the planet into its isothermal and convective components $\Sigma_p = \Sigma_{p,isoth} + \Sigma_{p,conv}$, with

$$\Sigma_{p,isoth} = \int_{r_=}^{r_{1p}} \sigma_p(r)dr \approx \int_{r_=}^{r_1} \sigma_0(r)dr = \frac{2E_pH_p}{\sqrt{P_{1p}}}\left(1 - \sqrt{\frac{P_{1p}}{P_{max}}}\right) \approx \frac{2E_pH_p}{\sqrt{P_{1p}}} \tag{6.117}$$

$$\Sigma_{p,conv} = \int_r A_4 \frac{T^{3/4}}{\sqrt{P}} exp\left(\frac{-E_K}{2kT}\right) dr \tag{6.118}$$

$$= \frac{A_4 T_{c,0}^{3/4}}{\sqrt{P_{c,0}}} \int_{r=0}^{r_=} (S(r))^{-1/4}\left[exp\left(\frac{-E_H}{2kT_{c,0}}\frac{1}{S(r)}\right) + \sqrt{f_K} exp\left(\frac{-E_K}{2kT_{c,0}}\frac{1}{S(r)}\right)\right].$$

where $P_{1p} = A_3\sqrt{T(r_{1p})}\mathcal{B}_*(a)$ is the pressure at the effective radius, $P_{max} = P(r_=)$ is the pressure at the transition with the convective zone, $E_p = A_4 T^{3/4}\sqrt{f_K}\exp\left(\frac{-E_K}{2kT}\right)$, and $H_p = \alpha T R_p^2/(GM_p)$ is the scale height.

For a planet like CoRoT-2b at $a = 0.028$ AU around a relatively young star (CoRoT-2), we obtain $T_p = 1500$K, $\mathcal{B}_*(a) = 10^{-4}$T, $P_{1p} = 11$Pa, $P_{max} = 3.8\times10^8$Pa, $H_p = 2.95\times10^5$m, $E_p = 7.6 \times 10^{-2}$, and we find $\Sigma_{p,isoth,young} \approx 1.3 \times 10^4$ for the isothermal region and $\Sigma_{p,conv,young} \approx 3 \times 10^{12}\text{ohm}^{-1}$ for the polytropic region (where the contribution of the hydrogen largely dominates that of the potassium).

We thus obtain $\mathcal{R}_\perp \approx 8.3 \times 10^{-13}$ for CoRoT2b threaded by a stellar field of 1G at its location.

Calculation of $\mathcal{R}_\parallel = \frac{1}{R_p^2}\left(\int_r dr/\sigma_p(r)\right)$ for a hot-Jupiter

The isothermal contribution to the total resistance is (after a change of variable),

$$\mathcal{R}_{\parallel,iso} = \frac{H_p}{E_p R_p^2}\int_{P_{1p}}^{P_=}\frac{dP}{\sqrt{P}} \approx \frac{2H_p\sqrt{P_=}}{R_p^2 E_p}. \tag{6.119}$$

For CoRoT-2b, we obtain $\mathcal{R}_{\parallel,iso} \approx 1.5 \times 10^{-5}$ohm, which is primarily determined by the interior ($\mathcal{R}_\parallel$ neglects the regions with smaller conductivity).

The convective contribution to the total resistance is,

$$\mathcal{R}_{\parallel,conv} = \frac{\sqrt{P_{c,0}}}{R_p^2 A_4 T_{c,0}^{3/4}}\int_{r=0}^{r_=}(S(r))^{1/4}\left[exp\left(\frac{-E_H}{2kT_{c,0}}\frac{1}{S(r)}\right) + \sqrt{f_K}exp\left(\frac{-E_K}{2kT_{c,0}}\frac{1}{S(r)}\right)\right]^{-1}, \tag{6.120}$$

with $\sqrt{P_{c,0}}/R_p^2 A_4 T_{c,0}^{3/4} \approx 4.7 \times 10^{-21}$, the integral approximatively equal to 6.1×10^{13}, and $\mathcal{R}_{\parallel,conv} \approx 2.9 \times 10^{-7}$ohm.

Therefore, $\mathcal{R}_\parallel \approx \mathcal{R}_{\parallel,iso} \approx 1.5 \times 10^{-5}$ ohm, which is primarily determined by the outer layers ($\mathcal{R}_\perp$ neglects the regions with larger conductivity).

Calculation of $\mathcal{R}_p$

Finally, we calculate $\mathcal{R}_p$,

$$\mathcal{R}_p = \left[\int_{z=0}^{R_{max}}\int_{y=0}^{\sqrt{R_{max}^2-z^2}} dydz\left(\int_{x=0}^{\sqrt{R_{max}^2-z^2-y^2}}\frac{dx}{\sigma_p(r)}\right)^{-1}\right]^{-1}, \tag{6.121}$$

with $R_{max} = r_1$ the radius for which $\omega_e \approx \nu_e$. For CoRoT-2b, we obtain $\mathcal{R}_p = 2 \times 10^{-6}$Ohm.

We then artificially vary the surface temperature T_0 (and the internal structure varies accordingly) but keep all the other parameter above constant (including the radius at the photosphere and the field strength). We find, $\mathcal{R}_p(T = 1000K) = 2 \times 10^{-2}$ohm, $\mathcal{R}_p(T = 1280K) = 6.7 \times 10^{-5}$ohm, $\mathcal{R}_p(T = 1500K) = 2 \times 10^{-6}$ohm, $\mathcal{R}_p(T = 1800K) = 1.5 \times 10^{-7}$ohm, $\mathcal{R}_p(T = 2000K) = 4 \times 10^{-8}$ohm, $\mathcal{R}_p(T = 2200K) = 10^{-8}$ohm.

Because we neglected the pressure ionization, our analytical model underestimates the electric conductivities in the planet's deep interior by a factor 100 when compared with Batygin & Stevenson 2011 [9] and a factor 10 when compared with Huang & Cummings 2012 [62]), which both use more realistic numerical models of the interior. Nevertheless, as we pointed out earlier, the value of the integrated resistance is dominated by the outer layer. For example, increasing the electric conductivity by 100 in the interior of the planet, leads to a change in the integrated resistance of a few percent.

6.9.3 Structure, electric conductivity, resistance, and Alfvén travel time in the footprint

Structure

A Sun-like star has a photosphere thickness of about 500 kilometers, and the chromosphere above is about 2000km thick. The temperature is about 6000K in the photosphere, and decreases slowly in most of the chromosphere to about 4000K. The thin transition zone between the chromosphere and the corona above sees a sharp increase in temperature. The density and pressure at the top of the photosphere (bottom of chromosphere) are roughly $\varrho \approx 2 \times 10^{-4}$ kgm^{-3} and $P \approx 10^4$ Pa, and decrease to $\varrho \approx 2 \times 10^{-11}$ and $P \approx 2 \times 10^{-3}$ Pa at the transition zone between the chromosphere and corona. The current typically crosses the footprint in the stellar atmosphere in the photosphere and the bottom of the chromosphere, which we model with an isothermal temperature T_*. The state variables in the footprint, photosphere, and chromosphere are,

$$P(r) = P_0 exp\left[\beta_*(1-x)\right] \quad (6.122)$$
$$\varrho(r) = \varrho_0 \exp\left[\beta_*(1-x)\right] \quad (6.123)$$
$$T(r) = T_0, \quad (6.124)$$

where the subscript 0 denotes the top of the photosphere.

Young or mature main sequence star. We use the perfect gas law, $\tau = 2/3$, and $\kappa = 10^{-38}\varrho^{1/3}T^{10}$ for the opacity due to H-scattering in SI units (converted from Bell & Lin 1994 [10]). For the top of the photosphere, we get the following values with our fiducial values given at the end of section (3.2.4), $g_* \approx 337\text{ms}^{-2}$, $\beta_* = 4576$, $P_0 = 1.2 \times 10^4$Pa, $\varrho_0 = 2.5 \times 10^{-4}\text{kgm}^{-3}$, $T_0 = 5600$K, $\kappa_0 = 1.8\text{m}^2\text{kg}^{-1}$.

TTauri star. The relatively lower temperatures of TTauri stars place them at the transition between an opacity dominated by molecules and H- scattering. Using the opacity tables (with X=0.8, Y=0.28, Z=0.02) from Cox & Tabor 1976 [25] and fit from Bell & Lin 1994 [10] for molecules (which gives a good match with the tables in Cox), we find $P_0 = 8 \times 10^3$Pa, $\varrho_0 = 2.4 \times 10^{-4}\text{kgm}^{-3}$, $T_0 = 4000$K, $\kappa_0 = 3 \times 10^{-3}\text{m}^2\text{kg}^{-1}$.

Stellar effective radius.

As with the planet, we assume that the current starts crossing the stellar atmosphere around $r = r_{1*}$, and we include layers below r_{1*} as part of the footprint. The corresponding pressure is $P_{1*} = A_3\sqrt{T}\mathcal{B}_*(R_*) \approx 6.5 \times 10^3$ Pa for a main sequence star (about one scale into the chromosphere), and $P_{1*} \approx 3.7 \times 10^4$Pa for a TTauri star (in the photosphere, about 1.5 scale height below the bottom of the chromosphere).

Electric conductivity and total resistance

As in the planet, we use equation (6.84) to write the electric conductivity in the footprint.

$$\sigma_p(r) \approx \sigma_0 = A_4 \frac{T^{3/4}}{\sqrt{P}} \exp\left(\frac{-E_H}{2kT}\right)\left[1+\sqrt{f_K}\,\exp\left(\frac{E_H-E_K}{2kT}\right)\right], \tag{6.125}$$

where $A_4 \approx 6.1\times10^6$. Since only a thin layer of the star is involved in the circuit (down to a depth of penetration d_{pn}), we use the thin-layer approximation,

$$\mathcal{R}_* = (2s\Sigma_*)^{-1} \tag{6.126}$$

$$\Sigma_* = \int_{zmin}^{zmax} \sigma_p(z)dz, \tag{6.127}$$

where $s = cos\theta_F = \sqrt{1-R_*/a}$ and the bounds of the integral are from $z = d_{pn}$ to $z = r_1$. For an isothermal region (near the photosphere and a few scale depth in thickness), we can write $\sigma_p(z) = E_* P^{-1/2}$ where $E_* = A_4 T^{3/4}\exp\left(\frac{-E_H}{2kT}\right)\left[1+\sqrt{f_K}\,\exp\left(\frac{E_H-E_K}{2kT}\right)\right]$. The height integrated Pedersen conductivity can then be integrated analytically,

$$\Sigma_* = \int_z E_* P^{-1/2} dz = \int_{Pmin}^{Pmax} E_* \frac{R_*}{\beta_*}\frac{dP}{P^{3/2}} = \frac{2E_*H_*}{\sqrt{P_{1*}}}\left(1-\sqrt{\frac{P_{1*}}{P_{max}}}\right), \tag{6.128}$$

where $H_* = R_*/\beta_* = \alpha T_* R_*^2/(GM_*)$ is the scale height in the photosphere and $P_{min} = P_{1*} = 2.9\times10^3\sqrt{T}\mathcal{B}_*(R_*)$. Therefore, Σ_* has a maximum value $\Sigma_{*,max} = 2E_*H_*/\sqrt{P_{1*}}$, but the footprint typically does not extend so deep that Σ_* reaches its maximum value. For a young or mature main sequence star (with $R_* = 0.9R_\odot$, $T_* = 5600$K), we find $\Sigma_{*,max} \approx 1.6\times10^8 \text{ohm}^{-1}$, and the resistance of the star is at least $\mathcal{R}_* > 3\times10^{-9}$ohm.

Total stellar resistance for different ages

We rewrite the relevant expression using scaling laws using CoRoT2 (a young main sequence star) as a reference,

$$\begin{aligned}
E_* &= 3.94\times10^9\left(\frac{T}{5600K}\right)^{3/4} exp\left(-14.1\left(\frac{T}{5600K}\right)^{-1}\right)\left[1+\sqrt{f_K}exp\left(9.6\left(\frac{T}{5600K}\right)^{-1}\right)\right]\\
H_* &= \frac{\alpha T_* R_*^2}{GM_*} = 1.38\times10^5 m\left(\frac{R_*}{0.9R_\odot}\right)^2\left(\frac{T_*}{5600K}\right)\left(\frac{M_*}{M_\odot}\right)^{-1}\\
P_{min} &= A_3\sqrt{T}\mathcal{B} = 6500Pa\left(\frac{T}{5600K}\right)^{1/2}\left(\frac{\mathcal{B}_*}{0.03T}\right)\\
\Sigma_{*,max} &= 1.34\times10^{13} ohm^{-1}\left(\frac{T}{5600K}\right)^{3/2}\left(\frac{R_*}{0.9R_\odot}\right)^2\left(\frac{\mathcal{B}_*}{0.03T}\right)^{-1/2}\left(\frac{M_*}{M_\odot}\right)^{-1}\\
&\quad exp\left(-14.1\left(\frac{T}{5600K}\right)^{-1}\right)\left[1+\sqrt{f_K}exp\left(9.6\left(\frac{T}{5600K}\right)^{-1}\right)\right].
\end{aligned} \tag{6.129}$$

For a TTauri star (we use $T = 4000$K, $\mathcal{B}_*(R_*) = 0.2T$, $R_* = 3R_\odot$), we obtain $E_* = 5.6 \times 10^3$, $H_* = 1.1 \times 10^6$m, $P_{1*} \approx 3.7 \times 10^4$ Pa, $\Sigma_{*,max} = 6.4 \times 10^7$ ohm^{-1}, and $\mathcal{R}_* > 7.9 \times 10^{-9}$ohm.

For a young main sequence star (we use the values for CoRoT-2, $T = 5600$K, $\mathcal{B}_*(R_*) = 0.03T$, $R_* = 0.9R_\odot$), $M_* = M_\odot$), we obtain Σ_* is 1.6×10^8ohm^{-1}, and $\mathcal{R}_* > 3 \times 10^{-9}$ohm.

For a mature star (we use $T = 5600$K, $\mathcal{B}_*(R_*) = 0.003T$), $E_* = 4.7 \times 10^4$, $H_* = 1.38 \times 10^5$m, $P_{min} = 650$Pa, $\Sigma_{*,max} = 5.1 \times 10^8$, and $\mathcal{R}_* > 10^{-9}$ohm.

Alfvén travel time in the footprint

As stated earlier, we consider the plasma with pressure larger than $P_{1*} = A_3\sqrt{T}\mathcal{B}_*(R_*)$ as part of the footprint (when the Pedersen conductivity becomes comparable to the parallel conductivity). This pressure is $P_{1*,TTauri} \approx 3.4 \times 10^4$Pa for a TTauri star, $P_{1*,young} \approx 6.5 \times 10^3$Pa for a young star such as CoRoT 2, and $P_{1*,mature} \approx 6.5 \times 10^2$Pa for a mature star like the Sun with weaker surface magnetic fields.

As an Alfvén wave is generated near the planet, it travels along the flux tube toward the star, taking a time $t_{A,FT}$ to reach the stellar atmosphere at r_{1*}. It may then be reflected to the planet or may continue deeper into the star. An Alfvén wave that penetrates too deep into the stellar atmosphere before it is reflected will not reach back to the planet within the time t_{max}. There is therefore a maximum penetration depth d_{pn} into the star. We therefore include as part of contribution of the footprint to the electric circuit any plasma between d_{pn} and r_1.

The Alfvén speed in the stellar atmosphere is

$$\upsilon_{A,*}(x) = \frac{\mathcal{B}_*(x)}{\sqrt{\mu_0 \varrho(x)}} = \frac{\mathcal{B}_*(R_*)}{\sqrt{\mu_0 \varrho_0}} \exp\left(\frac{-\beta_*}{2}(1-x)\right), \tag{6.130}$$

where we assumed the magnetic field to be constant throughout the footprint in the stellar atmosphere.

The Alfvén travel time in the footprint from $x_1 = r_1/R_p$ to a location x_{pn} (in the isothermal photosphere) to be determined is therefore,

$$t_{A,*} = \int_{r=r_{pn}}^{r_1} \frac{dr}{\upsilon_{A,*}} = \frac{2H_*}{\upsilon_{A,*}(x_1)}\left(\frac{\upsilon_{A,*}(x_1)}{\upsilon_{A,*}(x_{pn})} - 1\right) = \frac{2H_*}{\upsilon_{A,*}(x_1)}\left(\sqrt{\frac{P(x_{pn})}{P_{1*}}} - 1\right). \tag{6.131}$$

For a TTauri star, $H_* = 1.1 \times 10^6$m, $\beta_* = 1922$, $P_1 = 3.7 \times 10^4$Pa, $\varrho_1 = 1.1 \times 10^{-3}$, $\mathcal{B}_*(R_*) = 0.2$T, and $\upsilon_{A,*}(x_1) = 5.3$km/s.

For a main sequence star, $H_* = 1.4 \times 10^5$m, $\beta_* = 4576$, $P_1 = 6.5 \times 10^3$Pa, $\varrho_1 = 1.4 \times 10^{-4}$, $\mathcal{B}_*(R_*) = 0.03$T, and $\upsilon_{A,*}(x_1) = 2.26$km/s.

6.9.4 Structure and Alfvén travel time along the flux tube

Mass density in the flux tube

Since the planet is inside or near the stellar magnetosphere, we assume that the density in the interplanetary medium between the planet and star is set by the average stellar wind. If the system is very young, accretion may also play a role, depending on the location. We use a range of values around $10^{-8} M_\odot \mathrm{yr}^{-1}$, $\upsilon_{wind} = 400 km/s$ for TTauri stars, $10^{-11} M_\odot \mathrm{yr}^{-1}$ $\upsilon_{wind} = 200 km/s$ for young main sequence stars, and $3 \times 10^{-14} M_\odot \mathrm{yr}^{-1}$ $\upsilon_{wind} = 100 km/s$ for mature stars. Assuming an isotropic outflow, we get the density for the flux tube $\varrho_{FT}(r) = \dot{M} / (4\pi r^2 \upsilon_{wind})$ (where r denotes the distance to the center of the star) respectively for TTauri, young, and mature main sequence stars,

$$\varrho_{FT}(r) \approx 3.5 \times 10^{-12} kgm^{-3} \left(\frac{r}{0.04AU}\right)^{-2} \left(\frac{\dot{M}}{10^{-8} M_\odot/yr}\right) \left(\frac{\upsilon_{wind}}{400 km/s}\right)^{-1} \quad (6.132)$$

$$\varrho_{FT}(r) \approx 7 \times 10^{-15} kgm^{-3} \left(\frac{r}{0.04AU}\right)^{-2} \left(\frac{\dot{M}}{10^{-11} M_\odot/yr}\right) \left(\frac{\upsilon_{wind}}{200 km/s}\right)^{-1} \quad (6.133)$$

$$\varrho_{FT}(r) \approx 1.4 \times 10^{-17} kgm^{-3} \left(\frac{r}{0.04AU}\right)^{-2} \left(\frac{\dot{M}}{10^{-14} M_\odot/yr}\right) \left(\frac{\upsilon_{wind}}{100 km/s}\right)^{-1}. \quad (6.134)$$

Alfvén speed and travel time along the flux tube

Assuming a dipolar magnetic field, the Alfvén speed $\upsilon_{A,FT}(r) = \mathcal{B}_*(r)/\sqrt{\mu_0 \varrho(r)}$ along the flux tube is respectively for TTauri, young, and mature main sequence stars

$$\upsilon_{A,FT}(r) \approx 4 \times 10^6 ms^{-1} \left(\frac{r}{0.04AU}\right)^{-2} \left(\frac{\mathcal{B}_*(R_*)}{0.2T}\right) \left(\frac{R_*}{3R_\odot}\right)^3 \left(\frac{\dot{M}}{10^{-8} M_\odot/yr}\right)^{-1/2} \left(\frac{\upsilon_{wind}}{400 km/s}\right)^{1/2} \quad (6.135)$$

$$\upsilon_{A,FT}(r) \approx 3.7 \times 10^5 ms^{-1} \left(\frac{r}{0.04AU}\right)^{-2} \left(\frac{\mathcal{B}_*(R_*)}{0.03T}\right) \left(\frac{R_*}{0.9R_\odot}\right)^3 \left(\frac{\dot{M}}{10^{-11} M_\odot/yr}\right)^{-1/2} \left(\frac{\upsilon_{wind}}{200 km/s}\right)^{1/2} \quad (6.136)$$

$$\upsilon_{A,FT}(r) \approx 8.3 \times 10^5 ms^{-1} \left(\frac{r}{0.04AU}\right)^{-2} \left(\frac{\mathcal{B}_*(R_*)}{0.003T}\right) \left(\frac{R_*}{0.9R_\odot}\right)^3 \left(\frac{\dot{M}}{10^{-14} M_\odot/yr}\right)^{-1/2} \left(\frac{\upsilon_{wind}}{100 km/s}\right)^{1/2}. \quad (6.137)$$

Finally, the travel time along the flux tube between the planet and footprint $t_A = \int dr/\upsilon_A$ are (for TTauri, young, and mature main sequence stars)

$$t_{A,FT}(r) \approx 489s \left(\frac{a}{0.04AU}\right)^3 \left(\frac{\mathcal{B}_*(R_*)}{0.2T}\right)^{-1} \left(\frac{R_*}{3R_\odot}\right)^{-3} \left(\frac{\dot{M}}{10^{-8} M_\odot/yr}\right)^{1/2} \left(\frac{\upsilon_{wind}}{400 km/s}\right)^{-1/2} \quad (6.138)$$

$$t_{A,FT}(r) \approx 5.4 \times 10^3 s \left(\frac{a}{0.04AU}\right)^3 \left(\frac{\mathcal{B}_*(R_*)}{0.03T}\right)^{-1} \left(\frac{R_*}{0.9R_\odot}\right)^{-3} \left(\frac{\dot{M}}{10^{-11} M_\odot/yr}\right)^{1/2} \left(\frac{\upsilon_{wind}}{200 km/s}\right)^{-1/2} \quad (6.139)$$

$$t_{A,FT}(r) \approx 2.4 \times 10^3 s \left(\frac{a}{0.04AU}\right)^3 \left(\frac{\mathcal{B}_*(R_*)}{0.003T}\right)^{-1} \left(\frac{R_*}{0.9R_\odot}\right)^{-3} \left(\frac{\dot{M}}{10^{-14} M_\odot/yr}\right)^{1/2} \left(\frac{\upsilon_{wind}}{100 km/s}\right)^{-1/2}. \quad (6.140)$$

Travel time in the chromosphere. We also calculate the Alfvén travel time between r_{1*} and the top of the chromosphere below the transition region with the corona (where

we assume that the density becomes comparable to that imposed by the stellar wind). The chromosphere has a roughly isothermal profile until the transition region with the corona, where the density drops rapidly. We thus approximate the region above r_{1*} by extending the density $\varrho = \varrho_0 exp[\beta_*(1-x)]$. The Alfvén travel time from r_1 to the top of the chromosphere is thus

$$t_{A,chro} = \frac{2H_*}{\upsilon_{A,*}(r_1)}. \tag{6.141}$$

Travel time in the planetary atmosphere. The longest travel time is presumably in the planetary atmosphere of a hot-Jupiter (above the magnetic effective radius r_{1p}) because density is highest and the Alfvén wave is thus slowest (we consider the gas with $r < r_{1p}$ as part of the planet and is not included in the Alfvén travel time). We call $t_{A,p}$ the Alfvén travel time between r_{1p} and the top of the atmosphere where it merges with the interplanetary space. The profile in a the planetary atmosphere may be highly variable (depending on the stellar irradiation, opacities and clouds, composition, and mass loss if applicable, etc.). Since P_{1p} is small (around 11Pa for a temperature of 1500K and a field strength at the planet of 1G), the transition is at most within 10-15 scale heights (*i.e.* the ratios between P_{1p} and the pressure in the region dominated by the stellar wind is typically at most $exp(15)$). With an approximation of an isothermal atmosphere, the Alfvén travel time is calculated as above,

$$t_{A,p} = \frac{2H_p}{\upsilon_{A,p}(r_1)}. \tag{6.142}$$

Nevertheless, $t_{A,p}$ may be much lower. Because of the proximity to the star, the transition to the stellar wind may be much closer to r_{1p}. In addition, the stellar wind exerts a ram pressure and equilibrium balance may thus be reached with a much lower density on the side of the wind.

We include both $t_{A,p}$ and $t_{A,chro}$ as part of $t_{A,FT}$, the travel time along the flux tube. However, because of the uncertainties on $t_{A,p}$, we calculate separately the strength of the interaction with $t_{A,p}$ as above, and with $t_{A,p} = 0$.

6.9.5 Table of symbols

ω_p, ω_*	Planet's orbital angular velocity, Stellar spin angular velocity
$v_{p/*}$	Speed of the planet in the frame of the magnetosphere ($v_{p/*} = a(\omega_p - \omega_*)$)
P_p,P_*	Planet's orbital period, Stellar spin period
a,R_p,R_*	Semi-major axis, Radii of the planet and star
$\mathcal{B}_*$, m	Stellar dipolar magnetic field, Stellar magnetic dipole
θ_F	Angle between the stellar spin axis and the footprint
s	$s \stackrel{def}{=} cos\theta_F$
$\mathcal{E}_0$	Motionally induced electric field in the planet
U_0	Total difference of potential in the electric circuit analogy
y_*,x_*	Lengths of the axes of the footprint (ellipse); the current flows along the direction of y_*
σ_0	Electric conductivity along the magnetic field lines (or in the absence of magnetic field)
σ_p	Pedersen conductivity (perpendicular to $\mathcal{B}$, parallel to $\mathcal{E}$)
σ_H	Hall electric conductivity (parallel to $\mathcal{E} \wedge \mathcal{B}$)
$\sigma_p(r)$	Pedersen conductivity profile in the planet (the context makes it clear)
k	Boltzman constant
E_H, E_K	Hydrogen (13.6eV) and Potassium (4.34eV) ionization potential
$A_1A_3A_4$	Constants $A_1 \approx 0.18$, $A_3 \approx 2.9 \times 10^3$, $A_4 \approx 6.1 \times 10^6$
ω_e,ν_e	Electron gyrofrequency, electron-neutrals collision frequency
n_e	Number density of free electron
χ	Ionization fraction
f_K	Fraction of potassium ($f_K = 10^{-6}$)
$\sigma_*(r)$	Pedersen conductivity profile in the footprint (the context makes it clear)
Σ_*	Height integrated Pedersen conductivity in the footprint
$\Sigma_{*,max}$	Maximum value of Σ_* (it converges as the depth of (an isothermal) footprint increases)
$\mathcal{R}_*$,$\mathcal{R}_p$	Integrated resistance of the footprint and planet used in the calculations
$\mathcal{R}_f$	Integrated resistance of the flux tube (neglected)
$\mathcal{R}_\perp$	Formula for the integrated resistance valid in some cases $([2s]\int_z \sigma(z)dz)^{-1}$
$\mathcal{R}_\parallel$	Formula for the Integrated resistance valid in some cases $R_p^{-2}\int_z dz/\sigma(z)$
δR_{xyz}	Infinitesimal resistance of a parallelepiped of volume dxdydz
δR_{xy}	δR_{xyz} integrated along the z direction
$\mathcal{R}_{*,min}$	Minimum value for the integrated resistance of the footprint
$\mathcal{J}$, $\mathcal{I}$	Volumic (induced) electric current, Integrated current
$\mathcal{P}_p$ $\mathcal{P}_*$	Ohmic dissipation in the planet, in the footprint (usually for one hemisphere)
$\mathcal{P}_{Tot}$	Total ohmic dissipation (usually for one of the two equivalent circuits), $\mathcal{P}_{Tot} = \mathcal{P}_p + \mathcal{P}_*$
$\mathcal{T}_p$ $\mathcal{T}_*$	Lorentz torque on the planet and on the star (axis of the torque is the stellar spin axis)

ϱ_{FT}	Density of the flux tube
ϱ_{wind}, υ_{wind}, $\dot{M}$	Density and velocity of the stellar wind, Stellar mass loss rate
T,P,ϱ	Temperature, Pressure, Density
T_c,P_c,ϱ_c	Temperature, Pressure, Density in the planet's convective region
T_{c0},P_{c0},ϱ_{c0}	Temperature, Pressure, Density at the center of the planet
K, k, f	In the planet's polytropic region: $P = K\varrho^2$, $k = \pi/(fR_p)$, $\varrho = \varrho_{c0} sin(kr)/kr$
κ	Opacity in the stellar atmosphere
Λ_{Tot}, Λ_{vol}	Integrated cooling rate, Cooling rate per unit volume
λ_0	Coefficient in the cooling rate ($\lambda_0 \approx 10^{-39} - 10^{-37}$)Wm^3

E_*	E_* contains the T dependence of σ_* (Pedersen). E_*=cst if isothermal ($\sigma_p(r) = E_* P^{-1/2}$)
H_*, β_*	H_* is the scale-height in the footprint, $\beta_* = R_*/H_*$
H_p, β_p	H_p is the scale-height in the footprint, $\beta_p = R_p/H_p$
P_{min},P_{max}	Pressure at the shallower and deeper boundaries in the integrals in the footprint
r_{1p}, r_{1*}	The "Electromagnetic radius" of the planet and star (where $\omega_e(r) = \nu_e(r)$) It is also where σ_p becomes comparable to σ_0 It is also where the electron starts to cross the planet or the footprint
P_{1p}, P_{1*}	$P_{1p} = P(r_{1p})$, $P_{1*} = P(r_{1*})$
r_{pn}	Radius of the lower boundary of the footprint ("pn" indicates the depth of the footprint)
x, x_{pn}, P_{pn}	$x = r/R_p$ (dimensionless radius), $x_{pn} = r_{pn}/R_p$, $P_{pn} = P(r_{pn}) = P(x_{pn})$
ξ	$\xi = \sqrt{P_{pn}/P_{1*}}$. A dimensionless number which indicates the thickness of the footprint

υ_{A*}, $\upsilon_{A,FT}$	Alfvén speed in the footprint and along the flux tube
t_0	$t_0 = 2R_p/\upsilon_{p/*}$, the plasma advection time across $2R_p$ when there is no magnetic interaction (*e.g.* $\sigma = 0$ in the planet)
t_{max}	The maximum time available for the Alfvén wave to complete the round trip $t_{max} = t_0(1 + \mathcal{R}_*/\mathcal{R}_p)$.
t_{A*}	Alfvén wave travel time in the footprint (from r_{pn} to r_{1*})
$t_{A,FT}$	Alfvén travel time along the footprint, from r_{1p} to r_{1*}. $t_{A,FT}$ is composed of the three following parts, $t_{A,FT} = t_{A,chro} + t_{A,FT,0} + t_{A,p}$ $t_{A,p}$ or $t_{A,chro}$ may be 0 if the ϱ between the star and planet is determined by ϱ_{wind} (*i.e.* $t_{A,FT} = t_{A,FT,0}$)
$t_{A,chro}$	Travel time from r_{1*} to the area where the plasma density equals that of the stellar wind
$t_{A,p}$	Travel time from r_{1p} to the area where the plasma density equals that of the stellar wind
$t_{A,FT,0}$	Travel time along the flux tube proper (where the plasma density is ϱ_{wind}
t_A	Total Alfvén travel time ($t_A = t_{A*} + t_{A,FT}$

Table 6.1: Main symbols used in the chapter.

Chapter 7

Summary and perspectives

Close-in extrasolar planets are a unique subset of all known extrasolar planets as they occupy a parameter space associated with extreme surface temperatures, tidal disruption, irradiation, and electromagnetic interactions unlike any other groups of planets. On average, one percent of stars may harbor a hot-Jupiter (and this ratio may be larger for close-in super-Earths), of which, 10% may be observable by transit. Therefore, until direct imaging becomes widely successful, we may hope to obtain light curves from only a fraction of the close-in extrasolar planets. Yet this subset has already provided questions that challenge theoreticians to develop new models.

We have focused on the magnetic interaction between a close-in extrasolar planet and the magnetic dipole of its host star. In the time periodic interaction, we have chosen the most extreme interaction (that with a TTauri star) in order to obtain an upper boundary of the interaction. Our primary goal was to determine under which conditions the interaction arising from the time-dependent diffusion of the stellar field into a hot-Jupiter was suitable as a mechanism to slow the inward migration in young systems (which occurs on very short time-scales). We find that the maximum interaction by itself is inadequate or barely adequate.

Since young planets have not fully contracted yet, mass loss through Roche lobe overflow is easier to achieve than with mature planets. We thus calculate the maximum rate of mass loss achievable for planets still in the process of contracting, or for slightly older systems in equilibrium with a strong tidal dissipation. We find that the time-scale associated with this angular momentum transfer has the adequate order of magnitude and would result in significant mass loss.

We also model the time independent magnetic interaction as a unipolar inductor. We include both the planet and footprint resistances and introduce a more general calculation of the planetary resistance in the case where the current crosses the interior of the planet. We also allow the current to cross the footprint at variable depths and adapt the commonly used condition of Alfvén wave travel time into a self-consistent closure of the system of equations used in the model. With this feature of the model, the depth of the ohmic dissipation in the stellar envelope can be calculated. We find that it is likely to be in the range of pressures which correspond to the photosphere and bottom of the chromosphere. Such information leads us to the investigation of **potentially detectable spots** on the

star with a period similar to that of the close-in companion.

Although we have focused in this thesis on Solar-type stars, it may be worthwhile to consider **the unipolar inductor interaction between a close-in planet and an M-dwarf**. Indeed, 1) M-dwarfs are common. 2) the search for planets in the habitable zone seems to favor planets around M-dwarfs (since the observational techniques are biased toward planets near their host stars), and the number of detection of planetary systems around M-dwarfs may thus drastically increase in the near future. 3) The lower surface temperature of M-dwarfs is favorable to the Alfén wave closure condition in the unipolar inductor. Planets around M-dwarfs may thus be more likely to interact with their host star within the favorable regime of interaction.

The predictions of the expected Lorentz torque and ohmic dissipation can also be compared with the observed dynamics of the planet and its energy budget. We show that such observational constraints can put constraints on the strength of magnetic interaction, which can then be converted into constraints on the electric conductivity and state (solid, molten, partially molten, differentiated or not) of the outer layers of the planet. Using the example of one system for which a lower bound of the decay time-scale has been inferred, we show that stellar surface field strengths of a few tens of gausses and electric conductivities of the planet's outer layers between 10^{-2} to a few Sm^{-1} are consistent with the constraints. The observational constraints, although useful, are still scant, and more observational estimates (especially of decay time-scales and temperatures of the night side of transiting planets) would improve the constraints available.

We also join the discussion on the unexplained inflated radii of some hot-Jupiters. Focusing at first on CoRoT-2b, the system most inflated (after correcting for the stellar irradiation), we find that the amount of power needed can be provided within the assumptions of the unipolar inductor with a field strength of about 100G, but the precise value is dependent on the stellar mass loss rate and wind speed. As a natural further step, we are considering a wider range of effects which are likely to be present in some systems. For example, we have started to consider **the impact of a planetary ionosphere** and of a **temperature inversion in the planetary atmosphere**. Similarly, although it is not yet known whether close-in planets with synchronized spin of a few days can commonly generate strong dynamo fields, it may be worth investigating **the impact of a planetary magnetosphere**, especially in light of the potentially upcoming **radio-detection of extrasolar planets** (Zarka 2007 [121]). In addition, the field induced in the planet by the stellar magnetic field could be used in place of an intrinsic planetary field (for example in the model by Batygin & Stevenson or by Zarka), especially when the existence of an intrinsic planetary field is uncertain.

Finally, the question why some systems (*e.g.* WASP-19b) which parameters would also presumably result in large ohmic dissipations are not overly inflated also begs to be answered (although most models of inflation would also have to address this question). At the bottom line, it is an opportunity to consider more in detail both the mechanisms that may limit the applicability of the unipolar inductor model, and the corresponding regimes of interactions that are then substituted. For example, we have already considered the impact of the ohmic dissipation in the footprint which provides a feedback mechanism that can prevent the circuit closure condition to be met. When the circuit closure condition is

not met, the planet and footprint no longer directly influence each other, and the condition that the current is the same along the circuit is no longer valid. Instead, the planet and the footprint each generates an independent set of Alfvén waves. The waves generated near the planet may still reach the star (if the plasma flow is everywhere sub-Alfvénic), but they will not be reflected back to the planet. The impedance ascribed to a pure Alfvén wing ($\mu_0 v_A$, Neubauer 1980 [83]) is in the upper range of the resistances calculated in this work in the unfavorable closure regime. The **interaction as a pure Alfvén wing** would thus correspond to a weaker interaction.

Les planètes proches de leur étoile possèdent des charactéristiques uniques (par example leur température de surface ou l'intensité des interactions gravitationelles et électromagnétiques avec leur étoile) parmi les planètes extrasolaires découvertes jusqu'à ce jour. En moyenne, 1% des étoiles ont une planète géante proche (ce chiffre étant peut-être encore plus grand pour les planètes telluriques), dont environ 10% sont détectables par transit. Avant l'avènement de méthodes de détection directes, nous ne pouvons donc espérer étudier le spectre que d'une partie de ces planètes proches de leur étoile. Ce sous-groupe de planètes a cependant déjà soulevé de nombreuses questions intéressantes.

Nous nous intéressons à l'interaction magnétique entre une planète extrasolaire proche et le dipole magnétique de son étoile. Pour étudier l'interaction périodique dans le temps, nous considérons les conditions optimales (correspondant au champ magnétique d'une étoile TTauri) afin de déterminer quels sont les effets les plus forts possibles. En particulier, nous voulions savoir dans quelles conditions l'interaction correspondant au mode Transverse Electrique est suffisante pour arrêter la migration d'une planète vers son étoile. Nous concluons que ce mode d'interaction est insuffisant ou marginalement suffisant.

Puisque les planètes jeunes n'ont pas encore achevé leur contraction, une perte de masse est relativement plus facile à provoquer. Nous calculons le taux maximal de perte de masse par débordement du lobe de Roche pour une planète en contraction quasi-hydrostatique (ou pour une planète un peu plus vieille en équilibre avec des interactions de marées fortes). Nous concluons que la perte de masse associée à la dissipation ohmique permet de transferrer suffisamment de moment angulaire à la planète et serait associée à une perte de masse totale non-négligeable.

Nous modélisons l'interaction magnétique indépendente du temps comme un inducteur unipolaire. Nous incluons les résistances de la planète et du pied du flux de tube et introduisons une formule générale pour la conductivité intégrée de la planète lorsque le courant traverse l'intérieur de la planète. Nous introduisons aussi un paramètre qui permet de spécifier la profondeur à laquelle le courant traverse le pied du flux de tube; la condition de temps de trajet des ondes d'Alfvén complète alors le système d'équations de manière cohérente, et détermine la profondeur à laquelle l'énergie ohmique est dissipée dans l'atmosphère de l'étoile. Nous trouvons qu'elle est dissipée à des pressions correspondant à la photosphère et base de la chromosphère. Ceci permet alors d'envisager l'existence de **tâches stellaires potentiellement observables** dont la période est égale à celle de la période orbitale de la planète.

Bien que nous n'avons utilisé dans les applications numériques uniquement des étoiles de masse comparable au Soleil, il pourrait être intéressant d'appliquer le modéle d'interaction unipolaire aux **naines rouges**. En effet, 1) ces étoiles sont courantes, 2) la recherche de planètes dans la zone habitable est pour l'instant plus favorable aux naines rouges (puisque les méthodes de détections favorisent les planètes proches de leur étoile, et on peut donc s'attendre à une explosion dans le futur proche du nombre de détections de systèmes autour de naines rouges 3) les naines rouges ont une température de surface plus faible, ce qui est favorable à la fermeture du circuit dans le modèle d'interaction unipolaire.

Nous comparons aussi l'intensité du couple de Lorentz et de la dissipation ohmique dans le cadre de l'interaction unipolaire aux contraintes sur la dynamique et le budget énergétique de la planète obtenue par les observations. Nous proposons que ces contraintes observationelles permettent d'obtenir des contraintes sur l'intensité de l'interaction magnétique, et donc des informations sur la conductivité électrique et la phase (solide, liquide, différencié ou non) des couches externes d'une planète tellurique. En utilisant la planète Kepler-78b (KIC 8435766b) comme example (pour laquelle une borne minimale du taux de changement de demi-grand axe à été estimé observationellement), nous concluons qu'une intensité de champ magnétique à la surface de l'étoile de quelques dizaines de gauss et une conductivité électrique des couches externes de la planète de 0.01 à quelques Sm^{-1} sont consistents avec les contraintes. Bien qu'utiles, ces informations sont encore peu courantes et plus d'observations (en particulier le taux de réduction de semi-grand axe et la température de la face nuit des planètes en transit) permettraient d'affiner nos conclusions.

Nous proposons également que la dissipation ohmique dans une géante gaseuse permettrait d'expliquer l'aspect enflé de certaines planètes proches de leur étoile. Par example, nous montrons qu'un champ magnétique à la surface de l'étoile de 100G permettrait d'expliquer le rayon de CoRoT-2b (bien que la valeur exacte dépende de la perte de masse de l'étoile et de la vitesse du vent solaire). L'étude pourrait ensuite être élargie pour inclure des effets comme une **ionosphère** ou une **inversion de température dans l'atmosphère planétaire**. Bien que l'existence d'une **magnétosphère autour des planètes extrasolaires** dont la rotation est synchronisée avec leur orbite (d'une période de quelques jours) est encore débattue, il pourrait être intéressant d'inclure cet effet, en particulier au vu de la **détection potentielle d'émissions radios provenant des planètes extrasolaires** proches de leurs étoiles (Zarka 2007 [121]). De même, le champ magnétique induit dans la planète de part son interaction avec le champ stellaire peut être utilisé à la place d'un champ planétaire intrinsèque (par example dans le modèle de Zarka ou de Batygin & Stevenson), surtout dans les cas où l'existence d'un tel champ est incertain.

Finalement, une question importante (pour tout modèle cherchant à expliquer l'aspect enflé de certaines planètes) consiste à comprendre pourquoi certains systèmes (par example WASP-19b) qui devraient être associés avec une forte interaction magnétique avec l'étoile ne présentent pas un rayon aussi enflé que, par example, CoRoT-2b. Il s'agit donc de comprendre plus précisement les mécanismes qui limitent l'applicabilité du modèle d'induction unipolaire et les régimes d'interactions qui se substituent alors. Par example, nous avons déjà montré que la dissipation ohmique dans le pied du flux de tube peut rendre la condition de trajet des ondes d'Alfvén plus difficile à remplir. Lorsque cette condition n'est pas remplie, la planète et le pied du flux de tube ne s'influencent plus mutuellement, le courant n'est plus le même en tout point du circuit électrique, et la planète et le pied du flux de tube génèrent chacun une aile d'Alfvén. Les ondes d'Alfvén générées près de la planète se propagent jusqu'à l'étoile (si le plasma est partout sous-Alfvénique), mais ne sont pas réfléchies jusqu'à la planète. L'impédance correspondant à une aile d'Alfvén ($\mu_0 v_A$, Neubauer 1980 [83]) est comparable aux résistances les plus élevées typiquement obtenue dans le régime défavorable de fermeture du circuit. L'interaction correspondant au **régime d'aile d'Alfvén** correspondrait donc à une interaction plus faible.

Bibliography

[1] Richard Alexander. Lecture notes on the astrophysics of planet formation, 2013.

[2] H. Alfvén. *Cosmical Plasma*. D. Reidel Publishing Company, 1981.

[3] H. Alfvén. Existence of Electromagnetic-Hydrodynamic Waves. *Nature*, 150:405–406, October 1942.

[4] P. J. Armitage. *Astrophysics of Planet Formation*. Cambridge University Press, 2010.

[5] Philip J. Armitage. Lecture notes on the formation and early evolution of planetary systems, 2013.

[6] W. G. Baker and D. F. Martyn. Electric Currents in the Ionosphere. I. The Conductivity. *Royal Society of London Philosophical Transactions Series A*, 246:281–294, December 1953.

[7] C. Baruteau. *Toward predictive scenarios of planetary migration*. PhD thesis, CEA Saclay, Service d'Astrophysique, 91191 Gif/Yvette Cedex, France, 2008.

[8] K. Batygin and D. J. Stevenson. Inflating Hot Jupiters with Ohmic Dissipation. *ApJLett*, 714:L238–L243, May 2010.

[9] K. Batygin, D. J. Stevenson, and P. H. Bodenheimer. Evolution of Ohmically Heated Hot Jupiters. *ApJ*, 738:1, September 2011.

[10] K. R. Bell and D. N. C. Lin. Using FU Orionis outbursts to constrain self-regulated protostellar disk models. *ApJ*, 427:987–1004, June 1994.

[11] E. K. Bigg. Influence of the Satellite Io on Jupiter's Decametric Emission. *Nature*, 203:1008–1010, September 1964.

[12] P. Bodenheimer, D. N. C. Lin, and R. A. Mardling. On the Tidal Inflation of Short-Period Extrasolar Planets. *ApJ*, 548:466–472, February 2001.

[13] P. Bodenheimer and J. B. Pollack. Calculations of the accretion and evolution of giant planets The effects of solid cores. *Icarus*, 67:391–408, September 1986.

[14] A. P. Boss. Giant planet formation by gravitational instability. *Science*, 276:1836–1839, 1997.

[15] J. Bouvier, S. H. P. Alencar, T. J. Harries, C. M. Johns-Krull, and M. M. Romanova. Magnetospheric Accretion in Classical T Tauri Stars. *Protostars and Planets V*, pages 479–494, 2007.

[16] B. F. Burke and K. L. Franklin. Observations of a Variable Radio Source Associated with the Planet Jupiter. *JGR*, 60:213–217, June 1955.

[17] D. Buzasi. Stellar Magnetic Fields as a Heating Source for Extrasolar Giant Planets. *ApJLett*, 765:L25, March 2013.

[18] J. Cabrera, H. Bruntt, M. Ollivier, R. F. Díaz, S. Csizmadia, S. Aigrain, R. Alonso, J.-M. Almenara, M. Auvergne, A. Baglin, P. Barge, A. S. Bonomo, P. Bordé, F. Bouchy, L. Carone, S. Carpano, M. Deleuil, H. J. Deeg, R. Dvorak, A. Erikson, S. Ferraz-Mello, M. Fridlund, D. Gandolfi, J.-C. Gazzano, M. Gillon, E. W. Guenther, T. Guillot, A. Hatzes, M. Havel, G. Hébrard, L. Jorda, A. Léger, A. Llebaria, H. Lammer, C. Lovis, T. Mazeh, C. Moutou, A. Ofir, P. von Paris, M. Pätzold, D. Queloz, H. Rauer, D. Rouan, A. Santerne, J. Schneider, B. Tingley, R. Titz-Weider, and G. Wuchterl. Transiting exoplanets from the CoRoT space mission . XIII. CoRoT-13b: a dense hot Jupiter in transit around a star with solar metallicity and super-solar lithium content. *AAP*, 522:A110, November 2010.

[19] A. G. W. Cameron. Physics of the primitive solar accretion disk. *Moon and Planets*, 18:5–40, February 1978.

[20] C. G. Campbell. Magnetic coupling in AM Herculis binaries. *MNRAS*, 205:1031–1052, December 1983.

[21] S. Casassus, S. Perez M., A. Jordán, F. Ménard, J. Cuadra, M. R. Schreiber, A. S. Hales, and B. Ercolano. The Dynamically Disrupted Gap in HD 142527. *ApJLett*, 754:L31, August 2012.

[22] D. Charbonneau, T. M. Brown, D. W. Latham, and M. Mayor. Detection of Planetary Transits Across a Sun-like Star. *ApJLett*, 529:L45–L48, January 2000.

[23] U. R. Christensen and J. Aubert. Scaling properties of convection-driven dynamos in rotating spherical shells and application to planetary magnetic fields. *Geophysical Journal International*, 166:97–114, July 2006.

[24] D. S. Colburn. Electromagnetic heating of Io. *JGR*, 85:7257–7261, December 1980.

[25] A. N. Cox and J. E. Tabor. Radiative opacity tables for 40 stellar mixtures. *ApJSupp*, 31:271–312, June 1976.

[26] F. J. Crary and F. Bagenal. Coupling the plasma interaction at Io to Jupiter. *Geophys. Rev. Lett*, 24:2135, September 1997.

[27] M. Cuntz, S. H. Saar, and Z. E. Musielak. On Stellar Activity Enhancement Due to Interactions with Extrasolar Giant Planets. *ApJLett*, 533:L151–L154, April 2000.

[28] P. A. Deift and C. K. Goertz. The propagation of Alfven waves along Io's flux tube. *PSS*, 21:1417–1429, August 1973.

[29] I. dePater and J. L. Lissauer. *Planetary Sciences*. Cambridge University Press, 2001.

[30] S. F. Dermott. Modulation of Jupiter's decametric radio emission by Io. *MNRAS*, 149:35, 1970.

[31] I. Dobbs-Dixon, D. N. C. Lin, and R. A. Mardling. Spin-Orbit Evolution of Short-Period Planets. *ApJ*, 610:464–476, July 2004.

[32] J.-F. Donati, M. M. Jardine, S. G. Gregory, P. Petit, J. Bouvier, C. Dougados, F. Ménard, A. Collier Cameron, T. J. Harries, S. V. Jeffers, and F. Paletou. Magnetic fields and accretion flows on the classical T Tauri star V2129 Oph. *MNRAS*, 380:1297–1312, October 2007.

[33] J.-F. Donati, M. B. Skelly, J. Bouvier, S. G. Gregory, K. N. Grankin, M. M. Jardine, G. A. J. Hussain, F. Ménard, C. Dougados, Y. Unruh, S. Mohanty, M. Aurière, J. Morin, R. Farès, and MAPP Collaboration. Magnetospheric accretion and spin-down of the prototypical classical T Tauri star AA Tau. *MNRAS*, 409:1347–1361, December 2010.

[34] B. T. Draine. *Physics of the Interstellar and Intergalactic Medium*. Princeton University Press, 2010.

[35] B. T. Draine, W. G. Roberge, and A. Dalgarno. Magnetohydrodynamic shock waves in molecular clouds. *ApJ*, 264:485–507, January 1983.

[36] S. D. Drell, H. M. Foley, and M. A. Ruderman. Drag and Propulsion of Large Satellites in the Ionosphere: An Alfvén Propulsion Engine in Space. *JGR*, 70:3131–3145, July 1965.

[37] P. Driscoll and P. Olson. Optimal dynamos in the cores of terrestrial exoplanets: Magnetic field generation and detectability. *Icarus*, 213:12–23, May 2011.

[38] E. B. Fainberg and B. S. Singer. The Influence of Surface Inhomogeneities On Deep Electromagnetic Soundings of the Earth. *Geophysical Journal International*, 90:61–73, July 1987.

[39] R. Fares, J.-F. Donati, C. Moutou, M. M. Jardine, J.-M. Grießmeier, P. Zarka, E. L. Shkolnik, D. Bohlender, C. Catala, and A. Collier Cameron. Searching for star-planet interactions within the magnetosphere of HD189733. *MNRAS*, 406:409–419, July 2010.

[40] R. C. Fleck. A magnetic mechanism for halting inward protoplanet migration: I. Necessary conditions and angular momentum transfer timescales. *Astrophys. Space Sci.*, 313:351–356, February 2008.

[41] J. J. Fortney, M. Ikoma, N. Nettelmann, T. Guillot, and M. S. Marley. Self-consistent Model Atmospheres and the Cooling of the Solar System's Giant Planets. *ApJ*, 729:32, March 2011.

[42] King A. Frank, J. and D. Raine. *Accretion Power in Astrophysics*. Cambridge University Press, 2002.

[43] E. Gaidos, C. P. Conrad, M. Manga, and J. Hernlund. Thermodynamic Limits on Magnetodynamos in Rocky Exoplanets. *ApJ*, 718:596–609, August 2010.

[44] P. Ghosh and F. K. Lamb. Disk accretion by magnetic neutron stars. *ApJLett*, 223:L83–L87, July 1978.

[45] E. Giannini and J. I. Lunine. Microlensing detection of extrasolar planets. *Reports on Progress in Physics*, 76(5):056901, May 2013.

[46] M. Gillon, A. A. Lanotte, T. Barman, N. Miller, B.-O. Demory, M. Deleuil, J. Montalbán, F. Bouchy, A. Collier Cameron, H. J. Deeg, J. J. Fortney, M. Fridlund, J. Harrington, P. Magain, C. Moutou, D. Queloz, H. Rauer, D. Rouan, and J. Schneider. The thermal emission of the young and massive planet CoRoT-2b at 4.5 and 8 μm. *AAP*, 511:A3, February 2010.

[47] C. K. Goertz. Jupiter's ionosphere and magnetosphere. *PSS*, 21:1389–1398, August 1973.

[48] C. K. Goertz. The Io-controlled decametric radiation. *PSS*, 21:1431–1445, August 1973.

[49] C. K. Goertz and P. A. Deift. Io's interaction with the magnetosphere. *PSS*, 21:1399–1415, August 1973.

[50] T. Gold. Motions in the Magnetosphere of the Earth. *JGR*, 64:1219–1224, September 1959.

[51] P. Goldreich and D. Lynden-Bell. Io, a jovian unipolar inductor. *ApJ*, 156:59–78, April 1969.

[52] P. Goldreich and S. Tremaine. The excitation of density waves at the Lindblad and corotation resonances by an external potential. *ApJ*, 233:857–871, November 1979.

[53] S. G. Gregory, M. Jardine, C. G. Gray, and J.-F. Donati. The magnetic fields of forming solar-like stars. *Reports on Progress in Physics*, 73(12):126901, December 2010.

[54] S. G. Gregory, S. P. Matt, J.-F. Donati, and M. Jardine. The non-dipolar magnetic fields of accreting T Tauri stars. *MNRAS*, 389:1839–1850, October 2008.

[55] P.-G. Gu, P. H. Bodenheimer, and D. N. C. Lin. The Internal Structural Adjustment Due to Tidal Heating of Short-Period Inflated Giant Planets. *ApJ*, 608:1076–1094, June 2004.

[56] P.-G. Gu, D. N. C. Lin, and P. H. Bodenheimer. The Effect of Tidal Inflation Instability on the Mass and Dynamical Evolution of Extrasolar Planets with Ultrashort Periods. *ApJ*, 588:509–534, May 2003.

[57] T. Guillot. On the radiative equilibrium of irradiated planetary atmospheres. *AAP*, 520:A27, September 2010.

[58] T. Guillot and M. Havel. An analysis of the CoRoT-2 system: a young spotted star and its inflated giant planet. *AAP*, 527:A20, March 2011.

[59] T. Guillot and P. Morel. CEPAM: a code for modeling the interiors of giant planets. *AASupp*, 109:109–123, January 1995.

[60] T. W. Hill. Inertial limit on corotation. *JGR*, 84:6554–6558, November 1979.

[61] T. W. Hill. Corotation lag in Jupiter's magnetosphere - Comparison of observation and theory. *Science*, 207:301, January 1980.

[62] X. Huang and A. Cumming. Ohmic Dissipation in the Interiors of Hot Jupiters. *ApJ*, 757:47, September 2012.

[63] G. A. J. Hussain. T Tauri star magnetic fields and magnetospheres. *Astronomische Nachrichten*, 333:4, January 2012.

[64] W.-H. Ip, A. Kopp, and J.-H. Hu. On the Star-Magnetosphere Interaction of Close-in Exoplanets. *ApJLett*, 602:L53–L56, February 2004.

[65] P. B. Ivanov and J. C. B. Papaloizou. Close encounters of a rotating star with planets in parabolic orbits of varying inclination and the formation of hot Jupiters. *Celestial Mechanics and Dynamical Astronomy*, 111:51–82, October 2011.

[66] C. M. Johns-Krull. The Magnetic Fields of Classical T Tauri Stars. *ApJ*, 664:975–985, August 2007.

[67] C. A. Jones. Planetary Magnetic Fields and Fluid Dynamos. *Annual Review of Fluid Mechanics*, 43:583–614, January 2011.

[68] S. I. Karato and D. Wang. *Physics and Chemistry of the Deep Earth*. Wiley & Sons, 2013.

[69] M. G. Kivelson, K. K. Khurana, C. T. Russell, M. Volwerk, R. J. Walker, and C. Zimmer. Galileo Magnetometer Measurements: A Stronger Case for a Subsurface Ocean at Europa. *Science*, 289:1340–1343, August 2000.

[70] H. A. Knutson, D. Charbonneau, L. E. Allen, J. J. Fortney, E. Agol, N. B. Cowan, A. P. Showman, C. S. Cooper, and S. T. Megeath. A map of the day-night contrast of the extrasolar planet HD 189733b. *Nature*, 447:183–186, May 2007.

[71] R. O. Laine and D. N. C. Lin. *in preparation*.

[72] R. O. Laine and D. N. C. Lin. Interaction of Close-in Planets with the Magnetosphere of Their Host Stars. II. Super-Earths as Unipolar Inductors and Their Orbital Evolution. *ApJ*, 745:2, January 2012.

[73] R. O. Laine, D. N. C. Lin, and S. Dong. Interaction of Close-in Planets with the Magnetosphere of Their Host Stars. I. Diffusion, Ohmic Dissipation of Time-dependent Field, Planetary Inflation, and Mass Loss. *ApJ*, 685:521–542, September 2008.

[74] R. O. Laine, D. N. C. Lin, and T. Guillot. *in preparation*.

[75] A. F. Lanza. Stellar coronal magnetic fields and star-planet interaction. *AAP*, 505:339–350, October 2009.

[76] J. Li, L. Ferrario, and D. Wickramasinghe. Planets around White Dwarfs. *ApJLett*, 503:L151, August 1998.

[77] D. N. C. Lin, P. Bodenheimer, and D. C. Richardson. Orbital migration of the planetary companion of 51 Pegasi to its present location. *Nature*, 380:606–607, April 1996.

[78] D. N. C. Lin and W. Ju. *in preparation*.

[79] P. Machalek, P. R. McCullough, A. Burrows, C. J. Burke, J. L. Hora, and C. M. Johns-Krull. Detection of Thermal Emission of XO-2b: Evidence for a Weak Temperature Inversion. *ApJ*, 701:514–520, August 2009.

[80] S. Mao and B. Paczynski. Gravitational microlensing by double stars and planetary systems. *ApJLett*, 374:L37–L40, June 1991.

[81] M. Mayor and D. Queloz. A Jupiter-mass companion to a solar-type star. *Nature*, 378:355–359, November 1995.

[82] C. D. Murray and S. F. Dermott. *Solar System Dynamics*. Cambridge University Press, 2000.

[83] F. M. Neubauer. Nonlinear standing Alfven wave current system at Io - Theory. *JGR*, 85:1171–1178, March 1980.

[84] G. I. Ogilvie and D. N. C. Lin. Tidal Dissipation in Rotating Giant Planets. *ApJ*, 610:477–509, July 2004.

[85] J. C. B. Papaloizou. Protoplanet magnetosphere interactions. *AAP*, 463:775–781, February 2007.

[86] J. C. B. Papaloizou and C. Terquem. On the dynamics of multiple systems of hot super-Earths and Neptunes: tidal circularization, resonance and the HD 40307 system. *MNRAS*, 405:573–592, June 2010.

[87] E. Parker. *Conversations on electric and magnetic fields in the cosmos*. Princeton University Press, 2007.

[88] V. Parmentier and T. Guillot. Temperature inversion and the evolution of exoplanets. In *EPSC-DPS Joint Meeting 2011*, page 1367, October 2011.

[89] G. M. Partzsch, F. R. Schilling, and J. Arndt. The influence of partial melting on the electrical behavior of crustal rocks: laboratory examinations, model calculations, and geological interpretations. *Tectonophysics*, 317:189–203, 2000.

[90] J. H. Piddington. The motion of ionized gas in combined magnetic, electric and mechanical fields of force. *MNRAS*, 114:651, 1954.

[91] J. H. Piddington and J. F. Drake. Electrodynamic Effects of Jupiter's Satellite Io. *Nature*, 217:935–937, March 1968.

[92] K. Poppenhaeger, L. F. Lenz, A. Reiners, J. H. M. M. Schmitt, and E. Shkolnik. A search for star-planet interactions in the upsilon Andromedae system at X-ray and optical wavelengths. *AAP*, 528:A58, April 2011.

[93] D. Queloz. Extrasolar planets: Light through a gravitational lens. *Nature*, 439:400–401, January 2006.

[94] F. A. Rasio and E. B. Ford. Dynamical instabilities and the formation of extrasolar planetary systems. *Science*, 274:954–956, November 1996.

[95] R. Sanchis-Ojeda, S. Rappaport, J. N. Winn, A. M. Levine, M. C. Kotson, and D. W. Latham. Transits and occultations of an Earth-sized planet in an 8.5-hour orbit. *ArXiv e-prints*, May 2013.

[96] J. Saur. A model of Io's local electric field for a combined Alfvénic and unipolar inductor far-field coupling. *Journal of Geophysical Research (Space Physics)*, 109:1210, January 2004.

[97] J. Saur, F. M. Neubauer, J. E. P. Connerney, P. Zarka, and M. G. Kivelson. *Plasma interaction of Io with its plasma torus*, pages 537–560. 2004.

[98] G. Scandariato, A. Maggio, A. F. Lanza, I. Pagano, R. Fares, E. L. Shkolnik, D. Bohlender, A. C. Cameron, S. Dieters, J.-F. Donati, A. F. Martínez Fiorenzano, M. Jardine, and C. Moutou. A coordinated optical and X-ray spectroscopic campaign on HD 179949: searching for planet-induced chromospheric and coronal activity. *AAP*, 552:A7, April 2013.

[99] S. Schröter, S. Czesla, U. Wolter, H. M. Müller, K. F. Huber, and J. H. M. M. Schmitt. The corona and companion of CoRoT-2a. Insights from X-rays and optical spectroscopy. *AAP*, 532:A3, August 2011.

[100] K. Schwartz, C. P. Sonett, and D. S. Colburn. Unipolar Induction in the Moon and a Lunar Limb Shock Mechanism. *Moon*, 1:7–30, November 1969.

[101] ed. Seager, S. *Exoplanets (Space Science Series)*. University of Arizona Press, 2010.

[102] E. Shkolnik. *Chromospheric Activity Induced by Short-Period Planets: A Search for Modulation of Ca II H and K Emission*. PhD thesis, University of British Columbia, 2004.

[103] E. Shkolnik, D. A. Bohlender, G. A. H. Walker, and A. Collier Cameron. The On/Off Nature of Star-Planet Interactions. *ApJ*, 676:628–638, March 2008.

[104] E. Shkolnik, G. A. H. Walker, D. A. Bohlender, P.-G. Gu, and M. Kürster. Hot Jupiters and Hot Spots: The Short- and Long-Term Chromospheric Activity on Stars with Giant Planets. *ApJ*, 622:1075–1090, April 2005.

[105] E. Shkolnik, G. A. H. Walker, D. A. Bohlender, and S. Rucinski. Chromospheric Activity Induced by Short-Period Planets. In *American Astronomical Society Meeting Abstracts*, volume 35 of *Bulletin of the American Astronomical Society*, page 123, December 2003.

[106] A. P. Showman and T. Guillot. Atmospheric circulation and tides of "51 Pegasus b-like" planets. *AAP*, 385:166–180, April 2002.

[107] I. A. G. Snellen, E. J. W. de Mooij, and A. Burrows. Bright optical day-side emission from extrasolar planet CoRoT-2b. *AAP*, 513:A76, April 2010.

[108] C. P. Sonett and D. S. Colburn. Establishment of a Lunar Unipolar Generator and Associated Shock and Wake by the Solar Wind. *Nature*, 216:340–343, October 1967.

[109] C. P. Sonett, D. S. Colburn, and K. Schwartz. Formation of the lunar crust - an electrical source of heating. *Icarus*, 24:231–255, February 1975.

[110] D. J. Southwood and M. G. Kivelson. An approximate description of field-aligned currents in a planetary magnetic field. *JGR*, 96:67–75, January 1991.

[111] D. S. Spiegel, M. Zamojski, A. Gersch, J. Donovan, and Z. Haiman. Can We Probe the Atmospheric Composition of an Extrasolar Planet from Its Reflection Spectrum in a High-Magnification Microlensing Event? *ApJ*, 628:478–486, July 2005.

[112] O. Struve. Proposal for a project of high-precision stellar radial velocity work. *The Observatory*, 72:199–200, October 1952.

[113] C. Terquem and J. C. B. Papaloizou. Migration and the Formation of Systems of Hot Super-Earths and Neptunes. *ApJ*, 654:1110–1120, January 2007.

[114] A. A. Vidotto, M. Jardine, and C. Helling. Early UV Ingress in WASP-12b: Measuring Planetary Magnetic Fields. *ApJLett*, 722:L168–L172, October 2010.

[115] G. A. H. Walker, B. Croll, J. M. Matthews, R. Kuschnig, D. Huber, W. W. Weiss, E. Shkolnik, S. M. Rucinski, D. B. Guenther, A. F. J. Moffat, and D. Sasselov. MOST detects variability on τ Bootis A possibly induced by its planetary companion. *AAP*, 482:691–697, May 2008.

[116] J. N. Winn, J. A. Johnson, S. Albrecht, A. W. Howard, G. W. Marcy, I. J. Crossfield, and M. J. Holman. HAT-P-7: A Retrograde or Polar Orbit, and a Third Body. *ApJLett*, 703:L99–L103, October 2009.

[117] A. Wolszczan and D. A. Frail. A planetary system around the millisecond pulsar PSR1257 + 12. *Nature*, 355:145–147, January 1992.

[118] U. Wolter, S. Czesla, S. Schröter, K. Huber, and J. H. M. M. Schmitt. Transit and Spectral Studies of CoRoT-2. In C. Johns-Krull, M. K. Browning, and A. A. West, editors, *16th Cambridge Workshop on Cool Stars, Stellar Systems, and the Sun*, volume 448 of *Astronomical Society of the Pacific Conference Series*, page 1043, December 2011.

[119] Y. Wu and Y. Lithwick. Secular Chaos and the Production of Hot Jupiters. *ApJ*, 735:109, July 2011.

[120] H. Yang and C. M. Johns-Krull. Magnetic Field Measurements of T Tauri Stars in the Orion Nebula Cluster. *ApJ*, 729:83, March 2011.

[121] P. Zarka. Plasma interactions of exoplanets with their parent star and associated radio emissions. *PSS*, 55:598–617, April 2007.

[122] K. Zhang, C. A. Jones, and D. Chen. Estimates for the Effective Electrical Conductivity of the Core in the Interior of Jupiter and Saturn. *Earth Moon and Planets*, 73:221–236, June 1996.

[123] J. I. Zuluaga, S. Bustamante, P. A. Cuartas, and J. H. Hoyos. The Influence of Thermal Evolution in the Magnetic Protection of Terrestrial Planets. *ApJ*, 770:23, June 2013.

The Astrophysical Journal, 685:521–542, 2008 September 20

INTERACTION OF CLOSE-IN PLANETS WITH THE MAGNETOSPHERE OF THEIR HOST STARS. I. DIFFUSION, OHMIC DISSIPATION OF TIME-DEPENDENT FIELD, PLANETARY INFLATION, AND MASS LOSS

Randy O. Laine,[1] Douglas N. C. Lin,[2,3] and Shawfeng Dong[2]
Received 2007 November 24; accepted 2008 April 9

ABSTRACT

The unanticipated discovery of the first close-in planet around 51 Peg has rekindled the notion that shortly after their formation outside the snow line, some planets may have migrated to the proximity of their host stars because of their tidal interaction with their nascent disks. After a decade of discoveries, nearly 20% of the 200 known planets have similar short periods. If these planets indeed migrated to their present-day location, their survival would require a halting mechanism in the proximity of their host stars. Here we consider the possibility that a magnetic coupling between young stars and planets could quench the planet's orbital evolution. Most T Tauri stars have magnetic fields of several thousand gausses on their surface which can clear out a cavity in the innermost regions of their circumstellar disks and impose magnetic induction on the nearby young planets. After a brief discussion of the complexity of the full problem, we focus our discussion on evaluating the permeation and ohmic dissipation of the time-dependent component of the stellar magnetic field in the planet's interior. Adopting a model first introduced by Campbell for interacting binary stars, we determine the modulation of the planetary response to the tilted magnetic field of a nonsynchronously spinning star. We first compute the conductivity in the young planets, which indicates that the stellar field can penetrate well into the planet's envelope in a synodic period. For various orbital configurations, we show that the energy dissipation rate inside the planet is sufficient to induce short-period planets to inflate. This process results in mass loss via Roche lobe overflow and in the halting of the planet's orbital migration.

Subject headings: accretion, accretion disks — MHD — planetary systems: formation — planetary systems: protoplanetary disks — stars: individual (Peg 51b) — stars: magnetic fields

1. INTRODUCTION

Perhaps the most surprising finding in the search for extrasolar planets is the discovery of short-period ($P < 1$ week) Jupiter-mass (M_J) companions around solar-type main-sequence stars (Mayor & Queloz 1995; Marcy et al. 2000). Among the inventory of >200 presently known extrasolar planets, 20% have $P = 1$–7 days. Nearly 20 short-period planets have measured radii (R_p) that are comparable to or larger than that of Jupiter (R_J). While this information may be biased because of observational selection effects, these planets are most probably gas giants.

According to the conventional sequential accretion scenario (Pollack et al. 1996), the most likely birthplace for gas giant planets is just outside the snow line where volatile heavy elements can condense and coagulate into large planet building blocks (Ida & Lin 2004). In protostellar disks with surface density (Σ), metallicity ([Fe/H]), and temperature (T) distributions comparable to those of the minimum mass nebula model (Hayashi et al. 1985), protoplanets with $M_p \sim M_J$ induce the formation of a gap near their orbit as a consequence of their tidal torque on the nascent disks (Goldreich & Tremaine 1978, 1980; Lin & Papaloizou 1980, 1986a, 1993). In relatively massive and fast evolving disks, the outward transfer of angular momentum due to the disks' intrinsic turbulence can lead to an inward mass flux ($\dot{M}_d$) and the migration of the gas giant planets (Lin & Papaloizou 1986b). This process is commonly referred to as type II migration (Ward 1997).

This migration scenario was resurrected to account for the origin of the first known short-period extrasolar planet (Lin et al. 1996). Although type II migration provides a natural avenue for relocating some gas giants, a mechanism is needed to retain these planets close to their host stars. Moreover, many stars are born with rapid rotation (Stassun et al. 2001). When young planets venture close to their host stars, angular momentum would be transferred from the stellar spin to the planet's orbit if the stellar spin frequency ω_* is still larger than the planet's orbital frequency (Ω_k). The rate of the star-to-planet angular momentum transfer intensifies rapidly and may exceed that from the planet to the disk.

Two basic physical effects were suggested as potential migration barriers. The first one is tidal interaction between the host star and the planet. The gravitational perturbation of the star and close-in planet leads to responses in both the star and planet. For tidal frequencies smaller than twice the spin frequency, inertial waves are excited in the convective envelope of the host star and are dissipated there by turbulent viscosity (Ogilvie & Lin 2007). But, the tide excited by a close-in gas giant planet in a star, with a structure similar to that of the present Sun, marginally fails to achieve nonlinearity so that their survival is ensured. Nevertheless, during the formation epoch of solar-type stars, conditions at the center of the star evolve, so that nonlinearity may set in at a critical age, resulting in a relatively intense star-planet tidal interaction.

The second effect suggested is based on the magnetic interaction between the host star and the planet. Young T Tauri stars also have radii (R_*) 2–3 times that of the present-day Sun ($R_\odot$) and several thousand gauss fields (B_*) on their surface (Johns-Krull 2007). The stellar magnetosphere threads across the inner

[1] Ecole Normale Superieure, Paris, France; randy.laine@ens.fr.
[2] UCO/Lick Observatory, University of California, Santa Cruz, CA 95064; lin@ucolick.org, dong@ucolick.org.
[3] Kavli Institute of Astronomy and Astrophysics, Peking University, Beijing, China.

regions of the disk and clears a cavity out to a critical radius (R_c) which is determined by both the magnitude B_* and $\dot{M}_d$ (Konigl 1991). The subsequent complex interplay between accretion and outflow leads to angular momentum exchange which induces ω_* to evolve toward Ω_k at R_c (Shu et al. 1994). When the planet's orbital semimajor axis (a) reduces well inside R_c, its Lindblad resonances relocate inside the star's magnetospheric cavity. In principle, the planet's migration would stall due to its diminishing tidal torque on the disk.

However, if the star's magnetospheric interaction with the disk can lead to $\omega_* = \Omega_k(R_c)$, the planet inside the magnetospheric cavity would have $\Omega_k > \omega_*$. In this limit, the star-planet tidal interaction would induce a transfer of angular momentum from the planet to the star. In addition, the differential motion between the planet and the stellar spinning magnetosphere induces an electromagnetic field with the potential to generate a large current analogous to the interaction between the Jovian magnetosphere with its satellite Io (Goldreich & Lynden-Bell 1969). The associated Lorentz force drives an orbital evolution toward a synchronous state, in which case angular momentum would be transferred from the planets with $\Omega_k > \omega_*$ to their host stars, and the planets would continue their orbital decay.

In order to determine the necessary condition for the retention of close-in young planets, we examine, in this paper, their interaction with the magnetosphere of their host T Tauri stars. In § 2 we briefly recapitulate the essential concepts and validity of previous investigations on some related topics and give an overview of the key phenomena that will be discussed in this and later papers. In § 3 we adopt an existing model in order to examine the interaction between a planet and the magnetosphere of its host star. In § 4 we compute precisely the planet's magnetic diffusivity for a specific set of parameters, as well as the corresponding ohmic dissipation rate within that planet. In § 5 we suggest that the ohmic dissipation can generate sufficient heat to inflate the planet. In § 6 we construct an idealized self-consistent model in which the polytropic and isothermal equations of state are utilized. These equations represent the expected outcome of radiation transfer within the fully convective interior and the isothermal surface of a close-in planet which is exposed to the intense radiation from its host star. This internal model allows us to compute the magnetic diffusivity. With these tools, we discuss in § 7 the structural adjustment of the planet in response to this heating source, and we compute the ohmic dissipation and mass-loss rate for different sets of parameters. Finally in § 8 we summarize our results and discuss their implications.

2. PLANETARY AND STELLAR ANALOGUE

Two previous analyses are directly relevant to the present study: (1) the interaction of Io with the magnetosphere of Jupiter and (2) the spin-orbit synchronization in binary stars containing a magnetized white dwarf and its main-sequence or white dwarf or planetary companion.

2.1. *Unipolar Induction in Io*

Io orbits around Jupiter inside its magnetosphere once every 1.7 days, which is considerably longer than Jupiter's 10 hr spin period. This relative motion imposes a periodic variation in Jupiter's decametric emission (Duncan 1966). A class of models that accounts for the origin of this emission was developed based on the assumption that Io has a sufficiently high conductivity. In Io's rest frame, the electric field vanishes and the steady component of Jupiter's magnetic field permeates in Io's interior over time. When a steady state is established, the tube of constant magnetic flux is firmly frozen into Io (Piddington & Drake 1968) due to its high conductivity. The flux tube carried by Io moves through the surrounding field lines (which corotate with Jupiter) and slips through Jupiter's less conductive ionospheric surface. Plasma in Jupiter's ionosphere flows around the tube and introduces a potential difference across it (Goldreich & Lynden-Bell 1969). The associated electric field drives a current which travels down one half of the flux tube from Io and is sent back to Io along the other half. Within the flux tube connecting Io and Jupiter's ionosphere and those across it on Io, the electric field vanishes as a consequence of high conductivity. Thus, this DC circuit is closed by Io as a unipolar inductor.

The magnitude of the electric current is primarily determined by the Pedersen conductivity at the foot of the flux tube, i.e., on the ionosphere of Jupiter. Finite conductivity also determines the magnitude of the drag against the slippage of the flux tube through Jupiter. This drag results in energy dissipation on the surface of Jupiter and in a torque on the orbital motion of Io, driving the system toward a state of synchronization. This configuration is justified by the assumption that a constant flux tube is firmly anchored on and dragged along by Io, which requires the conductivity in Io to be much higher than that in Jupiter's ionosphere. A 10° inclination between Jupiter's magnetic dipole and rotation axis does introduce a periodic variation (over a synodic period) in the field felt by Io. The permeation and dissipation of this time-dependent AC field may be negligible in the limit of high conductivity in Io.

The validity of the key assumption for the unipolar induction model (i.e., conductivity on Io is larger than that in Jupiter's ionosphere) has also been challenged by Dermott (1970). A modest resistance in Io would distort the field, which may lead to field slippage through Io. In this case, the passage of Io through the magnetosphere of Jupiter would lead to the generation of Alfvén waves along the flux tube (Drell et al. 1965; Neubauer 1980). But, due to the field displacement, the waves, partially reflected at the foot of the flux tube on Jupiter's surface, may not be able to return to Io, in which case the DC circuit would be broken and the motion of Io would be decoupled from that of the flux tube. Nevertheless, the Alfvén waves are dissipated inside both Io and Jupiter, leading to a torque which must depend on their penetration depth.

An alternative class of scenarios has been proposed based on the assumption that the magnetosphere is everywhere anchored on Jupiter and the flux tube moves freely through Io (Gurnett 1972). This model requires the conductivity in Jupiter's ionosphere to be larger than that in Io. It assumes that the presence of Io creates a plasma sheath with an electric field to cancel the induced electromotive force associated with the motion of Io relative to Jupiter's magnetosphere (Shawhan 1976). The simplifying approximations in the development of this theory have been challenged by Piddington (1977), who questioned both the validity of the sheath-creation mechanism and the self-consistency of the internal and external field configurations, subjected to the electric currents in and around Io.

On the observational side, UV emissions from Io's footprint on Jupiter have been observed. But, it extends well beyond the intersection between Io's flux tube and Jupiter's ionosphere and the emission downstream is protracted (Clarke et al. 1996). These observations do not agree with the simple interpretation of either the unipolar induction or the plasma sheath scenarios.

2.2. *Magnetic Coupling in Interacting Binary Stars*

There are many close binary star systems with a white dwarf as their primary component. These systems also contain main-sequence stars and other white dwarfs as secondary components

in compact and circular orbits around each other. In some cases, mass is transferred from the secondary to the primary. In other cases, gravitational radiation may play an important role in determining the evolution of these systems.

A subclass of such interacting binary stars, AM Her systems, is composed of a magnetized white dwarf primary and a lower mass main-sequence star as its secondary in a fully synchronous orbit despite the ongoing mass transfer between them (Warner 1995). This orbital configuration is very similar to that of the Jupiter-Io system despite the enormous difference between the mass ratio in the two cases. The motivation for studying the impact of magnetic coupling between these stellar components is to assess whether this synchronous state can be achieved through the ohmic dissipation of the white dwarf's field in the main-sequence star's surface (Joss et al. 1979). Toward this goal, Campbell (1983, hereafter C83) adopted a novel approach by considering the penetration and dissipation of a periodically variable field, associated with an asynchronously spinning primary.

Campbell's approach is fundamentally different from that of the unipolar induction model. In this analysis, Campbell focussed on the flow in the envelope of the secondary and neglected the possibility of current flowing through the flux tube between the secondary star/satellite and the surface of the primary star/planet. This vacuum-surrounding approximation is justifiable since conductivity on the primary is likely to be much larger than that on the secondary and the stationary component of the field is frozen in the white dwarf primary but not in the main-sequence secondary. Campbell analyzed the time-dependent response of the secondary, including the modification of the field by the induced (AC) current in it (Campbell 2005), to the periodic modulation of the field. In contrast, the unipolar induction model depends on the explicit assumption that the field is anchored on the secondary and its distortion near the secondary must be small so that a complete current loop can be established between the primary and the secondary. Campbell determined the periodic diffusion of the field and the ohmic dissipation of the induced AC current in the companion, whereas that of the induced DC current is assumed to occur in the primary in the unipolar induction model.

In recent applications of the unipolar induction model in the context of interaction between white dwarf binary stars, the current induced by the unperturbed field has been computed, but the induced field generated by the current was neglected (Wu et al. 2002; Dall'Osso et al. 2006). A tidal torque is computed at the footprint of the flux tube, which is attached to the secondary white dwarf, on the surface of the magnetized primary white dwarf. A totally self-consistent solution of this difficult and complex problem remains outstanding. In addition to the uncertain anchorage location of the field, it is not clear whether the resulting misalignment of the total (original plus induced) field and current may be sufficiently large to break the circuit, in which case Campbell's model may be more appropriate.

2.3. *Mathematical Approximations Made by the Two Previous Models*

In this subsection we summarize the physical description of the two models just presented (the unipolar inductor vs. the periodic diffusion) by explicating the mathematical approximations made in each one of them. The complete MHD induction equation can be expressed as

$$\frac{\partial \boldsymbol{B}}{\partial t} = \nabla \wedge (\boldsymbol{v} \wedge \boldsymbol{B}) - \nabla \wedge (\eta \nabla \wedge \boldsymbol{B}), \qquad (1)$$

where the magnetic diffusivity $\eta = 1/\mu_0 \sigma$ and the electrical conductivity σ are functions of position and μ_0 is the permeability. If η is constant, the second term on the right-hand side becomes $-\nabla \wedge (\eta \nabla \wedge \boldsymbol{B}) = \eta \nabla^2 \boldsymbol{B}$, which reduces to a common expression of diffusion. The two models (unipolar induction vs. periodic diffusion) consider two complementary approximations of equation (1). In the problem where Io is treated as a unipolar inductor, its conductivity is explicitly assumed to be large so that the second term on the right-hand side (the diffusion term) is negligible compared to the first (i.e., the induction term). In this configuration, one can show that the field lines of the steady component of the magnetic field are moving with Io and appear to be "frozen" on Io (see Appendix A). Alternatively, in the model considered by Campbell, it is the first term on the right-hand side that is being neglected. Moreover, only the diffusion of the time-dependent component of the field is being considered. This approximation is valid if the two interacting bodies are almost in corotation (i.e., the relative speed v that appears in eq. [1] is small) or if the conductivity in the secondary is small.

2.4. *Overview of the Phenomena That Will Be Discussed*

The process under investigation in this paper is analogous to both the Jupiter-Io and the interacting binary star problems. In fact, the unipolar induction model has already been applied to study the orbital evolution of terrestrial planets and the cores of gas giants around white dwarfs (Li et al. 1998). There are even follow-up determinations of the radio flux densities from potential white dwarf/planet systems (Willes & Wu 2005). In this analysis, although the dissipation of the induced current due to the finite conductivities in the white dwarf was considered, the feedback modification of the field and the dissipation within the planet have been neglected (Li et al. 1998). As discussed above, it is not clear whether a DC circuit can be closed to promote the unipolar induction mechanism.

In light of these uncertainties, we consider both classes of models for the interaction of close-in planets with their magnetized host stars. In this paper we focus our discussion on the mechanism described by Campbell and apply it to a hot Jupiter revolving around its star. We will return to the unipolar induction problem in a later paper.

When young planets first arrive at the vicinity of their host stars, they are unlikely to be in a totally synchronized state. The stellar magnetic field felt by the planet may be dominated by the periodic modulation associated with the synodic (between the stellar spin and the planet's orbit) motion. In addition, the temperature in the planet's surface is expected to be $\sim 10^3$ K and the conductivity there may be moderate. In response to the modulation of the field, the interior of the planet continually adjusts to the magnetization effects so that the flux tube cannot be effectively frozen in the planet. All of these boundary condition suggest that at least over some regions of the planet (especially on the night side where the photoionization due to the stellar flux is negligible), the modulation of the field may lead to an induced current inside the planet which does not contribute to the closed circuit of a unipolar inductor.

Following the geometry introduced by Campbell (C83), we consider a close-in gas giant planet, with a finite conductivity, interacting with a time-dependent magnetic field generated by the star. An induced current is generated inside the planet, which is associated with an ohmic dissipation rate. Our main contributions to the model used by Campbell are (1) the relevant diffusivity inside the gas giant planets, (2) the effects of the ohmic dissipation on the planet's internal structure, and (3) the resulting

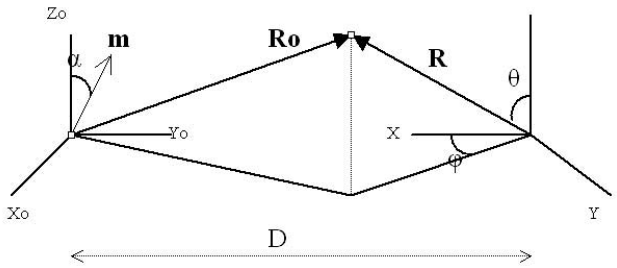

FIG. 1.—Geometry of the system. The star is on the left, at the center of the set of axes (x_0, y_0, z_0), and the planet is on the right, at the center of the set of axes (x, y, z).

orbital evolution of the planet. (Items 2 and 3 have negligible consequences in the interacting binary star problem considered by Campbell.) Since we are only considering the dissipation in the planet's interior, the associated torque applied on its orbit should be regarded as a lower limit.

In our scenario, we postulate that at a sufficiently close proximity to the host star, the stellar magnetic field is sufficiently intense for the ohmic dissipation of the periodically diffused field inside the planet to heat and inflate the planet until it overflows its Roche lobe. The hemisphere of the planet facing its host star is also exposed to the intense flux of UV radiation during the stellar infancy. It is possible for the planet to develop a substantial ionosphere regardless of the state of synchronization between the planet's orbit and spin (the timescale for establishing local ionization equilibrium is much faster than the planet's spin and orbital periods).

We will separately study these two phenomena (angular momentum transfer due to mass loss and presence of a ionosphere) in the follow-up papers of this series. We will show that the angular momentum transfer associated with the mass transfer can halt the orbital evolution of the planet. We will also present an analysis on the conductivities in the planet's dayside ionosphere and on the host star's surface. This will lead to an analysis on the condition for the unipolar induction to effectively operate and apply a significant slowdown torque on the planet's orbit.

3. MAGNETIC INDUCTION

In this section we are going to derive the governing equations that we use to compute the ohmic dissipation rate. Various equations are presented here for the purpose of introducing the algorithm of the numerical models to be presented in subsequent sections. Although we follow closely the approach made in C83, for brevity, we do not repeatedly cite this reference. But, wherever similarities occur, referral of Campbell's earlier work is implicitly implied. Also, throughout the paper, we use SI units.

We consider a protoplanetary system with a gas giant planet revolving around a T Tauri star with an angular frequency Ω_p. Well beyond the planet's semimajor axis, there is also a protoplanetary disk. The host star has a dipolar moment $\boldsymbol{m}$ tilted with an angle α with respect to its spinning axis (see Fig. 1). The angular frequency of the stellar spin is ω_*. The orbital axes of the disk and the planet are parallel to the star's spinning axis. The following analysis is applied to a frame of reference centered on the star and rotating with the planet.

In this frame, the planet is a fixed object (the planet's spin is neglected) in a periodic magnetic field with a frequency $\omega = \omega_* - \Omega_p$. From Ohm's law $\boldsymbol{J} = \sigma \boldsymbol{E}$ and Maxwell's equations $\partial \boldsymbol{B}/\partial t = -\nabla \wedge \boldsymbol{E}$ and $\nabla \wedge \boldsymbol{B} = \mu_0 \boldsymbol{J}$, the equation on the magnetic field becomes

$$\frac{\partial \boldsymbol{B}}{\partial t} = -\nabla \wedge (\eta \nabla \wedge \boldsymbol{B}). \tag{2}$$

It follows that in the mechanism considered by Campbell (as well as in this paper), it is the time-dependent stellar magnetic field, diffusing inside the secondary (for Campbell) or the hot Jupiter (in our paper), as well as the planet's induced magnetic field, that generate the current inside the planet, following the equation $\nabla \wedge \boldsymbol{B} = \mu_0 \boldsymbol{J}$. The relative speed between the planet and the stellar magnetic field thus intervenes not through $\boldsymbol{E} = -\boldsymbol{v} \wedge \boldsymbol{B}$ but through the time dependence in the stellar magnetic field that diffuses in the planet.

Following C83, we only consider the poloidal component ϕ of the magnetic field,

$$\boldsymbol{B} = \nabla \wedge [\nabla \wedge (\phi \boldsymbol{e}_r)], \tag{3}$$

where ϕ is a function of r, θ, and φ and can be expanded in terms of the spherical harmonics $Y_l^m(\theta, \varphi)$ (eq. [4]). Moreover, the variation in time of the magnetic field felt by the planet is periodic. In the limit where the field penetrates quickly in the planet compared to the timescale on which the field changes (so that the planet can respond "adiabatically"), we can account for the time dependence of ϕ by multiplying its spatial part by $e^{i\omega t}$ ($l \geq 0$ and $-l \leq m \leq l$),

$$\phi(\boldsymbol{r}, t) = \mu_0 \left[\sum_{l,m} C_l^m G_l(r) Y_l^m(\theta, \varphi) \right] e^{i\omega t}, \tag{4}$$

where C_l^m are constant coefficients and $G_l(r)$ is a function of r to be determined. We then replace $\boldsymbol{B}$ on the left-hand side of equation (2) by its expression in equation (3). After integration, we obtain

$$\nabla \wedge \boldsymbol{B} = -\frac{i\omega}{\eta} \nabla \wedge (\phi \boldsymbol{e}_r). \tag{5}$$

We then replace $\boldsymbol{B}$ on the left-hand side of this equation using equation (3) and develop both sides of the equation. After identification, we obtain

$$\frac{d^2 G_l}{dr^2}(r) - \left[\frac{l(l+1)}{r^2} + \frac{i\omega}{\eta} \right] G_l(r) = 0 \tag{6}$$

inside the planet. This equation holds inside and outside the planet (same as eqs. [16] and [18] in C83). However, outside the planet, the conductivity is assumed to be very low, and therefore, the magnetic diffusivity is extremely high compared to the diffusivity inside the planet. In the limit where the magnetic diffusivity outside tends to infinity (equivalent to a vacuum surrounding), equation (6) becomes

$$\frac{d^2 G_l}{dr^2}(r) - \left[\frac{l(l+1)}{r^2} \right] G_l(r) = 0 \tag{7}$$

outside the planet.

We consider the radial part of the poloidal scalar outside the planet. Following C83, we introduce $\phi_{\rm star}$, the radial part of the

poloidal scalar outside the planet due to the star's magnetic field, and ϕ_p, the radial part of the poloidal scalar outside the planet due to the planet (cf. C83, eqs. [21]–[22]),

$$\phi_{\rm star} = \frac{\mu_0 m \sin\alpha}{8\pi d^3} r^2 (2\cos\varphi \sin\omega t + \sin\varphi\cos\omega t) P_1^1 + \frac{\mu_0 m \sin\alpha}{8\pi d^4} r^3 \left(P_2^0 \sin\omega t\right) - \left[\left(\frac{1}{2}\cos 2\varphi \sin\omega t + \frac{1}{3}\sin 2\varphi \cos\omega t\right) P_2^2\right], \quad (8)$$

$$\phi_p = \mu_0 P_1^1 \left[\frac{\cos\varphi}{r}(\alpha_1 \sin\omega t + \alpha_2 \cos\omega t) + \frac{\sin\varphi}{r}(\alpha_3 \sin\omega t + \alpha_4 \cos\omega t)\right] + \frac{\mu_0 P_2^0}{r^2}(\beta_1 \sin\omega t + \beta_2 \cos\omega t) + \mu_0 P_2^2 \left[\frac{\cos 2\varphi}{r^2}(\gamma_1 \sin\omega t + \gamma_2 \cos\omega t) + \frac{\sin 2\varphi}{r^2}(\gamma_3 \sin\omega t + \gamma_4 \cos\omega t)\right], \quad (9)$$

where $P_1^1 = -\sin\theta, P_2^0 = \frac{1}{2}(3\cos^2\theta - 1)$, and $P_2^2 = 3\sin^2\theta$ are the associated Legendre polynomials (our convention for P_1^1 has an opposite sign to that adopted by Campbell). In addition, ϕ_p has the same time and angular dependence as $\phi_{\rm star}$, because the field inside the planet is induced by the stellar magnetic field.

The sum $\phi_{\rm out} = \phi_{\rm star} + \phi_p$ is the total poloidal scalar outside the planet, and $\phi_{\rm out}$ (given by eqs. [8] and [9]) is equal to $\phi_{\rm in}$ (given by eq. [4]) at the surface of the planet ($r = R_p$).

3.1. *Poloidal Scalar inside the Planet*

In order to determine the poloidal scalar inside the planet, we first numerically calculate the values of $G_l(r)$ (the radial part of ϕ, see eq. [4]) and $G_l'(r)$ inside the planet by solving equation (6). We then calculate the coefficients C_l^m, which appear in the decomposition of ϕ. They are determined by the boundary conditions which connect the interior and exterior solutions. In the rest of this section (§ 3), we assume that the conductivity profile is known, and we describe the procedure used to compute the ohmic dissipation rate inside the planet. In the following sections, we apply the method described in § 3 to compute the ohmic dissipation rate inside the planet.

3.1.1. *Computation of $G(r)$*

If the diffusivity $\eta(r)$ is known, we can solve equation (6) numerically, for $l = 1$ and 2, with a two-point boundary solver using the Newton-Raphson-Kantorovich method, and the equations and boundary conditions are given as

$$\begin{aligned} Y_1'(r) &= Y_3(r), \quad Y_2'(r) = Y_4(r), \\ Y_3'(r) &= -\frac{\omega}{\eta(r)} Y_2(r) + \frac{l(l+1)}{r^2} Y_1(r), \\ Y_4'(r) &= \frac{\omega}{\eta(r)} Y_1(r) + \frac{l(l+1)}{r^2} Y_2(r), \\ G_l'(R_p) &+ \frac{l}{R_p} G_l(R_p) - (2l+1) R_p^l = 0, \\ G_l'(r \simeq 0) &- \frac{l+1}{r} G_l(r \simeq 0) = 0, \end{aligned} \quad (10)$$

where $Y_1(r) = \mathrm{Re}[G(r)]$ and $Y_2(r) = \mathrm{Im}[G(r)]$.

3.1.2. *Computation of the $C(l, m)$*

The complex coefficients $C_l^m = \mu_l^m + i\nu_l^m$ have real and imaginary parts $\mu_l^m = \mathrm{Re}(C_l^m)$ and $\nu_l^m = \mathrm{Im}(C_l^m)$. We equate the real part of the decomposition of the poloidal scalar inside the planet given in equation (3) at $r = R_p$ (radius of the planet) with the expression of $\phi_{\rm out} = \phi_{\rm star} + \phi_p$ given in equations (8) and (9) at $r = R_p$.

Moreover, using the fact that (P_1^1, P_2^0, P_2^2) and then $(\cos\omega t\cos\varphi,$ $\cos\omega t\sin\varphi,$ $\sin\omega t\cos\varphi,$ $\sin\omega t\sin\varphi)$ $(\cos\omega t,$ $\sin\omega t)$, $(\cos\omega t\cos 2\varphi,$ $\cos\omega t\sin 2\varphi,$ $\sin\omega t\cos 2\varphi,$ $\sin\omega t\sin 2\varphi)$ are a set of bases, we get a set of linear equations which can be solved for $(\mu_1^1, \mu_1^{-1}, \nu_1^1, \nu_1^{-1}, \alpha_1, \alpha_2, \alpha_3, \alpha_4)$, $(\mu_2^0, \nu_2^0, \beta_1, \beta_2)$, and $(\mu_2^2, \mu_2^{-2},$ $\nu_2^2,$ $\nu_2^{-2},$ $\gamma_1,$ $\gamma_2,$ $\gamma_3,$ $\gamma_4)$ (the linear systems verified by these unknowns are given in Appendix B).

3.2. *Computation of the Ohmic Energy Dissipation Rate*

The potential generates an electric field $\boldsymbol{E}$ which induces a volumic current $\boldsymbol{J}$ inside the planet. The associated ohmic dissipation inside the planet is $\mathcal{P}_{\rm vol} = \mathrm{Re}(\boldsymbol{J})\mathrm{Re}(\boldsymbol{E})$. Using $\boldsymbol{E} = (1/\sigma)\boldsymbol{J}$ and $\boldsymbol{J} = (1/\mu_0)\nabla \wedge \boldsymbol{B}$, we can write

$$\mathcal{P} = \int_V \frac{1}{\sigma(r)} [\mathrm{Re}(\boldsymbol{J})]^2 dV = \int_V \frac{1}{\sigma(r)} \left[\mathrm{Re}\left(\frac{\nabla \wedge \boldsymbol{B}}{\mu_0}\right)\right]^2 dV. \quad (11)$$

Moreover, using equation (5), we can write

$$\mathcal{P} = \frac{\omega^2}{\mu_0} \int \frac{1}{\eta(r)} \left\{ \frac{1}{\sin\theta}\left[\frac{\partial \mathrm{Im}(\phi)}{\partial\varphi}(r,\theta,\varphi)\right]^2 + \sin\theta \left[\frac{\partial \mathrm{Im}(\phi)}{\partial\theta}(r,\theta,\varphi)\right]^2 \right\} dr\, d\theta\, d\varphi. \quad (12)$$

We use equation (4) to express the real and imaginary parts of Φ. After integrating over θ and φ, we are left with

$$\mathcal{P} = \int_r \langle \mathcal{P}_{\rm vol} \rangle r^2\, dr, \quad (13)$$

where

$$\langle \mathcal{P}_{\rm vol} \rangle = \frac{\mu_0 \omega^2}{\eta r^2} \left\{ \cos^2\omega t \left[\left(A_{11}^2 + A_{12}^2\right) + 3\left(A_{17}^2 + A_{18}^2\right) + \frac{3}{\pi} A_{15}^2 \right] + \sin^2\omega t \left[\left(A_{13}^2 + A_{14}^2\right) + 3\left(A_{19}^2 + A_{20}^2\right) + \frac{3}{\pi} A_{16}^2 \right] + \sin\omega t \cos\omega t \times \left[(A_{12}A_{14} + A_{11}A_{13}) + 3(A_{17}A_{19} + A_{18}A_{20}) + \frac{3}{\pi} A_{15}A_{16} \right] \right\},$$

where the expressions for A_{ij} are given in Appendix C.

4. CONDUCTIVITY PROFILE AND OHMIC DISSIPATION RATE

The general setting of the problem and the basic equations have been laid down. We have seen that once a conductivity profile is chosen, one can solve equation (10) and determine $G_l(r)$ inside the planet (the radial part of the poloidal scalar inside the planet). Then, one can compute the $C(l, m)$ and finally obtain the ohmic dissipation rate $\mathcal{P}$ inside the planet.

4.1. *Computation of $\mathcal{P}$ for One Specific Set of Parameters*

We compute the conductivity inside the planet with two parallel approaches. In §§ 5–7 we develop an idealized self-consistent internal structure model to determine the response of the planet to the ohmic dissipation of the induced current in it. But, in

this section, we first introduce a realistic, but non-self-consistent, model with the following set of parameters:

Planet's mass and radius.—0.63 M_J and $R_p = 1.4\ R_J = 10^8$ m;
Semimajor axis.—$a = 0.04$ AU $= 6 \times 10^9$ m.

These and other stellar parameters (such as mass and luminosity) are appropriate for the short-period planet around HD 209458 (Bodenheimer et al. 2001, hereafter BLM01). We compute the internal conductivity due to the ionization of the alkaline metals (see Appendix D for details). Although the planet is heated on the dayside, thermal circulation can redistribute the heat and reduce the temperature gradient between the two sides of the planet (Burkert et al. 2005; Dobbs-Dixon & Lin 2008). We adopt a spherically symmetric approximation for the surface temperature of the planet to be 1360 K. Here, we neglect the modification in the internal structure due to the ohmic dissipation which is considered with self-consistent models in the following sections. In Paper IV we will also consider the conductivity on the planet's upper atmosphere due to photoionization which only occurs on the dayside of the planet. Using this conductivity profile, we can approximate the magnetic diffusivity $\eta(r) = 1/\mu_0\sigma(r)$ by

$$\eta(r) \simeq 10^3 \exp\left[25\left(\frac{r}{R_p}\right)^2\right], \tag{14}$$

where the effects of the photoionization have been neglected in this paper.

To apply the procedure described in § 3, we also need to specify:
Relative angular velocity.—$\omega = 10^{-5}$ s^{-1};
Star's magnetic dipole.—$m = 4 \times 10^{34}$ A m^2;
Value of the tilt of the magnetic dipole.—$\sin(\alpha) = 1$.
We then obtain the following $\mathcal{P}$ [also see Fig. 2 for the graphs of $G_l(r)$]

$$\mathcal{P}(t) = 2.26 \times 10^{21} cos^2\omega t + 2.1 \times 10^{21} \times \sin^2\omega t + 1.3 \times 10^{21} \sin\omega t \cos\omega t. \tag{15}$$

We then take the average in time over one synodic period and obtain $\mathcal{P} \approx 2.18 \times 10^{21}$ J s^{-1}

The conductivity profile we have obtained here is sensitive to the planetary structure model. At the epoch of planet formation, the gas accretion and planetesimal bombardment history are stochastic (Zhou & Lin 2007). The opacity in the accretion envelope of proto–gas giant planets may also be subjected to variations due to dust coagulation (Iaroslavitz & Podolak 2007). The thermal evolution of these planets can be highly diverse. There may, therefore, be a dispersion in the magnitude of η.

4.2. *Comments on the Skin Depth and the Dependence of the Ohmic Dissipation on the Conductivity and on the Sign of ω*

Once the conductivity profile within the planet is determined, we are able to compute the energy dissipation rate inside the planet of the current induced by the star's magnetic field. In light of the possible uncertainties in the magnitude of η, we compute the ohmic dissipation rate for different η by artificially modifying the above determined η with a multiplicative factor. The resulting magnitude of the time-averaged value of $\mathcal{P}$ is listed below (Table 1).

These results indicate that the energy dissipation rate is insensitive to a change in the amplitude of the conductivity by several orders of magnitude (this conclusion is in agreement with a conjecture that Campbell made; C83). A high conductivity increases the energy dissipation in a given volume, but it also tends to prevent the magnetic field from penetrating inside the planet. On the other hand, a lower conductivity corresponds to less dissipation per unit of volume, but it also allows the field to penetrate deeper inside the planet (and therefore increases the volume where energy can be dissipated).

The skin depth [for reasonable values of $\eta(r)$] is of order $\delta = (\eta/\omega)^{1/2}$. For $\eta(r) = 10^3 \exp[25(x/R_p)^2]$ and $\omega = 10^{-5}$ s^{-1}, we have $\delta(r_{pn}) \approx 4 \times 10^7$ m (we define r_{pn} to be the radius of penetration, or the radius to which the magnetic field can diffuse inside the planet). This estimate is consistent with the numerical values of $G_l(r)$ inside the planet (see Fig. 2) in which we find that $G_1(r)$ for $r < r_{pn} \simeq 6.5 \times 10^7$ m is negligibly small compared to its value elsewhere.

These considerations suggest that the total rate of energy dissipation is well determined although the location where it occurs is less well established due to the uncertainties in η. Moreover, with our definition $\omega = \omega_\star - \Omega_p$, ω is positive outside corotation and negative inside corotation. However, the ohmic dissipation rate inside the planet $\mathcal{P}$ only depends on the absolute value of ω.

4.3. *Energy Source and Direct Influence on the Planet's Orbit*

The induced current $\boldsymbol{J}$ deduced in § 3 is due to the diffusion of a time-dependent magnetic field. This time dependence comes from the relative motion of the planet's orbit and the stellar magnetosphere. Thus, the ohmic dissipation must be supplied by the orbital kinetic energy of the planet and the rotational energy of the star. Our stated goal from § 1 is to consider whether the migration of some planets may be halted by their magnetic coupling with their rapidly spinning magnetized host stars. In the case where $\omega_* > \Omega_p$, the rotational energy of the star is transferred to the total orbital energy of the planet and provides a supply for the ohmic dissipation. The torque T associated with the ohmic dissipation is linked with the ohmic dissipation rate $\mathcal{P}$ and the relative angular velocity ω according to the following equation (see C83, eq. [55]),

$$\mathcal{P} = -\omega|T|. \tag{16}$$

Since the transfer of angular momentum involves the torque associated with the ohmic dissipation, a similar fraction of energy is being transferred to the planet's orbit and supplied to the ohmic dissipation. For this purpose, we qualitatively compare the magnitude of $\mathcal{P}(t)$ with the rate of energy change needed to stall the migration of a protoplanet. A detailed computation on the orbital evolution of the planet will be presented in Paper III.

For illustration purposes, we first consider the power associated with the migration (P_{mig}) of a planet with a 0.63 Jupiter mass and a 1.4 Jupiter radius toward a Sun-like star. At any semimajor axis a, the total energy of the Keplerian orbit is $|E| = GM_pM_s/2a$. If its orbit decays on a characteristic planet-disk interaction timescale (τ_{mig}) of about 3 Myr, the torque needed to halt the planet's migration would correspond to a power P_{mig} such that

$$P_{mig} = |\dot{E}| \simeq \frac{\mathcal{G}M_pM_\star}{2a\tau} \simeq 7.4 \times 10^{22}\ \text{J s}^{-1}.$$

Since this power is more than an order of magnitude larger than the time average value of $\mathcal{P}$ (see Table 1), it seems, therefore, not possible for the magnetic coupling to directly stall the planet's migration at a 0.04 AU Keplerian orbit within a few millions years, even in the limit of a positive ω.

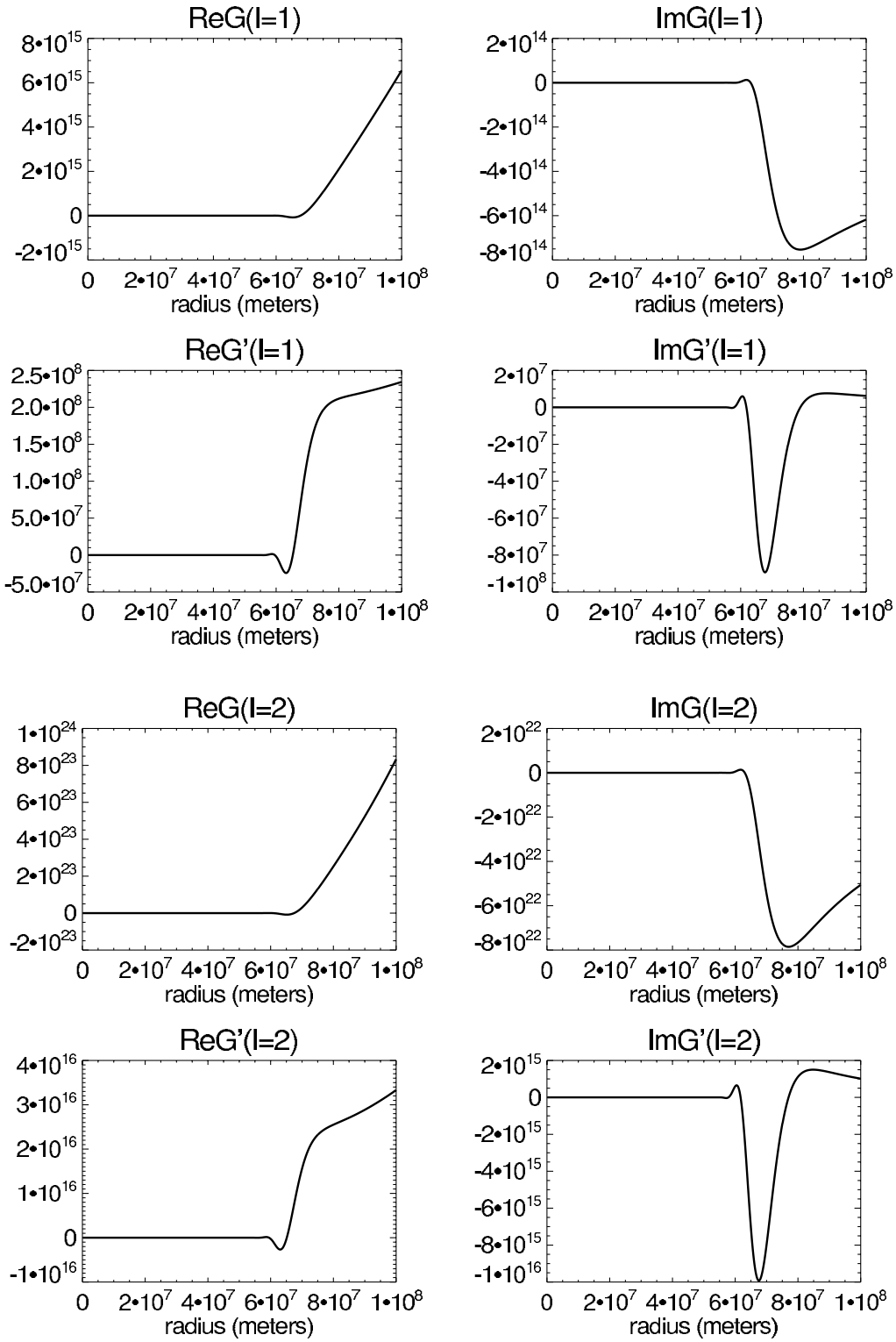

FIG. 2.—Plots of $\mathrm{Re}\,(G_{l=1})(r)$, $\mathrm{Im}\,(G_{l=1})(r)$, $\mathrm{Re}\,(G_{l=2})(r)$, $\mathrm{Im}\,(G_{l=2})(r)$, and their first derivatives, for $R_p = 10^8$ m $= 1.4\ R_J$, $a = 0.04$ AU, and $\eta(r) \simeq 10^3 \exp\,[25(r/R_p)^2]$. The shapes of G_l for $l = 1$ and 2 are very close, but the amplitudes for $l = 2$ are about $10^8 = R_p$ higher than for $l = 1$. Indeed, the major difference between $l = 1$ and 2 is found in the equations describing the boundary conditions (see eq. [10], where a factor 10^8 between $l = 1$ and 2 comes from the term R_p^l). In addition, we found that $|C(l, m)|$ for $l = 1$ is about 10^{10} times larger than for $l = 2$. Therefore, $|G_l C(l, m)|$ for $l = 1$ is much larger than for $l = 2$, which allows us to keep only the terms corresponding to $l = 1$ and 2 in the decomposition of ϕ on spherical harmonics.

TABLE 1
Ohmic Dissipation Rate as a Function of η

$\eta(r)$	$\mathcal{P}$ (J s^{-1})
$10^{-3}\exp[25(r/R_p)^2]$	1.26×10^{21}
$10^{0}\exp[25(r/R_p)^2]$	2.7×10^{21}
$10^{3}\exp[25(r/R_p)^2]$	2.18×10^{21}
$10^{5}\exp[25(r/R_p)^2]$	1.71×10^{21}
$10^{7}\exp[25(r/R_p)^2]$	1.12×10^{21}
$10^{9}\exp[25(r/R_p)^2]$	2.33×10^{20}
$10^{10}\exp[25(r/R_p)^2]$	2.5×10^{19}
$10^{12}\exp[25(r/R_p)^2]$	2.5×10^{17}

Note.—The value of η is artificially modified from the value computed in § 4 in order to evaluate how sensitive $\mathcal{P}$ is on the value of η.

However, in the model we have considered here $\mathcal{P}\propto B^2\propto m^2a^{-6}$. The power needed to drive the planet to migration with a specified speed is proportional to a^{-2} (these scalings are confirmed by numerical calculations that neglect any changes in the relative frequencies ω and the planetary internal structure). It means that there is a semimajor axis $a_{\rm stop}\sim0.01$ AU at which $\mathcal{P}$ and $P_{\rm mig}$ are comparable. This distance is comparable to the radius of typical T Tauri stars. Note that the requirement for $\omega_*>\Omega_p$ also implies that the planet must be outside the corotation radius. This condition is satisfied only in a disk with a low gas accretion rate around a rapidly spinning and weakly magnetized star. In Paper II, we will consider such a model for the newly discovered planet around TW Hyd (Setiawan et al. 2008). Under these circumstances, the planet-star magnetic interaction may also be overwhelmed by their tidal interaction.

5. PLANETARY INFLATION AND MASS LOSS

In this section we propose that ohmic dissipation in the planet's interior can indirectly halt its migration. The main physical mechanisms involve the heating of the planet's interior, its inflation and mass loss through Roche lobe overflow, and angular momentum transfer from the transferred material to the orbit of the planet.

Up to now, we have computed the planet's conductivity for one particular set of parameters (M_p, a, etc.) and the corresponding ohmic energy dissipation inside the planet due to the star's magnetic field. Although, this dissipation rate for most close-in planets is generally too small to directly provide the power needed to halt their migration over the timescale of a few Myr, it can modify their internal structure.

The ohmic dissipation is likely to increase the temperature, the ionization fraction, and the conductivity around the region where most of the dissipation occurs. In principle, the extra energy source would reduce the skin depth. However, the envelope of the young planet is likely to be fully convective, similar to the low-mass main-sequence secondary in interacting binaries. Campbell (C83) suggested that the dominant diffusivity may be due to turbulence (Cowling 1981). In § 4.2 we have already indicated that even though the skin depth may be affected by the magnitude of the diffusivity, the total energy dissipation rate in the planet's interior is not sensitively determined by the profile of η.

Nevertheless, the heat released by the dissipation is comparable to that associated with the Kelvin-Helmholtz contraction during the early stage of the planet's evolution (Bodenheimer et al. 2001, hereafter BLM01). In the proximity of its host star, this extra energy source may cause a planet to inflate beyond its Hill's radius and lose mass (Gu et al. 2004).

In the following sections (§§ 5–7) we adopt an idealized and self-consistent model of the planet's internal structure. This approach allows us to compute the conductivity of the planet for different sets of parameters. Considering the low dependence of the total ohmic dissipation $\mathcal{P}$ on η, an idealized but versatile prescription is adequate for the computation of $\mathcal{P}$ and the mass-loss rate ($\dot{M}$) for different values of the important parameters (the planet's mass and radius, the star's mass, luminosity, and dipolar magnetic field strength, the tilt between the magnetic dipole and the stellar spinning axis, and the relative orbital period). In § 5 we show how the mass-loss rate $\dot{M}$ is related to the ohmic dissipation $\mathcal{P}$. In § 6 we describe the model we used for the planet's interior, and in § 7, we calculate $\mathcal{P}$ and $\dot{M}$ for different sets of parameters.

5.1. *A Qualitative Description*

The planet receives energy, at its surface, from the star's radiation and, in the interior, from the ohmic dissipation. The surface heating diffuses inward until an isothermal structure is established in the planet's outer envelope. But, well below the surface region, the heat flux is generated by the planet's Kelvin-Helmholtz contraction and ohmic dissipation and is transported by convection. In the limit in which convection is efficient, the envelope attains a constant entropy profile. For computational simplicity, we adopt an isothermal model near the surface of the planet and a polytrope model for its deep interior.

There are two regions of interest. Very close to the host star, the ohmic dissipation rate is larger than that [$L_p=L_*(R_p/2a)^2$] due to the stellar irradiation (L_*) received by the planet. In this limit, the planet would rapidly expand beyond its Roche lobe and become tidally disrupted. In accordance with the results of § 4 (in which the effect of $\mathcal{P}$ on the internal structure of the planet has been neglected), $\mathcal{P}\propto a^{-6}$ and $L_p\propto a^{-2}$. Thus, the stellar heating dominates at larger semimajor axes. In this section we consider the effect of the planet's inflation due to the ohmic dissipation and show that $\mathcal{P}$ also increases with the planetary radius R_p at nearly the same rate as L_p ($\propto R_p^2$). Thus, during the thermal expansion of the planet, the ratio of $L_p/\mathcal{P}$ does not change. In the region where $L_p>\mathcal{P}$, the effective temperature at the planet's surface, with or without the contribution from the ohmic dissipation, remains the equilibrium value T_p. But, the planet's radius for thermal equilibrium increases with $\mathcal{P}$, which adds to the energy generation in the planet's interior (BLM01). If the new equilibrium R_p is larger than the planet's Roche radius, R_H, mass would be lost gradually through Roche overflow.

5.2. *Mass-Loss Rate*

We now derive the equations that allow us to calculate the mass-loss rate $\dot{M}$ and angular momentum transfer rate as functions of $\mathcal{P}$. We are in the second region where the ohmic dissipation is less than the radiation flux from the star ($\mathcal{P}\leqslant L_p$), and we set the Bond albedo to zero. We therefore assume that the equilibrium temperature at the surface of the planet is fixed by the radiation from the star $T_p^4=L_{\rm star}/(16\pi\sigma_r a^2)$ ($L_{\rm star}$ is the total luminosity of the star, $\sigma_r=5.67\times10^{-8}$ J s^{-1} m^{-2} T^{-4}), and that the ohmic dissipation provides the additional energy to inflate the planet.

An irradiated short-period planet establishes an isothermal surface layer. The hot interior continues to transport heat to this region and then radiates to infinity with a luminosity L_i despite the surface heating. Note that

$$L_i\ll L_p=4\pi\sigma_r T_p^4R_p^2, \tag{17}$$

so that the modification to T_p is negligible. The magnitude of L_i is a function of R_p, M_p, T_p, and the existence of the core. We

have previous computed an equilibrium model for the parameters for several short-period planets (BLM01). In the range $[10^{-8}\ L_\odot,\ 10^{-5}\ L_\odot]$, the numerical results of BLM01 can be approximated by

$$\log\frac{R_p}{R_\odot} = A(M_p) + B(M_p)\log\frac{L_i}{L_\odot} + C(M_p)\left(\log\frac{L_i}{L_\odot}\right)^2. \quad (18)$$

For HD 209458b (the 0.63 M_J model we presented in § 4), $(A, B, C) = (3.11, 1.01, 0.0642)$. BLM01 also determined the value of these coefficients for more massive planets around a solar-type star (they are modified by the stellar irradiation so that they are also functions of $M_\star$). The planet's radius R_p would contract unless there is an adequate energy source to replenish its loss of internal energy. If the ohmic dissipation can provide such a source, $R_p = R_e$ and $L_i = \mathcal{P}$ in a thermal equilibrium.

At $a = 0.04$ AU, the Roche radius of the planet is

$$R_H = a\left(\frac{M_p}{3M_\star}\right)^{1/3}. \quad (19)$$

From equation (18), we find that the equilibrium $R_e \sim R_H$ if $L_i \sim 10^{-5}\ L_\odot$, which is approximately the value of $\mathcal{P}$ ($\sim 10^{21}$ J s^{-1}) we have determined for HD 209458b. During the planet and star's infancy, this planet would inflate to fill its Roche lobe when it has migrated to this location.

Outside $\sim$0.04 AU, $\mathcal{P}$ decreases rapidly with a. Consequently, R_p reduces to the value which is essentially not modified by the ohmic heating. For the calculation presented in § 4, we neglected the inflation of the planet. In § 6 we construct a self-consistent model, taking into account the modification of the dissipation rate due to the internal structural changes. For $a = 0.04$ AU, the intense ohmic dissipation rate (with $L_i = \mathcal{P} \simeq 2 \times 10^{21}$ J s^{-1}) modifies the planet's internal structure and inflates its radius to $R_e \sim 0.5\ R_\odot$. The inflation is more severe at $a < 0.04$ AU because $\mathcal{P}$ is a rapidly decreasing function of a. If $R_e > R_H$ at this location, the planet would overflow its Roche lobe and lose mass. For the rest of this paper, we assume that we are in the case where the planet fills its Roche lobe, i.e., $R_p = R_H$.

Two remarks are appropriate here. First, in order for the Roche lobe overflow to provide angular momentum, the actual shape of the Roche lobe should be taken into account. However, for computational simplicity, we adopt in this paper a spherically symmetric approximation (refer to Gu et al. 2003, hereafter GBL03, for a detailed study). Second, we have only considered the contribution of ohmic dissipation $\mathcal{P}$ to the planetary inflation. The tidal (gravitational) interaction between the star and the planet can also significantly enhance the planet's inflation in some cases. More precisely, this tidal interaction can be strong for small semimajor axes (the tidal effect varies as $a^{-13/2}$) and for large radii (thus, the more inflated the planet, the stronger this effect becomes).

5.3. *The Governing Equations*

The mass-loss process is initiated when $R_e \geq R_H$. In this limit, a continuous flow would be established in which the inflation of the envelope drives a steady supply of gas to the Roche lobe region. Well inside the Roche lobe, the gravitational potential is primarily determined by the mass of the planet M_p, $\phi_g = -GM_p/r$; but near R_H, we need to take into account both the planet and the star. In a frame which corotates with the planet, the gravitational potential

$$U(r) = \frac{-GM_\star}{a}\left\{\left(1 - \frac{M_p}{M_\star}\right)\left[\frac{a}{a-r} + \frac{(a-r)^2}{2a^2}\right] + \frac{M_p}{M_\star}\left(\frac{a}{r} + \frac{r^2}{2a^2}\right)\right\}, \quad (20)$$

where r is the distance to the center of the planet. The value of R_H is determined from $dU/dr(R_H) = 0$.

In principle, this potential introduces a complex multidimensional flow pattern, especially near the Roche lobe. But the expansion of the envelope originates deep in the envelope where the ohmic dissipation occurs. In this region, spherical symmetry is adequate. Near the Roche lobe, we adopt the results obtained by GBL03. For computational convenience, we neglect the planet's spin.

We consider a low-velocity quasi-hydrostatic expansion of the envelope. Under this gravitational potential in equation (20), the radial component of the hydrodynamics momentum equation for a volume of gas is reduced to

$$v\frac{dv}{dr}(r) + \frac{1}{\rho(r)}\frac{dP}{dr}(r) = -\frac{1}{\rho(r)}\frac{dU}{dr}(r), \quad (21)$$

where v is the radial velocity. The radial component of the equation of mass conservation $\nabla[\rho(r)v(r)] = 0$ gives $r^2\rho(r)v(r) =$ const, and then the mass-loss rate $\dot{M}$ is constant,

$$\dot{M} = 4\pi r^2\rho(r)v(r) = \text{const}, \quad (22)$$

or equivalently, $(1/\rho)(d\rho/dr) = -(1/r^2v)(dr^2v/dr)$. Then using $(dP/dr) = (dP/d\rho)(d\rho/dr) = (d\rho/dr)\ c_s^2$ [$c_s^2(r)$ is the sound speed], the momentum equation becomes

$$\left(1 - \frac{c_s^2}{v^2}\right)\frac{d}{dr}\left(\frac{v^2}{2}\right) = -\frac{1}{\rho}\frac{dU}{dr}\left(1 - \frac{2c_s^2\rho}{r}\frac{1}{dU/dr}\right). \quad (23)$$

At a (sonic) radius r_2 near the inner Lagrangian point, the flow velocity becomes comparable to the sound speed (GBL03), i.e.,

$$v(r_2) = c_s(r_2), \quad (24)$$

where the magnitude of r_2 is the largest solution of $r^2 - rR_H + [(2c_s^2a^3)/(LGM_\star)] = 0$, with

$$L = \left(1 - \frac{M_p}{M_\star}\right)\left[\frac{2a^3}{(a-R_H)^3} + 1\right] + \frac{M_p}{M_\star}\left[2\left(\frac{a}{R_H}\right)^3 + 1\right] \simeq 9. \quad (25)$$

The expansion rate is determined by the rate of ohmic energy dissipation within the planet. In a steady state, the energy equation reduces to

$$\frac{1}{r^2}\frac{d}{dr}\left\{r^2\rho(r)v(r)\left[\frac{v^2}{2} + h(r) + \phi_g(r)\right]\right\} = \mathcal{P}_{\rm vol}, \quad (26)$$

where $\mathcal{P}_{\rm vol}$ is the volumic ohmic energy dissipation and ϕ_g is the gravitational potential (of the planet only or of both the planet

and the star, depending on the location). In this approximation, we assume that the distribution of enthalpy h is determined by both efficient convective transport (in term of an abiabat) and radiative diffusion inside the planet.

Using equation (22), we replace $r^2\rho(r)v(r)$ by $\dot{M}/4\pi$ in equation (26). We then can then integrate equation (26) between the radius $r_{\rm pn}$ (the radius at which the field can no longer penetrate into the planet) and r_2 so that

$$\dot{M}\left[\frac{v^2}{2}(r_2)-\frac{v^2}{2}(r_{\rm pn})+h(r_2)-h(r_{\rm pn})+\phi_g(r_2)-\phi_g(r_{\rm pn})\right] = \int 4\pi r^2\mathcal{P}_{\rm vol}(r)dr=\mathcal{P}. \quad (27)$$

Within an order of magnitude, $\Delta(h)\approx -\frac{1}{3}\Delta(\phi_g)$ and $\Delta(\frac{1}{2}v^2)\approx (1/10)\Delta(\phi_g)$ (this comes from calculating the order of magnitude of these three terms using an order of magnitude for the temperature, for the sound speed, and for $r_{\rm pn}$). In addition, the integrated energy equation is the result of an approximation, as the total ohmic dissipation rate $\mathcal{P}$ should be the integral of $\mathcal{P}_{\rm vol}$ between $r_{\rm pn}$ and R_p ($=R_H$ because we assumed that the planet fills its Roche lobe). However, this approximation is reasonable since $h(R_H)=h(r_2)$ (the surface region is approximately isothermal), $v^2(r_2)\approx v^2(R_H)$, and $\phi_g(r_2)\approx\phi_g(R_H)$ (because r_2 is very close to R_H).

We now can calculate $\rho(r_2)$ and $P(r_2)$. Equation (22) for $r=r_2$ with $\upsilon(r_2)=c_s(r_2)=10^4(T/10^4)^{1/2}$ m gives

$$\rho(r_2)=\frac{\dot{M}}{4\pi r_2^2 c_s(r_2)},\quad P(r_2)=\alpha\rho(r_2)T(r_2),\quad \alpha=\mathcal{N}_{\rm A}k_{\rm B}/(\mu\mathcal{M}_{\rm H}), \quad (28)$$

where $\mathcal{N}_{\rm A}$ is the Avogadro constant, $k_{\rm B}$ is the Boltzmann constant, $\mathcal{M}_{\rm H}$ is the hydrogen molar mass, and μ is a coefficient which depends on the ionization rate ($\mu=1$ for hydrogen atoms, and $\mu=0.5$ for fully ionized hydrogen gas, and we usually choose μ close to unity).

6. ISOTHERMAL AND POLYTROPIC MODEL

In § 4, the permeation and dissipation of the time-dependent external field is analyzed by neglecting any resulting changes in the planet's interior. In § 5 we show that the resulting ohmic dissipation can substantially modify the temperature and density distribution within the planet. Increases in the ionization rate modify the skin depth and relocate the region of maximum ohmic dissipation. However, the expansion of the planet's envelope does not affect the rate of ohmic dissipation. In this section we present a set of approximately self-consistent calculations to analyze the feedback effect of ohmic dissipation on the planet's internal structure.

6.1. *A Roche Lobe–Filling Structural Model*

In principle, the structure of the planet should be solved numerically with the standard planetary structure equations (BLM01). However, a semianalytic model based on simplifying assumptions may provide insight on the interdependent relation between various physical parameters. Based on BLM01's numerical models, we approximate the internal structure of the planet with an idealized model in which the outer region is isothermal (due to the stellar irradiation) and the inner region is polytropic (due to an efficient mix of entropy by thermal convection). In the computation of η, we only take into account the ionization of the hydrogen, because the internal temperature distribution is mostly determined by heat transfer rather than heat dissipation and the rate of $\mathcal{P}$ is a relatively insensitive function of η. The advantage of this approximation is that its application for the self-consistent analysis is relatively straightforward.

6.1.1. *The Isothermal Region*

The isothermal region extends from the surface to a transition radius $r_=$ which is to be determined self-consistently in § 6.2. In this region, the equation of state and the equation describing the hydrostatic equilibrium are

$$T(r)=\text{const}, \quad (29)$$

$$P(r)=\alpha\rho(r)T(r), \quad (30)$$

$$\frac{dP}{dr}(r)=-\frac{GM_{\rm int}(r)}{r^2}\rho(r), \quad (31)$$

where $\alpha=\mathcal{N}_{\rm A}k_{\rm B}/(\mu\mathcal{M}_{\rm H})$ and $M_{\rm int}(r)$ is the planet's mass inside a sphere of radius r centered on the planet's center. For all practical purposes, ρ is sufficiently low in the isothermal region that we can approximate $M_{\rm int}(r)\simeq M_p$ (one can verify, a posteriori, that the neglected mass is less than a few percent of the total mass). To calculate $P(r)$, we integrate equation (31) using equations (29) and (31). We then can calculate $\rho(r)$ using equation (31),

$$P(r)=C\exp\left(\frac{GM_p}{r}\frac{1}{\alpha T}\right),\quad \rho(r)=\frac{1}{\alpha T}C\exp\left(\frac{GM_p}{r}\frac{1}{\alpha T}\right), \quad (32)$$

where C is an integration constant, the value of which is obtained by injecting r_2 into the previous equations.

6.1.2. *The Polytrope Region*

The polytrope region extends from the center of the planet to $r_=$. In this region, we use the following equations,

$$P(r)=K\rho^{\gamma}(r), \quad (33)$$

$$\frac{d\phi_g}{dr}(r)=\frac{GM_{\rm int}(r)}{r^2}, \quad (34)$$

$$\frac{dP}{dr}(r)=-\frac{GM_{\rm int}(r)}{r^2}\rho(r), \quad (35)$$

$$\Delta\phi_g(r)=4\pi G\rho(r), \quad (36)$$

where ϕ_g is the gravitational potential and Δ is the Laplacian (in the Poisson equation). Using equations (33) and (34), equation (35) becomes $K\gamma\rho^{\gamma-1}(r)(d\rho/dr)(r)=-\rho(r)d\phi_g/dr$. And after integration, $\phi_g(r)=\text{const}-[K\gamma/(\gamma-1)]\rho^{\gamma-1}(r)$.

We then replace ϕ_g in the Poisson equation (36),

$$\Delta\rho^{\gamma-1}(r)=-\frac{\gamma-1}{K\gamma}4\pi G\rho(r). \quad (37)$$

For the condition appropriate in the interior of planets, the equation of state is reasonably approximated by a $\gamma=2$ polytrope (de Pater & Lissauer 2001). In spherical coordinates, the previous equation becomes

$$\frac{1}{r^2}\frac{d}{dr}\left[r^2\frac{d}{dr}\rho(r)\right]=-\frac{2\pi G}{K}\rho(r). \quad (38)$$

This equation has an analytical solution (Ogilvie & Lin 2004), and we can calculate $\rho(r)$, $P(r)$, and $T(r)$ in the region described by the polytropic equation of state,

$$\rho(r) = \rho_0 \frac{\sin kr}{kr},$$
$$P(r) = K\rho^2(r) = K\rho_0^2 \left(\frac{\sin kr}{kr}\right)^2,$$
$$T(r) = \frac{P}{\alpha\rho}(r) = \frac{1}{\alpha} K\rho_0 \frac{\sin kr}{kr},$$
$$k = \sqrt{\frac{2\pi G}{K}}. \quad (39)$$

6.2. *Transition between the Two Models*

In principle, the transition between the two regions is determined by the onset of convection. In the construction of hydrostatic equilibrium structure models (to be presented in Paper II), we will indeed use that condition to determine its photospheric radius. Qualitatively, we expect the transition radius which separates the two regions, $r_=$, to be larger than $r_{\rm pn}$, because only in the region interior to $r_=$ do we expect the temperature, ionization fraction, and conductivity to be sufficiently large to halt the penetration of the field. In a hydrostatic equilibrium, the actual value of $r_=$ is determined by the ratio of the ohmic dissipation rate in the convective region to the sum of the ohmic dissipation rate in the entire planet's interior and the stellar irradiative flux on the planet's surface. A set of fully self-consistent solutions requires the matching of the ohmic dissipation rate to be expected from the planetary structure and that which determines its density and temperature distribution (see Paper II).

In the present context, we are considering the situation in which the planet's radius is constrained by its Roche lobe and the density and temperature of the outer boundary is determined by equation (28). In this configuration, heat is also transported by advection which modifies the location of $r_=$. Moreover, the density ratio between the planet's center and the outer boundary is much larger than the temperature ratio. Therefore, the polytropic region cannot fill the entire interior region. Since the pressure scale height on the planet's surface is much smaller than its radius, the isothermal region also cannot occur in the entire planet's interior while containing all of its mass. Instead, the planet's interior adjusts to attain a balance between the requirement of mass loading and constraints set by hydrostatic equilibrium for appropriate equations of state.

In order to construct such an equilibrium model, we now determine ρ_0 and k at $r_=$, where the transition between the two regions occur. There are three equations that constrain these parameters, $T_{\rm iso}(r_=) = T_{\rm poly}(r_=)$, $P_{\rm iso}(r_=) = P_{\rm poly}(r_=)$, and the total mass is constant. The first two conditions also imply $\rho_{\rm iso}(r_=) = \rho_{\rm poly}(r_=)$. Therefore, we solve the following equations for ρ_0, k, and $r_=$,

$$k^2 = \frac{2\pi GC}{(\alpha T)^2} \exp\left(\frac{GM_p}{\alpha T r}\right),$$
$$\rho_0 = \frac{\alpha T}{2\pi G} k^2 \frac{kr_=}{\sin kr_=},$$
$$\int_0^a 4\pi r^2 \rho_{\rm poly}(r) dr + \int_a^R 4\pi r^2 \rho_{\rm iso}(r) dr = M_p. \quad (40)$$

By assuming an isothermal structure in the outer envelope, we have neglected the outward heat flux. This approximation is only adequate if the dissipation rate is above that which is needed to inflate R_p to the planet's Roche radius. If this condition is not satisfied, the planet's radius would attain equilibrium values for which the surface cooling is balanced by the ohmic dissipation and stellar irradiation. We will construct, in Paper II, the equivalent of equation (21) (for a 0.63 $M_\odot$ planet) which takes into account the effect of ohmic dissipation in the planetary interior.

Whereas the temperature on the planet's surface is determined by the stellar irradiation, the density at $r_2 = R_H$ is determined by the magnitude of $\dot{M}$ (through eq. [28]) which in turn is determined by the rate of ohmic energy dissipation $\mathcal{P}$ (see § 7). For very large values of $\mathcal{P}$, a set of fully self-consistent solutions also modifies the temperature at the disk surface as well as the thermal content of the outflowing gas. However, provided $\mathcal{P}$ is small compared with the stellar irradiative flux, a transition for convective stability occurs near $r_=$.

6.3. *Calculation of the Magnetic Diffusivity*

With these internal structure specified, we consider Saha's equation for the hydrogen atoms which gives the ionization fraction x (Kippenhahn & Weigert 1994, pp. 107–111),

$$\frac{x^2}{1-x^2} = K_{\rm H} = \frac{1}{P(r)} \frac{(2\pi m_e)^{3/2}}{h^3} (kT)^{5/2} \exp\left(-\frac{E}{kT}\right), \quad (41)$$

where the ionization energy of hydrogen is $E = 13.6$ eV. We also neglect here the radiation pressure as we write $P_{\rm gas}(r) = P(r)$.

If the ionization fraction x is small, $x^2 \approx K_{\rm H}$ (this is typically the case in the region where the ohmic dissipation occurs). We use $\sigma = N_e e^2/(m_e \nu_e)$, with $\nu_e = N_n 10^{-19} [128kT/(9\pi m_e)]^{1/2}$.

The electric conductivity we would obtain does not take into account higher ionization states or the ionization of elements other than hydrogen atoms. We then use for the following calculations an electric conductivity that is 10 times higher than that we would obtain with the Saha equation (eq. [41]) for the hydrogen atom only. We saw in Table 1 that the ohmic dissipation rate was quite insensitive to the magnetic diffusivity $\eta(r) = \mu_0 \sigma(r)$, and we verified that this is also the case with the internal model we used for the planet in §§ 5–8 (for example, in this model, a uniform change in the magnetic diffusivity by a factor 10 changes $\mathcal{P}$ and $\dot{M}$ by less than 20%, and a uniform change in the magnetic diffusivity by a factor 100 changes $\mathcal{P}$ and $\dot{M}$ by less than 40%). We then obtain the following expression for the magnetic diffusivity inside the planet,

$$\eta(r) = 1.28 \times 10^{-2} \frac{\sqrt{P(r)}}{T^{3/4}(r)} \exp\left(\frac{78909}{T}\right), \quad (42)$$

where $T(r)$ and $P(r)$ are the temperature and pressure of the isothermal or polytropic region, depending on the radius r.

7. OHMIC DISSIPATION RATE AND THE MASS-LOSS RATE FOR DIFFERENT SETS OF PARAMETERS

With the above idealized prescription for the planet's internal structure, we now calcultate self-consistently the ohmic dissipation rate $\mathcal{P}$ inside the planet as well as the mass-loss rate $\dot{M}$.

7.1. *Parameters Involved in the Calculation*

The model parameters involved in the calculation of the ohmic dissipation rate inside the planet are (1) the planet's mass M_p, (2) the semimajor axis a, (3) the relative angular velocity ω (the angular velocity of the field seen in a frame centered on the star and rotating with the planet), (4) the strength of the star's magnetic dipole moment m, and (5) the angle α between the spin axis of the star and the star's magnetic dipole.

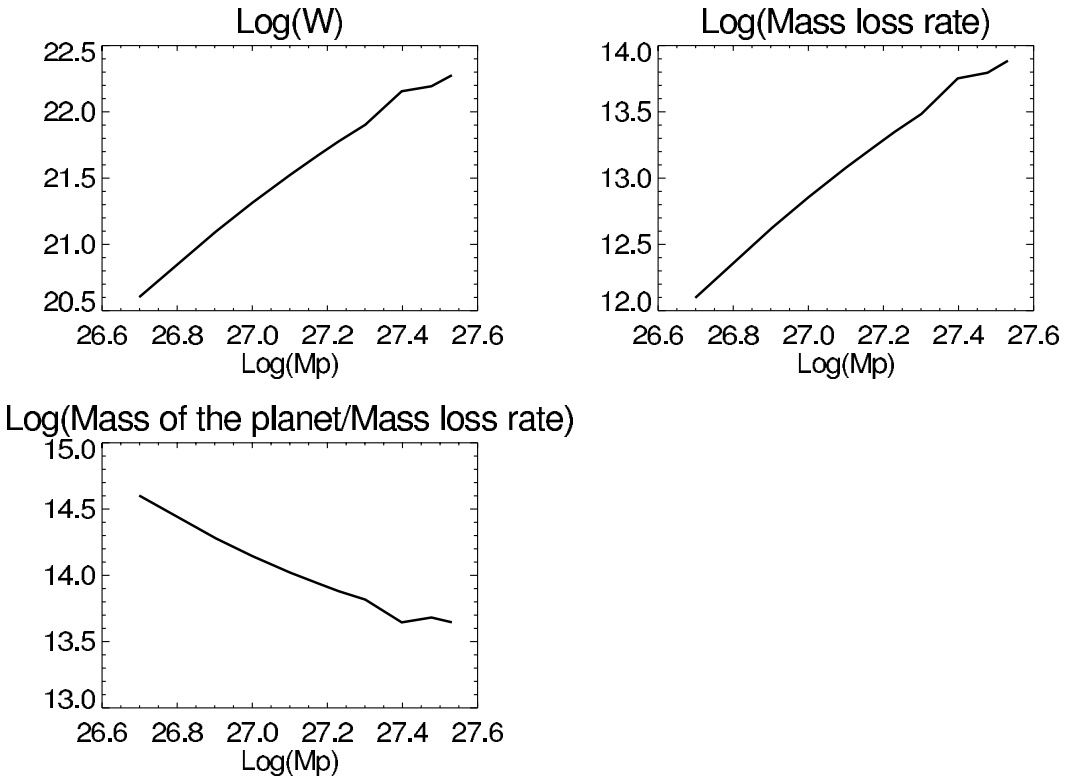

FIG. 3.—Ohmic dissipation rate, mass-loss rate, and timescale for different planetary masses.

We use the isothermal and polytropic prescription described in § 6 to model the planet's internal structure and calculate the conductivity profile inside the planet. To do so, we also need to specify (6) the mass of the star $M_\star$ and (7) the star's luminosity $L_\star$.

7.2. *Methodology*

The construction of a self-consistent model requires a loop of retroaction involving the determination of the internal structure of the planet and of the ohmic energy dissipation. For a specified internal structure of the planet, one can compute (following § 3) the conductivity profile and then the total ohmic dissipation rate $\mathcal{P}$. However, this energy dissipated inside the planet corresponds to an input of heat, which triggers an adjustment in the planet's internal parameters. Because of the efficient convection inside the planet, we assume that the adjustment of the internal parameters to this external heating is quick. We consider that the characteristic timescale for the planet to evolve from one equilibrium state to another is small compared to the variation timescale of the seven parameters mentioned in the previous paragraph. Therefore, we do not need to follow the planet's dynamical evolution at all times. Instead, we can take a series of "snap shots" of the planet in its equilibrium state for different sets of parameters.

Because of this feedback loop between the ohmic dissipation rate and the planet's internal parameters, we use an iterative method. For any chosen set of parameters, we start from an estimate for the ohmic dissipation rate $\mathcal{P}_0$ and internal structure $T_0(r)$, $P_0(r)$, and $\rho_0(r)$ corresponding to a magnetic diffusivity profile $\eta_0(r)$ (in our parametric analyses, we typically make small incremental changes in the model parameters from those for which we have already obtained equilibrium values). We then compute the new internal structure $T_1(r)$, $P_1(r)$, and $\rho_1(r)$ associated with $\mathcal{P}_0$. This enables us to compute the corresponding magnetic diffusivity $\eta_1(r)$. Finally, we use $\eta_1(r)$ to calculate the corresponding ohmic dissipation rate $\mathcal{P}_1$ and mass-loss rate $\dot{M}_1$. This process is iterated until convergence of $\mathcal{P}$, $\dot{M}$, and the internal parameters. Moreover, for some specific set of parameters M_p, a, ω, m, $\sin(\alpha)$, $M_\star$, and $L_\star$, we have started the iterative process from two different initial states in order to verify that they both converge to the same solution. Therefore, the iterative process does converge to a unique solution.

We consider the following fiducial model in which the mass of the planet and semimajor axis corresponds to HD 209458b and in which the other parameters are reasonable ones for the type of systems considered. An estimate of the order of magnitude for the strength of the magnetic dipole can be found in Johns-Krull (2007).

Mass of the planet.—$M_p = 0.63\ M_{\rm J} = 1.26 \times 10^{27}$ kg,
Semimajor axis.—$a = 0.04$ AU $= 6 \times 10^9$ m,
Relative angular velocity.—$\omega = 10^{-5}\ {\rm s}^{-1}$,
Star's magnetic dipole.—$m = 4 \times 10^{34}$ A m^2,
Value of the tilt of the magnetic dipole.—$\sin(\alpha) = 1$,
Mass of the star.—$M_\star = 1\ M_\odot = 2 \times 10^{30}$ kg,
Luminosity of the star.—$L_\star = 1.5\ L_\odot = 5.7 \times 10^{26}$ W.

7.3. *Computation of $\mathcal{P}$ and $\dot{M}$, Plots, and Mathematical Relations*

We present seven groups of plots (Figs. 3–9), one group for each parameter mentioned just above. For each group, we vary one parameter (x-axis), while keeping the others at the reference values mentioned above. On the y-axis, we plotted the ohmic dissipation rate $\mathcal{P}$, mass-loss rate $\dot{M}$, and characteristic timescale $\tau_M = M/\dot{M}$. Note that the magnitude of τ_M for a

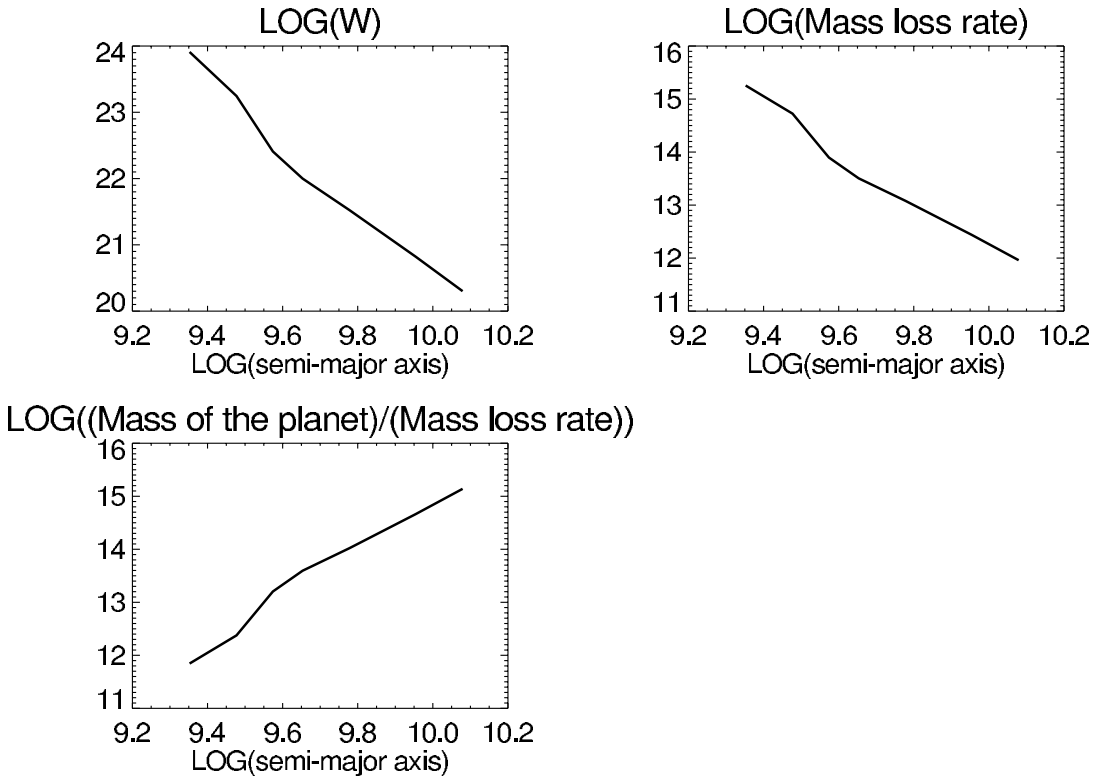

FIG. 4.—Same as Fig. 3, but for different semimajor axes.

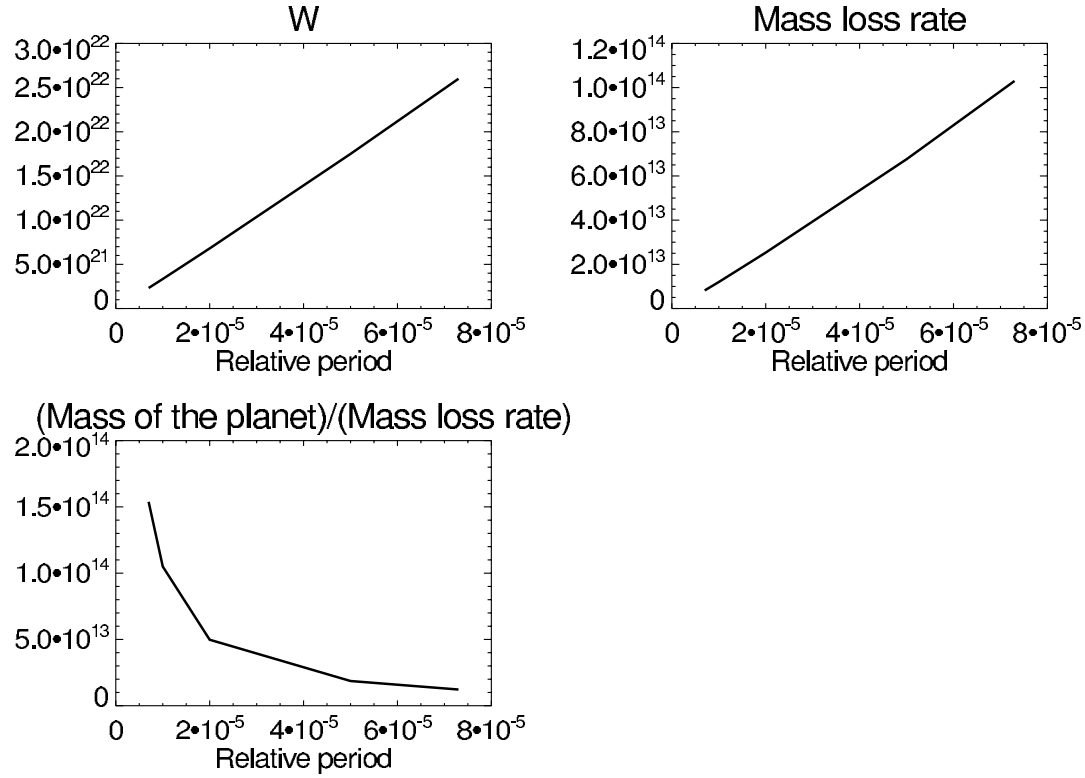

FIG. 5.—Same as Fig. 3, but for different relative angular velocities.

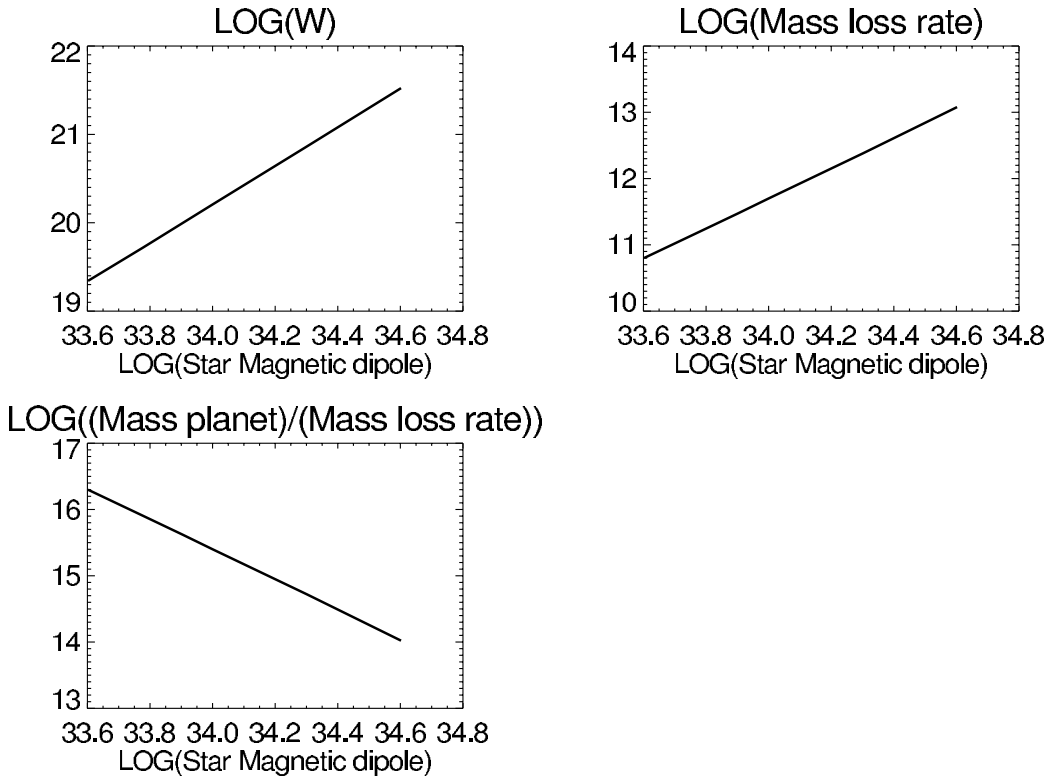

FIG. 6.—Same as Fig. 3, but for different stellar magnetic moments.

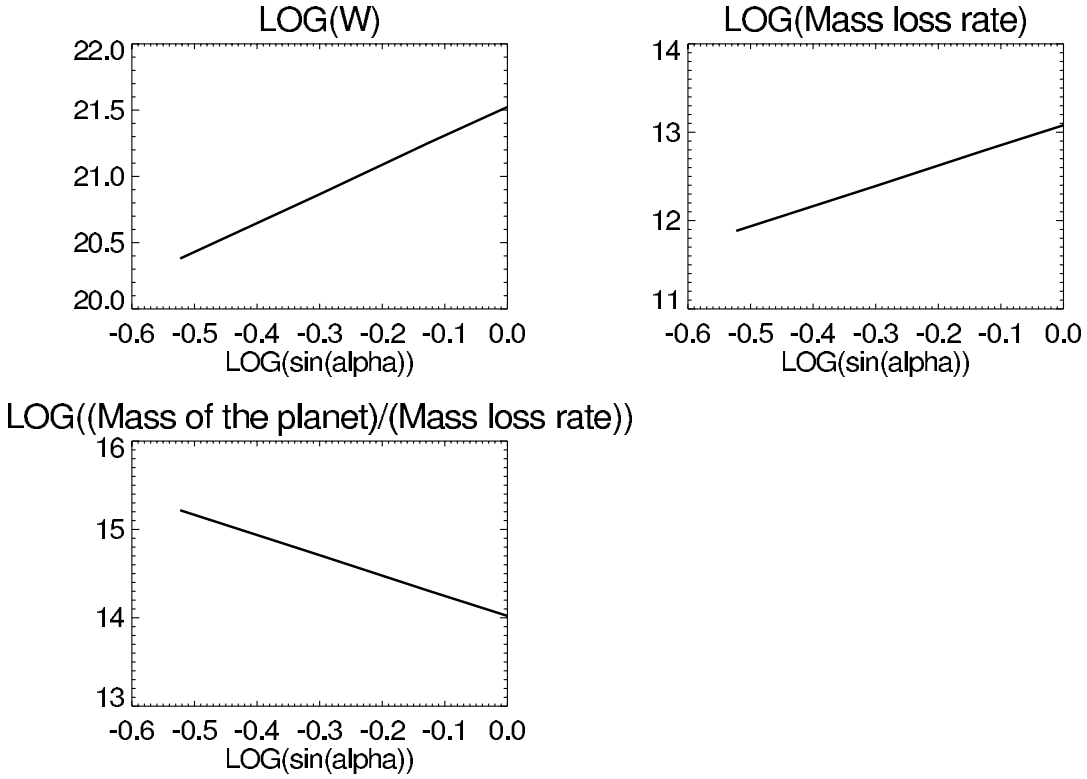

FIG. 7.—Same as Fig. 3, but for different tilts of the stellar magnetic dipole with regard to the stellar spin axis.

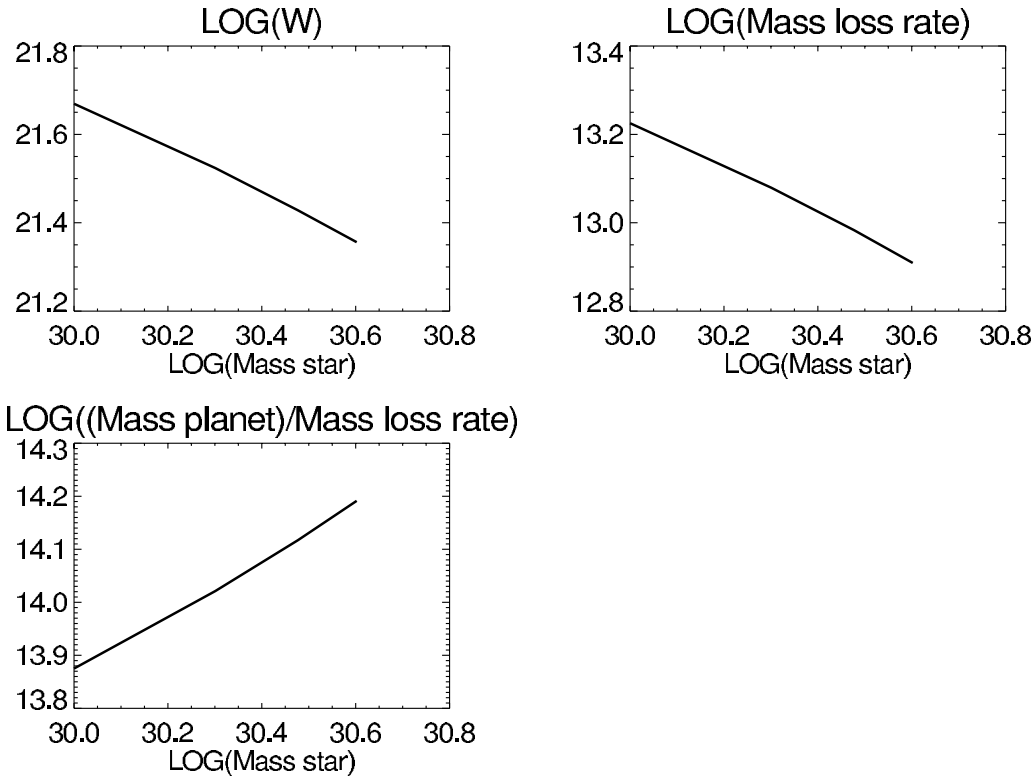

FIG. 8.—Same as Fig. 3, but for different stellar masses.

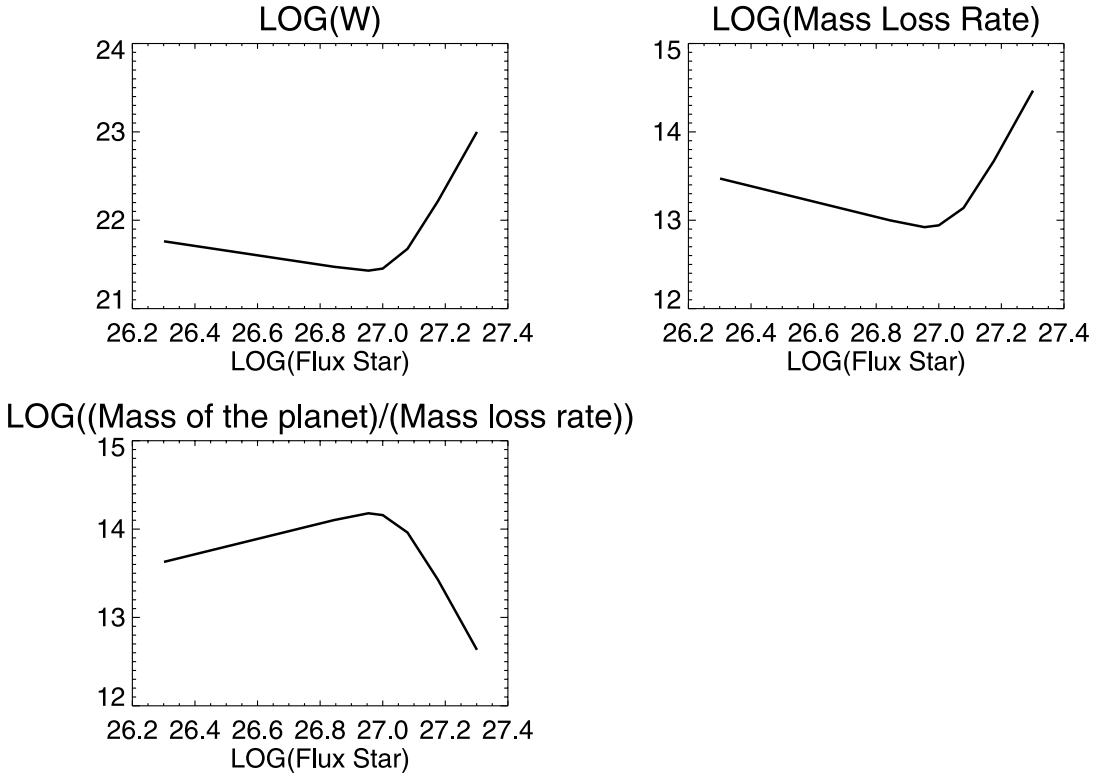

FIG. 9.—Same as Fig. 3, but for different stellar total flux.

TABLE 2
OHMIC DISSIPATION AND MASS-LOSS RATES AS A FUNCTION OF THE VARIED PARAMETER

Varying Parameter	$\mathcal{P}$ (W)	$\dot{M}$ (kg s^{-1})
$0.25\ M_J \leq M_p \leq 1.7\ M_J$	$\mathcal{P}_1 = 3.3\times10^{21}[M_p/(0.63\ M_J)]^{2.16}$	$\dot{M}_1 = 1.2\times10^{13}[M_p/(0.63\ M_J)]^{2.4}$
$0.015\ \mathrm{AU} \leq a \leq 0.08\ \mathrm{AU}$	$\mathcal{P}_2 = 3.3\times10^{21}[a/(0.04\ \mathrm{AU})]^{-4}$	$\dot{M}_2 = 1.2\times10^{13}[a/(0.4\ \mathrm{AU})]^{-3.8}$
$7\times10^{-6}\ \mathrm{s}^{-1} \leq \lvert\omega\rvert \leq 7.3\times10^{-5}\ \mathrm{s}^{-1}$	$\mathcal{P}_3 = 3.5\times10^{21}(\lvert\omega\rvert/10^{-5}) - 1.5\times10^{20}$	$\dot{M}_3 = 1.4\times10^{13}(\lvert\omega\rvert/10^{-5}) - 1.3\times10^{12}$
$6\times10^{33}\ \mathrm{A\ m^2} \leq m \leq 4\times10^{34}\ \mathrm{A\ m^2}$	$\mathcal{P}_4 = 3.3\times10^{21}[m/(4\times10^{34})]^{2.18}$	$\dot{M}_4 = 1.2\times10^{13}[m/(4\times10^{34})]^{2.3}$
$0.3 \leq \sin(\alpha) \leq 1$	$\mathcal{P}_5 = 3.3\times10^{21}\sin^{2.17}(\alpha)$	$\dot{M}_5 = 1.2\times10^{13}\sin^{2.28}(\alpha)$
$0.5\ M_\odot \leq M_\star \leq 1.5\ M_\odot$	$\mathcal{P}_6 = 3.3\times10^{21}(M_\star/M_\odot)^{-0.53}$	$\dot{M}_6 = 1.2\times10^{13}(M_\star/M_\odot)^{-0.5}$
$0.5\ L_\odot \leq L_\star \leq 2.6\ L_\odot$	$\mathcal{P}_7 = 3.3\times10^{21}[L_\star/(1.5\ L_\odot)]^{-0.5}$	$\dot{M}_7 = 1.2\times10^{13}[L_\star/(1.5\ L_\odot)]^{-0.8}$
$2.6\ L_\odot \leq L_\star \leq 5\ L_\odot$	$\mathcal{P}_7 = 7.5\times10^{19}[L_\star/(1.5\ L_\odot)]^{5.9}$	$\dot{M}_7 = 1.25\times10^{11}[L_\star/(1.5\ L_\odot)]^{5.8}$

Jupiter mass planet is about 1 Myr. In addition, the mass-loss rate determined here is many orders of magnitude larger than that due to photo evaporation. Only with such a large mass-loss rate can we compensate for the angular momentum transfer due to the planet-disk and planet-star tidal interactions.

We emphasize once again that in the construction of these models, we assume that there is adequate energy dissipation to inflate the planet with $R_e > R_H$. In later papers that use the Roche Lobe–filling model, we verify that $\mathcal{P}(R_H) > L_i(R_H)$ before these results are applied. If this condition is not satisfied, the planet would not fill its Roche lobe and not lose mass.

From each group of plots, we obtain $\mathcal{P}$ and $\dot{M}$ as a function of the parameter that is being varied (all the others are kept constant at the value of the fiducial model given above). These functions are given in Table 2.

7.4. *Model Parameter Dependence*

1. Mass of the planet M_p. The total ohmic dissipation is a volumic integral over the entire region where dissipation occurs. Therefore, one might expect $\mathcal{P}$ to be proportional to the volume. Since the planet fills its Roche lobe, the volume is determined by the mass (see eq. [19]). However, M_p also gives a constraint on the volumic mass at the center of the planet (see eq. [40]), which makes $\mathcal{P}$ mostly proportional to M^2. There is also a minor correction due to the weak dependence of $\mathcal{P}$ on η which depends on M_p through the calculation of the internal parameters T, P, and ρ (eqs. [32] and [39]).

2. Semimajor axis a. In the model we adopted in § 4, or more generally, in a model that would not take into account the planet's internal adjustment to the ohmic dissipation (especially in a

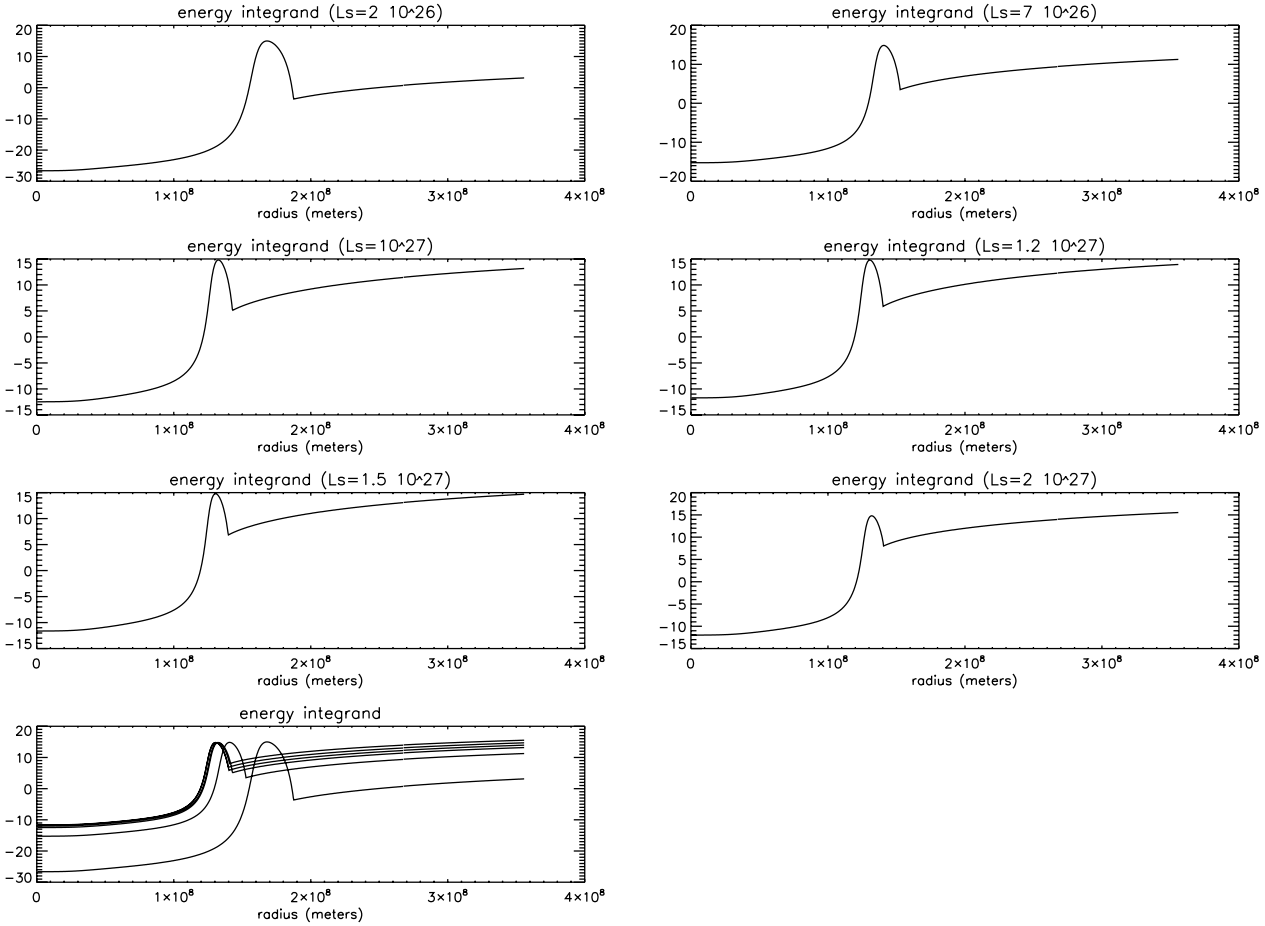

FIG. 10.—Integrand of the ohmic dissipation (log scale) for different values of the stellar luminosity.

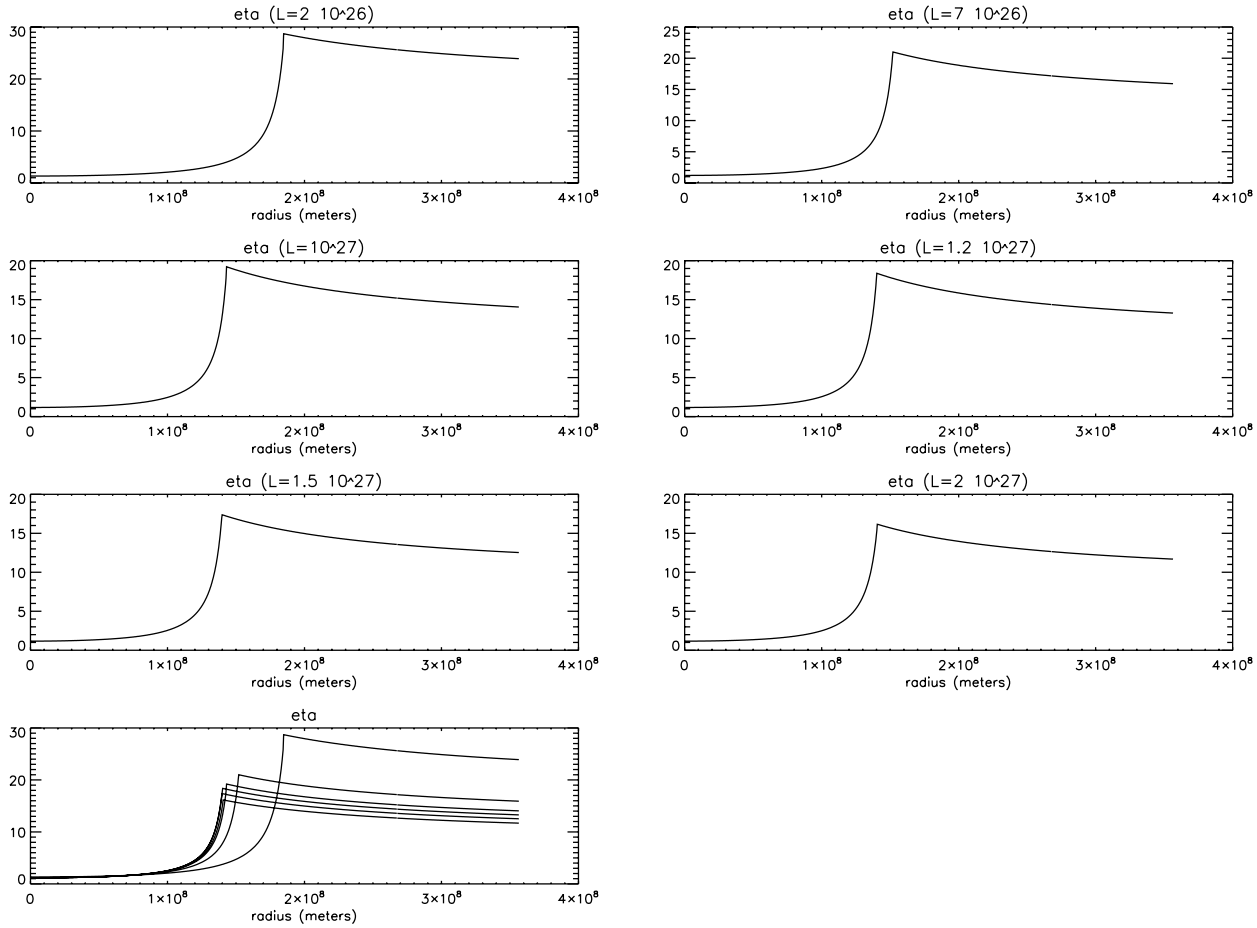

FIG. 11.—Magnetic diffusivity (log scale) for different values of the stellar luminosity.

model in which the radius of the planet is independent of the semimajor axis), the ohmic dissipation rate would be related to the semimajor axis according to the following law, $\mathcal{P} \propto B^2 \propto a^{-6}$. In the self-consistent model we adopted here and in the limit where the planet fills its Roche lobe ($R_p = R_H$), the radius of the planet varies with the semimajor axis. For example, when a planet moves closer to its host star, its Roche radius decreases linearly with the radius (see eq. [19]), and therefore, $\mathcal{P}$ increases less quickly than if the planet kept the same radius. Again, $\mathcal{P}$ also has a weak dependence on η which depends on the semimajor axis through the planet's surface temperature and through the dependence of r_2 on a. From these arguments, we thus expect the exponent in $\mathcal{P}_2$ to be greater than -6 and smaller than -3.

3. Relative angular velocity ω. In equation (12), the multiplicative constant in front of the volumic integral comes from the induction by the time-dependent stellar field (see eqs. [5] and [11]) and gives to $\mathcal{P}$ a dependence on ω^2. However, in addition, ω intervenes inside the volumic integral in equation (12) through the dependence of $G_l(r)$ on the δ^{-1}, with $\delta = (\eta/\omega)^{1/2}$, skin depth. Therefore, the volumic integral is proportional to ω^{-1} and $\mathcal{P}$ is proportional to ω.

4. Magnetic dipole m and tilt of the magnetic dipole α. Without any adjustment of the planet's interior to the ohmic dissipation, we would expect $\mathcal{P}_4$ and $\mathcal{P}_5$ to vary, respectively, in m^2 and $\sin^2(\alpha)$. The fact that both exponents that have been computed numerically are slightly larger than 2 means, in the self-consistent model we adopted here, that the adjustment of the planet's interior tends to have a small positive retroaction on the amount of energy that is deposited inside the planet through ohmic dissipation.

5. Mass of the star $M_\star$. The mass of the star intervenes in the computation of the Roche radius ($R_H \propto M_\star^{-1/3}$). With $\mathcal{P}$ being a volumic integral, one would, therefore, expect it to vary proportionally to $M_\star^{-1}$. However, $M_\star$ also intervenes in the computation of r_2 [r_2 is the sonic point, or the largest solution of $r^2 - rR_H + 2c_s^2 a^3/(LGM_\star) = 0$; see eq. (25)], which brings a correction to the dependence of $\mathcal{P}$ on M_s. Indeed, r_2 is used to compute $P(r_2)$ and $\rho(r_2)$ (see eq. [28]) which are the boundary conditions we adopted to calculate the pressure and volumic mass in the isothermal region (see eq. [32]). As a side note, this dependence of $\mathcal{P}$ on r_2 could also affect the dependence of $\mathcal{P}$ on a and $M_\star$.

6. Stellar total luminosity $L_\star$. From Figure 9, one can see that $L_\star = 10^{27}$ W corresponds to a minimum for $\mathcal{P}$ and that $\mathcal{P}$ varies slowly for $L_\star \leq 10^{27}$ W and much faster for $L_\star \geq 10^{27}$ W. In the model we adopted here, the stellar total luminosity fixes the planet's equilibrium surface temperature, which is also the temperature of the isothermal region (for $L_\star = 10^{27}$ W, $T_p \simeq 1767$ K). It in turn determines the temperature profile inside the planet (the surface temperature is used as a boundary condition) and influences the internal structure and magnetic diffusivity profile inside the planet $\eta(r)$. The temperature T_p varies proportionally to $L_\star^{1/4}$ (for constant semimajor axis), and therefore, η is roughly proportional to $\exp(78,909/L_\star^{1/4})$.

We plotted the integrand of the ohmic dissipation ($\langle \mathcal{P}_{\rm vol} \rangle r^2$ in eq. [13]) as well as the magnetic diffusivity (see Figs. 10 and 11) for $L_\star = 2 \times 10^{26}$, 7×10^{26}, 10^{27}, 1.2×10^{27}, 1.5×10^{27}, and

2×10^{27} W. One can notice two parts corresponding to the isothermal and the polytropic regions. In the isothermal region, the energy integrand decreases slowly from the surface to the center of the planet. The transition between the two regions corresponds to a sharp increase in conductivity and, therefore, a quick increase in the ohmic dissipation. This accounts for the sharp increase in the integrand (around 1.5×10^8 m), and most of the remaining magnetic energy is dissipated in this region. Moreover, an increase in the stellar luminosity results in a decrease in the magnetic diffusivity as well as a deeper penetration and a deeper transition between the isothermal and the polytropic regions.

When one increases $L_\star$ starting from low values ($L_\star = 2 \times 10^{26}$ W), the energy integrand also increases in the isothermal region. Nevertheless, the extent and amplitude of the sharp increase at the transition between the isothermal and the polytropic regions are also reduced. Therefore, these two effects compensate each other, and for low stellar luminosity (e.g., $L_\star$ between 2×10^{26} and 10^{27} W), the total ohmic dissipation in the planet increases slowly with the stellar luminosity.

On the other hand, for higher values of the stellar luminosity, the penetration depth as well as the transition depth saturates [when the coupling term in eq. (6), $\omega/\eta(r)$, between the real and imaginary parts of $G_l(r)$ becomes comparable to the other term $l(l+1)/r^2$]. One can see that an increase in the stellar luminosity results only in changes in the energy integrand that would increase the total ohmic dissipation. This results in a much sharper increase of the ohmic dissipation with the stellar luminosity.

7. Attempts of generalized function. We consider the generalized expression of the ohmic dissipation rate and mass-loss rate in the case where the variables are separable,

$$\mathcal{P}_{\rm gen} = 3.3 \times 10^{21}\ {\rm W} \left(\frac{M_p}{0.63\ M_{\rm J}}\right)^{2.16} \left(\frac{a}{0.04\ {\rm AU}}\right)^{-4} \times \left(\frac{|\omega|}{10^{-5}\ {\rm s}^{-1}} - 0.045\right) \left(\frac{m}{4 \times 10^{34}\ {\rm A\ m}^2}\right)^{2.18} \times (\sin\alpha)^{2.17} \left(\frac{M_\star}{M_\odot}\right)^{-0.53} \left(\frac{L_\star}{1.5\ L_\odot}\right)^{-0.5}, \quad (43)$$

$$\dot{\mathcal{M}}_{\rm gen} = 1.2 \times 10^{13}\ {\rm kg\ s}^{-1} \left(\frac{M_p}{0.63\ M_{\rm J}}\right)^{2.4} \left(\frac{a}{0.04\ {\rm AU}}\right)^{-3.8} \times \left(\frac{|\omega|}{10^{-5}\ {\rm s}^{-1}} - 0.1\right) \left(\frac{m}{4 \times 10^{34}\ {\rm A\ m}^2}\right)^{2.3} \times (\sin\alpha)^{2.28} \left(\frac{M_\star}{M_\odot}\right)^{-0.5} \left(\frac{L_\star}{1.5\ L_\odot}\right)^{-0.8}. \quad (44)$$

The above formulae have been written for the first interval of $\mathcal{P}_7$ in Table 2, but one can write the corresponding formulae for the second interval by using the corresponding expression of $\mathcal{P}_7$. We compute, using the iterative procedure described above (§ 7.2), the ohmic dissipation $\mathcal{P}$ and mass-loss rate $\dot{\mathcal{M}}$ for sets of parameters in which more than two parameters are different from the fiducial parameters. We then compare these values with the values of $\mathcal{P}_{\rm gen}$ and $\dot{\mathcal{M}}_{\rm gen}$ for these sets of parameters. This test enables us to determine if the hypothesis of separation of variables is accurate or not. The first set of parameters that we consider is $M_p = 1.5\ M_{\rm J}$ and $a = 0.03$ AU, all the other parameters being kept equal to the fiducial parameters. We get $\mathcal{P} = 4.2 \times 10^{22}$ W and $\dot{\mathcal{M}} = 1.5 \times 10^{14}$ kg s^{-1}. However, using the formula of the ohmic dissipation rate and mass-loss rate with the approximation of separation of variables, we get $\mathcal{P}_{\rm gen} = 7 \times 10^{22}$ W and $\dot{\mathcal{M}} = 2.9 \times 10^{14}$ kg s^{-1}.

We now consider a set of parameters in which all parameters are taken different from the fiducial value, $M_p = 1.5\ M_{\rm J}$, $a = 0.03$ AU, $\omega = 2.9 \times 10^{-5}$ s^{-1}, $m = 2 \times 10^{34}$ A m^2, $M_\star = 1.5\ M_\odot$, and $L_\star = 0.8\ L_\odot$ (this value of ω corresponds, for example, to a system in which the planet is at Keplerian angular velocity and the star has a period of 4 days). We get $\mathcal{P} = 1.7 \times 10^{22}$ W and $\dot{\mathcal{M}} = 7 \times 10^{13}$ kg s^{-1}, and using the formula of the ohmic dissipation rate and mass-loss rate with the approximation of separation of variables, we get $\mathcal{P}_{\rm gen} = 3.5 \times 10^{22}$ W and $\dot{\mathcal{M}} = 1.6 \times 10^{14}$ kg s^{-1}.

From these two tests, we deduce that the approximation of separation of variables gives a reasonable order of magnitude, but nevertheless, does not seem to be accurate. This result means that the exponents in the functions given in Table 2 can themselves be a function of the parameters, and the generalized functions that describe the ohmic dissipation and mass-loss rate as a function of all parameters can be fairly complicated. Nevertheless, even if a generalized formula is still unknown, for a given set of parameters, one could still compute the mass-loss rate and ohmic dissipation using the procedure described in §§ 3–7.

7.5. *Mass Loss and Migration Stalls*

From equation (44), we find

$$\tau_m = \frac{M_p}{\dot{\mathcal{M}}_{\rm gen}} \simeq 3\ {\rm Myr} \left(\frac{0.63\ M_{\rm J}}{M_p}\right)^{2.4} \left(\frac{a}{0.04\ {\rm AU}}\right)^{3.8} \times \left(\frac{|\omega|}{10^{-5}\ {\rm s}^{-1}} - 0.1\right)^{-1} \left(\frac{m}{4 \times 10^{34}\ {\rm A\ m}^2}\right)^{-2.3} \times (\sin\alpha)^{-2.28} \left(\frac{M_\star}{M_\odot}\right)^{0.5} \left(\frac{L_\star}{1.5\ L_\odot}\right)^{0.8}. \quad (45)$$

The same mass loss provides angular momentum to the planet. We neglect any variations in eccentricity and assume that all the mass is accreted into the star. Using GBL03 (their eq. [96]), we link the mass-loss rate to a rate of change of semimajor axis,

$$\frac{\dot{a}}{a} = -2\frac{\dot{M}}{Mp}. \quad (46)$$

Thus, $\tau_a \equiv |\dot{a}|/a = -2\tau_m$.

These relations indicate that, within ~0.04 AU, the ohmic dissipation within the planet may indeed generate sufficient energy to inflate its radius beyond its Roche lobe. The resulting mass transfer not only reduces the planet's mass but also stalls its orbital migration. The impact of this process on the mass-period distribution of gas giants will be discussed in Paper III.

8. SUMMARY

In this paper we applied a model described by Campbell (in the context of interacting binary stars) to the situation of a planet in a protoplanetary disk interacting with the stellar periodic magnetic field. In § 3 we showed that with a well-determined electrical conductivity profile inside the planet as well as the characteristic parameters of the system (such as the stellar magnetic field strength and angular velocity spin, planet radius and semimajor axis), one can compute the total ohmic dissipation rate $\mathcal{P}(t)$ inside the planet and its average value over one synodic

period. This dissipation rate gives a good estimate of the strength of the Lorentz torque exerted on the planet due to the interaction between the stellar magnetic field and the induced current inside the planet. When the planet is outside corotation, this torque will provide angular momentum to the planet from the star and slow down the planet's migration. In § 4 we computed $\mathcal{P}$ for one specific set of parameters ($R_p = 0.63\ R_J$, $a = 0.04$ AU) and also showed that the conductivity profile (all the other parameters being kept constant) had some influence on the location of maximum dissipation, but fairly little influence on the total dissipate rate $\mathcal{P}$. We noted that this value of $\mathcal{P}$ seemed too low to directly provide an adequate rate of angular momentum transfer to the planet to stop its migration toward the host star. However, this energy input can inflate the planet's envelope and trigger mass loss $\dot{M}$ through Roche lobe overflow. The mass that overflows toward the central star provides angular momentum to the planet (GBL03). In order to estimate this mass-loss rate, we first linked the ohmic dissipation rate to the mass-loss rate (§ 5). Then we used an isothermal-polytropic model to describe the adjustment of the planet's interior to the heat deposited through ohmic dissipation (§ 6). Finally, we computed $\mathcal{P}$ and $\dot{M}$ at equilibrium for several set of parameters (§ 7). A detailed calculation on the orbital evolution of the planet due to this process will be presented in Paper III.

We thank P. Garaud, J. E. Pringle, and F. Rasio for constructive discussions. This work is supported by NASA (NAGS 5-11779, NNG 04G-191G, NNG 06-GH45G, NNX 07-AL13G, HST-AR-11267), JPL (1270927), and NSF (AST 05-07424).

APPENDIX A

PERFECT CONDUCTOR MOVING RELATIVE TO A MAGNETIC FIELD

Let us consider the flux Φ of the magnetic field $\boldsymbol{B}$ across a surface $S(t)$ that changes with time or moves in space. One can show that

$$\frac{d\Phi}{dt} \equiv \frac{1}{dt}\left[\int_a \boldsymbol{B}(\boldsymbol{r}, t+dt)\, d\boldsymbol{S} - \int_b \boldsymbol{B}(\boldsymbol{r}, t)\, d\boldsymbol{S}\right] = \int_a \left[\frac{\partial \boldsymbol{B}}{\partial t} - \nabla \wedge (\boldsymbol{v} \wedge \boldsymbol{B})\right] d\boldsymbol{S}, \tag{A1}$$

with $a = S(t + dt)$ and $b = S(t)$. Therefore, using the MHD induction equation

$$\frac{\partial \boldsymbol{B}}{\partial t} = \nabla \wedge (\boldsymbol{v} \wedge \boldsymbol{B}) - \nabla \wedge \left(\frac{1}{\mu_0 \sigma} \nabla \wedge \boldsymbol{B}\right), \tag{A2}$$

we get

$$\frac{d\Phi}{dt} = -\frac{1}{\sigma}\int_c \boldsymbol{J}(\boldsymbol{r}, t)\, d\boldsymbol{l}, \tag{A3}$$

which tends to zero when the electric conductivity is large (the above integral is a closed integral along a closed curve). Therefore, the magnetic field's flux will be constant if σ is large enough that the second term on the right-hand side is negligible. In such a case, the field lines will move with the body and appear to be "frozen."

APPENDIX B

SET OF LINEAR EQUATIONS

We give below the linear set of equation that we solved for (μ_1^1, μ_1^{-1}, ν_1^1, ν_1^{-1}, α_1, α_2, α_3, α_4), (μ_2^0, ν_2^0, β_1, β_2), and (μ_2^2, μ_2^{-2}, ν_2^2, ν_2^{-2}, γ_1, γ_2, γ_3, γ_4). The values of $G_l(r)$ considered are for $r = R_p$, the radius of the planet. We have

$$\left(\mu_1^1 - \mu_1^{-1}\right)\mathrm{Re}(G_1) + \left(-\nu_1^1 + \nu_1^{-1}\right)\mathrm{Im}(G_1) - \alpha_2 \frac{1}{R_p}\sqrt{\frac{8\pi}{3}} = 0,$$

$$\left(-\nu_1^1 - \nu_1^{-1}\right)\mathrm{Re}(G_1) + \left(-\mu_1^1 - \mu_1^{-1}\right)\mathrm{Im}(G_1) - \alpha_4 \frac{1}{R_p}\sqrt{\frac{8\pi}{3}} = \frac{m \sin\alpha}{8\pi d^3} R_p^2 \sqrt{\frac{8\pi}{3}},$$

$$\left(-\nu_1^1 + \nu_1^{-1}\right)\mathrm{Re}(G_1) + \left(-\mu_1^1 + \mu_1^{-1}\right)\mathrm{Im}(G_1) - \alpha_1 \frac{1}{R_p}\sqrt{\frac{8\pi}{3}} = 2\frac{m \sin\alpha}{8\pi d^3} R_p^2 \sqrt{\frac{8\pi}{3}},$$

$$\left(-\mu_1^1 - \mu_1^{-1}\right)\mathrm{Re}(G_1) + \left(\nu_1^1 + \nu_1^{-1}\right)\mathrm{Im}(G_1) - \alpha_3 \frac{1}{R_p}\sqrt{\frac{8\pi}{3}} = 0,$$

$$\left(\mu_1^1 - \mu_1^{-1}\right)\mathrm{Re}\left(\dot{G}_1\right) + \left(-\nu_1^1 + \nu_1^{-1}\right)\mathrm{Im}\left(\dot{G}_1\right) + \alpha_2 \frac{1}{R_p^2}\sqrt{\frac{8\pi}{3}} = \frac{m \sin\alpha}{8\pi d^3} 2R_p \sqrt{\frac{8\pi}{3}},$$

$$\left(-\nu_1^1 - \nu_1^{-1}\right)\mathrm{Re}\left(\dot{G}_1\right) + \left(-\mu_1^1 - \mu_1^{-1}\right)\mathrm{Im}\left(\dot{G}_1\right) + \alpha_4 \frac{1}{R_p^2}\sqrt{\frac{8\pi}{3}} = 2\frac{m \sin\alpha}{8\pi d^3} 2R_p \sqrt{\frac{8\pi}{3}},$$

$$\left(-\nu_1^1+\nu_1^{-1}\right)\mathrm{Re}\left(\dot{G}_1\right)+\left(-\mu_1^1+\mu_1^{-1}\right)\mathrm{Im}\left(\dot{G}_1\right)+\alpha_1\frac{1}{R_p^2}\sqrt{\frac{8\pi}{3}}=0,$$

$$\left(-\mu_1^1-\mu_1^{-1}\right)\mathrm{Re}\left(\dot{G}_1\right)+\left(\nu_1^1+\nu_1^{-1}\right)\mathrm{Im}\left(\dot{G}_1\right)+\alpha_3\frac{1}{R_p^2}\sqrt{\frac{8\pi}{3}}=0, \tag{B1}$$

$$\left(\mu_2^2+\mu_2^{-2}\right)\mathrm{Re}\left[G_2(R_p)\right]+\left(-\nu_2^2-\nu_2^{-2}\right)\mathrm{Im}\left[G_2(R_p)\right]-\gamma_2\frac{1}{R_p^2}12\sqrt{\frac{2\pi}{15}}=0,$$

$$\left(-\nu_2^2+\nu_2^{-2}\right)\mathrm{Re}\left[G_2(R_p)\right]+\left(-\mu_2^2+\mu_2^{-2}\right)\mathrm{Im}\left[G_2(R_p)\right]-\gamma_4\frac{1}{R_p^2}12\sqrt{\frac{2\pi}{15}}=-\frac{1}{3}\frac{m\sin\alpha}{8\pi d^4}R_p^3 12\sqrt{\frac{2\pi}{15}},$$

$$\left(-\nu_2^2-\nu_2^{-2}\right)\mathrm{Re}\left[G_2(R_p)\right]+\left(-\mu_2^2-\mu_2^{-2}\right)\mathrm{Im}\left[G_2(R_p)\right]-\gamma_1\frac{1}{R_p^2}12\sqrt{\frac{2\pi}{15}}=-\frac{1}{2}\frac{m\sin\alpha}{8\pi d^4}R_p^3 12\sqrt{\frac{2\pi}{15}},$$

$$\left(-\mu_2^2+\mu_2^{-2}\right)\mathrm{Re}\left[G_2(R_p)\right]+\left(\nu_2^2-\nu_2^{-2}\right)\mathrm{Im}\left[G_2(R_p)\right]-\gamma_3\frac{1}{R_p^2}12\sqrt{\frac{2\pi}{15}}=0,$$

$$\left(\mu_2^2+\mu_2^{-2}\right)\mathrm{Re}\left[\dot{G}_2(R_p)\right]+\left(-\nu_2^2-\nu_2^{-2}\right)\mathrm{Im}\left[\dot{G}_2(R_p)\right]+2\gamma_2\frac{1}{R_p^3}12\sqrt{\frac{2\pi}{15}}=0,$$

$$\left(-\nu_2^2+\nu_2^{-2}\right)\mathrm{Re}\left[\dot{G}_2(R_p)\right]+\left(-\mu_2^2+\mu_2^{-2}\right)\mathrm{Im}\left[\dot{G}_2(R_p)\right]+2\gamma_4\frac{1}{R_p^3}12\sqrt{\frac{2\pi}{15}}=-\frac{m\sin\alpha}{8\pi d^4}R_p^2 12\sqrt{\frac{2\pi}{15}},$$

$$\left(-\nu_2^2-\nu_2^{-2}\right)\mathrm{Re}\left[\dot{G}_2(R_p)\right]+\left(-\mu_2^2-\mu_2^{-2}\right)\mathrm{Im}\left[\dot{G}_2(R_p)\right]+2\gamma_1\frac{1}{R_p^3}12\sqrt{\frac{2\pi}{15}}=-\frac{3}{2}\frac{m\sin\alpha}{8\pi d^4}R_p^2 12\sqrt{\frac{2\pi}{15}},$$

$$\left(-\mu_2^2+\mu_2^{-2}\right)\mathrm{Re}\left[\dot{G}_2(R_p)\right]+\left(\nu_2^2-\nu_2^{-2}\right)\mathrm{Im}\left[\dot{G}_2(R_p)\right]+2\gamma_3\frac{1}{R_p^3}12\sqrt{\frac{2\pi}{15}}=0, \tag{B2}$$

$$\mu_2^0\mathrm{Re}\left[G_2(R_p)\right]-\nu_2^0\mathrm{Im}\left[G_2(R_p)\right]-\beta_2\frac{1}{R_P^2}\sqrt{\frac{4\pi}{5}}=0,$$

$$-\nu_2^0\mathrm{Re}\left[G_2(R_p)\right]-\mu_2^0\mathrm{Im}\left[G_2(R_p)\right]-\beta_1\frac{1}{R_P^2}\sqrt{\frac{4\pi}{5}}=\sqrt{\frac{4\pi}{5}}\frac{m\sin\alpha}{8\pi d^4}R_p^3,$$

$$\mu_2^0\mathrm{Re}\left[\dot{G}_2(R_p)\right]-\nu_2^0\mathrm{Im}\left[\dot{G}_2(R_p)\right]+\beta_2\frac{2}{R_P^3}\sqrt{\frac{4\pi}{5}}=0,$$

$$-\nu_2^0\mathrm{Re}\left[\dot{G}_2(R_p)\right]-\mu_2^0\mathrm{Im}\left[\dot{G}_2(R_p)\right]+\beta_1\frac{2}{R_P^3}\sqrt{\frac{4\pi}{5}}=\sqrt{\frac{4\pi}{5}}\frac{m\sin\alpha}{8\pi d^4}3R_p^2. \tag{B3}$$

APPENDIX C

COEFFICIENTS INTERVENING IN THE EXPRESSION OF THE OHMIC DISSIPATION RATE

We have

$$A_{11}(r)\equiv\left(\nu_1^1-\nu_1^{-1}\right)\mathrm{Re}(G_1(r))+\left(\mu_1^1-\mu_1^{-1}\right)\mathrm{Im}(G_1(r)),$$
$$A_{12}(r)\equiv\left(\mu_1^1+\mu_1^{-1}\right)\mathrm{Re}(G_1(r))-\left(\nu_1^1+\nu_1^{-1}\right)\mathrm{Im}(G_1(r)),$$
$$A_{13}(r)\equiv\left(\mu_1^1-\mu_1^{-1}\right)\mathrm{Re}[G_1(r)]-\left(\nu_1^1-\nu_1^{-1}\right)\mathrm{Im}[G_1(r)],$$
$$A_{14}(r)\equiv-\left(\nu_1^1+\nu_1^{-1}\right)\mathrm{Re}[G_1(r)]-\left(\mu_1^1+\mu_1^{-1}\right)\mathrm{Im}[G_1(r)],$$
$$A_{15}(r)\equiv\nu_2^0\mathrm{Re}[G_2(r)]+\mu_2^0\mathrm{Im}[G_2(r)],$$
$$A_{16}(r)\equiv\mu_2^0\mathrm{Re}[G_2(r)]-\nu_2^0\mathrm{Im}[G_2(r)],$$

$$A_{17}(r) \equiv \left(\nu_2^2 + \nu_2^{-2}\right)\mathrm{Re}[G_2(r)] + \left(\mu_2^2 + \mu_2^{-2}\right)\mathrm{Im}[G_2(r)],$$
$$A_{18}(r) \equiv \left(\mu_2^2 - \mu_2^{-2}\right)\mathrm{Re}[G_2(r)] + \left(-\nu_2^2 + \nu_2^{-2}\right)\mathrm{Im}[G_2(r)],$$
$$A_{19}(r) \equiv \left(\mu_2^2 + \mu_2^{-2}\right)\mathrm{Re}[G_2(r)] - \left(\nu_2^2 + \nu_2^{-2}\right)\mathrm{Im}[G_2(r)],$$
$$A_{20}(r) \equiv \left(-\nu_2^2 + \nu_2^{-2}\right)\mathrm{Re}[G_2(r)] - \left(\mu_2^2 - \mu_2^{-2}\right)\mathrm{Im}[G_2(r)]. \quad \text{(C1)}$$

APPENDIX D

CONDUCTIVITY AND RESISTANCE OF SHORT-PERIOD EXTRASOLAR PLANETS

We now calculate the conductivity and resistance (the reciprocal of conductivity) of short-period extrasolar planets. The conductivity of the planet is determined by the density of charged particles. We consider separately the contribution from the collisional ionization within the planet's interior and from the photoionization near its surface.

D1. IONIZATION OF THE PLANET'S INTERIOR

The cores and the inner envelopes of Jovian planets are mostly ionized. They are shielded by cool, mostly neutral gaseous envelopes, where the ionization is dominated by elements with low ionization potentials, such as sodium and potassium.

The planetary model used in our calculation of the ionization fraction is model A3 presented by Bodenheimer et al. (2001). It is a spherically symmetric model for the short-period planet around HD 209458. The following parameters are assumed: the planetary mass is 0.63 Jupiter masses (M_J); the equilibrium temperature at the surface of the planet due to irradiation from the star is $T_s = 1360$ K; there is a solid core with a density $\rho_c = 5.5 \times 10^3$ kg m^{-3} and a mass 0.139 M_J (=44 $M_\oplus = 0.22 M_p$) in the center. An energy source, uniformly distributed through the gaseous part of the planet, with an energy input rate $\dot{E}_d = 8.5 \times 10^{19}$ J s^{-1}, is also imposed to take into account the effect of tidal dissipation of energy. Those model parameters result in an asymptotic radius of 1.41 R_J at $t = 4.5$ Gyr, which is consistent with the photometric occultation observations of HD 209458 (Henry et al. 2000; Charbonneau et al. 2000)

The cores and the inner envelopes of Jovian planets are mostly ionized by the pressure ionization effect, where the Saha equation breaks down. We have to resort to various equation of state tables, including the equation of state tables for hydrogen and helium by Saumon et al. (1995). These tables are calculated using the free-energy minimization methods, with a careful study of the nonideal interactions. They cover temperatures in the range $2.10 < \log T(\mathrm{K}) < 7.06$ and pressure in the range $5 < \log P(\mathrm{N\ m^{-2}}) < 20$. The calculations on which these tables were constructed also include the treatments of partial dissociation and ionization caused by both pressure and temperature effects. Given the internal structure data of ρ, T, and P for model A3, we use those equation of state tables to calculate the electron number density distribution for the inner part of the planet. In this approximation, we bear in mind that the ionization fractions calculated from the free-energy minimization are of limited accuracy. Moreover, in the interpolation regions of both the H and He equations of state, the data have very little physical basis but are reasonably well behaved by construction.

In the envelope, hydrogen and helium are mostly neutral, and free electrons are exclusively provided by thermal ionization of elements with low ionization potentials. Among them, potassium and sodium have the highest concentrations with a relative abundance $\log(N_\mathrm{K}/N_\mathrm{H}) \simeq -6.88$ and $\log(N_\mathrm{Na}/N_\mathrm{H}) \simeq -5.67$ for the solar composition. The lowest ionization potentials for these two elements are $\chi_\mathrm{K} = 4.339$ eV and $\chi_\mathrm{Na} = 5.138$ eV. We identify these two elements to be the sources of most of the free electrons in the planetary envelope.

We solve the Saha equations for ionization of Na and K jointly (see Allen 1955),

$$\frac{N_\mathrm{Na}^1}{N_\mathrm{Na}^0} 10^6 N_e = -\chi_\mathrm{Na}\Theta - \frac{3}{2}\log\Theta + 20.9388, \quad \text{(D1)}$$

$$\frac{N_\mathrm{K}^1}{N_\mathrm{K}^0} 10^6 N_e = -\chi_\mathrm{K}\Theta - \frac{3}{2}\log\Theta + 20.9388, \quad \text{(D2)}$$

where $\Theta = (5040\ \mathrm{K})/T$, N_Na^1 and N_Na^0 are, respectively, the singly ionized and neutral number density of sodium (SI units), N_K^1 and N_K^0 are, respectively, the singly ionized and neutral number density of potassium, and N_e is the electron density.

D2. CONDUCTIVITY AND RESISTIVITY

Using the electron number density profile, we then calculate the conductivity using the formulae given by Fejer (1965). Three kinds of conductivity are of interest here. The conductivity σ_0, which determines the current parallel to the magnetic lines of force and which would exist for all directions in the absence of the magnetic field, is given by

$$\sigma_0 = \frac{N_e e}{B}\left(\frac{\omega_i}{\nu_i} - \frac{\omega_e}{\nu_e}\right) \cong \frac{N_e e^2}{m_e \nu_e}, \quad \text{(D3)}$$

where e is the electron charge, $\omega_e = -eB/m_e$ and $\omega_i = eB/m_i$ are the gyrofrequencies of electrons and ions, respectively, while ν_e and ν_i are the collisional frequencies associated with the momentum transfer of electrons and ions.

The Pedersen conductivity, which determines the current parallel to the electric field, is given by

$$\sigma_p = \frac{N_e e}{B}\left(\frac{\nu_i\omega_i}{\nu_i^2+\omega_i^2} - \frac{\nu_e\omega_e}{\nu_e^2+\omega_e^2}\right) \cong \frac{\sigma_0}{1+(\omega_e/\nu_e)^2}. \tag{D4}$$

The Hall conductivity, which determines the current perpendicular to both the electric and magnetic fields, is given by

$$\sigma_{\rm H} = \frac{N_e e}{B}\left(\frac{\omega_e^2}{\nu_e^2+\omega_e^2} - \frac{\omega_i^2}{\nu_i^2+\omega_i^2}\right) \cong \frac{\sigma_0(\omega_e/\nu_e)}{1+(\omega_e/\nu_e)^2}. \tag{D5}$$

In the limit of low ionization fraction, ν_e is closely related to the mean collisional frequencies of the electrons with molecules of the neutral gas such that (see Draine et al. 1983)

$$\nu_e^{(1)} = N_n\langle\sigma v\rangle_{e\text{-}n} \simeq N_n 10^{-19}\left(\frac{128kT}{9\pi m_e}\right)^{1/2}, \tag{D6}$$

where N_n is the number density of neutral particles and $\langle\sigma v\rangle_{e\text{-}n}$ is the average product of collisional cross section and the relative speed between electrons and neutral particles. In the other limit of a completely ionized gas, we take into account both electron-ion and electron-electron encounters. The collisional frequency of the electrons is given by (see Sturrock 1994)

$$\nu_e^{(2)} \simeq 10^{8.0} N_e T^{-3/2}. \tag{D7}$$

In the intermediate range, we use $\nu_e = \max(\nu_e^{(1)}, \nu_e^{(2)})$.

The resistance of the planet cannot be specified exactly because an unknown shape factor is involved. Following Dermott (1970), we use the following expression for the resistance,

$$R_p = \frac{f_R}{r_p^2}\int_0^{r_p}\frac{dr}{\sigma_p(r)}, \tag{D8}$$

where f_R is a parameter of order unity for the geometry. In the aligned geometry we consider here, the planet's resistance comes from Pedersen resistivity (conductivity). The core of the planet is assumed to be a perfect conductor. From equation (D8), we can see that it is the cold, mostly neutral envelope that gives rise to most of the resistance.

REFERENCES

Allen, C. W. 1955, Astrophysical Quantities (London: Univ. London Press)
Bodenheimer, P., Lin, D. N. C., & Mardling, R. A. 2001, ApJ, 548, 466 (BLM01)
Burkert, A., Lin, D. N. C., Bodenheimer, P. H., Jones, C. A., & Yorke, H. W. 2005, ApJ, 618, 512
Campbell, C. G. 1983, MNRAS, 205, 1031 (C83)
———. 2005, MNRAS, 359, 835
Charbonneau, D., Brown, T. M., Latham, D. W., & Mayor, M. 2000, ApJ, 529, L45
Clarke, J. T., et al 1996, Science, 274, 404
Cowling, T. G. 1981, ARA&A, 19, 115
Dall'Osso, S., Israel, G. L., & Stella, L. 2006, A&A, 447, 785
de Pater, I., & Lissauer, J. 2001, Planetary Sciences (Cambridge: Cambridge Univ. Press)
Dermott, S. F. 1970, MNRAS, 149, 35
Dobbs-Dixon, I., & Lin, D. N. C. 2008, ApJ, 673, 513
Draine, B. T., Roberge, W. G., & Dalgarno, A. 1983, ApJ, 264, 485
Drell, S. D., et al. 1965, J. Geophys. Res., 70, 3131
Duncan, R. A. 1966, Planet. Space Sci., 14, 173
Fejer, J. A. 1965, J. Geophys. Res., 70, 4972
Goldreich, P., & Lynden-Bell, D. 1969, ApJ, 156, 59
Goldreich, P., & Tremaine, S. 1978, ApJ, 222, 850
———. 1980, ApJ, 241, 425
Gu, P.-G., Bodenheimer, P., & Lin, D. N. C. 2003, ApJ, 588, 509 (GBL03)
———. 2004, ApJ, 608, 1076
Gurnett, D. A. 1972, ApJ, 175, 525
Hayashi, C., Nakazawa, K., & Nakagawa, Y. 1985, in Protostars and Planets II, ed. D. C. Black & M. S. Matthews (Tucson: Univ. Arizona Press), 1100
Henry, G. W., Marcy, G. W., Butler, R. P., & Vogt, S. S. 2000, ApJ, 529, L41
Iaroslavitz, E., & Podolak, M. 2007, Icarus, 187, 600
Ida, S., & Lin, D. N. C. 2004, ApJ, 604, 388
Johns-Krull, C. M. 2007, ApJ, 664, 975
Joss, P. C., Rappaport, S. A., & Katz, J. I. 1979, ApJ, 230, 176
Kippenhahn, R., & Weigert, A. 1994, Stellar Structure and Evolution (Berlin: Springer)
Konigl, A. 1991, ApJ, 370, L39
Li, J., Ferrario, L., & Wickramashinghe, D. 1998, ApJ, 503, L151
Lin, D. N. C., Bodenheimer, P., & Richardson, D. C. 1996, Nature, 380, 606
Lin, D. N. C., & Papaloizou, J. C. B. 1980, MNRAS, 191, 37
———. 1986a, ApJ, 307, 395
———. 1986b, ApJ, 309, 846
———. 1993, in Protostars and Planets III, ed. E. H. Levy & J. I. Lunine (Tucson: Univ. Arizona Press), 749
Marcy, G. W., Cochran, W. D., & Mayor, M. 2000, in Protostars and Planets IV, ed. V. Mannings, A. P. Boss, & S. S. Russell (Tucson: Univ. Arizona Press), 1285
Mayor, M., & Queloz, D. 1995, Nature, 378, 355
Neubauer, F. M. 1980, J. Geophys. Res., 85, 1171
Ogilvie, G. I., & Lin, D. N. C. 2004, ApJ, 610, 477
———. 2007, ApJ, 661, 1180
Piddington, J. H. 1977, Moon, 17, 373
Piddington, J. H., & Drake, J. F. 1968, Nature, 217, 935
Pollack, J. B., Hubickyj, O., Bodenheimer, P., Lissauer, J. J., Podolak, M., & Greenzweig, Y. 1996, Icarus, 124, 62
Saumon, D., Chabrier, G., & Van Horn, H. M. 1995, ApJS, 99, 713
Setiawan, J., Henning, T., Launhardt, R., Muller, A., Weise, P., & Kurster, M. 2008, Nature, 451, 38
Shawhan, S. D. 1976, J. Geophys. Res., 81, 3373
Shu, F., Najita, J., Ostriker, E., Wilkin, F., Ruden, S., & Lizano, S. 1994, ApJ, 429, 781
Stassum, K. G., Mathieu, R. D., Vrba, F. J., Mazeh, T., & Henden, A. 2001, AJ, 121, 1003
Sturrock, P. A. 1994, Plasma Physics (Cambridge: Cambridge Univ. Press)
Ward, W. R. 1997, ApJ, 482, L211
Warner, B. 1995, Cataclysmic Variable Stars (Cambridge: Cambridge Univ. Press)
Willes, A. J., & Wu, K. 2005, A&A, 432, 1091
Wu, K., Cropper, M., Ramsay, G., & Sekiguchi, K. 2002, MNRAS, 331, 221
Zhou, J. L., & Lin, D. N. C. 2007, ApJ, 666, 447

The Astrophysical Journal, 745:2 (18pp), 2012 January 20 doi:10.1088/0004-637X/745/1/2

INTERACTION OF CLOSE-IN PLANETS WITH THE MAGNETOSPHERE OF THEIR HOST STARS. II. SUPER-EARTHS AS UNIPOLAR INDUCTORS AND THEIR ORBITAL EVOLUTION

Randy O. Laine[1,2] and Douglas N. C. Lin[3,4]
[1] Ecole Normale Superieure, Paris, France; laine@ens.fr, randy.laine@normalesup.org
[2] LPC2E, Universite d'Orleans/CNRS, Orleans, France
[3] Department of Astronomy and Astrophysics University of California, Santa Cruz, CA 95064, USA; lin@ucolick.org
[4] Kavli Institute of Astronomy & Astrophysics, Peking University, Beijing, China
Received 2010 October 12; accepted 2011 August 8; published 2011 December 27

ABSTRACT

Planets with several Earth masses and orbital periods of a few days have been discovered through radial velocity and transit surveys. Regardless of their formation mechanism, an important evolution issue is the efficiency of their retention in the proximity of their host stars. If these "super-Earths" attained their present-day orbits during or shortly after the T Tauri phase of their host stars, a large fraction of these planets would have encountered an intense stellar magnetic field. These rocky planets have a higher conductivity than the atmosphere of their host stars and, therefore, the magnetic flux tube connecting them would slip though the envelope of the host stars faster than across the planets. The induced electromotive force across the planet's diameter leads to a potential drop which propagates along a flux tube away from the planet with an Alfvén speed. The foot of the flux tube would sweep across the stellar surface and the potential drop across the field lines drives a DC current analogous to that proposed for the electrodynamics of the Io–Jupiter system. The ohmic dissipation of this current produces potentially observable hot spots in the star envelope. It also heats the planet and leads to a torque which drives the planet's orbit to evolve toward both circularization and a state of synchronization with the spin of the star. The net effect is the damping of the planet's orbital eccentricity. Around slowly (or rapidly) spinning stars, this process also causes rocky planets with periods less than a few days to undergo orbital decay (or expansion/stagnation) within a few Myr. In principle, this effect can determine the retention efficiency of short-period hot Earths. We also estimate the ohmic dissipation interior to these planets and show that it can lead to severe structure evolution and potential loss of volatile material in them. However, these effects may be significantly weakened by the reconnection of the induced field.

Key words: magnetohydrodynamics (MHD) – planetary systems – planets and satellites: dynamical evolution and stability – planets and satellites: formation – planet–star interactions – stars: magnetic field

Online-only material: color figures

1. INTRODUCTION

An important milestone in planetary astronomy is the discovery of a Jupiter-mass planet, 51 Peg b (Mayor & Queloz 1995). Its extraordinary four-day orbital period rekindled a theoretical expectation that protoplanets may undergo orbital decay (Goldreich & Tremaine 1980; Lin & Papaloizou 1986) as a consequence of their tidal interaction with their natal disks. Today, more than 500 planets have been discovered around nearby stars. Among them, there is a pile up of ∼100 planets with periods (P) less than a week and masses (M_p) two orders of magnitude larger than that of the Earth ($M_\oplus$). Transit observations of some of these planets indicate that they have a radius and density comparable to that of Jupiter and Saturn and are commonly referred to as hot Jupiters.

These hot Jupiters, including 51 Peg b, were formed presumably at some preferred locations (beyond the snow line) of their natal disks (Ida & Lin 2008, 2010). After acquiring sufficient masses to open gaps in their natal disk, they undergo type II migration along with the viscous diffusion of their surrounding gas. In order to account for their survival, we proposed that the migration of 51 Peg b and other short-period gas giant planets may have stalled when they entered into the magnetospheric cavity of their host star during their infancy (Lin et al. 1996). Since protostellar disks are expected to be truncated within the magnetosphere of their central stars (see below), once any protoplanet enters into this region, its migration would slow to a halt as the intensity of its tidal interaction with its nascent disk weakens.

The existence of the magnetosphere around T Tauri stars was proposed (Konigl 1991) to account for the observed period distribution which peaks around eight days (Bouvier et al. 1993). If efficient angular momentum flow between protostellar disks and the magnetosphere of their central stars can enforce corotation at their interface where the magnetic and viscous torques are balanced (Shu et al. 1994), we would infer kilogauss fields. Today, Zeeman splitting of emission lines have been directly measured for many T Tauri stars and these observations confirm the presence of kilogauss fields on their surface (Johns-Krull 2007). If this field strength represents that of a dipole stellar field, the magnetospheric radius for T Tauri stars with accretion rates in the range of 10^{-8} to $10^{-7}\ M_\odot\ \mathrm{yr}^{-1}$ would extend to regions beyond the orbits of their close-in planets. The radius of this magnetospheric cavity expands during the depletion of the disk gas and the decline of the accretion flux through the disk.

Although the magnetospheric-cavity scenario provides a useful qualitative model for the abundant population of short-period planets, a detailed reconstruction of the observed period distribution requires a quantitative determination of short-period planets' retention efficiency. After they have entered the magnetospheric cavity of their host stars or after they have been engulfed by the magnetospheric cavity, protoplanets continue to interact with the stellar magnetic field. It is not clear whether

this process can induce planets to undergo further orbital interaction.

In order to understand the nature of this physical mechanism, we carry out a series of investigations. In Paper I (Laine et al. 2008), we provided a general description of the relevant physical effects. We first consider the retention of short-period gas giant planets inside the stellar magnetosphere. We decompose the stellar magnetic field into a steady and a periodically modulating component and the planet into a day and night side. In this previous investigation, we considered the periodically modulating component of the field, which can be due to either the planet's eccentric orbit or the star's non-synchronous (with respect to the planet's orbital angular frequency) and non-aligned (with respect to the star's magnetic poles) spin. On the night side of the planet where the magnetic diffusivity is relatively high, this time-dependent field can permeate into the planet's envelope and induce an AC current. The ohmic dissipation of this current not only heats the planet but also provides a torque which drives the planet's orbit toward a state of circularization and synchronization with the star's spin. We also found that close to the host star where the stellar magnetosphere is intense, ohmic dissipation can cause a planet's interior to heat up such that it expands and overflows its Roche lobe. The gas flow from the planet to its host star via the inner Lagrangian point also transfers angular momentum to the orbit of the planet (Gu et al. 2003). This process can halt the migration of the planet despite its loss of angular momentum as a consequence of its tidal interaction with the disk and the host star and the direct torque applied by the stellar magnetosphere on it. The results of this analysis will be presented elsewhere.

Another class of planets have been discovered with $M_p \sim$ a few $M_\oplus$ and P in the range of a few days to two months. In contrast to their Jupiter-mass siblings, these planets probably have rocky or icy internal structures and are commonly referred to as super-Earths (Mayor et al. 2008; Howard et al. 2010). Recently Kepler mission led to the discovery of over 1200 planetary candidates. Since they all have radii more than twice that of the Earth, they may also be super-Earths, albeit their masses are yet to be determined. These super-Earths too are probably formed at locations ranging from a fraction to several AUs from their host stars (Ida & Lin 2008, 2010). In contrast to the gas giants, super-Earths may not have adequate mass to open a gap and undergo type II migration. Nevertheless, they do tidally interact with their natal disk and undergo type I migration, due to an imbalance between the torque they exert on the disk at the Lindblad and corotation resonances both interior and exterior to their orbits (Tanaka et al. 2002).

In most regions of the disk, type I migration is directed inward. However, due to the corotation torque, there are migration barriers where the orbital decay of isolated super-Earths may be halted (Masset et al 2006; Paardekooper et al. 2010). These barriers occur at gas surface density (Σ_g) maximum near the snow line ($a_{\rm ice}$ where water vapor condensate), at the inner edge of a dead zone ($a_{\rm dead}$ where the ionization fraction near the midplane is too small to maintain coupling between turbulent magnetic field and disk gas), and just outside the magnetospheric cavity, $a_{\rm mag}$ (Kretke & Lin 2007; Kretke et al. 2009).

Since Σ_g and the midplane temperature of the disk decline with time, the location of these barriers also evolves with them. During the advanced stages of disk evolution, Σ_g may be sufficiently small that the dead zone essentially vanishes and the stalled embryos near $a_{\rm ice}$ and $a_{\rm dead}$ resume their migration. Assuming the field strength decreases slowly or remains unchanged, the location of $a_{\rm mag}$ also expands beyond the orbital semimajor axis of the super-Earths, $a_{\rm SE}$, during the transition from classical to weak-line T Tauri phases on a timescale of $\sim$10 Myr (Kretke & Lin 2010). After the disk depletion, the stellar magnetic field and spin rate decrease (Skumanich 1972) on a timescale $\sim$100 Myr (Soderblom et al. 1993). During these evolutionary stages, the location ($a_{\rm corote}$) where the frequency of the Keplerian motion matches that of the stellar spin also evolves relative to $a_{\rm SE}$. Thus, we anticipate that some super-Earths are located interior to the corotation radius while others are located beyond it.

In this paper, we consider the interaction between close-in super-Earths with the steady component of their host stars' magnetic field. Besides differences between their masses and radii, rocky planets have much larger electric conductivity on their surface than the envelope and atmosphere on the night side of close-in young gas giant planets. The day side of gas giant planets is exposed to the stellar ionizing photons and may have much higher ionization fraction and electrical conductivities than their night side. We will consider this more complex aspect of the hot Jupiter problem elsewhere.

The super-Earth problem we are considering here is analogous to the *Echo* satellite (in the form of a conductor) moving relative to background (Earth) field line, which was analyzed by Drell et al. (1965). In general, an electric field is induced across the conductor (in directions orthogonal to the field and motion). However, the electric field must vanish (in its frame) inside a perfect conductor (with an infinite conductivity). On its surface, the electric field generates a current which leads to an induced magnetic field. The induced field cancels the unperturbed field inside the conductor so that there is no relative motion between the perfect conductor and the net (unperturbed plus induced) field inside it. Outside the moving conductor, the net field appears to wrap around it. At large distances from the moving conductor, the induced field propagates away from it with the Alfvén speed.

In a slightly different context, Goldreich & Lynden-Bell (1969) analyzed the electrodynamic interaction between Io and Jupiter. They treated Io as a conductor moving in Jupiter's magnetosphere. Because Io's conductivity is larger than that of Jupiter, it drags a flux tube of field lines. They showed that an electromagnetic field is induced across Io's surface. Provided that the conductivity is high along and low across the field lines, the electric potential drop across them would propagate and be maintained along the field lines connecting Io and Jupiter with an Alfvén speed. At the foot of the flux tube where it enters into Jupiter's atmosphere and envelope, conductivity across the field lines increases with the density of the surrounding gas such that the potential drop drives a DC current across the potential drop. Provided that the induced field can propagate back to Io before the unperturbed field slips through it, the current forms a close circuit. In this scenario, Io acts as a unipolar inductor.

In this paper, we apply Goldreich & Lynden-Bell's model to the study of a super-Earth moving in its host star's magnetosphere. For computational simplicity, we neglect the planet's intrinsic magnetic field, as we have done in the previous paper. In the problem we are considering, a steady component of the stellar magnetic field is present regardless of the differential motion between the star's spin and the planet's orbit. In an asynchronous system, a flux tube of magnetic field between the planet and the star cannot be infinitely anchored on both entities. If the planet's conductivity is smaller than that on the surface of the host star, the flux tube would tend to be anchored on the

surface of the star along with all other unperturbed field lines and it would slip through the planet.

In Section 2, we introduce a qualitative discussion and schematic illustration to show in the limit that the electric conductivity in the super-Earth planet is higher (but not by an infinite amount) than that of its host star's envelope; the relative motion between the planet and the stellar magnetic field leads to an induced electromotive force (emf) and a potential drop across the planet. Outside the planet, a flux tube of (unperturbed plus induced) magnetic fields would appear to be approximately anchored on the planet. In the tenuous regions between the planet and its host star, the conductivity along the field lines is much higher than that across them and the electric current flows freely to maintain constant electric potential along them. In the absence of field reconnection, Alfvén waves propagate to infinity on open lines and the electric current flows to the surface of the host stars along closed field lines. Due to the finite resistance of the surrounding (stellar) gas, the foot of the flux tube on the surface of the host star slips through the stellar atmosphere and the electrical potential drop across the foot of the flux tube drives an electric current with an associated rate of ohmic dissipation.

Based on the above qualitative scenario, we construct a quantitative model in this paper. In Section 3, we introduce the values of the different parameters we use in the numerical applications and derive the analytical expressions for the induced electric field, intensity, ohmic dissipation, and torque. In our numerical applications, we adopt a set of fiducial physical parameters for a rocky super-Earth planet with two Earth radii, $2R_\oplus \approx 1.4 \times 10^7$ m on a three-day circular orbit ($a \approx 6 \times 10^9$ m around a T Tauri star with a mass equal to that of the Sun ($1\,M_\odot \approx 2 \times 10^{30}$ kg) and a radius twice that of the Sun $R_* = 2\,R_\odot \approx 1.4 \times 10^9$ m. We also assume that it has a solar luminosity ($1\,L_\odot$), a surface temperature of $T_* = 4 \times 10^3$ K, and a dipole field with a strength 0.2 T (i.e., 2×10^3 G) on the stellar surface (which corresponds to a magnetic dipole strength of 5.4×10^{33} Am^2).

With these parameters, we first analyze two limiting cases of rapid and slow stellar spin. We discuss the condition of validity of the model in Section 4 and derive in Section 5 the expressions and values of the resistances and Alfvén speed. We will consider more general sets of model parameters elsewhere. In Section 6, we calculate the values of the induced intensity, ohmic dissipation, and torque, and discuss the relevance of these values. In the context of planetary migration in the presence of their natal disk, we show that if the planet orbits around the host star outside its corotation radius (i.e., the Keplerian frequency of the planet's orbit is smaller than the stellar spin frequency), the net torque associated with this induced current would provide an adequate rate of angular momentum transfer to balance against the rate of tidally induced angular momentum loss by the rocky planet to the disk. In the limit that the planet is inside its host star's corotation radius, the planet's orbit would continue to decay. Finally, we summarize our results and discuss their implications in Section 7.

2. QUALITATIVE ILLUSTRATION AND DESCRIPTION OF THE PHENOMENA AND BRIEF OUTLINE OF THE CALCULATION

We consider a rocky planet with a mass of several $M_\oplus$ moving in the dipole magnetic field of the star it is orbiting. The relative motion of such a conductor in an external stellar magnetic field generates an induced emf across the planet. There are two complementary effects (see Paper I) described by the complete magnetohydrodynamic (MHD) equation: the diffusion of the magnetic field in the planet and the magnetic induction (with its associated drag).

The MHD equation describing the electrodynamics of the planet in the stellar field can be written as

$$\frac{\partial \mathbf{B}}{\partial t} = \nabla \wedge (\upsilon \wedge \mathbf{B}) - \nabla \wedge (\eta \nabla \wedge \mathbf{B}), \quad (1)$$

where η is the magnetic diffusivity (which is equal to $(\mu_0 \sigma)^{-1}$ where σ is the electric conductivity).

In Paper I, we focused on the diffusion of the stellar magnetic field inside a hot Jupiter. In order to do so, we considered the periodic component of the stellar magnetic field felt by a planet when the axis of the stellar magnetic moment is not aligned with the planetary orbital axis, or when the planet is on an eccentric orbit. The drag of the magnetic field by the planet due to induction can be neglected if the planet's orbit corotates with the star's spin or if the electrical conductivity of the planet is low compared with that of the outer layers of the star (which is the case at least in the night side of a hot Jupiter).

In this limit, the diffusion of the stellar magnetic field inside the planet is modulated by the electric conductivity (inversely proportional to the magnetic diffusivity) profile in the planet. A somewhat higher electric conductivity in the planet would tend to decrease the penetration depth of the stellar magnetic field and the volume where the electric current induced by the field can be dissipated, but it would also increase the volumic ohmic (power) dissipation rate. Likewise, a lower conductivity in the planet would enable the stellar magnetic field to penetrate deeper into it, albeit the induced current also encounters a lower volumic ohmic dissipation rate. Consequently, we found that the total ohmic dissipation rate over the entire planet does not change significantly over a reasonable range of electric conductivity for a hot Jupiter (neglecting the effect of photoionization in its atmosphere).

In the present paper, we describe the induction (and associated "drag" of the field lines) which was neglected in Paper I. For simplicity, we neglect the damping of the magnetic field in the planet associated with the diffusion term and focus on the case where the planet is able to significantly drag the stellar magnetic field lines which are enclosed in the flux tube that passes through the planet.

Throughout this paper, this "flux tube which passes through the planet" is simply referred to as "the flux tube" (we are interested in the part that extends between the interior of the planet and above the surface of the star). The "foot of the flux tube" refers to that part of the flux tube which extends below the surface of the star for a distance $D_{\rm pn}$ (the subscript "pn" refers to penetration) to be estimated below.

Between the planet and the surface of the star, the volumic current flows along the flux tube (parallel to the magnetic field lines—the electrons in fact gyrate around the magnetic field lines), but the volumic current crosses the flux tube in the planet and at the foot of the flux tube (perpendicular to the magnetic field lines in the stellar atmosphere). Figures 1 and 2 present the general overview of the system.

In this model, we make a distinction between the regular (unperturbed) stellar dipole magnetic field (magnetosphere), which corotates with the stellar spin, and the field lines that define the flux tube (composed of both the stellar field in the planet and the induced flux tube), which appear to be dragged along with the planet and thus move relative to the rest of the

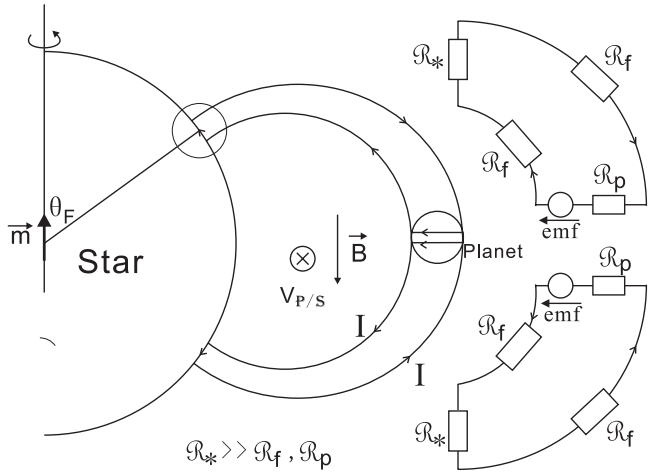

Figure 1. Schematic illustration of the planet–magnetosphere interaction system. The circuit diagram idealizes the basic physics, which is described in the text. In this context, a planet with a non-negligible motion (into the plane of the diagram) relative to the stellar magnetosphere induces an emf. At the location of the planet, the direction of the unperturbed stellar dipole field is pointing downward. The potential difference across the flux tube generates a current with a flux, which is primarily determined by the electrical resistivity in the atmosphere of the host star. Arrows indicate the flow direction of the current.

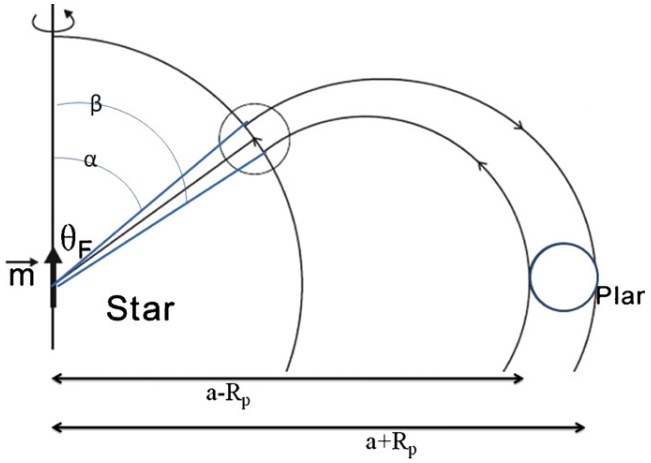

Figure 2. Main parameters in the calculation of y_1 and y_2, which defines the geometry of the foot of the flux tube.

(A color version of this figure is available in the online journal.)

stellar magnetosphere. This drag is significant when the electric conductivity of the planet is large compared to that of the outer layers of the star (Piddington & Drake 1968).

A large conductivity in the planet's interior would lead to a large surface current which induces a field and cancels the external (unperturbed stellar dipole) field. With small magnetic diffusivity, the planet's interior would appear to be shielded from any time-dependent external magnetic field. We therefore consider only the time-independent component of the stellar magnetic field. In this model, the time-independent component of the stellar magnetic field permeates the planet. The motion of the planet relative to the stellar magnetosphere induces an electric field $\mathcal{E}$, an induced volumic electric current $\mathcal{J}$, and an induced difference of potential U across the planet's diameter. In Figure 3, we provide a schematic illustration on the field lines and current inside the planet.

For the flux tube between the planet and its host star, we adopt the assumption of high electric conductivity along the magnetic field lines and low conductivity across them, which was introduced by Goldreich & Lynden-Bell (1969) for the system Io–Jupiter. In this case, the difference of electric potential (induced by the planet's relative motion with respect to the magnetic field of its host star) drives an electrical current out of the planet, along the flux tube, across its foot on the atmosphere of the star, and back to the planet along its other half (Figure 1).

In the limit of negligible electrical conductivity in the direction normal to the flux tube, the electric current can only cross the field lines in the planet or in the atmosphere of the host star. The assumption of high electric conductivity along the magnetic field lines also implies (1) that the difference of potential U across the planet's diameter is transmitted along the flux tube without significant drop in potential and (2) that the plasma enclosed in the flux tube is dragged along by the motion of the magnetic field lines. An electric circuit is therefore created, where the flux tube acts as electric wires, the planet as a unipolar inductor with internal resistance $\mathcal{R}_p$, and the foot of the flux tube as the largest resistance.

We see that there are in fact two circuits (see Figure 1). The first one is composed of the foot of the flux tube on the northern hemisphere of the star, its corresponding flux tube, and the northern hemisphere of the planet. The second is equivalent and symmetric to the first one (the plane of symmetry being the plane of the planetary disk). Except when explicitly stated, the calculations (current, resistances, ohmic dissipation, torques, etc.) describe only one circuit (the northern one).

In an electric circuit composed of a generator (with an emf $\int \mathcal{E} dl$ and resistance $\mathcal{R}_g$ over a length scale l) and other resistances along the circuit $\mathcal{R}$ (here primarily the resistance of the foot of the flux tube), the intensity of the current I is determined by $\int \mathcal{E} dl - \mathcal{R}_g I \approx \int \mathcal{E} dl = U = \mathcal{R} I$. With the parameters we have adopted here, we show in Section 5 that the resistance along the flux tube $\mathcal{R}_{\rm tube}$ and the resistance across the planet $\mathcal{R}_{\rm p}$ are small compared to that across the foot of the flux tube on the star $\mathcal{R}_*$. In this limit, (1) the potential drop across the planet with a radius R_p is $U \sim 2\mathcal{E} R_p$, (2) the magnitude U is approximately constant along each field lines in the flux tube between the planet and its host star because the resistance of the tube $\mathcal{R}_{\rm tube}$ and the induction are negligible, and (3) the total current is determined by the largest resistance along the circuit, i.e., that at the foot of the flux tube in the stellar atmosphere.

3. DESCRIPTION OF THE MODEL: VALUES OF THE PARAMETERS, GEOMETRY, ANALYTICAL EXPRESSIONS, AND EQUATION OF EVOLUTION OF THE PLANET'S ORBIT

3.1. Values of the Parameters for a Fiducial Model

Except when explicitly stated otherwise, we consider a system composed of a super-Earth closely orbiting a young T Tauri star with a time-independent magnetic dipole. We assume that the magnetosphere corotates with the star, and adopt the following numerical values (SI units) for the parameters intervening in the model:

For the star we adopt the following model parameters.

1. Temperature of the isothermal outer layer: $T_* = 4000$ K;
2. radius: $R_\star \approx 2\, R_\odot \approx 1.4 \times 10^9$ m;
3. mass: $M_\star \simeq M_\odot \simeq 2 \times 10^{30}$ kg;
4. opacity at the photosphere: $\kappa \simeq 3$ m^2 kg^{-1} (which is equivalent to taking a surface pressure of about 15 Pa);
5. magnetic dipole strength: $m = 5.4 \times 10^{33}$ Am^2, which corresponds to a magnetic field of 0.2 T (Tesla) $\equiv 2 \times 10^3$ G (Gauss) at the stellar surface (Yang et al. 2008); and

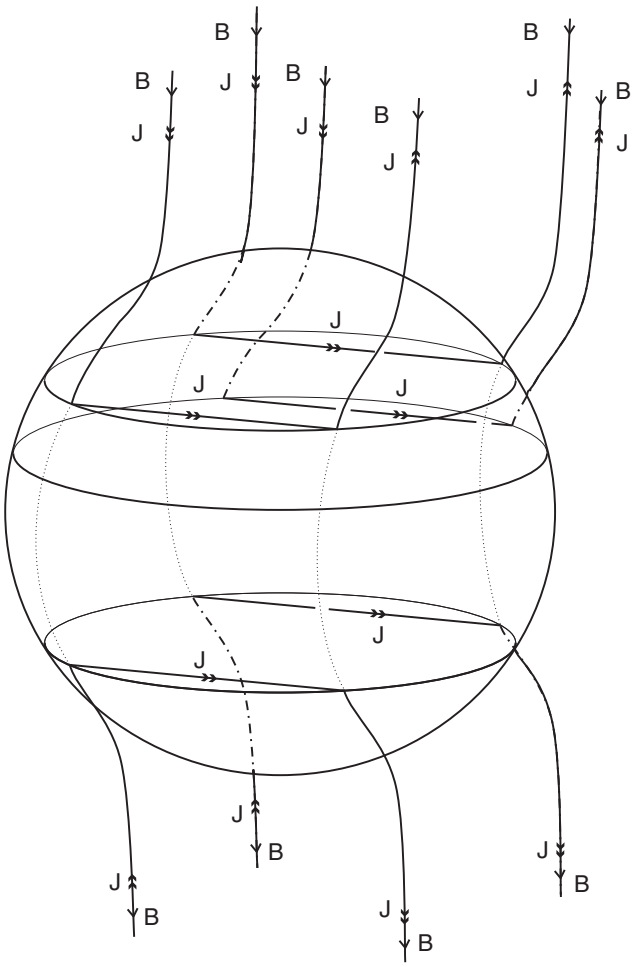

Figure 3. External and induced field around a planet moving relative to the magnetosphere of its host star. The planet is moving out of the plane and toward the lower left side of the illustration. Arrows in this idealized cartoon illustrate the direction of current flow across the potential drop due to the induced emf. The current also lead to an induced field which distorts the field near the planet. Information on the induced emf propagates along the field lines in the direction of the host star.

6. spin period: 8 days (slow-rotator) or 0.8 days (fast-rotator).

We will consider more general stellar models elsewhere. For a super-Earth, we consider the following case.

1. Radius: $R_p \simeq 2\,R_\oplus \simeq 1.4 \times 10^7$ m; and
2. semimajor axis: $a \simeq 0.04\,\mathrm{AU} \simeq 6 \times 10^9$ m (which corresponds to a period of 3 days).

In the electrodynamics of super-Earths, the magnitude of M_p does not enter explicitly (it does implicitly through the radius) the calculation of the torque, albeit their orbital evolution timescale does depend on it (for example, see Equation (16). The linear speed in a frame corotating with the star ($\upsilon_{p/s} = (\omega_p - \omega_*)a$) of such a planet orbiting a star rotating slowly is 9×10^4 m s^{-1} and 4×10^5 m s^{-1} around a star rotating fast (these are the absolute values).

3.2. Length and Width of the Foot of the Flux Tube in a Spherical Approximation

As defined above, the "flux tube" refers to the flux tube composed of the field lines of the magnetosphere that pass through and are dragged along by the planet. This flux tube connects the planet and the surface of the star and its foot penetrates into the star to a depth which will be determined later.

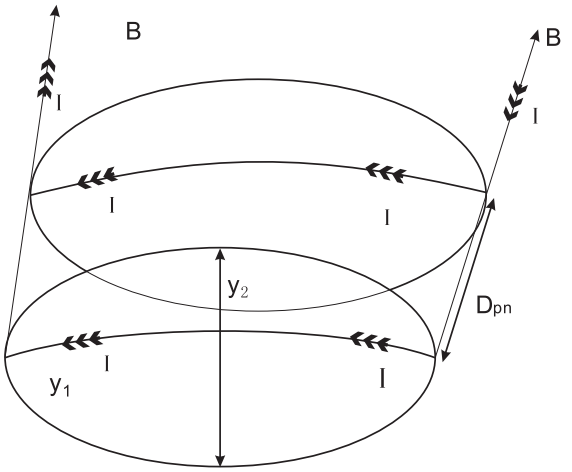

Figure 4. Penetration of the flux tube in the stellar atmosphere. Potential difference across the planet would be maintained at its foot print on the surface of its host star if there is sufficient time for the Alfvén waves to transit this information. Arrows indicate the flow direction of the electrical current. The values of y_1 and y_2 are given by Equations (2). The top circle represents the stellar surface and the penetration depth $D_{\rm pn} = R_* - r_{\rm pn}$ is evaluated in Section 5.3.

The stellar magnetic field has the geometrical structure of a magnetic dipole field. Thus, the foot of the flux tube at the stellar envelope (the circled area in Figure 2) is, at the first order in $\sqrt{R_*/a}$, an ellipse whose axes have respective lengths

$$y_1 = \left(\frac{R_p}{s}\right)\left(\frac{R_*}{a}\right)^{3/2}, \tag{2}$$

$$y_2 = 2R_p\left(\frac{R_*}{a}\right)^{3/2}, \tag{3}$$

$$\sin\theta_F = \sqrt{\frac{R_*}{a}} \tag{4}$$

$$\cos\theta_F = \sqrt{1 - \frac{R_*}{a}} \equiv s, \tag{5}$$

where θ_F is the angle between the stellar spin axis and the location of the foot of the flux tube. When the current **J** crosses the foot of the flux tube in the stellar envelope, it covers a length y_1. In the rest of the paper, we take $\cos\theta_F$ as roughly equal to 1. We represent it with the symbol s in analytical equations and take it to be equal to 1 in numerical applications.

In Figure 4, we zoom in on the foot of the flux tube at the stellar atmosphere. In order to derive y_1 and y_2 (at the first order in R_*/a), we first solve $\mathcal{B} \wedge dl = 0$ and obtain $\sin\alpha = \sqrt{R_*/(a + R_p)}$ and $\sin\beta = \sqrt{R_*/(a - R_p)}$ with α and β defined in Figure 2. We then write $y_1 = R_*(\alpha - \beta)$ and $y_2 = (2R_p/2\pi a)2\pi R_* \sin\theta_F$.

For a super-Earth (using the model parameters listed above), we find $y_1 = 1.6 \times 10^6$ m and $y_2 = 3.2 \times 10^6$ m. For a hot Jupiter, we would typically need to multiply these values by a factor 10. The height of the foot of the flux tube is derived below in Section 5.3.3. The numerical applications are for $s = 1$. For semimajor axes comparable to the stellar radius, the multiplicative factor $(1 - R_*/a)^{-1/2}$ in y_1 would significantly affect the length of the foot of the flux tube.

3.3. Induced Difference of Potential

The planet is a conductor moving in the stellar magnetosphere with relative linear speed $\upsilon_{p/s}$. Modeling the stellar magnetic field as the one created by a magnetic dipole (of magnetic moment m), the magnitude of the induced electric field in the planet $\mathcal{E}_p$ is

$$\mathcal{E}_p = \upsilon_{p/s}\mathcal{B}_*(a) = (\omega_p - \omega_*)a\frac{\mu_0 m}{4\pi a^3} \tag{6}$$

with $\mathcal{B}_*(a)$ representing the stellar magnetic field at the location of the planet. Numerical applications for a super-Earth give $\mathcal{E}_p = 240\,\mathrm{V\,m^{-1}}$ (slow-rotator), $1000\,\mathrm{V\,m^{-1}}$ (fast rotator) (a slow or fast rotator depends on the spin frequency of the star, as described in Section 3.1).

The magnitude of the difference of potential U (or emf) generated across the planet is thus

$$U = 2R_p\mathcal{E}_p = 2R_p(\omega_p - \omega_*)a\frac{\mu_0 m}{4\pi a^3}. \tag{7}$$

For the super-Earth models under consideration, $U = 6.7 \times 10^9 V$ (slow rotator) and $2.8 \times 10^{10} V$ (fast rotator). This difference of potential is transmitted across the flux tube (with the assumption of infinite conductivity along the flux tube that passes through the planet) and generates a uniform electric field $\mathcal{E}_*$ in the stellar envelope (see Figure 1) at the foot of the flux tube

$$\mathcal{E}_* = \frac{U}{y_1} = 2\frac{\mu_0 m}{4\pi a^3}(\omega_p - \omega_*)a\left(\frac{a}{R_s}\right)^{3/2} s. \tag{8}$$

The value of $\mathcal{E}_*$ does not depend on the radius of the planet, and for our values of the parameters for a young T Tauri star, $\mathcal{E}_* = 4.2 \times 10^3\,\mathrm{V\,m^{-1}}$ (slow rotator), $1.8 \times 10^4\,\mathrm{V\,m^{-1}}$ (fast rotator).

3.4. Analytical Expressions: Intensity in the Circuit, Ohmic Dissipation, and Torque in the Planet and Star

The induced current I is given by

$$\begin{aligned} I &= \int_z\int_y \mathcal{J}dydz = \mathcal{E}_* y_2\int_z \sigma_*(z)dz = U\frac{y_2}{y_1}\int_z \sigma_*(z)dz \\ &= 4R_p(\omega_p - \omega_*)a\frac{\mu_0 m}{4\pi a^3}s\int_z \sigma_*(z)dz. \end{aligned} \tag{9}$$

In the previous equation, $\mathcal{J}$ is the volumic electric current in the stellar atmosphere at the foot of the flux tube (induced by U), y varies from 0 to y_2 (the width of the foot of the flux tube), and z varies from $r_{\rm pn}$ (the radius to which the flux tube can penetrate into the stellar atmosphere) to R_* and $(y_2/y_1) = 2s$ (see Figure 4). In this circuit, the total resistance is the sum of that across the planet, the foot print of the flux tube on the stellar surface, and along the flux tube. Here we consider only the largest contribution and neglect that across the planet. In Section 5.3, we determine the magnitude of $r_{\rm pn}$ and evaluate

$$\Sigma = \int_{r_{\rm pn}}^{R_*}\sigma_p(z)dz \tag{10}$$

such that $I = 2U\Sigma s$. In the above equation, $\sigma_p(z)$ is the local Pedersen conductivity (see Equation (47)). The total resistance of the stellar atmosphere at the foot of the flux tube is

$$\mathcal{R}_* = \frac{U}{I} = \frac{y_1}{y_2}\frac{1}{\Sigma} = \frac{1}{2\Sigma s}. \tag{11}$$

The total ohmic power dissipation in the stellar atmosphere at the foot of both flux tubes (one for each hemisphere, thus the multiplicative factor 2) $\mathcal{P}_*$ and in the planet $\mathcal{P}_p$ are

$$\begin{aligned} \mathcal{P}_* &= 2\mathcal{R}_* I^2 = 2UI = 4U^2\Sigma s \\ &= 16R_p^2(\omega_p - \omega_*)^2 a^2(\mu_0 m/4\pi a^3)^2\Sigma s \end{aligned} \tag{12}$$

$$\mathcal{P}_p = 2\mathcal{R}_p I^2 = 2\mathcal{R}_p(2U\Sigma s)^2 = \mathcal{P}_*\frac{\mathcal{R}_p}{\mathcal{R}_*}, \tag{13}$$

where $\mathcal{R}_*$ is the resistance of the foot of the flux tube (on one hemisphere), and $\mathcal{R}_p$ is the resistance of one hemisphere of the planet. Since the resistance in the planet is considerably smaller than that in the star, most of the power is dissipated in near the foot of the flux tube on the surface of the star. Note that the magnitude of both $\mathcal{P}_*$ and $\mathcal{P}_p$ is determined by I and $\mathcal{R}_*$.

The total torque (for both circuits, one circuit for each hemisphere) due to the Lorentz force (the axis is the stellar spin axis) on the star (equal in absolute value to that on the planet) is

$$\begin{aligned} \mathcal{T}_* &= 2\int_x\int_y\int_z r\wedge(\mathcal{J}\wedge\mathcal{B})dxdydz \\ &= 2(R_*\sin\theta_F)(y_1 I)\left(\frac{2\mu_0 m\cos\theta_F}{4\pi R_*^3}\right) \\ &= 4R_p a\frac{\mu_0 m}{4\pi a^3}I\mathbf{e}_z, \end{aligned} \tag{14}$$

$$\mathcal{T}_* = 16R_p^2 a^2(\omega_p - \omega_*)\left(\frac{\mu_0 m}{4\pi a^3}\right)^2\Sigma s\mathbf{e}_z, \tag{15}$$

where $s = \cos\theta_F$ as defined in (2) and I is the integral of the volumic current across a cross section (we take an averaged view of the volumic current rather than determining its complex geometry inside the planet). We have calculated here the total ohmic dissipation and torque (i.e., for both hemispheres).

3.5. Equation of Evolution of the Stellar Spin and Planet's Orbital Angular Velocity and Semimajor Axis

The torque on the planet $\mathcal{T}_p$ is equal and opposite to that on the star $\mathcal{T}_*$. Consequently, the semimajor axis of a super-Earth on a circular orbit evolves at a rate

$$\dot{a} = \frac{2a}{H_p}\mathcal{T}_p, \tag{16}$$

where the total angular momentum of the planet's orbit is $H_p = M_p a^2\omega_p$. Since the total angular momentum of the system is conserved, the changing rate of the stellar spin is

$$\dot{\omega}_* = \frac{\mathcal{T}_*}{c_* M_* R_*^2}, \tag{17}$$

where $c_* \simeq 2/5$ is the inertial constant of the star. According to the above expression, the planet would undergo orbital decay and its host star would spin up if it is inside corotation (or equivalently if $\omega_p > \omega_*$). Similarly, the planet's orbit would expand and its host star would spin down if it is outside corotation.

The planet's orbital frequency ω_p is related to the semimajor axis, $\omega_p = (\sqrt{GM_*}/a^{3/2})$. Using the expressions calculated for the torques and Equations (16) and (17), we find

$$\dot{\omega}_* = \frac{M_p(GM_*)^{2/3}}{3C_*M_*R_*^2}\frac{\dot{\omega_p}}{\omega_p^{4/3}} \approx 3\times10^{-10}\frac{\dot{\omega}_p}{(\omega_p\ \tilde{s})^{4/3}}, \quad (18)$$

where the numerical application was for a planet with 10 Earth masses ($M_p = 6\times10^{25}$ kg) and $\tilde{s}$ represent second. Therefore, we can estimate the variation of ω_* during the evolution of the planet's migration:

$$|\triangle\omega_*| = -\frac{M_p(GM_*)^{2/3}}{C_*M_*R_*^2}\left|\triangle\left(\frac{1}{\omega_p^{1/3}}\right)\right|, \quad (19)$$

which is negligibly small.

We can thus consider that the star's angular velocity is roughly unaffected by this transfer of angular momentum. Using Equation (16), $a^3 = (GM_*/\omega_p^2)$, $(\dot{a}/a) = (-2/3)(\dot{\omega_p}/\omega_p)$, and the expression for the torque on the planet (equal to $-\mathcal{T}_*$ with $\mathcal{T}_*$ given in Equation (15)) we find

$$\frac{\dot{\omega_p}}{\omega_p^4(\omega_p-\omega_*)} = 48\frac{R_p^2}{M_p}\left(\frac{\mu_0 m}{4\pi}\right)^2\frac{\Sigma s}{(GM_*)^2} = \alpha, \quad (20)$$

where ω_* is constant and $\alpha = 48(R_p^2/M_p)(\mu_0 m/4\pi)^2 \times (\Sigma s/(GM_*)^2)$ (of unit s^3), and s in the numerator of the expression for α is defined as in Equation (2). The previous equation becomes

$$-\frac{1}{\omega_*}\frac{\dot{\omega_p}}{\omega_p^4}-\frac{1}{\omega_*^2}\frac{\dot{\omega_p}}{\omega_p^3}-\frac{1}{\omega_*^3}\frac{\dot{\omega_p}}{\omega_p^2}-\frac{1}{\omega_*^4}\frac{\dot{\omega_p}}{\omega_p}+\frac{1}{\omega_*^4}\frac{\dot{\omega_p}}{(\omega_p-\omega_*)} = \alpha. \quad (21)$$

After integration, we find

$$\frac{\Omega^3(t)}{3}+\frac{\Omega^2(t)}{2}+\Omega(t)+\ln(|1-\Omega(t)|) = \frac{\Omega_i^3}{3}+\frac{\Omega_i^2}{2}+\Omega_i+\ln(|1-\Omega_i|)+\alpha\omega_*^4(t-t_0), \quad (22)$$

where we define $\Omega(t)\equiv\omega_*/\omega_p(t)$ and $\Omega_i\equiv\Omega(t=t_0)$.

Near corotation (i.e., $\Omega\simeq1$), the ln function is dominant and we find

$$\ln(|1-\Omega(t)|) = \ln(|1-\Omega_i|)+\alpha\omega_*^4(t-t_0). \quad (23)$$

If ω_p is greater than ω_*, then

$$\frac{\omega_p(t)}{\omega_*} = \frac{1}{\Omega(t)} = \left[1-\left(1-\frac{\omega_*}{\omega_p(t_0)}\right)\exp\left(\alpha\omega_*^4(t-t_0)\right)\right]^{-1}. \quad (24)$$

Similarly, if ω_p is less than ω_*, then

$$\frac{\omega_p(t)}{\omega_*} = \frac{1}{\Omega(t)} = \left[1+\left(\frac{\omega_*}{\omega_p(t_0)}-1\right)\exp\left(\alpha\omega_*^4(t-t_0)\right)\right]^{-1} \quad (25)$$

with a timescale

$$\tau = \frac{1}{\alpha\omega_*^4} = \frac{M_p(GM_*)^2}{48\omega_*^4R_p^2\Sigma s}\left(\frac{\mu_0 m}{4\pi}\right)^{-2}. \quad (26)$$

In the general case, $\omega_p(t)$ follows Equation (22), or written differently:

$$\omega_p^3(t)\left[f(t)-\ln\left|1-\frac{\omega_*}{\omega_p(t)}\right|\right]-\omega_*\omega_p^2(t)-\frac{\omega_*^2}{2}\omega_p(t) = \frac{\omega_*^3}{3}, \quad (27)$$

where $f(t) = A + B(t-t_0)$ with $A = \Omega_i^3/3+\Omega_i^2/2+\Omega_i+\ln(|1-\Omega_i|)$ and $B = \alpha\omega_*^4$.

In order to get an equation of evolution of the semimajor axis, one can replace in Equation (23) (near corotation) or (22) (in the general case) $\Omega_p(t)$ by $(a(t)/a_c)^{3/2}$ and Ω_i by $(a(t_0)/a_c)^{3/2}$ with a_c the corotation radius. Near corotation, we find

$$a(t) = a_c\left[1-\left[1-\left(\frac{a(t_0)}{a_c}\right)^{3/2}\right]\exp\left(\frac{t-t_0}{\tau}\right)\right]^{2/3}, \quad (28)$$

for the case where a is smaller than a_c.

4. CONDITION FOR THE VALIDITY OF THE MODEL: $t_A \leqslant t_{\max}$

In order to apply the model described above, one needs to verify that the time t_A required for the Alfvén waves to travel along the flux tube (to a depth $D_{\rm pn}$ inside the star to be determined), and back to the planet is smaller than the time $t_{\max}$ it takes the flux tube to slip ahead of the planet by more than its diameter. This condition ensures that a perturbation along a field line of the flux tube has the time to travel back and forth while the field line is still part of the flux tube that passes through the planet. Figures 5 and 6 illustrate this condition. Figure 7 shows the field lines near the planet in the case where the condition is not met.

In order to calculate t_A, we need to estimate the Alfvén speeds along the flux tube between the planet and the star and in the stellar ionosphere (at the foot of the flux tube). Similarly, the calculation of $t_{\max}$ requires the value of the conductivities (or resistance) of the different components of the circuit. Indeed, the ratio of $\mathcal{R}_p$ (resistance of the planet) and $\mathcal{R}_*$ (resistance of the foot of the flux tube in the stellar atmosphere) determines the amount of relative slippage between the flux tube and the planet (Dermott 1970).

In the limit where $\mathcal{R}_p$ is comparable to or larger than $\mathcal{R}_*$ (as in the night side of synchronously spinning hot Jupiter; see Paper I), the flux tube would tend to slip through the planet. In this case, the flux tube would slip ahead of the planet by a distance $\sim 2R_p$ in a relatively short time t_A, and it might not be possible to maintain a closed circuit.

In the most unfavorable case ($\mathcal{R}_p/\mathcal{R}_* = \infty$, i.e., the flux tube passes through the planet completely undisturbed), $t_A = 2R_p/\upsilon_{p/s}$ (where $\upsilon_{p/s}$ represents the speed of the planet in the frame rotating with the stellar magnetosphere). In the opposite extreme limit, $\mathcal{R}_p/\mathcal{R}_* = 0$ and $t_A = \infty$ such that the flux tube is completely anchored in the planet. Differential motion steadily stretches the field lines until they reconnect. A more realistic situation falls somewhere between these two extreme limits, and the smaller $\mathcal{R}_p/\mathcal{R}_*$, the easier it is to satisfy the condition of validity.

4.1. Qualitative Estimate of the Relative Slippage

A first qualitative criterion is given by the following argument. We want to determine whether the magnetic flux tube

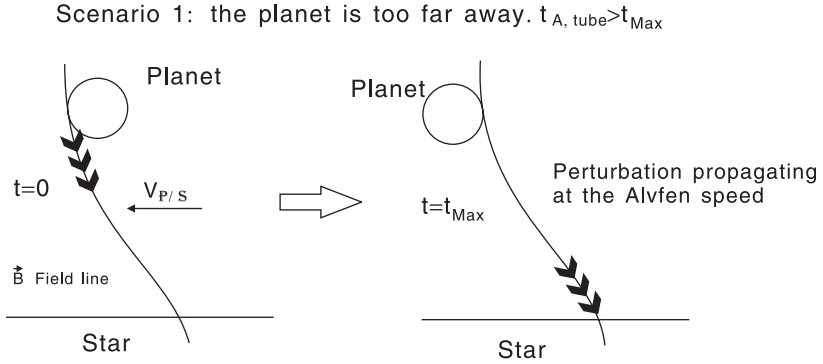

Figure 5. Propagation of the Alfvén wave between a relatively distant planet and its host star. The planet's motion relative to the stellar field induces a potential drop across the flux tube in the proximity of the planet. This information propagates along the flux tube toward the host star with an Alfvén speed. Due to finite diffusion and the relative motion between the planet and the stellar magnetosphere, the net field lines also slip through the planet. In this illustration the timescale required for the Alfvén wave to reach the host star is long compared with that required for the slippage of the field. The circuit is not established in this case.

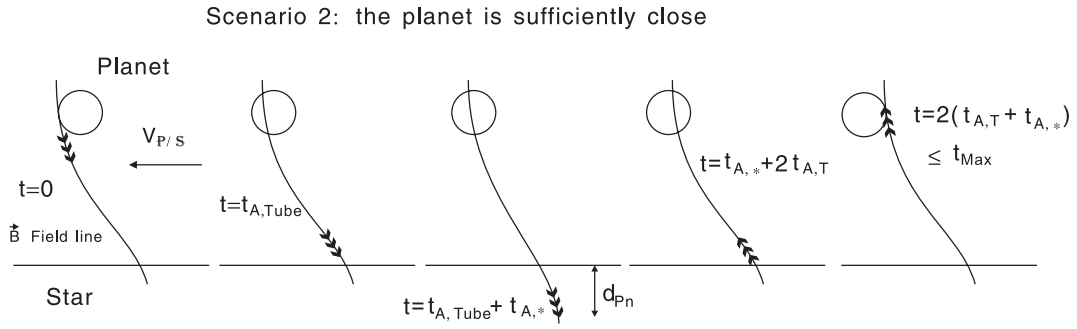

Figure 6. Necessary condition for a complete unipolar inductor circuit. Similar to the illustration in Figure 5, the potential drop across the planet propagates along the flux tube toward the planet with an Alfvén speed. In this illustration, the planet is sufficiently close to its host star that the potential drop can be established on the surface of the host star before the fields slip through the planet. This potential drop induces a current which is determined by the resistivity on the stellar surface. In this case, it is possible to complete the circuit induced by the motion of the planet.

slips on the planet or on the star. In the absence of any companions, the magnetic field in the magnetosphere of a star rotates with the star. A close-in planet would tend to drag the stellar magnetic field lines that pass through it along with its motion.

Let us define ω_p, ω_*, and ω_B to be the angular velocity of the planet, star, and magnetic field in an absolute frame. We then consider the relative motion between the planet and the field lines, and between the field lines and the star. We write $\Omega_p = \omega_p - \omega_B$ and $\Omega_* = \omega_B - \omega_*$ and our goal is to estimate the magnitude of Ω_p/Ω_*. In these notations, the planet's speed relative to the magnetic field is then $\upsilon_p = \Omega_p\, a$ (a is the semimajor axis), and the speed of the field lines (that pass through the planet) relative to the star is $\upsilon_* = \Omega_* R_*$ (R_* being the stellar radius).

Considering the DC component of the field, we can write the complete MHD induction Equation (1) for the star and the planet:

$$\frac{\partial \vec{\mathcal{B}}_p}{\partial t} = \nabla \wedge (\vec{\upsilon}_p \wedge \vec{\mathcal{B}}_p) + \nabla \wedge (\eta_p \nabla \wedge \vec{\mathcal{B}}_p)$$
$$\frac{\partial \vec{\mathcal{B}}_*}{\partial t} = \nabla \wedge (\vec{\upsilon}_* \wedge \vec{\mathcal{B}}_*) + \nabla \wedge (\eta_* \nabla \wedge \vec{\mathcal{B}}_*). \quad (29)$$

In a steady state, the first and second equations imply $\upsilon_p \approx \eta_p/R_p$ and $\upsilon_* \approx \eta_*/R_*$, respectively. Therefore, we obtain

$$\frac{\Omega_p}{\Omega_*} \approx \frac{\sigma_*}{\sigma_p}\frac{R_*^2}{R_p a}. \quad (30)$$

In the context of Io–Jupiter interaction $R_*^2/R_p a \approx 7$. Since the electrical conductivity on Io is estimated to be much larger than that on Jupiter, the flux tube which passes through Io moves with Io and drags its foot on the surface of Jupiter (Goldreich & Lynden-Bell 1969). For a Jupiter-mass planet orbiting a young T Tauri star (with radius twice that of the sun) at 0.04 AU (three-day period), $R_*^2/R_p a \approx 4$, and the anchorage of the flux tube which passes through the hot Jupiters is thus determined by the ratio of the diffusivity through the planet to that through its host star. For a super-Earth with radius twice that of the Earth at 0.04 AU, $R_*^2/R_p a \approx 20$.

4.2. Analytical Expression of the Time Constraint, $t_{\max}$

The magnitude of $t_{\max}$ is the time it takes for the field lines in the flux tube to slip pass through the planet by a distance equal to the planetary diameter. We consider a planet with an electrical conductivity σ_p moving relative to a magnetic field at speed $\upsilon_{p/s} = (\omega_p - \omega_*)a$. If the planet does not drag the field at all (for example, if $\sigma_p = 0$), the field lines would move relative to the planet with a linear speed $\upsilon_{p/s}$. Thus, the minimum value for $t_{\max}$ is $t_{\max} = 2R_p/\upsilon_{p/s}$. On the other hand, if the field lines are perfectly anchored in the planet (for example, when $\sigma_p = \infty$) then $t_{\max} = \infty$. The induced field lines would wrap around the host stars with the planet's synodic orbit (i.e., its motion relative to the stellar spin).

Based on extrapolation from analogous considerations (Aly 1985; Aly & Kuijpers 1990; van Ballegooijen 1994), we hypothesize that magnetic reconnection may occur when the azimuthal component of the induced (and "dragged") mag-

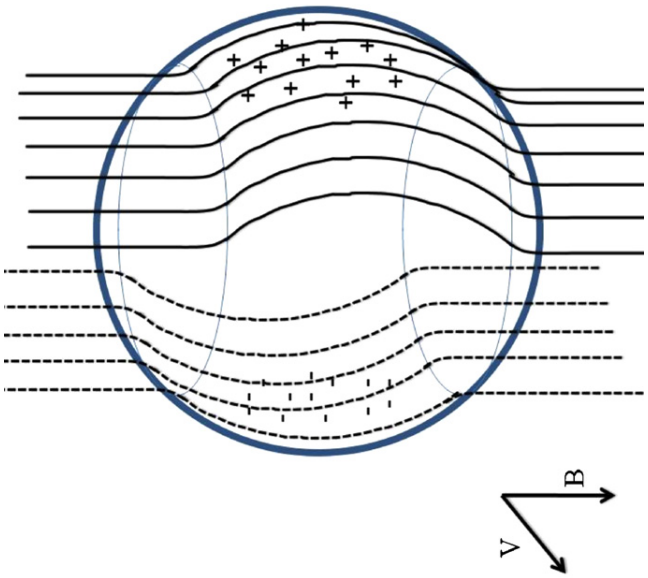

Figure 7. Magnetic field lines in the case where the circuit is not closed. The planetary motion relative to the stellar magnetic field induces charge separation. Without any connection (at infinity) between the separated charges, there is no current in the frame of the moving planet. In a infinitely conducting planet, the separated charges are concentrated near its surface. The magnitude of the induced field $\mathcal{E}_p$ is determined by Equation (6). In the stationary frame (centered on the host star), the separated surface charges carried by the planets generate two opposite currents as well as a finite $\nabla \wedge \mathcal{E}_p$ in the moving planet. Interior to the infinitely conducting moving planet, the induced field exactly cancels the unperturbed field as if there is no diffusion of the stellar magnetic field into the planet. In the external region close to the moving planet, the induced field strongly perturbs the stellar magnetic field. The net field distortion is symmetric around an infinitely conducting moving planet (analogous to an invisic flow around a spherical object) such that there is no net torque acting between the planet and the stellar field. This symmetry would be broken and the drag on the planet would be finite if its conductivity is sufficiently low to permit significant slippage of the stellar magnetic field or if a complete circuit connecting two sides of the planet can be established on the surface of its host star.

(A color version of this figure is available in the online journal.)

netic field well outside the planet becomes comparable to the unperturbed stellar dipole field. We assume the time growth timescale for the azimuthal component of the field to the period $t_{\rm syn} = 2\pi/(\omega_p - \omega_*)$ of the planet's synodic period. If it occurs, reconnection would lead to short-circuit and a burst of intense ohmic dissipation in the planet. We discuss the possibility of magnetic reconnection again in Section 6.4. In the limit of infinite $t_{\rm max}$, the relative motion between the planet and the stellar field would restore the electric field and reestablish the circuit on the timescale of t_A with a reduced effective conductivity (or equivalently an enhanced resistivity and magnetic diffusivity). We shall consider elsewhere the possibility of such an episodic electrodynamic process.

In general, the conductivity σ_p would fall between 0 and ∞ and the field is dragged without being completely anchored on the planet. The induced field lines are distorted and partially wrapped around the host star. In the limit that $t_A < t_{\rm max} < t_{\rm syn}$, it is possible to complete a steady circuit of unipolar induction without reconnection.

The same argument also holds for the star with electrical conductivity σ_* dragging its own field lines so that the intensity of the slippage between the field lines and the planet depends on both the conductivity of the planet and star. Modeling the interaction between Io and Jupiter, Goldreich & Lynden-Bell (1969) took into account σ_{Io} and $\sigma_{\rm Jupiter}$. Dermott (1970) included the contribution of the flux tube's conductivity in the expression of the slippage of the field relative to both Io and Jupiter.

In the present context, the linear speed of the slippage between the flux tube and the planet is

$$\upsilon_{\rm slip} = \frac{\upsilon_{p/s}}{1 + (\mathcal{R}_* + \mathcal{R}_{\rm tube})/(\mathcal{R}_{\rm tube} + \mathcal{R}_p)} \tag{31}$$

(In the above expression, we use $\mathcal{R}_p$ instead of $2\mathcal{R}_p$ as in Dermott).

In a complete circuit, the maximum time available for the Alfvén waves to propagate from the planet to the star and return to the planet is

$$t_{\rm max} = \frac{2R_p}{\upsilon_{\rm slip}} = 2R_p \frac{(1+w)}{(\omega_p - \omega_*)a}, \tag{32}$$

where $w = (\mathcal{R}_* + \mathcal{R}_{\rm tube})/(\mathcal{R}_p + \mathcal{R}_{\rm tube})$. It is common to neglect $\mathcal{R}_{\rm tube}$.

5. RESISTANCE AND ALFVÉN SPEED ALONG THE CIRCUIT

We derived the analytical expressions of the total intensity (Section 3.4) and the time available for the Alfvén waves to travel back and forth between the planet and the foot of the flux tube (Section 4.2). In order to determine their numerical values, we calculate in this section 1) the planet's integrated resistance $\mathcal{R}_p$, 2) the resistance $\mathcal{R}_{\rm tube}$ and Alfvén speed $\upsilon_{A,\rm tube}$ along the flux tube, and 3) the resistance across the foot of the flux tube just below the star's surface $\mathcal{R}_*$ (perpendicular to the magnetic field and parallel to the electric potential gradient) and the Alfvén speed along the foot of the flux tube $\upsilon_{A,\rm tube}$. Figures 5 and 6 provide a summary of the condition of validity.

5.1. Resistance in the Planet $\mathcal{R}_p$

The electrical conductivity profile of a super-Earth is unclear. We thus first discuss the (better characterized) conductivity profile of present-day Earth. Lorrain et al. (2006) estimated the electric conductivity of the present-day Earth mantle to range between 10^{-2} ohm^{-1} m^{-1} and 10^3 ohm^{-1} m^{-1} and 10^5 ohm^{-1} m^{-1} for the inner core (also see Stevenson, 2003). Merrill et al. (1996, pp. 273–277) similarly argues for an electrical conductivity of about 5–8 $\times 10^5$ ohm^{-1} m^{-1} for the core of the Earth, and between 3 and 100 ohm^{-1} m^{-1} for the lower mantle. For the upper mantle (and crust), Obiekezie & Okeke (2010) calculate an electrical conductivity increasing from the surface (about 3×10^{-2} ohm^{-1} m^{-1}) to 10^{-1} ohm^{-1} m^{-1} at around 500 km. The electrical conductivity of the Earth is therefore minimal and between 3×10^{-2} and 10^{-1} ohm^{-1} m^{-1} for a few hundred kilometers and then increases with depth.

In the present application, we are primarily interested in the interaction between super-Earths and their host stars when they are relatively young (up to a few 10^7 yr). During this stage, the stellar magnetic field is intense and the close-in super-Earths may be intensely heated by giant impacts and tidal and ohmic dissipation. Super-Earths with a molten crust are likely to have higher conductivities than the present-day terrestrial planets (for example, Rikitake (1966) expressed the conductivity of rocks and metals on the Earth as a sum of $\exp(-E_i/kT)$, and Umemoto et al. (2006) estimated a conductivity at the core of a super-Earth and hot-Jupiter to be around 10^6 ohm^{-1} m^{-1}. The stellar radiation alone would raise

the super-Earth's surface temperature to about 1500 K. Ohmic dissipation inside the planet may provide an additional source of thermal energy (see Section 6.3). In a thermal equilibrium, the planet's surface temperature may sometimes exceed 2000 K, at which silicate melts, and raise the electric conductivity to around 10 ohm^{-1} m^{-1} (for 1400 K, Waff & Weill 1975).

It is therefore reasonable to assume that the electrical conductivity of a super-Earth is most likely higher but at least that of the Earth. The electrical conductivity in a super-Earth would thus be several orders of magnitude higher than 1 ohm^{-1} m^{-1} in the core and lower mantle and arguably also in the upper mantle. Besides, a conductivity of 0.1–1 ohm^{-1} m^{-1} (i.e., 10 times lower than the value we use) in an area spanning 10 % of the planet (roughly the thickness of the upper mantle) would at most double total the resistance.

In addition, for a super-Earth, the characteristic speed (for example, the planet linear speed in a frame corotating with the star) is much faster that for the field to diffuse across it, i.e., $\upsilon \gg (\eta/L) = (1/\mu_0 \sigma L)$ where L is the characteristic length. Therefore, we can neglect the diffusion (second term on the right hand side of the MHD Equation (1)) compared to the induction (first term).

The integrated resistance in the geometry of the planet is

$$\mathcal{R}_p = \frac{1}{S}\frac{L}{\sigma} = \frac{1}{R_p \sigma_p}, \tag{33}$$

where S is the cross section. Depending of the geometry of the current inside the planet, the formula could have multiplicative factors, usually of order unity.

With these approximations, we find

$$\mathcal{R}_p = \frac{1}{R_p \sigma} \ll 7 \times 10^{-8}\,\mathrm{Ohm}. \tag{34}$$

The value we use in our fiducial calculation is $\mathcal{R}_p = 7 \times 10^{-8}$ Ohm. If our assumption that the conductivity in a super-Earth is higher than that in the present-day Earth is inappropriate, this resistance could be higher. But it may also be much lower if the super-Earth has a substantial atmosphere, which is extensively photoionized or a fully molten core where the alkali metals are partially ionized.

5.2. Resistance and Alfvén Speed along the Flux Tube

Electrodynamics along the flux tube determines the propagation of the induced electric field between the planet and its host star. The total resistance along the flux tube determines changes in the electric potential at the foot of the flux tube. The Alfvén speed determines the propagation speed of the disturbance.

5.2.1. Total Resistance Along the Flux Tube $\mathcal{R}_{\rm tube}$

The resistance of the flux tube is also difficult to estimate accurately. Goldreich & Lynden-Bell (1969) simply assumed the electric conductivity to be infinite along the magnetic field lines and did not include $\mathcal{R}_{\rm tube}$ in their equations. Dermott included $\mathcal{R}_{\rm tube}$ in the equations but, during numerical applications, assumed it to be negligible in front of the resistance of the satellite Io. In all previous investigations, conductivity across the field lines in the tenuous region between the planet and the star is assumed to be negligible.

We provide here an estimate of the order of magnitude of the resistance of the flux tube. If we assume the plasma between the star and the planet to be fully ionized, the electric conductivity along (parallel) to the magnetic field line would be

$$\sigma_0 = \frac{n_e e^2}{m_e \nu_e}, \tag{35}$$

where n_e is the volumic number of free electrons, e and m_e are the charge and mass of the electron, and ν_e the collisional frequency of the electrons with electrons and ions/protons (we assume these two collisional frequency to be the same).

We take $\nu_e = (n_e e^4/16\pi\epsilon_0^2 m_e^2 \langle \upsilon_e \rangle^3)$ with the electron thermal speed $\langle \upsilon_e \rangle = \sqrt{2k_B T/m_e}$. We thus get $\nu_e = n_e 1.2 \times 10^{-6} T^{-3/2}$ and $\sigma_0 = (e^2 T^{3/2}/1.2 \times 10^{-6} m_e)$. In our model, we consider a star with a surface temperature $T_* = 4000$ K, and a planet with the equilibrium temperature $T_p \sim 1{,}500$ K for the planet with an $a = 0.04$ AU. For an average temperature of 2000 K between the star and the planet, we find $\sigma_0 \simeq 2000\,\mathrm{Ohm}^{-1}\,\mathrm{m}^{-1}$ so that

$$\mathcal{R}_{\rm tube} = \frac{L}{\sigma_0 S} = \frac{a}{(\pi R_p)(R_p f_{\rm tube})\sigma_0} = \frac{4.6 \times 10^{-9}}{f_{\rm tube}}\,\mathrm{Ohm}, \tag{36}$$

where $f_{\rm tube}$ is between 0 and 1 such that $R_p f_{\rm tube}$ is equal to the thickness of the volumic current that flows along the field lines. This resistance is usually negligible compared to the other resistances involved in the model (especially that of the star), except if the volumic currents are confined in an extremely thin layer at the surface of the flux tube. Therefore, we neglect the potential difference, along each field line in the flux tube between the surfaces of the planet and star.

5.2.2. Travel Time along the Flux Tube between the Planet and (the Top of) the Stellar Surface

We assume that the plasma between the star and the planet is fully ionized and estimate $\upsilon_{A,\rm tube}$ under various different situations.

(1) We first consider the epoch shortly after the super-Earth has migrated to the stellar proximity through planet–disk tidal interaction. In opaque inner regions of their natal disks, super-Earths' type I migration generally stalls at a radius r where the Σ_d has a positive radial gradient with a scale height $\Delta r = \Sigma_d/(\partial \Sigma_d/\partial r)$ which is a fraction ($\sim$0.1–0.2) of r (Masset et al 2006). Special locations include narrow transition regions between the active inner region and dead zone as well as outer edge of magnetospheric cavity (Kretke et al. 2009).

We consider a super-Earth to be embedded in a disk with an effective thickness $H_d \simeq c_s/\omega_p \sim 0.01$–$0.1r$ and a steady state mass transfer rate of $\dot{M}_d = 2\pi \Sigma_d U_a r$ throughout the disk where Σ_d and c_s are the surface density and sound speed of the gas, respectively. Using an ad hoc α prescription for the effective viscosity $\nu = \alpha \omega_p H_d^2$, the radial velocity of the disk gas is $U_d \simeq -3\nu/2r = -3\alpha H_d^2 \omega_p/2r$ and the characteristic density at the disk midplane is

$$\rho_d \simeq \Sigma_d/2H_d = \frac{\dot{M}_d}{6\pi\alpha\Omega H_d^3}, \tag{37}$$

where α is the turbulent transport efficiency factor and may have an effective magnitude $\sim 10^{-2}$–10^{-3} (Hartmann et al. 1998). In untruncated protostellar disks around classical T Tauri with $\dot{M}_d \sim 10^{-7}$–$10^{-8}\,M_\odot\,\mathrm{yr}^{-1}$, $\rho_d \sim 10^{-6}$–$10^{-7}\,\mathrm{kg\,cm}^{-3}$ at the edge of the magnetospheric cavity $r \sim 0.04$ AU. The corresponding Alfvén speed is

$$\upsilon_{A,\rm tube} = \frac{\mathcal{B}}{\sqrt{\mu_0 \varrho}} = \frac{m}{4\pi a^3}\sqrt{\frac{\mu_0}{\varrho}}. \tag{38}$$

Near the disk inner edge, the characteristic wave propagation timescale $t_{\rm tude} \sim \Delta r/v_{A,\rm tube} \sim 10^4$ s may be too long to maintain a circuit. Note that if the super-Earth is stalled near the transition region between active and dead zones, $t_{\rm tube}$ would be longer not only because this region is further away from the host star, but also because Σ_d interior to it does not vanish.

However, around stars with ages larger than 10^7 yr, $\dot{M}_d$ may decline below that found around T Tauri stars and $t_{\rm tube}$ can be reduced substantially. If the observed weak (or absences of) near-IR excess around young stellar objects (Sicilia-Aguilar et al. 2006) in clusters with ages of ∼10 Myr is due to the depletion of inner holes in both gas and dust, Σ_d and hence ρ_d would be substantially smaller than the values estimated above. Thus in the post T Tauri phase, the Alfvén speed around the host stars of super-Earths would increase to sufficiently large values to enable the circuit to be closed, especially if we take into account the resistances in the calculation of the speed of slippage through the planet.

(2) Density around the flux tube does not decline indefinitely. Even after the disk is completely depleted or truncated in the proximity of the planet's orbit, the planet may be surrounded by a spherically symmetric component of stellar outflow with a speed $v_{\rm flow}$ and a mass flux. In this case, the volumic mass distribution is

$$\varrho_w(r) = \frac{\dot{M}_w}{4\pi r^2 v_{\rm flow}}. \tag{39}$$

The Alfvén speed between the planet and the star at radius r (with the origin at the center of the star) is thus

$$v_{A,\rm tube}(r) = \frac{m}{r^2}\sqrt{\frac{\mu_0 v_{\rm flow}}{4\pi\ \dot{M}}}. \tag{40}$$

Using $v_{\rm flow} = 100\,{\rm km\,s^{-1}}$, the numerical applications give $v_{A,\rm tube}(R_*) \simeq 10^8$ m s^{-1} and $v_{A,\rm tube}(a) \simeq 6 \times 10^6$ m s^{-1}. The time it takes the Alfvén waves to travel down the flux tube is

$$t_{\rm tube} = \int dr\ \frac{r^2}{m}\sqrt{\frac{4\pi\ \dot{M}}{\mu_0 v_{\rm flow}}} = \frac{a^3}{3m}\sqrt{\frac{4\pi\ \dot{M}}{\mu_0 v_{\rm flow}}}\left[1 - \left(\frac{R_*}{a}\right)^3\right], \tag{41}$$

with the integral being for r varying from the surface of the star to the planet. If one takes $\dot{M} = 10^{-10}\,M_\odot\,{\rm yr^{-1}}$ and $v_{\rm flow} = 100\,{\rm km\,s^{-1}}$, the numerical application then gives $t_{A,\rm tube} \simeq 300$ s. The magnitude of $t_{A,\rm tube}$ would be smaller for winds with faster speeds or lower mass loss rate.

5.3. Resistance in the Star across the Foot of the Flux Tube and Alfvén Speed along the Magnetic Field in the Star at the Foot of the Flux Tube

The resistance of the foot of the flux tube determines the total intensity in the circuit, and most of the travel time of the Alfvén waves occur at the foot of the flux tube.

5.3.1. Temperature and Pressure of the Stellar Outer Layer in an Isothermal Approximation

For the outer layer of the star, we adopt an isothermal approximation and assume a spherical symmetry. The pressure and temperature, $P(r)$ and T, are then given by

$$T(r) = T_* \tag{42}$$

$$P(r) = P(R_*)\ \exp\left[\frac{GM_*\mu}{R_g T(r) R_*}\left(\frac{R_*}{r} - 1\right)\right] \tag{43}$$

$$P(R_*) = \frac{2}{3}\frac{g_s}{\kappa}, \tag{44}$$

where κ and μ are the opacity and molecular weight at the photosphere and $R_g = \mathcal{N}_A k_B/\mathcal{M}_H \simeq 8.3 \times 10^3$ in SI units, with $\mathcal{N}_A$ the Avogadro number, k_B the Boltzmann constant, and $\mathcal{M}_H$ the molar mass of the hydrogen atom. The volumic mass can also be calculated using the ideal gas equation of state. For the models presented here, we neglect any change in $T(r)$ and $P(r)$ due to the local ohmic heating at the foot of the flux tube. Discussions in Section 6.2 show the possible existence of a hot spot at the foot of the flux tube. Self-consistent treatment of a potential feedback effect will be analyzed elsewhere.

5.3.2. Conductivity in the Stellar Atmosphere

The details of the derivation of the conductivity in the stellar atmosphere (foot of the flux tube) are given in Appendix A. In Figure 4, we show that, at the foot of the flux tube, current flows across the field lines, as a series of parallel circuits. We calculate the effective resistance and Alfvén travel timescale to determine the depth of penetration. We use Saha's equation to derive the ionization fraction. Following Fejer (1965) we refer to σ_0 as the electric conductivity parallel to the magnetic field lines, and $\sigma_p = \sigma_0/\{1 + (\omega_e/\nu_e)^2\}$ is the Pedersen conductivity parallel to the electric field. We define $\omega_e = eB/m_e$ to be the electron gyro-frequency, ν_e to be the mean collision frequency of the electrons with the neutral gas (see Equations (A7) and (A8)) and $r_=$ to be the radius at which

$$\nu_e(r_=) = \omega_e(r_=). \tag{45}$$

We find $r_= \approx 1.3962 \times 10^9$ m (given with several significant figures as an intermediate value in the series of numerical applications). Since $\omega_e(r) << \nu_e(r)$ at $r \leqslant r_=$ and $\omega_e(r) > \nu_e(r)$ at $r \geqslant r_=$, we write the Pedersen conductivity

$$\sigma_p(r \leqslant r_=) = \sigma_0(r) \tag{46}$$

$$\sigma_p(r \geqslant r_=) = \sigma_0(r)\left(\frac{\nu_e}{\omega_e}\right)^2. \tag{47}$$

In contrast to the region between the planet and its host star, gas in the stellar atmosphere is partially ionized. Substituting the appropriate value for σ_0 from Equations (A4) and (A5) we find

$$\sigma_p(r \leqslant r_=) = L_a \exp\left(\frac{-E}{2k_B T(r)}\right)\ \frac{T(r)^{3/4}}{\sqrt{P(r)}} \tag{48}$$

$$\sigma_p(r \geqslant r_=) = \frac{L_a}{Q_a^2}\ \frac{1}{m^2 T(r)^{1/4}} \exp\left(\frac{-E}{2kT(r)}\right)\ r^6\ (P(r))^{3/2} \tag{49}$$

$$\frac{L_a}{Q_a^2} = 10^{-19}\ \left(\frac{\mu_0}{4\pi}\right)^{-2}\ \frac{(2\pi m_e)^{3/4}}{h^{3/2}} k_B^{-1/4}\ \left(\frac{128 m_e}{9\pi}\right)^{1/2}, \tag{50}$$

where the numerical values of the constants in SI units are $L_a = 6.17 \times 10^6$, $Q_a = 2.93 \times 10^{-4}$, and $L_a/Q_a^2 = 7.2 \times 10^{13}$.

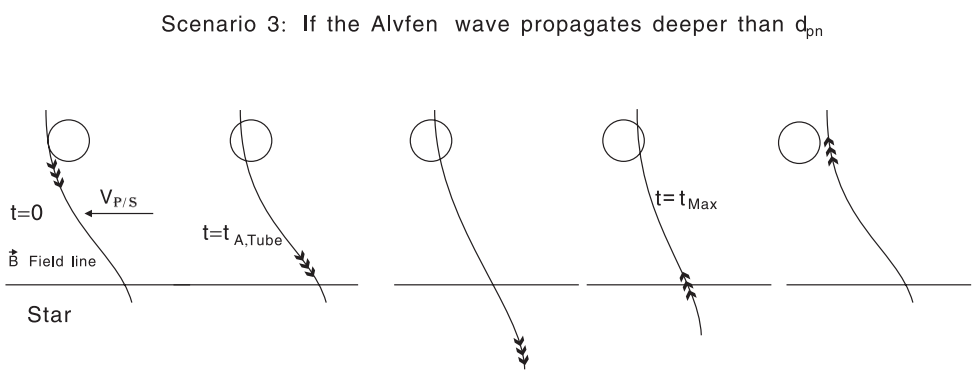

Figure 8. Penetration depth of the unipolar induction circuit. The propagation of the induced disturbances from the planet to the stellar surface is $t_{A,\mathrm{tube}}$. Below the stellar surface, gas density increases exponentially and the Alfvén speed decreases accordingly. The penetration depth of the planet's induced field is determined by the requirement that the timescale for the Alfvén waves to complete the circuit equals the field slippage timescale across the planet. The net resistivity at the stellar surface is determined by the gas across the flux tube in the form of "parallel resistors."

5.3.3. Alfvén Speed and Resistance

In Equation (11), we showed that $\mathcal{R}_*$ is given by

$$\mathcal{R}_* = \frac{1}{2\Sigma s}, \tag{51}$$

where s has been previously defined as $\cos\theta_F$. Here, we decompose Σ, the integral from r_{pn} to R_* of the electric conductivity, into two parts Σ_1 and Σ_2, respectively, the integral of the electric conductivity $\sigma_p(z)$ from r_{pn} to $r_=$ and from $r_=$ to R_* such that

$$\Sigma = \int_r \sigma_p(r)dr = \Sigma_1 + \Sigma_2 \tag{52}$$

$$\Sigma_1 = \int_{r_{\mathrm{pn}}}^{r_=} \sigma_p(r)dr = L_a \frac{T(r)^{3/4}}{\sqrt{P(R_*)}} \exp\left(-\frac{E}{2k_B T(r)}\right) \times \int_{r_{\mathrm{pn}}}^{r_=} \exp\left[-\frac{GM_*\mu}{2R_g T(r) R_*}\left(\frac{R_*}{r} - 1\right)\right] dr \tag{53}$$

$$\Sigma_2 = \int_{r_=}^{R_*} \sigma_p(r)dr = \frac{L_a}{Q_a^2} \exp\left(-\frac{E}{2k_B T(r)}\right) \frac{(P(R_*))^{3/2}}{m^2 T(r)^{1/4}} \times \int_{r=}^{R_*} r^6 \exp\left[\frac{3}{2}\frac{GM_*\mu}{R_g T(r) R_*}\left(\frac{R_*}{r} - 1\right)\right] dr \tag{54}$$

where $y_1 = (R_p/s)(R_*/a)^{3/2}$ and $y_2 = 2R_p(R_*/a)^{3/2}$ are, respectively, the length and width of the foot of the flux tube, $r_=$ is defined above, and the penetration radius r_{pn} is to be determined below (see Figure 4). The numerical application gives $\Sigma_2 \approx 1.5 \times 10^4\,\mathrm{ohm}^{-1}$, and the analytical expression of Σ_1 depends on r_{pn}. Nevertheless, in our fiducial model, the numerical value of Σ_1 does not depend significantly on r_{pn} and we get $\Sigma_1 \approx 4.3 \times 10^4\,\mathrm{ohm}^{-1}$. These values lead to $\mathcal{R}_* = 8.6 \times 10^{-6}$ ohm.

At the foot of the flux tube on the surface of the star, the volumic mass is $\varrho(r) = P(r)m_p/k_B T$ and the expression for the ionization x is given in Appendix A. Therefore, the Alfvén speed in the stellar atmosphere and the time t_A is thus

$$\upsilon_{A,*}(r) = \sqrt{\frac{\mathcal{B}^2 k_B T(r)}{\mu_0 m_p P(r) x(r)}} \tag{55}$$

$$= W \frac{m}{r^3 T(r)^{1/8}} \exp\left(\frac{E}{4k_B T(r)}\right) \frac{1}{(P(R_*)^{1/4})} \times \exp\left[\frac{GM_*\mu}{4R_g T(r) R_*}\left(1 - \frac{R_*}{r}\right)\right] \tag{56}$$

$$W = \frac{1}{2\pi}\sqrt{\frac{\mu_0}{m_p}} \frac{h^{3/4}}{(2\pi m_e)^{3/8}} \frac{1}{k_B^{1/8}}. \tag{57}$$

In SI units, $W = 0.038$, $\mathcal{B}(r) = 2\cos\theta_F \mu_0 m/(4\pi R_*^3)$ (with $\cos\theta_F \approx 1$, and the integral going from r_{pn} to R_* (r_{pn} is the radius that determines the effective height $R_* - r_{\mathrm{pn}}$ of the foot of the flux tube). Using the fiducial values for the parameters, we get $\upsilon_{A,*} \simeq 2.6 \times 10^8 \exp[-717.5(R_s/r) - 1]$. Clearly, $\upsilon_{A,*}$ decreases sharply from the surface toward the interior. r_{pn} is thus the smallest radius that still enables the model to be valid (i.e., the deepest that a perturbation of the field line can penetrate inside the star and back to the planet in less than t_{max} (see Figure 8).

The time it takes for the Alfvén wave to travel from the surface of the star to the bottom of the flux tube is

$$t_{A,*} = \int_z \frac{dz}{\upsilon_{A,*}(z)}. \tag{58}$$

We then equate the total travel time $2(t_{A,*} + t_{\mathrm{tube}})$ (there is a coefficient "2" since the wave needs to go from the planet to the star and back to the planet) defined in Equations (58) and (41) with the total time available, t_{max}, defined in Equation (32)

$$2(t_{A,*} + t_{\mathrm{tube}}) = t_{\mathrm{max}} \tag{59}$$

and solve for r_{pn}. The numerical application gives $r_{\mathrm{pn}} \approx 1.3718 \times 10^9$ m for a fast rotating star and $r_{\mathrm{pn}} \approx 1.3746 \times 10^9$ m for a slow rotating star (given here with several significant digits simply as an intermediate value in the thread of numerical applications). Having determined r_{pn}, one could now calculate self-consistently Σ_1 and $\mathcal{R}_*$.

6. NUMERICAL APPLICATIONS AND DISCUSSION

The quantities we have determined above are applicable for the fiducial model we adopted here. A more general application (for host stars of different masses) will be presented elsewhere.

6.1. Numerical Applications

The numerical values of the intensity, ohmic dissipation, and torque in the star and the planet, respectively, for a slow rotating star (with a spin period eight days) and a fast rotating star (with a spin period 0.8 days) are given below. The values below for U and I correspond to one of the two circuits (each circuit has the same value of U and I), and the values for $\mathcal{P}$ and $\mathcal{T}$ are for the entire planet and entire star (both circuits combined).

$U = 6.7 \times 10^9$ V and 2.8×10^{10} V (for slow and fast rotator, respectively)

$$I = 7.8 \times 10^{14}\text{A and } 3.2 \times 10^{15}\text{A}$$
$$\mathcal{P}_* = 10^{25}\text{ W and } 2 \times 10^{26}\text{ W}$$
$$\mathcal{P}_p = 4 \times 10^{22}\text{ W and } 7 \times 10^{23}\text{ W}$$
$$|\mathcal{T}_*| = |\mathcal{T}_p| = 6 \times 10^{29}\text{ Nm and } 2 \times 10^{30}\text{ Nm}.$$

6.2. Ohmic Dissipation at the Foot of the Flux Tube on the Star and Hot Spots

A super-Earth orbiting at $a = 0.04$ AU from its host star induces an ohmic dissipation at the foot of the flux tube on the surface of the star of 5×10^{24} W (for a stellar spin period of eight days) and 9×10^{25} W (for a spin period of 0.8 days, which is about 1 to 5% of the stellar luminosity ($L_{*,\rm total} = 3.6 \times 10^{26}$ W). This effect would create an observable hot spot at the surface of the star. The rate of energy dissipation per surface area at the foot of the flux tube would be about $2 \times 10^{10}\,\mathrm{W\,m^{-2}}$, which is three orders of magnitude higher than the intrinsic radiative flux from the surface of a typical T Tauri star.

Since $\Sigma_1 > \Sigma_2$, most of the dissipation occurs in the region between $r_{\rm pn}$ and $r_=$. We note that the density scale at the photosphere (R_*), $\delta r_* = R_g T_* R_*^2 / G M_* \mu \sim 5 \times 10^5$ m is much smaller than $R_* - r_= = 3.8 \times 10^6$ m and $R_* - r_{\rm pn} = 1.55 \times 10^7$ m. When the dissipated energy emerges from the stellar photosphere, the actual area of the hot spot may be diffused to several times the area of the foot of the flux tube. The corresponding temperature of the hot spot would be ~2–3 that elsewhere on the stellar surface. In our model, we consider a star with a surface temperature $T_* = 4000$ K. Ohmic dissipation at the foot the flux tube increases the local ionization, conductivity, current, and torque. We will construct a self-consistent model in a follow-up analysis.

6.3. Ohmic Dissipation in the Planet and the Induced Mass Loss

In Paper I, we considered the structural adjustment due to ohmic dissipation. In this paper, we have not yet considered the structural adjustment of super-Earth structure due to ohmic dissipation. For the slow-rotator model, the rate of ohmic dissipation is six times that which the planet receives from its host star's irradiation. In the absence of any structural adjustment, the super-Earth may attain a thermal equilibrium with an effective blackbody temperature $T_p \simeq 2{,}300$ K (and much higher for the fast-rotator model). With this temperature, planet's core crust would surrounded by an ocean and an extensive atmosphere where water and hydrogen molecules readily dissociate but their ionization fraction remains negligible. The local density scale height is $\delta r_p = \lambda R_p$ where

$$\lambda = R_g T_p R_p / G M_p \mu \sim 1/17\mu. \tag{60}$$

The density scale height of the hydrogen atoms is much larger than that of all other elements including carbon, oxygen, and silicates. The mean free path for a hydrogen atom to collide with an heavy element with a density n_z is $l_{H-Z} = 1/(n_z A)$ where $A \sim 10^{-19}$ m^2 is a typical cross section. Within $\delta r_{\rm de} \sim 2$–3 hydrogen atoms' scale heights there are so few heavy-elemental atoms left that they essentially become thermally decoupled, i.e., $l_{H-Z} > \delta r_{\rm de}$ for hydrogen atoms. We refer to this location as the decoupling radius, $r_{\rm de} = R_p + \delta r_{\rm de} \sim (1.1$–$1.2) R_p$, and the local hydrogen density at $r_{\rm de}$ as $\rho_{\rm de}$. The local temperature $T_{\rm de} = T(r_{\rm de})$ is set by the blackbody temperature T_p of the heavy elements in the planet's photosphere. The magnitude of $\rho_{\rm de} = \rho(r_{\rm de})$ for a rocky or icy planet can be estimated to be

$$\rho_{\rm de} = 3 f_H M_p / 4\pi R_p^3 \exp -\delta_{\rm de} \sim 10\,\mathrm{kg\,m^{-3}}, \tag{61}$$

where typical fractional abundance of the hydrogen atoms $f_H \leqslant 0.1$.

Next, we consider the possibility of significant loss of hydrogen atmosphere. Planetary outflow is usually analyzed in the limit that atmosphere is heated by stellar irradiation. For the present configuration, simple estimates indicate that the hydrogen atmosphere is opaque to incident ionizing photons from the host star, i.e., they are mostly absorbed by hydrogen atoms in the upper atmosphere. Provided hydrogen atmosphere remains mostly atomic, most visual stellar photons would stream pass it and be absorbed by heavy elements near R_p. Transit light curves of such a super-Earth in Lyα photons would be much deeper than that for visual photons, as in the case of HD 209458b (Vidal-Madjar et al. 2003). Thus, most regions of the atmosphere are not affected by either ohmic dissipation or irradiation.

The most important heat input is the ohmic dissipation which takes place at the base of the atmosphere. If we neglect energy deposition and loss in the atmosphere, our problem would reduce to a simple spherical Bondi (or Parker) solution. In a steady state, the governing continuity and momentum equations at a location r would reduce to

$$\dot{M}_H = 4\pi \rho_H V_H r^2 \tag{62}$$

$$V_H \frac{\partial V_H}{\partial r} = -\frac{c_s^2}{\rho_H}\frac{\partial \rho_H}{\partial r} - \frac{G M_p}{r^2} + \frac{3 G M_* r}{a^3}, \tag{63}$$

where the last term represents the host star's tidal force (Dobbs-Dixon et al. 2007) and V_H is the radial velocity. Together they reduce to

$$\frac{\left(V_H^2 - c_s^2\right)}{r}\frac{\partial \ln V_H}{\partial \ln r} = \frac{2 c_s^2}{r} - \frac{G M_p}{r^2} + \frac{3 G M_* r}{a^3}. \tag{64}$$

The transonic point (where $V_H = c_s$) occurs (Lubow & Shu 1975; Gu et al. 2003) near the Roche radius, $r \simeq R_R = (M_p/3M_*)^{1/3} a$. Interior to the transonic point, flow is subsonic.

In order to make further progress, we need to estimate the energy budget of the atmosphere. At the base of the atmosphere, ohmic dissipation occurs primarily due to the collision of charged (provided by the heavy elements) and neutral particles. Most of the dissipated energy is emitted to space at R_p as blackbody radiation. Below $r_{\rm de}$, hydrogen atoms

attain $T_p(\sim 2300$ K) through conduction as all other particles. Above $r_{\rm de}$, hydrogen atoms attain different density distribution.

For computational simplicity, let us first consider an isothermal equation of state. For an analytic approximation, we neglect the advection contribution to the momentum equation and obtain

$$\rho(r) \simeq \rho_{\rm de} \exp(r_{\rm de}/\lambda r - 1/\lambda). \quad (65)$$

At large distances ($r > (2\text{–}3)r_{\rm de} \sim 3R_p$) but still well within $R_R(\sim 10^{10}$ cm $\sim 7R_p)$, hydrogen's density approaches an isochoric limiting value of $\rho_\infty \sim 4 \times 10^{-8}\rho_{\rm de} \sim 10^{-7}$ kg m^{-3}. The mass loss rate at R_R (Li et al. 2010) becomes

$$\dot{M}_{\rm hydro} \simeq 4\pi R_R^2 \rho_\infty c_s \sim 5 \times 10^{12} \,{\rm kg\,s^{-1}}. \quad (66)$$

At this rate, the total hydrogen mass in the planet $f_H M_p$ is depleted in a few Myr.

Note that hydrogen atoms contained within this region are negligible compared with M_p as we have assumed in the momentum equation. In addition, the collisional mean free path between hydrogen atoms $l_{H-H} = m_H/(\rho A)$ is small compared to the density scale height δr_p and more importantly R_R. In these limits, it is more appropriate consider outflow in the hydrodynamic limit (Murray-Clay et al. 2009), as we have done above, rather than use the Jeans' escape formula (Lecavelier des Etangs et al. 2006).

If the planet's atmosphere is maintained above the recombination temperature so that it is primarily composed of hydrogen atoms, the main cooling process would be the emission of Lyα photons at a rate of

$$\Lambda \simeq 7.5 \times 10^{-20} x n_H^2 \exp -(1.2 \times 10^5 K/T)\,{\rm J\,m^{-3}\,s^{-1}}. \quad (67)$$

After integrating over the entire volume $\sim 4\pi R_R^3/3$, the total energy loss rate is $L_{{\rm Ly}\alpha} \sim 10^{16} x$ Watt, which is substantially below the fraction of the dissipated energy flux ($f_H \mathcal{P}_p$) carried by the hydrogen atoms. (In the above estimate, we use the asymptotic value of ρ_∞ to estimate Λ.) However, with the magnitude of $\dot{M}_{\rm hydro}$ in Equation (67), we find that a significant fraction of $f_H \mathcal{P}_p$ may be advected with the escaped hydrogen gas.

Based on hydrogen atoms' ineffective absorption and emission rates, it is natural to contemplate the possibility that the planet's atmosphere expands adiabatically. In the limit that ohmic dissipation provides the only source of heating at its base, a planet's atmosphere may be convectively unstable. Efficient convection also leads to constant entropy.

Using the conventional polytropic approximation (in which $P = K\rho^\gamma$ and $\gamma = 1.4$) for an adiabatic hydrogen atmosphere, a stationary quasi-hydrostatic solution can be constructed with

$$1 - \left(\frac{\rho(r)}{\rho_{\rm de}}\right)^{\gamma-1} = \left(\frac{\gamma-1}{\lambda}\right)\left(1 - \frac{R_{\rm de}}{r}\right). \quad (68)$$

The above equation implies that with an adiabatic equation of state, both density and temperature in the hydrogen atmosphere vanish within $\delta r_{\rm de}/(\gamma - 1) \sim 2.5\delta r_{\rm de}$. Unless a planet's photospheric radius can expand (see Paper I) significantly, there would be no outflow, despite the intense ohmic dissipation below R_p, and all the thermal energy generated would efficiently be radiated by atomic emission from heavy elements.

However, a planet's atmosphere may be heated to prevent its temperature from plummeting below that ($\sim$2000 K) for hydrogen molecules to recombine. Rotational and vibrational bands of hydrogen molecules not only provide emission mechanisms but also opacity sources to absorb the incident stellar irradiation and to diffuse thermal energy in the planet's atmosphere from its heated base to its upper layers. In the mildly heated case, we anticipate the planet's hydrogen atmosphere to attain an equilibrium temperature so that the incident deposition of stellar photon energy would be balanced by planet's reprocessed luminosity. (For our fiducial model, the equilibrium temperature is $T_p \sim 2000$ K.) In this limit, the loss of a planet's hydrogen atmosphere relies more critically on the atmosphere ability to maintain a shallow temperature gradient than that to generate energy through ohmic dissipation. This situation has already been analyzed in the context of HD 209458b (Murray-Clay et al. 2009).

However, enhanced sources of energy may also expand the radius of a planet's photosphere well beyond R_p. This is a distinctive possibility for the fast-rotator model in which case $\mathcal{P}_p$ is another 18 times larger. This increase in the ohmic dissipation rate is due to the relatively large differential motion between the planet and the magnetosphere of its host star. If the planet's photosphere remains at R_p, the enhanced energy source would increase T_p by a factor of two, which is comparable to the magnitude of T_*. At this temperature, opacity due to H^- process becomes significant. A planet's envelope and photosphere may well expand, leading to a possible runaway ohmic heating. The above discussion clearly warrants further discussions and detailed treatments of radiation transfer in this type of super-Earth. We shall carry out and present this analysis in a future paper.

The loss of a planet's atmospheric hydrogen is likely to occur at a more rapid pace. It remains to be demonstrated for the intense heating cases how far up in the atmosphere thermal decoupling between hydrogen and heavy elements occurs. If the planet's photosphere is well within R_R, the density scale height of most other heavy elements such as carbon and oxygen above are sufficiently small that they may be effectively retained near R_p. Oxygen atoms may combine with Mg, Fe, Ca, Na, Al, and Ti silicates to form high-density minerals such as enstatites, olivines, and pyroxenes. Planets composed mostly of such substances are expected to have compact sizes (Valencia et al. 2010). Thus, it is likely that super-Earths which migrated early to the proximity of their strongly magnetized host stars may attain relatively compact sizes as in the case of CoRoT 7-b (Leger et al. 2009) and planets around Kepler 11.

The rate of ohmic dissipation in short-period super-Earths is likely to diminish as their host stars magnetic field weakens with age. As their semimajor axis increases, planets which undergo outward migration around rapidly spinning host stars also encounter less intense stellar dipole field. Some residual oxygen atoms in the atmosphere may recombine to form oxygen molecules during the decline of the ohmic dissipation rate. Oxygen molecules are particularly important because they have been suggested as a bio-marker for the detection of life elsewhere in the universe (DesMarais et al. 2002).

6.4. Discussion about Some Approximations

We have presented here a preliminary model for the unipolar induction model. Some approximations were made for computational convenience, and we briefly discuss here the validity of the approximations which have not yet been discussed in the paper.

We only took into account hydrogen for the calculation of the conductivity/resistance of the star. In a realistic model, especially for low-mass stars, other elements may become important

contributors of the ionization fraction. A more comprehensive study will be presented elsewhere. In addition, we suggested that the foot of the flux tube at the stellar atmosphere would be significantly heated. However, we used $T = 4000$ K for the stellar surface temperature (usual T Tauri star). The feedback on the stellar temperature due to the circuit may be included in later models.

Evaluation of the planet's electrical resistivity. The value we adopted (7×10^{-8} ohm) seems to be the most uncertain value in our calculation. This value of the resistance of the planet used here is likely to be a lower boundary for the mantle of the planet (a metallic core might have even higher conductivity). If the real resistance were to be lower, then (1) the time $t_{\max}$ available for the Alfvén waves to travel around the circuit would increase, which would result in a deeper foot of the flux tube and would also enable the model to hold for larger semimajor axes and (2) the ohmic dissipation in the planet would decrease. Nevertheless, an increase in the depth of the foot of the flux tube would not affect much the total resistance of the foot of the flux tube $\mathcal{R}_*$.

Induction at the foot of the flux tube. Since the conductivity is very high along the magnetic field lines, the plasma in the star's magnetosphere rotates with the magnetic field lines. Therefore, the plasma contained in the flux tube also moves with the magnetic field lines as they are dragged along by the planet, and thus moves relative to the unperturbed magnetic field line. Therefore, just as the induction in the planet is due to the relative motion between the frame co-moving with the planet and the frame rotating with the magnetosphere, there can also be a magnetic induction in the plasma enclosed by the foot of the flux tube. The order of magnitude of this phenomenon will be at most comparable to the order of magnitude of the phenomenon presently described. Ferraro & Plumpton (1966) provide a brief discussion of the problems raised by two good concentric conductors rotating in a magnetic field at different angular speeds.

As mentioned earlier, there may be a magnetic reconnection if the induced field dominates over the unperturbed stellar dipole field. The field lines also tend to wrap around the planet when the synodic period ($T_{\rm synod} = 2\pi/(\omega_p - \omega_*)$) is small compared to $t_{\max}$, the time required for the field lines constituting the flux tube to move across the diameter of the planet. Using (32), we find that $t_{\max} = (R_p/\pi a)(1 + w)T_{\rm synod}$ with $w = ((\mathcal{R}_* + \mathcal{R}_{\rm tube})/(\mathcal{R}_p + \mathcal{R}_{\rm tube})) \approx (\mathcal{R}_*/\mathcal{R}_p)$. For our parameters, this corresponds to $t_{\max} \approx 0.091 T_{\rm synod}$ (using $\mathcal{R}_p = 7 \times 10^{-8}$ ohm according to (34) and $\mathcal{R}_* = 8.6 \times 10^{-6}$ ohm according to section (5.3.3).

This also provides an upper limit on the ratio of resistances w in order to stay with a model without reconnection. Indeed, magnetic reconnection may occur when $t_{\max}$ is larger than a few $T_{\rm synod}$, and one would thus arguably stay in the regime without frequent magnetic reconnection when

$$1 + w \leqslant K \frac{\pi a}{R_p} \tag{69}$$

with K larger than 1, and w as defined above. Using $R_p = 2R_\oplus$ and $a = 0.04$ AU, we find $(\pi a/R_p) \approx 1300$. We have neglected the resistance of the flux tube $\mathcal{R}_{\rm tube}$ in front of $\mathcal{R}_p$ and $\mathcal{R}_*$ but this approximation may break down in extreme cases. Nevertheless, in most cases, Equation (70) means that $\mathcal{R}_*/\mathcal{R}_p$ is smaller than 1300. The resistance of the planet depends mainly on its composition, and structure, which would adjust to the strong ohmic dissipation in its interior. The resistance of the foot of the flux tube in the stellar atmosphere would depend on the metallicity and the temperature, which would also adjust to the strong ohmic dissipation.

Previously in the paper, we also discussed that the Alfvén travel time can be at most $t_{\max}$ (Equation (59)). $\mathcal{R}_*$, through its relationship with the variable depth of penetration, would self-consistently adjust depending on the parameters of the model. Indeed, larger $\mathcal{R}_*$ leads to larger w, then larger $t_{\max}$, and thus larger depth of penetration since the Alfvén waves have more time to travel between the planet and the star along the flux tube, into the stellar atmosphere at the foot of the flux tube, and back to the planet. Deeper depth of penetration then results in smaller $\mathcal{R}_*$ (equivalent resistance with resistances in parallel).

The value $\mathcal{R}_p$ is less directly constrained by the model, although it of course depends on the parameters chosen for the model. Nevertheless, changes in the value of $\mathcal{R}_p$ would result in adjustments in $\mathcal{R}_*$ through the mechanism just mentioned above.

Goldreich & Lynden-Bell also interpret the torque calculated above (Section 6.1) in terms of a toroidal magnetic stress due to a distortion of B_ϕ in the azimuthal direction, i.e., the direction of the motion. Neglecting the induced field in the $r-z$ (meridional) direction, they determined the longitude of the flux tube from the ratio of the induced B_ϕ and the unperturbed stellar-dipole field. They then determined, for the Jupiter-Io system, the forward-sweeping angle (or the backward-sweeping angle in the case of a slowly rotating star) of each field line as it leaves the Io to be 13°. When a similar approach is adopted in the present model, we find this angle may be close to 90°. This large distortion is due to a strong torque induced by the unipolar circuit with a relatively small $\mathcal{R}_*$ (and thus a large intensity). For such a large field distortion, Goldreich & Lynden-Bell suggested that the induction circuit may be broken by field reconnection. We shall further examine this possibility elsewhere and determine whether it may significantly weaken the effective torque.

7. SUMMARY AND DISCUSSIONS

With the advent of high-precision radial velocity and transit surveys, we have entered an era of super-Earth discovery. Although the detection probability (due to observational selection effects) decreases with a planet's period, three times more planets are found with periods between 3 and 10 days than between 1 and 3 days. We suggest that super-Earths' interaction with the magnetosphere of their host stars may be one possible mechanism for this dichotomy.

In this paper, we analyze the electrodynamics of super-Earths orbiting in the proximity of strongly magnetized T Tauri stars. We constructed a fiducial model in which the planet's orbital frequency is not synchronized with the star's spin. Their relative motion enables the planet to continually encounter field lines which are locked on the star. As a good (but not perfect) conductor, an emf is induced across the planet (along the semimajor axis). We estimate the planet's conductivity and show that the stellar fields slip through the planet with a drift speed considerably slower than its Keplerian speed.

We show that conductivity along the field line is likely to be large and the perturbed potential (due to the induced electric field) propagates along a flux tube away from the planet with an Alfvén speed. We show that for planets with periods less than three or so days, the disturbance can reach the surface of the star and return before stellar fields have drifted through the planet.

The foot of the flux tube is implanted to the stellar surface. As density increases with depth below the photosphere, the Alfvén

speed decreases. Penetration depth of the flux tube is determined by the condition that the timescale required for Alfvén waves to complete a circuit between the planet and its host star is comparable to that for the stellar field to drift through the planet.

Across the foot of the flux tube on the stellar surface, the potential drop induces a current to flow across it. We show that the resistance on the surface of the star is larger than that in the planet. Consequently, the intensity of the current is determined by the resistivity on the star. We quantitatively determine this resistivity, the associated current, ohmic dissipation rate, and torque due to the Lorentz force. The ohmic dissipation in the star at the foot of the flux tube could also induce an observable hot spot.

The source of energy is the differential motion between the planet and the magnetosphere of its host star. The Lorentz force on the planet and its host star leads to an evolution toward a state of synchronous rotation. Inside the corotation radius, planets tend to lose angular momentum and migrate inward and the opposite trend occurs outside the corotation radius. Consequently, planets inside corotation migrate inward and those outside corotation migrate outward.

For super-Earths with periods less than three days, the timescale for orbital evolution can be comparable or shorter than a few Myr (the timescale over which intense stellar magnetic field is maintained). The low abundance of super-Earths with periods less than three days may be due to their infant mortality.

Due to their finite conductivity, ohmic dissipation also occurs within the super-Earths. The heating rate depends on planet's poorly determined resistivity. Its magnitude can be comparable to or larger than that which the planet received from the stellar irradiation. The intense rate of ohmic dissipation may cause water and hydrogen molecule to become dissociated and hydrogen atoms to segregate from other heavy elements. It is unclear whether a substantial fraction of the hydrogen atom may escape though hydrodynamic outflows. As the field decays with maturing stars, remaining excess oxygen atoms may either be incorporated in high density minerals or form oxygen molecules. Either of these processes can lead to consequences which may be observable in the near future.

There are several uncertainties which warrant further investigation. Conductivity in super-Earths and their host stars need further study. We have not yet applied these results to a wide range of stellar and planetary models. The effect of feedback due to the adjustment of the planet's and star's heated atmosphere also need to be examine. Perhaps the largest uncertainty is whether the intense induced field can lead to magnetic reconnection and the breaking of the circuit. Reconnection would increase the effective magnetic diffusivity and severely weaken the effective torque.

In order to directly compare with observations, we also need to consider a diverse range of planetary orbits. For example, this process may not work for planets with periods longer than a few days. Finally, it would be of interest to determine whether the intense electromagnetic interaction between super-Earths and their host stars can be directly observed in the radio-wave frequency range.

Nevertheless, we show that electrodynamic interaction is an important process for the orbital and structure evolution of super-Earths as well as hot Jupiters. Along with many other physical processes it introduces diversity in the present-day configuration of extra solar planetary systems.

We thank A. Cumming, F. de Colle, S. F. Dong, G. Ogilvie, G. Glatzmaier, and Q. Williams for useful discussions. This work is supported by NASA (NNX07A-L13G, NNX07AI88G, NNX08AL41G, and NNX08AM84G), and NSF (AST-0908807).

APPENDIX A

ELECTRIC CONDUCTIVITY AT THE FOOT OF THE FLUX TUBE

Saha's equation gives the ionization fraction of the hydrogen atom $x = \sqrt{K_H/1 + K_H}$, where

$$K_H(r) = \frac{1}{P(r)} \frac{(2\pi m_e)^{3/2}}{h^3} (kT)^{5/2} \exp\left(-\frac{E}{kT}\right), \quad \text{(A1)}$$

where $P(r)$ is the pressure, m_e the electron mass, h Planck's constant, and E the ionization energy of the hydrogen atom. K_H is a function of r which, in the isothermal region, decreases as one moves from the surface of the star toward the interior. Since, in the situations considered in this paper, K_H is small compared to unity at the surface of the star, we get the following expression for the ionization rate x everywhere in the isothermal region

$$x(r) \approx \sqrt{K_H(r)}. \quad \text{(A2)}$$

Using the formulas given by Fejer (1965), we calculate the electric conductivity profile in the stellar (isothermal) outer layer. The conductivity $\sigma_0(r)$, which determines the current parallel to the magnetic lines of force, is given by

$$\sigma_0(r) = x(r)\ 10^{19} \frac{e^2}{m_e} \sqrt{\frac{9\pi m_e}{128 k_B T(r)}}. \quad \text{(A3)}$$

Using (A1) and (A2), we obtain the following expression for σ_0

$$\sigma_0(r) = L_a \exp\left(\frac{-E}{2kT(r)}\right) \frac{T(r)^{3/4}}{\sqrt{P(r)}} \quad \text{(A4)}$$

$$L_a = 10^{19} \frac{e^2}{m_e} \sqrt{\frac{9\pi m_e}{128 k_B}} \frac{(2\pi m_e)^{3/4}}{h^{3/2}} k_B^{5/4} \quad \text{(A5)}$$

which decreases as one moves from the surface of the star toward the interior. The numerical value of the constant L_a in SI units is $L_a \simeq 6.17 \times 10^6$.

The (Pedersen) conductivity $\sigma_p(r)$, which determines the current parallel to the electric field, is given by

$$\sigma_p = \frac{\sigma_0}{1 + (\omega_e/\nu_e)^2}, \quad \text{(A6)}$$

where ω_e (the gyro-frequency of the electron) and ν_e (in the limit of a gas with low ionization fraction, ν_e, is related to the mean collisional frequencies of the electrons with molecules of the neutral gas; see Draine et al. 1983) are given by

$$\omega_e(r) = \frac{e\mathcal{B}_s(r)}{m_e} \quad \text{(A7)}$$

$$\nu_e(r) = 10^{-19}\, n \left(\frac{128kT(r)}{9\pi m_e}\right)^{1/2} = 10^{-19}\, P(r) \left(\frac{128}{9\pi m_e kT(r)}\right)^{1/2} \quad \text{(A8)}$$

with n the number density of neutral particles. Since the ionization rate is small, n is also the number density of particles which is equal to P/kT for a perfect gas. Using (A7) and the expression of a dipole magnetic field $\mathcal{B}_s(r) = \mu_0\, m/(4\pi r^3)$ (with m being the stellar magnetic moment), we obtain

$$\frac{\omega_e}{\nu_e}(r) = Q_a\, \frac{m\sqrt{T(r)}}{r^3 P(r)} \tag{A9}$$

$$Q_a = \frac{e}{m_e}\frac{\mu_0}{4\pi} 10^{19} \left(\frac{9\pi m_e k_B}{128}\right)^{1/2}, \tag{A10}$$

where the numerical value of the constant Q_a in SI units is $Q_a = 2.93 \times 10^{-4}$.

In order to compare $(\omega_e/\nu_e)(r)$ with unity, we define $r_=$ such that

$$\frac{\omega_e}{\nu_e}(r_=) = 1 \tag{A11}$$

or, equivalently,

$$P(r_=) = \frac{Q\, m\sqrt{T(r)}}{r_=^3}. \tag{A12}$$

Using the numerical values for the star listed above, we deduce $r_= = 1.3962 \times 10^9$ (note that in Paper I, what we defined $r_=$ to be the transition between the isothermal and the polytropic region in the star, which is an unrelated quantity defined here).

Since $P(r)$ increases rapidly when r decreases (from the stellar surface inward), one may distinguish two regimes by

$$\sigma_p(r \leqslant r_=) = \sigma_0(r) \tag{A13}$$

$$\sigma_p(r \geqslant r_=) = \frac{\sigma_0(r}{(\omega_e/\nu_e)^2} \tag{A14}$$

i.e.,

$$\sigma_p(r \leqslant r_=) = L_a\, \exp\left(\frac{-E}{2k_B T(r)}\right) \frac{T(r)^{3/4}}{\sqrt{P(r)}} \tag{A15}$$

$$\sigma_p(r \geqslant r_=) = \frac{L_a}{Q_a^2}\, \frac{1}{m^2 T(r)^{1/4}} \exp\left(\frac{-E}{2kT(r)}\right) r^6\, (P(r))^{3/2} \tag{A16}$$

$$\frac{L_a}{Q_a^2} = 10^{-19} \left(\frac{\mu_0}{4\pi}\right)^{-2} \frac{(2\pi m_e)^{3/4}}{h^{3/2}} k_B^{-1/4} \left(\frac{128 m_e}{9\pi}\right)^{1/2} \tag{A17}$$

where the numerical value of the constant in SI units is $L_a/Q_a^2 = 7.2 \times 10^{13}$.

APPENDIX B

ANOTHER ESTIMATE OF THE ALFVÉN SPEED ALONG THE FLUX TUBE

The volumic current passing through the tube is $\mathcal{J} = e\upsilon_e f \varrho/m_p$. In this expression, we adopt the current propagation υ_e to be the thermal speed of the electrons $m_e\upsilon_e^2/2 = k_B T$ and we define f to be the fraction of gas particles that are ionized. The total flux $\mathcal{J}$ is the total intensity I divided by the cross section of the flux tube through which the current passes. It is a fraction g_2 of the cross section πR_p^2 of the planet. With these notations, we get $\mathcal{J} = I/g_2\pi R_p^2$.

We thus obtain the following Alfvén speed and $t_{A,\mathrm{tube}}$

$$\upsilon_{A,\mathrm{tube}} = \frac{\mu_0 m}{4\pi}\sqrt{\frac{1}{\mu_0}\frac{\pi R_p^2}{I}\frac{e}{m_p}}\left(\frac{2k_B T}{m_e}\right)^{1/4}\frac{\sqrt{g_2}}{r^3} \tag{B1}$$

$$t_{A,\mathrm{tube}} = \frac{2}{m}\sqrt{\frac{\pi I m_p}{\mu_0 R_p^2 e}}\left(\frac{m_e}{2k_B T}\right)^{1/4} a^4\left[1-\left(\frac{R_*}{a}\right)^4\right]\frac{1}{\sqrt{f g_2}}, \tag{B2}$$

which gives, for $f g_2 = 1$, $t_{A,\mathrm{tube}} \simeq 450$ s.

REFERENCES

Aly, J. J. 1985, A&A, 143, 19
Aly, J. J., & Kuijpers, J. 1990, A&A, 227, 473
Bouvier, J., Cabrit, S., Fernandez, M., Martin, E. L., & Mattews, J. M. 1993, A&A, 272, 176
Dermott, S. F. 1970, MNRAS, 149, 35
Des Marais, D. J., Hawitt, M. O., Jucks, K. W., et al. 2002, Astrobiology, 2, 153
Dobbs-Dixon, I., Li, S. L., & Lin, D. N. C. 2007, ApJ, 660, 791
Draine, B. T., Roberge, W. G., & Dalgarno, A. 1983, ApJ, 264, 485
Drell, S. D., Foley, H. M., & Ruderman, M. A. 1965, J. Geophys. Res., 70, 3131
Fejer, J. A. 1965, J. Geophys. Res., 70, 4972
Ferraro, V. C. A., & Plumpton, C. 1966, An Introduction to Magneto-fluid Mechanics (Oxford: Clarendon)
Goldreich, P., & Lynden-Bell, D. 1969, ApJ, 156, 59
Goldreich, P., & Tremaine, S. 1980, ApJ, 241, 425
Gu, P-G., Bodenheimer, P., & Lin, D. N. C. 2003, ApJ, 588, 509
Hartmann, L., Calvet, N., Gullbring, E., & D'Alessio, P. 1998, ApJ, 495, 385
Howard, A. W., Marcy, G. W., Johnson, J. A., et al. 2010, Science, 330, 653
Ida, S., & Lin, D. N. C. 2008, ApJ, 685, 584
Ida, S., & Lin, D. N. C. 2010, ApJ, 719, 810
Johns-Krull, C. M. 2007, ApJ, 664, 975
Konigl, A. 1991, ApJ, 370, L39
Kretke, K., & Lin, D. N. C. 2007, ApJ, 664, L55
Kretke, K., & Lin, D. N. C. 2010, ApJ, 721, 1585
Kretke, K., Lin, D. N. C., Garaud, P., & Turner, N. J. 2009, ApJ, 690, 407
Laine, R. O., Lin, D. N. C., & Dong, S. 2008, ApJ, 685, 521 (Paper I)
Lecavelier des Etangs, A., Vidal-Madjar, A., McConnell, J. C., & Hebrard, G. 2006, A&A, 418, 1
Leger, A., Rouan, D., Schneider, J., et al. 2009, A&A, 506, 287
Li, S. L., Miller, N., Lin, D. N. C., & Fortney, J. 2010, Nature, 463, 1054
Lin, D. N. C., Bodenheimer, P., & Richardson, D. C. 1996, Nature, 380, 606
Lin, D. N. C., & Papaloizou, J. C. B. 1986, ApJ, 309, 846
Lorrain, P., Lorrain, F., & Houle, S. (ed.) 2006, Magneto-fluid Dynamics: Fundamentals and Case Studies of Natural Phenomena (Berlin: Springer)
Lubow, S. H., & Shu, F. H. 1975, ApJ, 198, 383
Masset, F. S., D'Angelo, G., & Kley, W. 2006, ApJ, 652, 730
Mayor, M., Bonfils, X., Forveille, T., et al. 2008, A&A, 507, 487
Mayor, M., & Queloz, D. 1995, Nature, 378, 355
Merrill, R. T., McElhinny, M. W., & McFadden, P. L. 1996, The Magnetic Field of the Earth (London: Academic Press)
Murray-Clay, R. A., Chiang, E. I., & Murray, N. 2009, ApJ, 693, 23
Obiekezie, T. N., & Okeke, F. N. 2010, Int. J. Phys. Sci., 5, 637
Paardekooper, S.-J., Baruteau, C., Crida, A., & Kley, W. 2010, MNRAS, 401, 1950
Piddington, J. H., & Drake, J. F. 1968, Nature, 217, 935
Rikitake, T. 1966, Electromagnetism and the Earth's Interior (Amsterdam: Elsevier)
Shu, F., Najita, J., Ostriker, E., et al. 1994, ApJ, 429, 781

Sicilia-Aguilar, A., Hartmann, L., Calvet, N., et al. 2006, ApJ, 638, 897
Skumanich, A. 1972, ApJ, 171, 565
Soderblom, D. R., Stauffer, J. R., MacGregor, K. B., & Jones, B. F. 1993, ApJ, 409, 624
Stevenson, D. J. 2003, Earth Planet. Sci. Lett., 208, 1
Tanaka, H., Takeuchi, T., & Ward, W. R. 2002, ApJ, 565, 1257
Umemoto, K., Wentzcovitch, R., & Allen, P. 2006, Science, 311, 986
Valencia, D., Ikoma, M., Guillot, T., & Nettelmann, N. 2010, A&A, 516, 20
Van Ballegooijen, A. A. 1994, Space Sci. Rev., 68, 299
Vidal-Madjar, A., Lecavelier des Etangs, A., Desert, J.-M., et al. 2003, Nature, 422, 143
Waff, H. S., & Weill, D. F. 1975, Earth Planet. Sci. Lett., 28, 254
Yang, H., Johns-Krull, C., & Valenti, J. A. 2008, AJ, 136, 2286

Randy Olivier LAINE

MODÉLISATION DE L'INTERACTION ENTRE LE CHAMP MAGNÉTIQUE D'UNE ÉTOILE ET UNE PLANÈTE EXTRASOLAIRE PROCHE

La découverte de nombreuses planètes extrasolaires depuis 1995 est une source d'inspiration pour les modèles de formation et évolution des systèmes solaires. Une fraction de ces planètes ont un demi-grand axe inférieur à 0.1 UA; une planète qui migre à proximité de son étoile subit donc d'abord un fort vent solaire et, après son entrée dans la magnétosphère stellaire, un fort champ magnétique.

Nous étudions séparemment l'interaction entre ces planètes et la composante périodique et indépendente du temps du champ magnétique dipolaire stellaire. L'interaction périodique est associée à des courants induits confinés dans la planète. Nous étudions deux effets qui pourraient augmenter le moment angulaire d'une planète gaseuse géante qui migre vers son étoile: un torque de Lorentz qui transferre du moment angulaire de la rotation de l'étoile vers l'orbite de la planète et une perte de masse induite par la dissipation ohmique dans la planète qui peut donner du moment angulaire à la planète lorsque cette masse est accrétée sur l'étoile.

Nous modellisons l'interaction indépendente du temps comme un modèle d'inducteur unipolaire, dans lequel le courant induit circule dans une boucle fermée formée par la planète, le flux de tube, et le pied du flux de tube dans l'atmosphère stellaire. Nous calculons de fa con cohérente la dissipation ohmique dans la planète et le pied du flux de tube ainsi que le couple de Lorentz. Nous utilisons alors ce modèle pour expliquer l'aspect enflé de certaines planètes géantes. Finalement, nous suggérons que ce modèle permettrait également d'estimer la conductivité électrique des super-Terres qui interagissent magnétiquement avec leur étoile.

Mots clés : Planète extrasolaire, Inducteur unipolaire, courants induits, Migration, inflation, et différenciation planétaire.

INTERACTION OF A CLOSE-IN EXTRASOLAR PLANET WITH THE MAGNETIC FIELD OF ITS HOST STAR

The numerous and diverse extrasolar planets detected since 1995 provide much inspiration for planetary astrophysics. A fraction of these extrasolar planets orbit their host stars at semi-major axes less than 0.1 AU; a planet which has migrated toward its host star would thus first encounter a strong magnetized wind and, as it enters the stellar magnetosphere, strong magnetic fields.

We model the interaction of such a close-in extrasolar planet with the dipolar magnetic field of its host star and study separately the time-dependent and independent components. The time-dependent interaction gives rise to Eddy currents confined in the planet. We investigate two effects that may transfer angular momentum to a planet approaching its host TTauri star through type II migration: a Lorentz torque that transfers angular momentum from the stellar spin to the planetary orbit and a mass loss induced by the ohmic dissipation in the planet, which may transfer angular momentum to the planet as the gas is accreted onto the star.

We model the time-independent interaction with the unipolar inductor model, which allows the current induced in the planet to flow along a closed loop constituted by the planet, the flux tube, and its footprint on the stellar atmosphere. We self-consistently calculate the ohmic dissipation in the planet and the star and the associated Lorentz torque. We then suggest that the ohmic dissipation may provide the extra energy needed to explain some planets with inflated radii. Finally, we propose that the model may also be used to remotely infer the electric conductivity of the outer layers of super-Earths interacting magnetically with their host stars.

Keywords: Close-in extrasolar planet, Unipolar inductor, Eddy currents, Remote sounding, Planetary migration, inflation, and differentiation.

LPC2E UMR7328
CNRS–Université d'Orléans
3A, Avenue de la Recherche Scientifique
45071 Orléans Cedex 2
France